Structure-reactivity relationships through-ray and neutron diffraction studies

Wilson, Claire

Structure-Reactivity Relationships through X-ray and Neutron Diffraction Studies

Claire Wilson

May 14, 1995

[1]Thesis submitted to the University of Durham for the degree of Ph.D. containing work conducted in the Department of Chemistry.

Abstract

Author:Claire Wilson

Thesis Title:

Structure-Reactivity Relationships through X-ray and Neutron Diffraction Studies

This thesis is primarily concerned with the investigation of a structure-reactivity relationship in a series of pentacyclic Isodrin derivatives. These compounds undergo a two-hydrogen atom dyotropic rearrangement at vastly differing rates when apparently small structural changes are made. Two pairs of these isomers (with the formulas $C_{16}H_8Cl_{10}$ and $C_{16}H_9Cl_9$) have been investigated using both X-ray and neutron single crystal diffraction studies, at ambient and low temperatures. The experimental details of these studies are given for five experiments and the results of the least-squares refinements made using the data from these experiments are reported herein.

In addition to conventional crystallographic studies, an experimental charge density study of one of these compounds, $C_{16}H_9Cl_9$, has been made at 123K. The electron density was modelled using a multipole model which allows explicitly for the aspherical nature of the electron density. The results of this study, including a topological analysis of the charge density are reported in this thesis.

The structures of six organometallic, four molybdenum bis(imido) and two half-sandwich niobium imido complexes, are also reported herein. Their structures were determined from single crystal diffraction data. These compounds show the expected structures predicted using the pseudo-isolobal relationship to the Group 4 bent metallocenes of which they may be considered analogues.

Contents

List of Figures

List of Tables

Declaration The work contained in this thesis was carried out between September 1991 and May 1995 at the University of Durham and the Institut Laue-Langevin, Grenoble. Unless otherwise stated it is the individual work of the author and has not been submitted previously for a degree at the University of Durham or any other university.

Acknowledgements

I'd like to thank the many people who have helped me during the period of my thesis:-

To Judith for a great deal of help, moral support and encouragement and for dealing with my poor grammar, amongst other things, in the last few months.

To my ILL supervisor Sax Mason. To Garry McIntyre for a massive amount of patient and good humoured help and for answering endless stupid questions. To Ken Mackenzie for not only supplying the crystals but also a great deal of enthusiastic background information and interest in this project. To the ILL for financial support. To Paul Mallinson for his help with the charge density study of KM25.

To the various members of the lab in Durham who made the time that I spent there very enjoyable. To Ness for lots of things including revolutionising the final stages of my thesis writing with the ctrl-k key and her postscript skills. To Roy for lots of help and encouragement, to Jacqui for lots of entertainment. As well as to my contempories Jason and Nigel, and to all the other members of the lab: Susanna, Pete, Garry, Dima. To other friends in Durham including Phil, Matt and Martyn.

In Grenoble to the friends that have made living here very enjoyable - especially to Steve and Jostein and to Jo for lots of manic lunchbreaks and for her efforts to keep me at least as sane as I started out and for lots of things more entertaining than bowls of fruit. To Emilio for his efforts to keep me going and for his epic stint of proof-reading and to many people at the ILL, especially to John, Iain and Miles, for making work a more enjoyable time.

Glossary of units and abbreviations

KM5	1,5,6,7,8,12,13,14,15,15-decachloropentacyclo- [10.2.1.1^{3,10}.0^{2,11}.0^{4,9}] hexadeca-5,7,13-triene.
KM9	1,5,6,7,8,12,13,14,15,15-decachloropentacyclo- [10.2.1.1^{3,10}.0^{2,11}.0^{4,9}] hexadeca-4(9),5,7-triene.
KM22	endo,endo,exo-1,5,6,7,8,12,13,14-anti-15-nonachloropentacyclo- [10.2.1.1^{3,10}.0.^{2,11}0^{4,9}]hexadeca-5,7,13-triene.
KM25	endo,endo-1,5,6,7,8,12,13,14-anti-15-nonachloropentacyclo- [10.2.1.1^{3,10}.0.^{2,11}0^{4,9}]hexadeca-4(9),5,7-triene.
Å	Ångstroms 10^{-10} metres
barn	10^{-24}cm^2
fm	10^{-15} metres
esd	estimated standard deviation esds given for refined parameters are from the least-squares refinements esds for average values are variances of the mean
rms	root mean square
rmsd	root mean square deviation
NMR	Nuclear Magnetic Resonance
TDS	Thermal Diffuse Scattering
BPB	Background - Peak - Background
adp	atomic displacement parameter
IAM	Independent Atom Model
Displex	Two-stage closed-cycle helium cryorefrigerator from Air Products and Chemical, Inc. Model number CS201 was used at Risø, Denmark and CS202 at BNL, USA.
@	trade mark

Me	Methyl, CH_3
Et	Ethyl, C_2H_5
Ph	Phenyl, C_6H_5
^{i}Pr	isopropyl, CH_3CHCH_3
Bu^t	tertiary butyl, $C(CH_3)_3$
Cp	cyclopentadienyl, C_5H_5
R(F^2)	$\sum \Delta / \sum F(\mathbf{h})^2_{obs}$
wR(F^2)	$[\sum w\Delta^2 / \sum (w\mathrm{F}(\mathbf{h})^2_{obs})^2]^{\frac{1}{2}}$
S	the Goodness of Fit given by $[\sum w\Delta^2/(n-p)]^{\frac{1}{2}}$ where $\Delta = \lvert \mathrm{F}(\mathbf{h})^2_{obs} - \mathrm{F}(\mathbf{h})^2_{calc} \rvert$ and n and p are the number of observations and parameters respectively
R	$\sum \Delta / \sum F(\mathbf{h})^2_{obs}$
Rw	$[\sum w\Delta^2 / \sum (w\mathrm{F}(\mathbf{h})^2_{obs})^2]^{\frac{1}{2}}$
Goof	$[\sum w\Delta^2/(n-p)]^{\frac{1}{2}}$ where $\Delta = \lvert \mathrm{F}(\mathbf{h})_{obs} - \mathrm{F}(\mathbf{h})_{calc} \rvert$ and n and p are the number of observations and parameters.

Chapter 1

Introduction

The broad concern of this thesis is the relationship between structure and reactivity. It is an area which is of importance to many branches of science, including chemistry and biology. Often, the detailed molecular structure of a compound allows many of its other properties to be derived and or understood.

1.1 The history of the project

We have been studying a series of organic compounds which undergo a two hydrogen atom intramolecular rearrangement [1]. These pentacyclic Isodrin (which is shown in Figure 1.1) derivatives are thought to rearrange via a pericyclic mechanism. The reaction is best seen as a $[4\sigma + 2\pi]$ thermal rearrangement which is exothermic and irreversible. It is an example of a 'dyotropic' rearrangement, *i.e.*

> an uncatalysed process in which two σ-bonds simultaneously, but not necessarily via a fully synchronous mode, migrate intramolecularly [2].

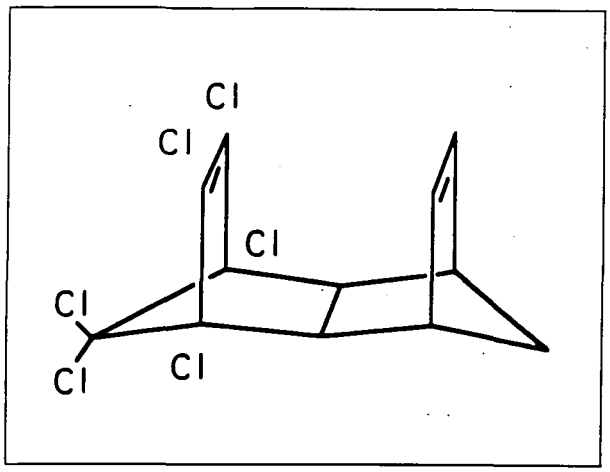

Figure 1.1: Isodrin

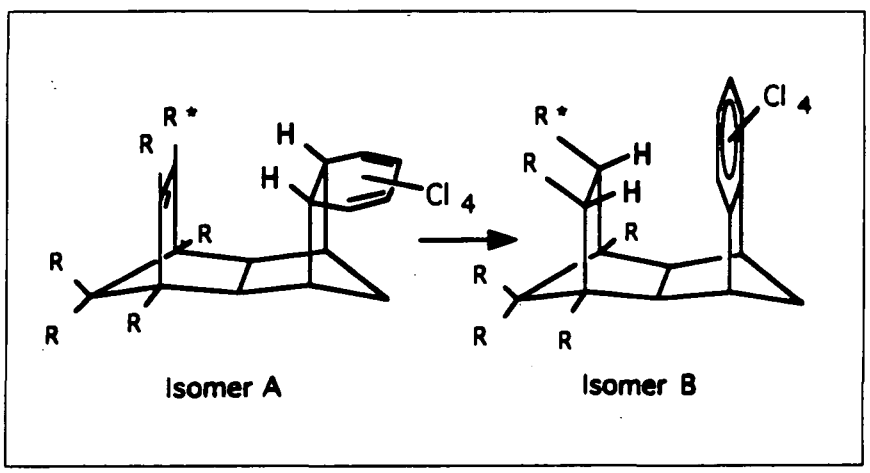

Figure 1.2: Rearrangement of isomer A to form isomer B.

These compounds initially were found to undergo this interesting rearrangement when an attempt to synthesise isomer **A** (see Figure 1.2) produced only trace amounts and the expected ClC=CCl chromophore was not present [3]. The product was found to be isomer **B**. Similar compounds were synthesised where R*=Cl was replaced by R*=OCH_3 and R*=OC_2H_5. In these cases, isomer **A** was formed but on heating, the pure crystalline compound melted at $\sim$ 180°C and resolidified as isomer **B**. The different rates of rearrangement found for these three compounds, relative stability OMe>OEt>Cl, prompted a further systematic program of synthesis to be started.

A number of compounds, (see Table 1.1 for examples and for the labelling scheme) modelled on compound KM5, have been synthesised in which the substituents were varied in order to alter the properties of the π-receptor site, especially its electronic properties. The rate of rearrangement of these compounds has been investigated using ultraviolet spectroscopy [4]. An obvious target model was the dechlorinated triene KM17. Its aromatic isomer KM18 is known [3] but it has proved impossible to isolate the triene as the rearrangement proceeds too rapidly. The rate ratio KM17:KM5 has been calculated by suitable extrapolation to be $\sim 2 \times 10^5$ at 36°C. Such a large difference in rate accompanying a relatively small structural change provoked further interest in the mechanism of this rearrangement. However, current explanations appear to be somewhat controversial.

Several intermolecular esterification and intramolecular lactonisation reactions have been studied in an attempt to understand the greatly enhanced rates of reaction often observed for intramolecular reactions over the corresponding *inter*molecular reaction. Rate accelerations of factors as great as 10^8 have been observed. These types of reactions may then be useful as models of enzyme reactions, which generally show great rate enhancements under very mild conditions. A great deal of work has been carried out in an attempt to pinpoint the origin of this acceleration and may potentially provide information

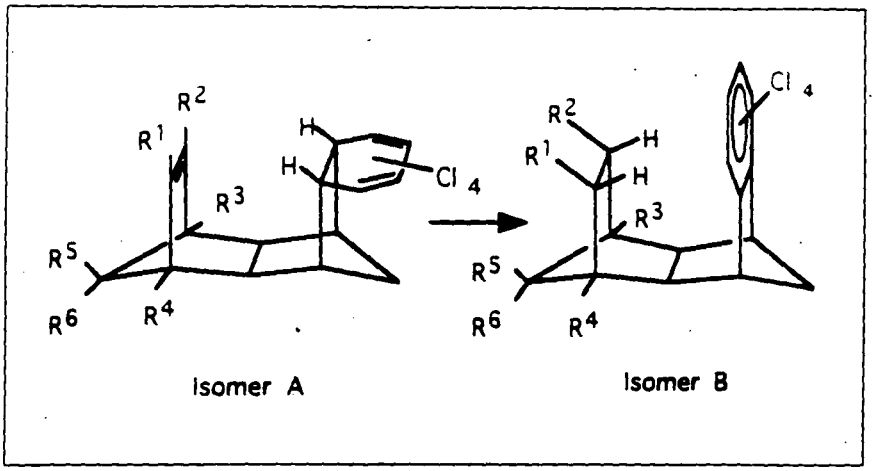

	Isomer A		Isomer B		
Substituents	Compound Number	Crystal info	Compound Number	Crystal info	
R^{1-6}=Cl	KM5	X , N †15K $P2_12_12_1$	KM9	X † C2/c	MM
R^1=OEt, R^{2-6}=Cl	KM7	X $P2_1/c$	KM11		MM
$R^{1,6}$=H, R^{2-5}=Cl	KM8		KM12		
R^{1-6}=H	KM17		KM18	X $P2_1/c$	MM
$R^{1-4,6}$, R^5=H	KM22	X, N 123K † $P2_1/c$	KM25	X , N 123K † $P\bar{1}$	MM
R^{1-5}=Cl, R^6=H	KM23		KM26		MM
R^{1-4}=Cl, $R^{5,6}$=H	KM24	X, N 15K C2/c	KM27	X, N 120K $P2_1/n$	MM

Table 1.1: Some of the compounds studied in the series of trienes. MM signifies that Molecular Mechanics calculations have been made for both isomer A and B of this compound. †Reported herein.

concerning our dyotropic rearrangement.

One early proposal suggested that the covalent linking of the two reactants would not make a great contribution to the rate enhancement [5]. A maximum 55-fold acceleration was calculated although this was subsequently disputed [6] as it ignored any attractive or repulsive forces between the reactants.

It was later proposed that the rate enhancement could be entirely explained by the entropy differences between bimolecular and unimolecular reactions [7]. This proposal does not explain why *all* intramolecular reactions do not show great rate accelerations, which they do not [8], nor why rate differences are seen between closely related intramolecular reactions. The poor correlation with experimental results also means that relative rates cannot be predicted purely from such entropy differences.

Two theories were then suggested which relied on reactions having a strong angular dependence. The first of the theories, *orbital steering* [9], stated that the precise orientation of the reacting groups was of critical importance. This theory was very quickly questioned by Bruice [6] who pointed out that for the observed rate enhancements to be accounted for entirely by the orientation factor the reactions would have to have unfeasibly narrow angular 'windows'. Displacements of only tenths of a degree and hundredths of an ångstrom would be necessary to pass from the most to the least favourable conformation; well within normal vibrational and torsional displacements. In addition, no such strong angular dependence has been observed experimentally in representative types of reactions [10].

The second theory with a strong angular dependence was that of *stereopopulation control* [11]. This theory suggested that the freezing of a molecule into a 'favourable' conformation, *i.e.* one from which the transition state is more easily accessible, was the important factor in the determination of the rate. This freezing could be effected by various interactions; hydrogen bond-

ing, steric and/or electrostatic interactions. This idea found some support with Bruice [6]. However, it has subsequently been thought that much of the rate enhancement in this case is due to relief of strain and that the contribution from freezing the molecules in a particular conformer is much less important [12].

An explanation which did not consider that there is an important angular dependence was Menger's *spatiotemporal* theory. This suggested that the rate of reaction was proportional to the time that the two functional groups were within a critical distance, where the distance and the critical time were reaction dependent.

A different approach again was taken by Dorigo and Houk [13], using models of transition states with partially formed bonds. The conclusion drawn from this study was that the reactivity was determined by the energy required to distort the functional groups into the geometry of the rate determining transition state. They did not find any supporting evidence for Koshland's orbital steering or for Menger's spatiotemporal theories.

The Dorigo and Houk paper received a rapid reply from Sherrod and Menger [14], maintaining that the ground state distances between the reacting units were of importance. They also found better correlations with experimental results when using models which had intermediates with 'ground state' type structures, *i.e.* those with fully formed covalent bonds rather than those with partially formed bonds.

Even from this brief summary it is easy to see that the situation is still unclear.

1.2 The Compounds

The pentacyclic Isodrin derivatives we have been studying rearrange cleanly at conveniently measurable rates, no side reactions take place and they have very little conformational freedom. In general they crystallise to form good quality, stable crystals suitable for X-ray and neutron diffraction studies. They therefore provide suitable models for the investigation of the kinetic and structural effects of changes to their electronic and steric character.

In addition to the trienes with which this work is concerned primarily, other related series of compounds, based on both Isodrin and Homoisodrin, have been synthesised. One of these series has been synthesised in which a 2,3-diazacyclohexadiene element replaces the cyclohexadiene element of the trienes to form 1,3-bisarylpyrazolines [15] (see the Figures accompanying Tables 1.2 and 1.3).

Although all the pyrazoline compounds, except KM35 (see Table 1.2 for labelling scheme), show dyotropy, they do so considerably less readily than the trienes. The rates of rearrangement are typically a factor of $\sim 10^2 - 10^3$ times slower than those of the trienes: e.g. rate ratio KM5:KM37 1.7×10^3 [1]. This slower rate of rearrangement may be due to the two cyclohexadiene, the alicyclic and heterocyclic, elements having different requirements for aromatisation. Despite these differences comparisons within the series show remarkably similar trends when equivalent structural changes are made: *e.g.*

for trienes	KM5	: KM23	: KM22	: KM24
the rate ratios are	7.2	: 1.8	: 1.7	: 1.0
for pyrazolines	KM36	: KM44	: KM45	: KM46
	7.3	: 2.4	: 1.4	: 1.0

suggesting that these structural modifications remote to the reaction cavity cause similar changes in the receptor π-bond energy in both cases.

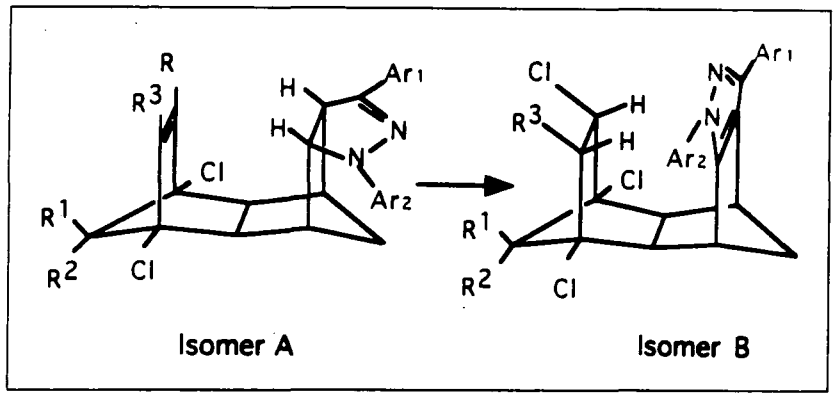

	Isomer A		Isomer B	
Substituents	Compound	Crystal	Compound	Crystal
$R^{1,2}$=Cl, R^3=OEt, $Ar^{1,2}$=Ph	KM35			
R^{1-3}=Cl, $Ar^{1,2}$=Ph	KM36		KM40	
R^{1-3}=Cl, $Ar^{1,2}$=p-MeC_6H_4	KM37	*Pbca*	KM41	$P2_1/n$
R^{1-3}=Cl, Ar^1=p-MeC_6H_4, Ar^2=p-ClC_6H_4	KM39	*Pbca*	KM43	
R^1=H, $R^{2,3}$=Cl, $Ar^{1,2}$=Ph	KM44		KM47	
$R^{1,3}$=Cl, R^2=H, $Ar^{1,2}$=Ph	KM45		KM48	
$R^{1,2}$=H, R^3=Cl, $Ar^{1,2}$=Ph	KM46		KM49	

Table 1.2: Labelling scheme for pyrazoline/pyrazole pairs.

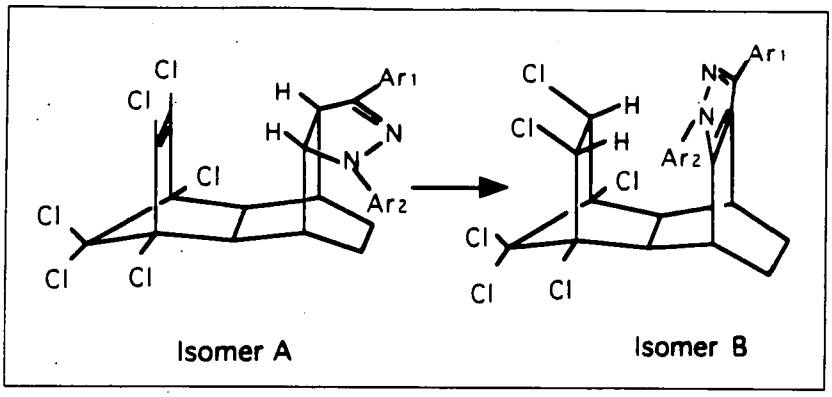

	Isomer A		Isomer B	
Substituents	Compound	Crystal	Compound	Crystal
$Ar^{1,2}$=Ph	KM60	$P2_1/n$	KM62	$Ama2$
$Ar^{1,2}$=p-ClC_6H_4	KM61		KM63	$P2_1/c$

Table 1.3: Pyrazolines derived from Homoisodrin.

The driving force for the rearrangement is thought to come from; the aromatisation of the 1,3-cyclohexadiene element, or replacement heterocycle, which accompanies the rearrangement, changes in the π-energy, E_π, and changes in the strain energy, E_s. Other examples of dyotropic rearrangements have been reported (see Figure 1.3). The gain in π-energy on formation of an aromatic element is also important to other related rearrangments [16, 17]. It is not, however, a prerequisite for such reactions as shown by the thermoneutral, reversible $[4\sigma + 2\pi]$ thermal rearrangement reported by Vogel [18]. In this case the 'lack' of aromatisation is compensated for by the presumed compressed nature of the molecule. Nor are all these reactions $[4\sigma + 2\pi]$ type rearrangements as shown by Grimme who has reported an example of a $[4\sigma + 6\pi]$ hydrogen migration [19].

A recent paper [20] suggests that the two-hydrogen transfer might occur via a two-step asynchronous tunnelling process. This suggestion does not appear to take into account several experimental observations. Both chlorine and alkoxy substituents would be expected to have a stabilising, and therefore rate-

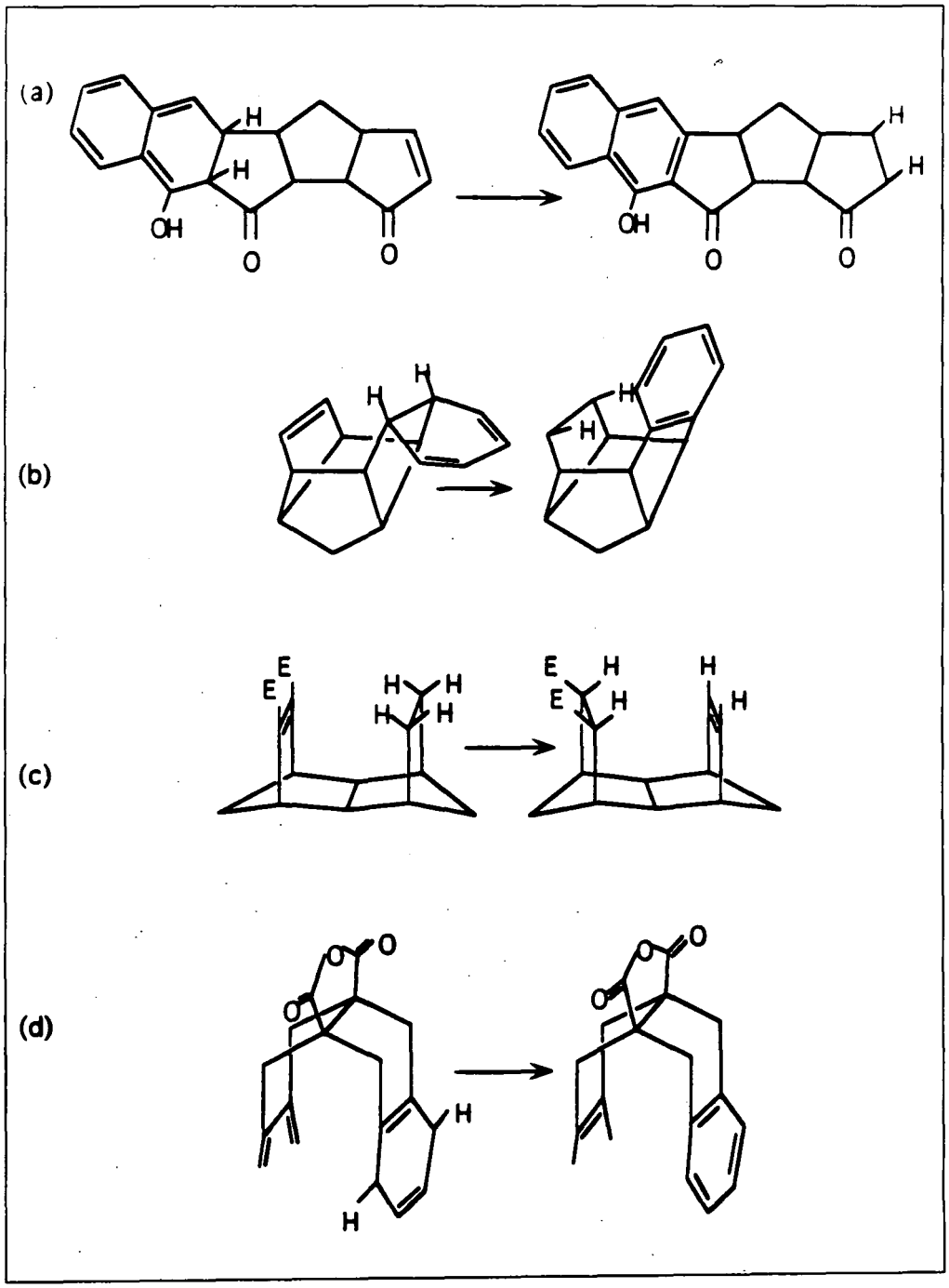

Figure 1.3: Other examples of dyotropic rearrangement reactions: see References (a) [16] (b) [17], (c) [18] and (d) [19].

enhancing effect but in fact, they have a retarding one; dramatically so in the case of the trienes where the rate ratio KM17:KM5 (dechlorinated:chlorinated) is 2×10^5 at 36°C.

Similarly, the aryl substituents and nitrogen atoms of the heterocyclic 4π-element of the pyrazolines should act to stabilise a diradical intermediate. In fact, as a series, the pyrazolines rearrange significantly more slowly than do the trienes which lack any such stabilising groups. Furthermore, changes to the aryl substituent appear to have only a small effect on the kinetics of the rearrangement.

A further indication that a diradical intermediate is not involved is provided by the melting point behaviour of both the trienes and the pyrazolines. Radical reactions often have side reactions and produce by-products. The sharp melting points of these compounds after the rearrangement has taken place implies that no substances other than the aromatic rearrangement product are present.

Results from recent kinetic studies by Mackenzie [21] also contradict the proposed asynchronous, tunnelling process. For triene KM5 the Arrhenius relationship is essentially linear over a temperature range of more than 70°C which is inconsistent with a tunnelling contribution. However non-classical behaviour is suspected for the pyrazolines.

1.3 Crystallographic Studies

A key part of this project, adding to the impressive body of kinetic and synthetic work, some of which has been discussed above, has been a number of crystallographic studies of these compounds.

Crystallography, both X-ray and neutron, has the unique ability to provide

very detailed information about the geometry of the molecule as a whole in a crystal environment. Neutron diffraction studies have an important role to play in the determination of structures containing hydrogen atoms (see Chapter 2) which are only poorly determined by X-ray studies. Neutrons are of particular importance to this project as the hydrogen atoms in these molecules are of vital interest, especially those directly involved in the rearrangement.

The structures of several compounds in the triene series, as in the pyrazoline/pyrazole and homoisodrin derivative series, have been determined by X-ray and in some cases neutron crystallographic studies. This has enabled a small database of structural information to be built up. Comparisons can thus be made between pairs of isomers, within series of related compounds and also between series.

There are very few other research groups studying these dyotropic rearrangements who make use of crystallographic work. The structures of some isolated compounds have been determined but not generally in any systematic way. Paquette and co-workers [22, 23] are one of few groups who have benefitted from the use of crystallographic data. They have been studying a dyotropic rearrangement reaction which occurs in a series of syn-sesquinorbene disulphones (see Figure 1.4). By changing the substituent 'X' they have been attempting to tailor the distance, d_{CC}, across the reaction cavity. In their initial work [22] they found this distance and the rate of rearrangement to be closely correlated; a variation of a little over 0.3Å resulting in a rate spread of more than a factor of 10^4. However, results in a later paper [23] suggest that other factors are also involved, for example, the strain energy and π-electronic effects on the reaction thermodynamics.

There does not appear to be a clear, simple relationship between these cross-cavity separations and the rate of rearrangement in our compounds. The investigation into such a correlation has been greatly aided by the neutron studies which have been made, allowing the d_{CH} distance as well as the d_{CC}

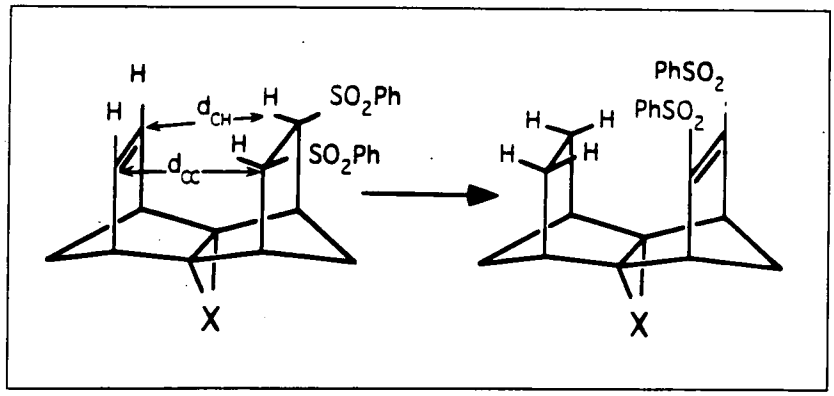

Figure 1.4: Dyotropic rearrangement observed in the syn-sesquinorbene disulphones [22].

separation to be accurately determined. This suggests that other factors have an important influence on the rate of rearrangement. These may be other steric factors away from the reaction zone or electronic factors. In either case, crystallographic studies have an important contribution to make. Structural features away from the reaction cavity may be of interest in themselves or as indicators of other characteristics of the molecules such as the level of strain. Additionally, Molecular Mechanics (MM) calculations have been made for several of these compounds, see Table 1.1 and structural parameters determined by crystallographic studies are a useful check of the corresponding calculated parameters.

X-ray diffraction studies also probe the electronic structure of the molecule directly as it is the electrons which interact with X-rays. In general, peaks in the electron density are used to determine the atomic positions. However, far more information than this is contained in the diffracted intensities and it is possible to study the detailed charge density distribution in the crystal. Neutron studies are also used in combination with X-rays in such studies.

The overall aim of the structure determinations, neutron studies and now a charge density study is to obtain information which will allow further insights into the mechanism of this rearrangement and into which factors have the

greatest influence on the rate of rearrangement. There is always some argument that such experiments determine the time averaged structures and electron densities in the crystal and so they may not provide information relevant to the transition states or to the factors important to the rearrangement in other states. However, the rearrangement does proceed in the solid state and kinetic studies suggest that the transition states are reactant-like in character thus supporting the validity of our studies.

The work reported herein adds considerably to the database of structural information. The determination of the room temperature structure of KM9 is reported, as are the results of three neutron diffraction studies, of KM5, KM22 and KM25, at low temperatures. Both KM5 and KM9, and KM22 and KM25 form pairs of isomers, therefore allowing the structural changes accompanying the rearrangement to be studied. In the case of the latter pair, KM22 and KM25, it is the first time that neutron data for a pair of isomers have been measured at the same temperature, 123K, and only the second pair of isomers which have been studied using neutrons; the other pair being that of KM24 and KM27.

An extensive X-ray data set has also been collected for KM25, again at 123K, which has been used in conjunction with the neutron data to investigate the detailed electron density distribution in this molecule.

1.4 Organisation of the thesis

This thesis is arranged along the following lines. Chapter 2 contains details of the five experiments; three neutron and two X-ray, on the compounds KM5, KM9, KM22 and KM25. Some relevant backgound material is also included in this chapter and in Chapter 3. Details of the data reduction and least squares refinements of the conventional models are given in Chapter 3. Chapter 4 dis-

cusses the results of these conventional refinements and Chapter 5 is concerned with the charge density model refinements for KM25. Chapter 7 is concerned with the conclusions which may be drawn from this work and some suggestions for future work.

Chapter 6 reports on the results of the structure determinations of six novel organometallic compounds. This work was carried out as a separate study of several half-sandwich niobium imido and molybdenum bis-imido compounds which can be considered as analogues of the Group 4 bent metallocenes. This was in collaboration with Prof. V.C. Gibson and his research group, also at the University of Durham. It is also concerned with the relationship between structure and reactivity.

Bibliography

[1] K. MacKenzie, J.A.K. Howard, E.C. Gravett, K.B. Astin, Liu Shi-Xiong, A.S. Batsanov, D. Vlaovic, J.P. Maher, M. Murray, D. Kendrew, C. Wilson, R.E. Johnson, T. Preiβ and R. Gregory (1993). *J. Chem. Soc. Perkin. Trans.* 2, 1211-1228.

[2] M.T. Reetz (1973). *Tetrahedron* **29**, 2189-2194.

[3] K. Mackenzie (1965). *J. Chem. Soc.,* 4646-4653.

[4] J.A.K. Howard, K. Mackenzie, R.E. Johnson and K.B. Astin (1989). *Tetrahedron Letters* **30**, 5005-5008.

[5] D.E. Koshland Jr. (1962). *J. Theor. Biol.* **2**, 75.

[6] T.C. Bruice, A. Brown and D.O. Harris (1971). *Proc. Natl. Acad. Sci. U.S.A.* **68**, 658-661.

[7] M.I. Page and W.P. Jencks (1971). *Proc. Natl. Acad. Sci. U.S.A.* **68**, 1678-1683.

[8] A.J. Kirby (1980). *Adv. Phys. Org. Chem.* **17**, 183-278.

[9] D.R. Storm and D.E. Koshland Jr. (1970). *Proc. Natl. Acad. Sci. U.S.A.* **66**, 445-452.

[10] F.M. Menger (1985). *Acc. Chem. Res.* **18**, 128-134.

[11] S. Milstien and L.A. Cohen (1972). *J. Am. Chem. Soc.* **94**, 9158-9165.

[12] C. Danforth, A.W. Nicholson, J.C. James and G.M. Loudon (1976). *J. Am. Chem. Soc.* **98**, 4275-4281.

[13] A.E. Dorigo and K.N. Houk (1987). *J. Am. Chem. Soc.* **109**, 3698-3708.

[14] M.J. Sherrod and F.M. Menger (1989). *J. Am. Chem. Soc.* **111**, 2611-2613.

[15] K. Mackenzie, G. Proctor and D.J. Woodnutt (1987). *Tetrahedron* **43**, 5981-5993.

[16] A.P. Marchand, P. Annapurna, W.H. Watson and A. Nagl (1989). *J. Chem. Soc., Chem. Commun.* 281-282.

[17] T.J. Chow and M-F. Ding (1986). *Angew. Chem. Int. Ed. Engl.* **25**, 1121-1122.

[18] J-P. Hagenbuch, B. Stampfli and P. Vogel (1981). *J. Am. Chem. Soc.* **103**, 3934-3935.

[19] H. Geich, W. Grimme and K. Proske (1992). *J. Am. Chem. Soc.* **114**, 1492-1493.

[20] Z.K. Smedarchina and W. Siebrand (1993). *J. Mol. Struct.* **297**, 207-213.

[21] K. Mackenzie, E.C. Gravett, R.J. Gregory, J.A.K. Howard and J.P. Maher (1992). *Tetrahedron Letters* **33**, 5629-5632.

[22] L.A. Paquette, M.A. Kesselmayer and R.D. Rogers (1990). *J. Am. Chem. Soc.* **112**, 284-291.

[23] L.A. Paquette, G.A. O'Doherty and R.D. Rogers (1991). *J. Am. Chem. Soc.* **113**, 7761-7762.

Chapter 2

Data Collection

2.1 The Background

A crystal is made up of a regular arrangement of atoms with a repeating pattern in three dimensions. This internal periodicity means that the crystal can act as a three-dimensional diffraction grating for radiation of suitable wavelengths. In this case, where the atomic spacing is of the order of $\sim$1Å it is X-rays and thermal neutrons which have these suitable wavelengths [1]. To observe any diffracted intensity there must be constructive interference between all the waves diffracted by the crystal. In any one direction the Laue conditions state that for constructive interference to occur the phase shift, *i.e.* the change of the position of the wave crests relative to one another, must be an integer number of wavelengths. If we assume the phase shift to be caused purely by path length differences then the differences corresponding to lattice translations must equal an integral number of wavelengths.

To obtain a resultant beam from a 3-dimensional grating the interference must be constructive with respect to all three axes. This depends on the wavelength, λ, and the lattice spacing, d, and determines the acceptable angles, θ,

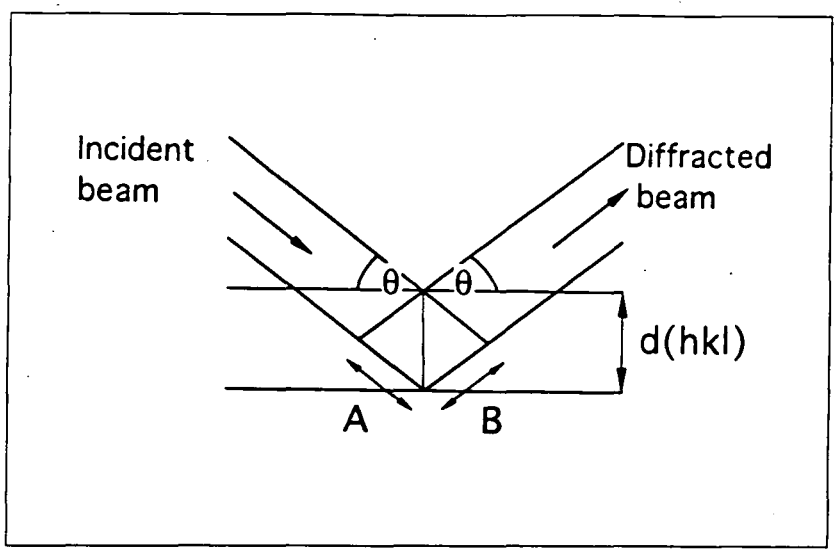

Figure 2.1: Reflection from the planes (*hkl*) with interplanar separation d(hkl).

of the incident and diffracted beams relative to the lattice rows. A simple way of predicting these angles was given by Bragg who considered the diffraction as reflection from the lattice planes, thus giving Bragg's law which is given below in Equation 2.1. Hence diffracted beams are often called reflections and labelled with the indices, (*hkl*), of the 'reflecting' lattice planes. Figure 2.1 shows this reflection and the path length differences A and B which must equal an integer number of wavelengths.

$$2d(hkl)sin\theta = n\lambda \tag{2.1}$$

The structure factor and the density of the scattering material, $\rho(\mathbf{r})$, are related to one another by Fourier transform:

$$F(\mathbf{h}) = \int \rho(\mathbf{r}) \exp(2\pi i \mathbf{r}.\mathbf{h}) d\mathbf{r} \tag{2.2}$$

and

$$\rho(\mathbf{r}) = \frac{1}{V} \sum \mathrm{F}(\mathbf{h}) \exp\left(-2\pi i \mathbf{r}.\mathbf{h}\right) \tag{2.3}$$

where $\mathbf{r}$ is the position vector, (xyz) , and $\mathbf{h}$ is the reciprocal lattice vector,

(hkl), V is the unit cell volume and ρ is the density (electron or nuclear) of the scattering material. The reason for there being a summation rather than an integral in Equation 2.3 is that the diffraction pattern is only observed at discrete points.

The observed intensities of the reflections are related to the square of the amplitude of the structure factor, $|\mathrm{F}(\mathbf{h})|^2_{\mathrm{obs}}$, and can be converted by applying several corrections such as those for Lorentz, polarisation and absorption effects.

Equation 2.3 thus shows that if the phase and the amplitude of the structure factors for all indices, ($\mathbf{h}$), were known, the density ρ at any point $\mathbf{r}$ could be computed and so a complete picture of the density obtained. Unfortunately the phase information is lost and only the intensities are measured.

Xrays and neutrons

The reason for using the term scattering material is that X-rays and neutrons interact differently with matter and are not scattered by the same components of the crystal. X-rays are scattered by electrons, whereas it is the atomic nuclei which scatter neutrons. Therefore, the information obtained from an X-ray diffraction study concerns the electron density distribution, whereas a neutron experiment gives the nuclear positions and displacements.

This difference between X-rays and neutrons has a number of consequences, some of which give rise to the useful complementarity of X-ray and neutron studies. For X-rays the scattering power of an atom, given by the atomic scattering factor (f_j), increases in a regular way with atomic number and may be calculated. For neutrons the equivalent quantity is the experimentally determined atomic scattering length (b_j), and due to the random effect of resonance scattering it does not vary in any regular way with atomic number; even isotopes of a given element may have very different scattering lengths, (see Figure 2.2).

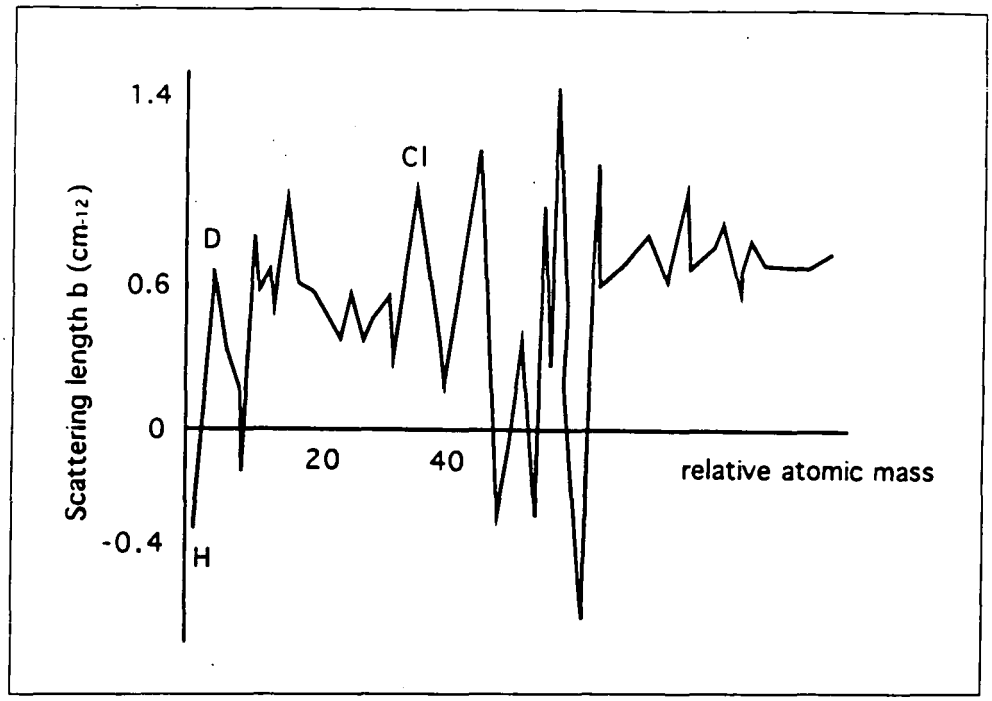

Figure 2.2: Scattering length (cm^{-12}) versus atomic mass for neutrons.

A light atom (low atomic number) and hence weak X-ray scatterer may not be a weak neutron scatterer. The neutron atom scattering lengths, b, only vary by a factor of two or three over all types of nuclei. This is a far narrower range than that of X-ray scattering factors. The narrow range is particularly useful when studying compounds which contain light atoms, the classic example being hydrogen, in the presence of strong X-ray scatterers. The non-periodic variation in scattering length with atomic number is also useful when studying neighbouring elements in the periodic table, as they may have very different neutron scattering lengths hence allowing them to be easily distinguished.

The scattering power for the two types of radiation not only varies differently with atomic number but also with $\sin\theta/\lambda$. Atomic nuclei are small compared to the wavelengths of thermal neutrons and so act as point scatterers, scattering isotropically. Consequently many more high angle data are

attainable to higher precision in neutron studies than they are with X-rays, where the scattering power falls off rapidly with $\sin\theta/\lambda$. The fall-off in X-ray scattering power is due to the fact that the electrons are distributed over a finite volume which is of comparable dimensions to the X-ray wavelengths used. Therefore, X-rays which are scattered from one part of an atom can interfere with those scattered from another, at all scattering angles greater than $\theta = 0°$.

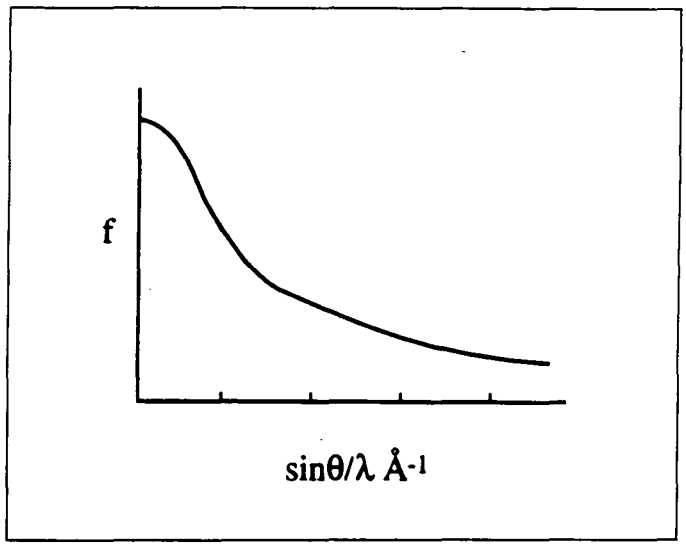

Figure 2.3: X-ray scattering factor variation with $\sin\theta/\lambda$ showing the reduction in scattering power at high angles.

However, for both X-ray and neutron radiation the intensity of the high angle data is reduced by thermal vibrations. The structure factor for X-rays then becomes:-

$$F(\mathbf{h}) = \sum f_j \exp\left(-2\pi i \mathbf{h_j}.\mathbf{r_j}\right) . \exp\left(-T_j\right) \tag{2.4}$$

and for neutrons:-

$$F(\mathbf{h}) = \sum b_j \exp\left(-2\pi i \mathbf{h_j}.\mathbf{r_j}\right) . \exp\left(-T_j\right) \tag{2.5}$$

where

$$T_j = 8\pi^2 \frac{sin^2\theta}{\lambda^2} . \langle U^2 \rangle \tag{2.6}$$

$\langle U^2 \rangle$ is the mean square amplitude of displacement of the atom from its equilibrium position.

2.2 The Diffractometer

The aim of the experiment is usually to measure, as precisely and accurately as required, a set of integrated intensities and to calculate their estimated standard deviations (esds). These intensities and esds are then used to obtain the corresponding structure factor amplitudes, $|\mathrm{F}(\mathbf{h})|$ or their squares $|\mathrm{F}(\mathbf{h})|^2$. 4-circle diffractometers are now most commonly used to collect the data using some level of automation. In the case of diffractometers equipped with a single detector the intensities are measured one by one, which, although time consuming, allows measurements to be made precisely.

The diffractometer consists of a radiation source, a computer controlled goniostat to orient the crystal and a detector to record the intensity of the diffracted beam.

The Source

X-rays

A continuous or 'white' X-ray spectrum, called Bremsstrahlung, is produced by a beam of electrons, accelerated by a high voltage, striking a metal target. This white beam is also accompanied by several spectral lines that give a characteristic spectrum for the target metal. The spectral lines result when the incoming electrons striking the target have sufficient energy to eject electrons from one of the inner shells of the metal target atoms. The ejected electrons are then replaced by electrons from a higher energy level which emit the energy difference of the two levels as photons of the characteristic wavelength. The two most commonly used target materials for single crystal diffraction experiments are copper and molybdenum. The X-ray experiments reported here used Mo

$K_{\overline{\alpha}}$ X-radiation produced using a high vacuum sealed tube source. The tube, sealed after evacuation, consists of an electron gun to produce a well defined electron beam which is accelerated towards a water-cooled anode or 'target'. The X-ray beam then leaves the tube at a low 'take-off' angle, typically 2-6°, through a Be window.

Neutrons

All the neutron diffraction experiments in this thesis were carried out at reactor sources. The neutrons are produced by a self-sustaining fission reaction:

$$n_{therm} + U^{235} \longrightarrow 2 fission fragments + 2.5n + 200MeV$$

The fast neutrons so produced are then 'moderated' or slowed down by collisions with the moderator, usually D_2O or graphite to give 'thermal' neutrons which have wavelengths in the range $0.5\text{Å} \leq \lambda \leq 2.0\text{Å}$. The neutron energies have a Maxwellian distribution , *i.e.* a broad continuous white spectrum, with energies centered around the temperature of the moderator.

Monochromatisation

A narrow wavelength band is selected by diffracting the incident beam using a single crystal positioned at the correct Bragg angle for a given plane to diffract radiation of the chosen wavelength (Equation 2.1). In the case of X-rays this wavelength is that of the K_α spectral lines. For neutrons the choice is slightly different as there is a continuous spectrum. A wavelength slightly shorter than the maximum of the distribution is usually selected in order to reduce the $\lambda/2$ contribution, that is, the radiation of half the wavelength of that desired which will be diffracted from higher order planes according to Equation 2.1.

The Rigaku AFC6S and CAD4 X-ray diffractometers used for this work both have graphite single crystal monochromators. On the neutron instruments, TAS2 at Risø and H6M at BNL, the beam was reflected from the (002) planes of a beryllium single crystal.

The beam is then collimated to define a narrow beam as parallel as possible and of dimensions such that the background caused by scattering from air and from the sample environment is minimised.

The Goniostat

There are two commonly used designs of 4-circle diffractometer; either Kappa or Eulerian geometry. Both types of diffractometer have been used for the experiments described herein.

A geometric construction which is very useful in visualising the machine movements necessary to bring a plane into diffracting position is the Ewald sphere. See Figure 2.4.

For a reciprocal lattice point to satisfy the diffraction condition it must lie on the surface of the sphere. In equatorial-plane geometry, which was used for each of the data collections described in this thesis, the detector moves in a horizontal plane using rotations about the 2θ axis. When using an Eulerian cradle two rotations are needed to bring a given crystal plane into diffracting position: a ϕ-rotation brings the reciprocal lattice point into contact with the Ewald sphere then a χ-rotation is needed to bring the point into the equatorial plane (see Figure 2.5). The detector is then placed at the correct 2θ setting and ω set to $\theta°$, so that the χ-circle bisects the angle between the incident and diffracted beams. This is known as the bisecting position and is most commonly used to make measurements.

For a machine of Kappa geometry, as an alternative to the full χ-circle, there is a κ-axis which is inclined at an angle of 50° to the ω-axis about which it can be rotated. The ϕ-axis is then mounted on this κ-axis. The 'Kappa' geometry machines have the advantage of having much clearer access to the crystal and most of the data available when using a Eulerian cradle are accessible.

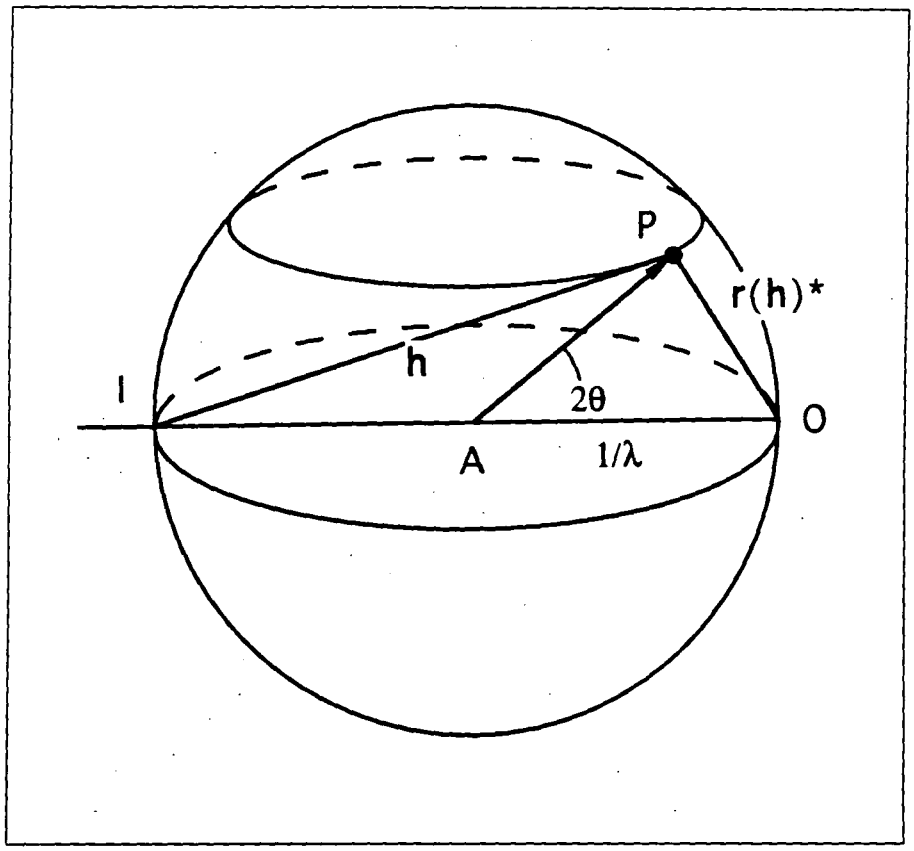

Figure 2.4: Ewald Sphere construction. The incident beam passes along the diameter IO of the sphere of radius $1/\lambda$. O is the origin of the reciprocal lattice amd $\mathbf{r}^*(\mathbf{h})$ is a reciprocal lattice vector. When the reciprocal lattice point P lies on the surface of the sphere: OP = $\mathbf{r}^*(\mathbf{h})$= 1/d($\mathbf{h}$) = IO $\sin\theta$ = 2 $\sin\theta/\lambda$ and hence obeys Bragg's Law.

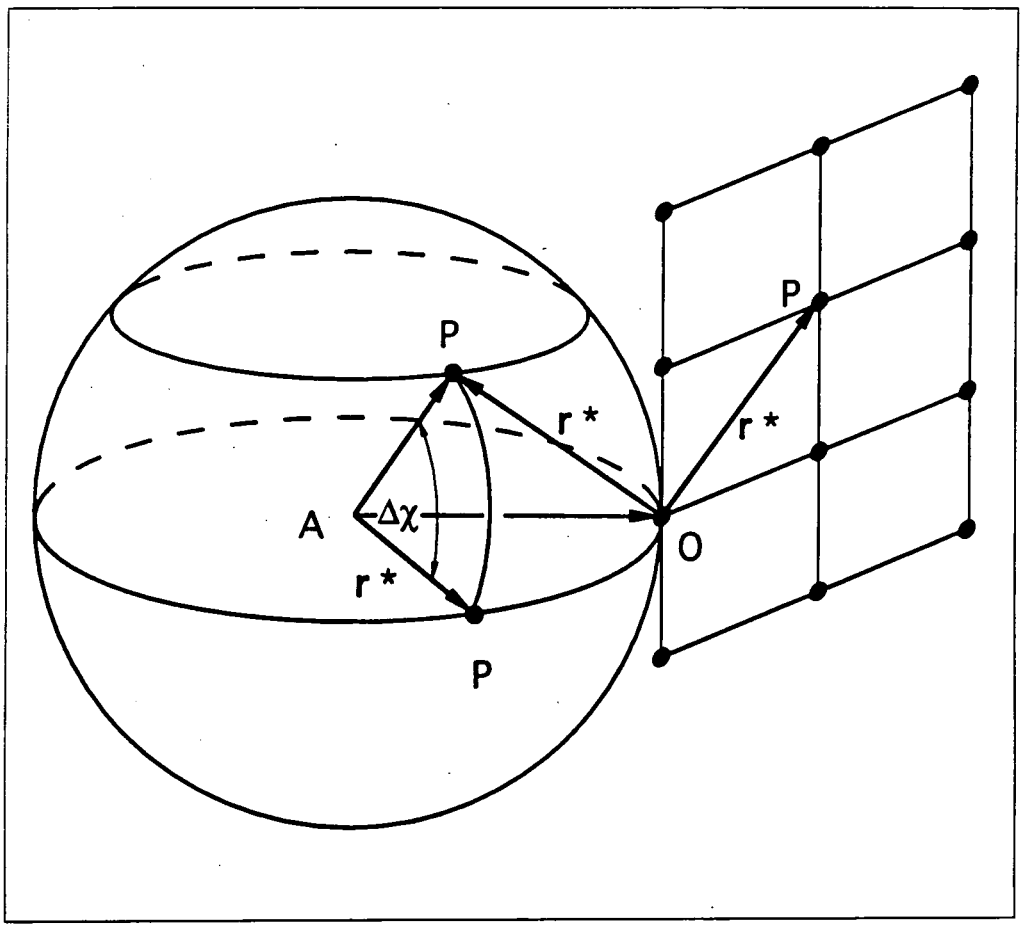

Figure 2.5: Ewald sphere construction showing the two rotations necessary to bring a reciprocal lattice point P into diffracting position in the equatorial plane.

The Detector

Both X-rays and neutrons are neutral and so must be absorbed and modified or reacted in some way in order to be detected. Two types of detector have been used in these experiments; proportional detectors for the neutron experiments and scintillation counters for the X-ray experiments.

The proportional counters contain a pressurised absorbing gas, ^{3}He in the TAS2 detector at Risø and BF_3 in the H6M detector at BNL. The neutrons are first involved in a neutron-capture or absorption reaction with these gas molecules

$$\begin{aligned} {}^3He + n &\longrightarrow H^+ + {}^3H^- \\ or\ {}^{10}B + n &\longrightarrow {}^7Li + {}^4He^+ + \gamma \end{aligned} \tag{2.7}$$

which produces secondary, charged particles. These charged particles are then involved in collisions which ionise other gas molecules. The electrons produced by this ionisation then go on to ionise further gas molecules, causing an avalanche of electrons which give a signal at the wire anode proportional to the number of primary particles.

Proportional counters have a low efficiency for Mo $K_{\overline{\alpha}}$ X-radiation and so scintillation counters are more commonly used with X-radiation. These detectors contain a fluorescent crystal, usually Tl doped NaI, which absorbs the incoming X-rays, causing an electron to be promoted from the valence to the conduction band. Excited ions returning to the ground state emit a flash of light which enters a photomultiplier tube and so produces a detectable pulse of electrons for each quantum absorbed.

The Cooling Devices

As shown by Equations 2.4, 2.5 and 2.6, thermal vibrations have an important effect on the intensities of Bragg peaks. This effect restricts the number of significant data which may be collected, especially at high values of $\sin\theta/\lambda$, and so limits the resolution and precision of the study being made. Collecting the data at reduced temperatures therefore helps to increase the number of observable data and increases the precision of all the measured reflections. Two types of cooling device were used in the experiments reported herein; one cold inert gas flow and one conduction type device.

Cryostream nitrogen gas-stream cryostats [2] were used with both the CAD4 in Experiment 5 and for certain experiments in Chapter 6. These cryostats are designed to be stable over the temperature range 77.4 - 323.0K and work as outlined below.

Liquid nitrogen is drawn up from an unpressurised Dewar vessel through a vacuum insulated supply line and into an evaporation coil, by a small diaphragm pump. Most of the liquid is evaporated to gaseous nitrogen at its boiling point (77.4K), passed through a heat exchanger to bring it to just below room temperature and then passed through the diaphragm pump. The nitrogen gas is then pumped back through the heat exchanger at a constant flow rate, controlled by the pump and a flow regulating valve. The gas then passes from the cold end of the heat exchanger over a heater, which allows the temperature to be controlled, and on to the sample. A temperature sensor is situated at the tip of the delivery nozzle.

There is usually some temperature gradient between the position of this sensor and the crystal so the device needs to be calibrated. This calibration was carried out by observing the phase transition between the tetragonal and orthorhombic phases of KDP (KH_2PO_4) which occurs at 122K [3].

The particular feature of this gas flow cryostat is the positioning of the pump, between the liquid supply and the gas output. This prevents the problem of temperature variation when the liquid supply is replenished. The heat exchanger is required as the pump operates at room temperature. Generally, the flow rate is set at around $0.5lhr^{-1}$ which is reasonably economical and ensures a stable temperature. To reduce the problem of frosting the cold gas stream is surrounded by a flow of dry air.

The second type of cooling device, which can achieve much lower temperatures, minimum 10K, was used for the neutron experiments (Experiments 1, 3 and 4). Displex® two-stage closed-cycle helium cryorefrigerators were used to cool the crystals by conduction. These cryostats consist of two linked parts; an expander and a compressor.

Helium gas from the compressor unit enters the expander unit and cools a cold stage by means of adiabatic expansion. The expanded gas exits to the compressor unit, cooling part of the displacer unit as it does so, and the cycle begins again. Although the Displex always works at its maximum level, which would produce a temperature of 10K, intermediate temperatures may be achieved by heating against the cryorefrigeration. Heating is effected by a resistor placed around the copper block to which the crystal is attached.

The crystal is held in thermal contact with the cold stage, so materials, such as copper and aluminium, with good thermal conductivity are needed for mounts and attachments. Both the crystal and cold stage are contained within radiation shields to prevent heating from the exterior and frosting. For Experiments 1 and 3 the inner (of three) aluminium 'can' or radiation shield contained helium gas, and for Experiment 4 air. The outer cans are evacuated. In all cases the 'cans' were made from aluminium, which has low absorption properties for neutrons typically $\sim 1\%$ for $\lambda = 1$Å[4] although it does produce powder diffraction lines.

The details of the method of mounting the Displex on the diffractometer differ in the two laboratories, BNL and Risø. However, both methods allow small adjustments of the crystal position to be made in order that the crystal is correctly centered.

2.3 The Experiment

Several single crystal diffraction experiments, using both X-ray and neutron radiation, are reported in this thesis. The experiments were carried out in four laboratories using as many different instruments. Although there are many important differences between X-rays and neutrons, some of which are outlined in Section 2.1, much of the experimental set up is common to all of the data collections. The following is an attempt to give a general outline of a typical experiment, to highlight some of the differences between the various experiments and to outline some of the experimental factors which should be taken into consideration. Details of the individual experiments are given afterwards in Tables 2.3 to 2.7.

Crystal Selection

The first step is the choice of the crystal to be used in the experiment. Initially, the quality of the crystal is assessed optically using a microscope, preferably a polarising one. Ideally a crystal with clean, sharp edges and no obvious flaws is sought. This is not always possible and many perfectly adequate crystals do not have an ideal appearance.

An important consideration when choosing a crystal is its size. The choice depends upon a number of factors, for example: the dimensions of the homogeneous region of the incident beam, the absorption coefficient and the scattering strength of the sample. These factors vary greatly between X-rays and neutrons. The interaction between neutrons and matter is generally much weaker

than for X-rays and the incident flux, relative to X-ray sources, is much lower. Consequently, in order to have reasonably intense scattering, samples with volumes of several cubic millimetres are required. The homogeneous region of the neutron beam is generally of the order of a square centimetre, allowing such samples to be completely bathed in the beam.

The greater intensity of X-ray sources and the stronger interaction with matter allow smaller crystals to be studied. The smaller homogeneous region of the X-ray beam (typically 0.4mm in diameter) and the fact that absorption is, in general, more significant with X-rays than neutrons promote the use of smaller samples. Where a suitably sized crystal cannot be found it may be necessary to cut or to cleave a crystal.

Crystal Mounts

A number of different methods of supporting the crystal were used for data collection:-

Experiment	Radiation	Temperature	Mount	Adhesive
1	N	15	Al pin	Fluorocarbon grease
2	X	295	Glass fibre	®Araldite (Epoxy resin)
3	N	123	Al pin	®Goo (rubber base)
4	N	123	Al pin	Varnish
5	X	123	capillary	Epoxy resin

Table 2.1: Details of the mounts used in Experiments 1 to 5. For an explanation of the experiment numbers see Page 65.

In all cases the adhesives and mounts should provide an inert, rigid support without putting undue stress on the crystal. Additionally, they should be stable over the temperature range of the experiment and should not greatly increase the background scattering. Epoxy resins such as "Araldite" can 'pull' on the crystal as they set but are generally satisfactory. The fluorocarbon grease used in Experiment 1 solidifies as it cools, without putting excessive stress on the crystal. However, it is not rigid at room temperature and as

the crystal used in Experiment 3 was examined for some time at ambient temperature, it could not be used. The crystal used for the X-ray study Experiment 5 was mounted in a glass capillary, despite its stability to air and moisture, as it did not appear to be rigidly fixed when mounted on a fibre and the experiment was required to last for more than 6 weeks. This was decided after the loss of the first crystal, see Page 68

Capillaries are generally used for crystals which are air or moisture sensitive such as the studies of the organometallic compounds reported in Chapter 6. These crystals were mounted in dry glass tubes under nitrogen gas, using dried ®Apiezon grease.

Crystal centring and initial investigations

Initially the mounted crystal must be positioned at the centre of the circles. There is no need for any particular alignment with respect to a specific crystallographic axis. Indeed, alignment of a crystallographic axis with the ϕ-axis increases the chance of multiple reflection, which is to be avoided.

The physical centring of the crystal was carried out optically in the case of all the X-ray experiments reported herein. The neutron data collections were all performed at low temperatures using Displex® cryorefrigerators where it is impossible to see the crystal. Therefore, a different method is used to ensure that the crystal is correctly positioned (see Page 56).

The next step is to locate some Bragg reflections. In X-ray experiments, where the flux is relatively high, counting times are such that this is usually carried out using an automated process which systematically searches a given region of reciprocal space. The reflections which are found are then centred, that is the setting angles 2θ, ω and χ are optimised for the maximum observed scattered intensity. ϕ is usually fixed at the value at which the reflection was initially found. These reflections must then be assigned indices, *hkl*. This process generally involves finding the three shortest non-coplanar reciprocal

lattice vectors from the results of the initial search. For the reciprocal space method of indexing [5], the three vectors are then assigned as the reciprocal cell axes and then used to describe a simple unit cell and orientation matrix (see below). This matrix is then used to assign indices to all the other reflections from the search. It is important that reflections found in the initial search are well distributed in reciprocal space, are not too few in number and do not belong to a special subset of the data as this may result in an incorrect cell determination. The cell determined in this way may not be the conventional one nor show the metric symmetry, *i.e.* the symmetry of the lattice, so some further processing is generally required.

The orientation matrix relates a set of cartesian crystal axes to the laboratory or machine based axes. Strictly speaking it is only the 3×3 matrix **U** which is the orientation matrix. However, the **UB** matrix is often also referred to as the orientation matrix although this actually consists of two matrices, **U** and **B**. **B** is another 3×3 matrix which relates the, usually triclinic, reciprocal lattice axes to a set of cartesian axes fixed to the reciprocal lattice axes. **U** is a second matrix which relates these crystal cartesian axes to the laboratory or machine axes. It is therefore possible, using **UB**, to calculate the machine angles for a particular reflection or the indices of a reflection observed at a given angle.

A manual, rather than fully automated, search is made to locate the first reflections in a neutron experiment. The counting times required are so much longer than those in X-ray experiments that an automated random search of reciprocal space would be a waste of neutron beam time. As an X-ray study is always made prior to a neutron one, the resulting structural model can be used to compute a list of calculated intensities. From this list a strong, low angle reflection is chosen and the diffractometer angles 2θ and ω set to the bisecting position, ϕ and χ are then rotated to search for the peak. At least two centred reflections combined with the cell parameters determined from the X-ray data

are then used to calculate an initial orientation matrix.

Although the crystal could be cooled from the start (and in some cases this is necessary) the cooling is often carried out after the indexing. During careful cooling, typically at around 2-5 $Kmin^{-1}$, at least one reflection is repeatedly scanned or in some cases a list of reflections are repeatedly recentred in order to monitor the effect of the cooling. A gradual increase in intensity of the monitored reflections is expected due to the reduction of thermal motion as the temperature is lowered. However, this may be offset slightly by changes in the peak position as the cell dimensions alter, requiring the peak to be recentred occasionally. Any sudden changes in the intensity are more alarming and may indicate, for example, that the crystal has undergone a phase transition. Repeated warming and cooling of a crystal is known to cause changes in the mosaicity.

In both types of experiments, X-ray and neutron, a more precise orientation matrix is often determined using more reflections. In theory reflections with higher 2θ values should give a more precise matrix, however, these reflections are generally weaker and often broad so some compromise is usually reached. Before the higher angle orientation matrix is calculated the crystal must be physically centred at the centre of the diffractometer circles, at the relevant temperature. As was stated previously, this cannot be achieved optically when the crystal is contained within a Displex® cryorefrigerator and so a different procedure is required.

The procedure used for centring the crystal in Experiments 1 and 3 was as follows. A reflection with $\chi \sim 90°$ is used. Two settings, A and B, for this reflection are found at ϕ at 0 and 90° such that each of the translational sledges are contained in the plane of the χ-circle. Two further settings, C and D, are calculated using form 2 of settings A and B (from Hamilton's 8 forms [6]). The peak at each of these 4 settings is then centred and the angle differences, $\Delta 2\theta$ and $\Delta\chi$, are then used to determine the magnitudes of the translational

corrections required.

$$\Delta 2\theta = \frac{1}{2}(2\theta_A + 2\theta_B) - \frac{1}{2}(2\theta_C + 2\theta_D)$$

$2\theta_A$ and $2\theta_B$ should be equal if there is no difference in crystal height. $\Delta 2\theta$ gives the correction to be made in crystal height at $\chi = 0°$. The x and y translational corrections are determined from $\Delta\chi = (\chi_A - \chi_C)$ and $\Delta\chi = (\chi_B - \chi_D)$. This is an iterative process as the translational corrections are not completely independent of one another.

The initial cell given is often triclinic and a check must be made for cells of higher symmetry. A routine to do this is usually included in the data collection software. Nowadays, photographic work is often not carried out so extra care must be taken that the cell has been correctly chosen.

A further important check to be made before data collection is the determination of the Laue symmetry, that is, the symmetry of the diffraction pattern. This is done by comparing diffracted intensities of reflections which could be related by symmetry. For example, for a crystal of Laue symmetry $2/m$ the following reflections are of equal intensity: $|F_{hkl}| \equiv |F_{h\bar{k}l}| \equiv |F_{\bar{h}k\bar{l}}| \equiv |F_{\bar{h}\bar{k}\bar{l}}|$. The Laue symmetry determines which regions of data are related to one another and therefore how many data need to be collected to have a unique set of reflections. For the above case only one of the four sets of equivalent reflections need be collected.

Several sets of such symmetry equivalents are often included in the list of reflections measured when determining a more precise orientation matrix. They provide a check on the centring of the crystal as well as the symmetry although strong absorption by a crystal can make it difficult to decide if two potential symmetry-equivalents are indeed equivalent. If in doubt, and time permits, it is safer to assume to lower symmetry. If the higher symmetry is in fact correct an extra set of equivalent reflections will have been collected.

Data Collection Strategy

A number of decisions still remain to be made concerning the data collection. The main choices are the type of scan, the width of these scans and the speed with which they are measured, as well as which data are to be collected.

If the crystals studied were infinite and perfect and the radiation used completely monochromatic and also infinite, the diffracted intensities would be delta functions. However, this is not the case. The crystals are not infinite which causes the reciprocal lattice points to have a volume, nor are they usually made of perfectly aligned planes but consist of slightly misaligned blocks, *i.e.* they have a mosaic character. The radiation used is also finite and slightly polychromatic; too perfect a monochromator crystal would result in too great a reduction in the intensity of the incident beam.

The combination of the above factors results in measurable intensity over a small range of ω for any given plane, *hkl*. It is therefore the integrated intensity over this range that should be measured. This is achieved by rotating the crystal around ω so that the entire reciprocal lattice point is swept through the Ewald sphere with constant angular velocity.

There are two commonly used methods of scanning the peak; the ω-scan and the $\omega/2\theta$-scan, both of which have their advantages and disadvantages. In an ω-scan the crystal is rotated about the ω-axis while the detector is kept fixed at the calculated 2θ value. This moves the reciprocal lattice point across the Ewald sphere in the direction shown below in Figure 2.6. An $\omega/2\theta$-scan involves the coupled movement of both crystal and detector in the ratio of 1:2, although other ratios are possible. The section of the peak which is sampled in an $\omega/2\theta$-scan is different to that of an ω-scan and lies in the direction of the reciprocal lattice row. This difference may cause problems if the unit cell has a long axis where the lattice points are closely spaced in which case an ω-scan may be favoured. The background sampled in the two cases also

differs. For example, white radiation streaks spread out radially from the origin of reciprocal space along the lattice rows and so do not contribute to the background of an ω-scan, therefore causing an overestimation of the peak intensity to be made [7].

Several studies have been made which examine the relative merits of the different types of scan [7, 8, 9]. These studies show the character of the profiles to be due to a combination of the properties of the crystal and the instrument, *e.g.* the mosaic spread, the wavelength spread and the beam divergence. These properties affect the various modes of scanning differently, as mentioned above for the background, and there does not appear to be any hard and fast rule for choosing the 'best' method. Two dimensional scans have been recommended [9] and though these are very time consuming with a scintillation counter, they could be a useful way of examining a small set of reflections to select the scan parameters required for collection of the full data set. Such information is always provided if an area detector is used, which is increasingly the case.

Another factor which must be considered is the width of scan to be made. This needs to be decided for each crystal studied. The scan should be broad enough to ensure that the reflection is fully contained within the scan and allow an estimate of the background to be made. This background scatter is due to several factors, for example, scattering from air, thermal diffuse scattering (TDS), electronic noise and incoherent scattering. Some allowance also needs to be made for errors in setting angles and in the unit cell parameters, both of which will result in the reflection not being perfectly centred in the scan. However, too broad a scan is not desirable as it wastes beam time, risks the possibility of including intensity from neighbouring peaks in the estimate of the background and increases the estimated standard deviation.

The scan width is usually varied with the Bragg angle, 2θ, in some way, often as a function of $\tan\theta$. This is to take into account the broadening of the peak due to wavelength dispersion, the $\tan\theta$ term coming from differentiating

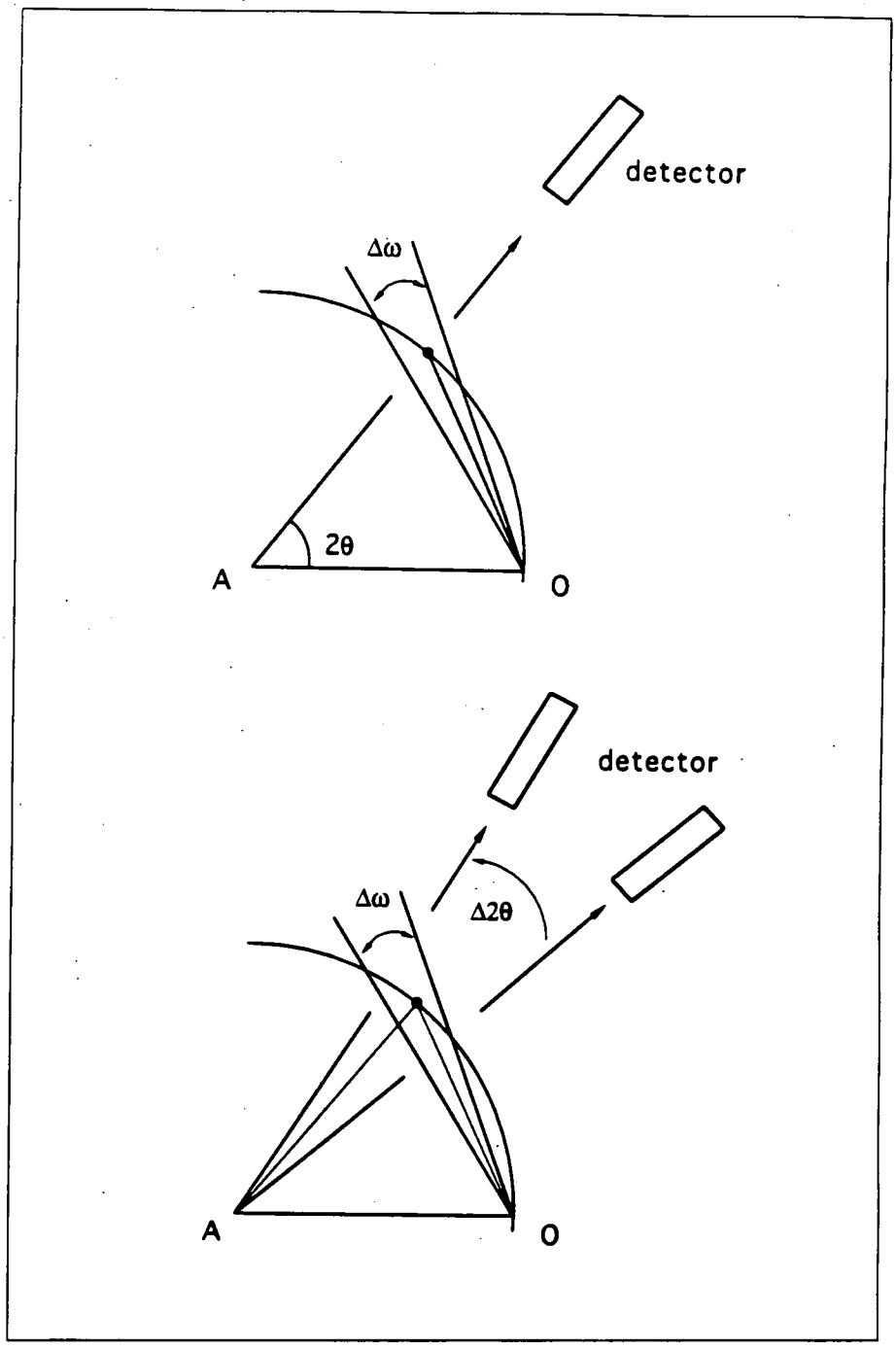

Figure 2.6: Representation of the two scanning modes: ω shown above and $\omega/2\theta$ below, using the Ewald sphere construction.

the Bragg equation 2.1 to give $\Delta\theta = (\Delta\lambda/\lambda)tan\theta$. A function of the form:-

$$\Delta\omega = A + Btan\theta \tag{2.8}$$

is often used for the scan width where A and B are constants. A is usually determined experimentally for each crystal to account for peak broadening due to the crystal mosaicity, the beam divergence, the crystal volume and B is a typical value reflecting the wavelength. X-rays from a laboratory source also have the added problem of the K_α-doublet splitting which becomes more pronounced at higher 2θ-angles.

This type of variable scan width was used in all the experiments reported here apart from the neutron data collection made at Risø, Experiment 4, where the scan width was calculated using a resolution curve.

The precision of the measurement of a reflection is linked to the time spent measuring it. Fluctuations in the source, for both X-rays and neutrons, are said to obey Poisson statistics hence, in its simplest form, the esd, $\sigma(\mathrm{I}(\mathbf{h}))$, is given by:-

$$\sigma(\mathrm{I}(\mathbf{h})) = \sqrt{\mathrm{N}} \tag{2.9}$$

where N is the total number of counts in the scan. Therefore, to improve the precision of a measurement the number of counts accumulated must be increased. However, it is clear that for a count time four times as long, the precision is only improved by a factor of two.

In neutron experiments, where the flux is low, sufficient counting time is needed so that variations in the flux at the sample are not significant. Rather than measure for a fixed time per step, the counts for each step are measured for the time needed to accumulate a given incident beam monitor count. The beam monitor count is a set number of counts at a detector (with low attenuation) placed in the beam before the sample and should be chosen to give satisfactory precision within a reasonable time.

X-ray diffraction measurements are made slightly differently. The incident

beam flux is much higher than that of neutron beams, so the corresponding times per scan step are shorter. Usually an attempt is made to measure all reflections to the same relative precision. An $I(\mathbf{h})/\sigma(I(\mathbf{h}))$ ratio is chosen and based on an initial scan the effective scan speed is calculated which will give this required precision. The software for the two X-rays diffractometers used here, the CAD4 and the Rigaku AFC6S [10, 11] , achieves this in different ways. The CAD4 carries out a prescan at some given speed $(\omega)(^\circ\ \mathrm{min}^{-1})$ and then sets the scan speed for the true scan accordingly, up to a maximum preselected time. The Rigaku software is set up such that instead of changing the scan speed the number of scans made of a particular reflection is changed in order to obtain the desired precision. This is evaluated on the completion of each scan and in this case, it is the scan speed and the maximum number of rescans which are set when using this diffractometer.

For both the CAD4 and the Rigaku it is possible to set a threshold below which a reflection will not be measured as the initial scan indicates it is too weak for the required precision to be attained within the maximum time limit. As well as the above choices of scan type there are also various methods of assessing the peak limits. This will be discussed in more detail in Chapter 3.

For a simple BPB scan the esd of the intensity $\sigma(I(\mathbf{h}))$ based on counting statistics is given by the following equation:-

$$\sigma(I(\mathbf{h})) = \sqrt{(I(\mathbf{h})_P + I(\mathbf{h})_B)} \tag{2.10}$$

where the intensity of the peak is the total peak intensity $I(\mathbf{h})_P$ minus the estimate of the background intensity $I(\mathbf{h})_B$:-

$$I(\mathbf{h}) = I(\mathbf{h})_P - I(\mathbf{h})_B \tag{2.11}$$

This shows that the peak to background ratio is an important factor contributing to the precision of the measurement and efforts should be made to minimise the background level.

One way in which the background may be reduced is by limiting the size of the detector window used. This is effected using some kind of slit or mask placed in front of the detector. Careful choice of the aperture size is needed to ensure that it is only the background which is reduced and that the peak is not clipped, especially at high 2θ-angles. This becomes a more serious problem when using ω-scans. As with the scan width and speed, the aperture size is decided upon by examining several scans and looking at the effect of changes in the aperture size.

Once these scan parameters have been decided upon then the data collection can be started.

Data are usually collected in shells of increasing θ and in most cases, all the possible reflections in the selected region of reciprocal space are recorded or at least an initial scan of them is made. Occasionally, where many weak, high angle data are to be measured and where time is limited, only a subset of reflections, whose intensities are calculated to be above some threshold value, are measured. This list of reflections is calculated using a structural model refined against the lower angle data.

This type of list-driven data collection was used in two cases; in Experiment 5 for one set of equivalents with $30° \leq \theta \leq 50°$ and for a shell of high angle data in the neutron diffraction study, Experiment 3.

As well as adjusting the scan speed, it is also possible and in some ways preferable, to improve the precision of the measurement of a particular reflection, by measuring two or three symmetry-equivalents. These scans are measured at twice or three times the scan speed of a single, slow measurement so taking the same total measuring time. This method has the advantage of averaging or cancelling out certain errors, for example in the setting angles. In general, it is better to first collect a unique set of data and then to measure each of the equivalent sets in turn.

A check is usually made on the quality and stability of the data collection as it proceeds by means of the repeated measurement of certain 'standard' reflections at regular intervals. Usually two or three reasonably intense reflections, which are well distributed in reciprocal space, are chosen as standard reflections. If any change in intensity is observed then it may indicate that the crystal has moved, some instrument fault has occurred or that the crystal has suffered radiation damage. As well as giving an immediate indication of such problems, these measurements can also be used to scale the data during data reduction if necessary, see Chapter 3.

Although the absorption correction is made as part of data reduction (again see Chapter 3) some experimental input is required. The intensity of the beam after it has passed through the crystal is attenuated as follows:-

$$I = I_o \exp -\mu t \tag{2.12}$$

I is the attenuated intensity, I_o the incident intensity, μ the linear absorption coefficient (mm^{-1}) (which is a function of the type and wavelength of the radiation used and the composition of the crystal) and t is the pathlength (mm) of the radiation through the crystal. To obtain this last quantity, the shape, size and orientation of the crystal relative to the incident beam must be known. If possible, the crystal faces are indexed and the distance from each face to a reference point within the crystal is measured.

In some cases, where the faces are not regular or difficult to see, such a description of the crystal is impossible and an empirical correction based on ψ-scans is made. These scans are made by measuring the intensity of a reflection as it is rotated about the scattering vector, *i.e.* at different values of the azimuthal angle (ψ). Even if an analytical or numerical correction is to be made the ψ-scan provides a useful check of its correctness.

On a four-circle diffractometer of Eulerian geometry, a reflection with a χ-value close to 90° is selected for this measurement. If the reflection is exactly

at $\chi = 90°$ then the ψ and ϕ-axes coincide and only a ϕ-rotation is needed. In general a combination of rotations about the ω, χ is required. Although previously there has been some ambiguity about ψ-rotations due to different angle conventions being used on different instruments, a standard definition has now been proposed [12].

2.4 The Details

The five data collections reported in this Chapter were made in four different laboratories, (see Table 2.2). The neutron studies were necessarily made at central facilities; the HFBR (High Flux Beam Reactor) at Brookhaven National Laboratories, USA for Experiments 1 and 3 and DR3 at Risø National Laboratory, Denmark for Experiment 4. The help of R.K. McMullan (BNL) and B. Lebech (Risø) is gratefully acknowledged. Experiment 2 was carried out in the Department of Chemistry, University of Durham and Experiment 5 in the Department of Chemistry, Glasgow University in collaboration with P.R. Mallinson.

Experiments 1, 2 and 3 were carried out very much as described in the preceding sections. Details of these experiments are given in Tables 2.3 to 2.6. Both Experiments 4 and 5 were more problematic and are described in more detail.

Data for Experiment 4 were collected in several stages over a period of approximately 2 months. An initial period of beam time was used in checking the crystal; face indexing, ψ-scan measurements and scan parameter determination. A shell of data to $\theta = 25°$ in the hemisphere $\overline{h} \pm k \pm l$ was collected at 123K, (see Tables 2.5 and 2.6).

During a second period of beam time the data collection was continued.

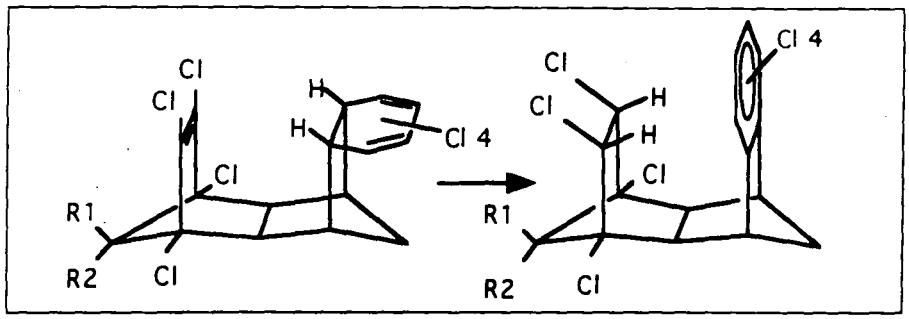

Substituents $R^1 = R^2 = Cl$

Isomer	KM5	KM9
	Experiment 1	Experiment 2
Radiation	Neutron	X-ray
Instrument	BNL H6M	Rigaku AFC6S

Substituents $R^1 = Cl, R^2 = Cl$

Isomer	KM22	KM25	
	Experiment 3	Experiment 4	Experiment 5
Radiation	Neutron	Neutron	X-ray
Instrument	BNL H6M	Risø TAS2	CAD4

Table 2.2: Details and labelling of experiments reported herein.

	Experiment 1	Experiment 2
Formula	$C_{16}D_6H_2Cl_{10}$	$C_{16}H_8Cl_{10}$
Crystal size (mm^3)	6.35	0.4 x 0.35 x 0.2
Radiation	neutron	Mo $K_{\overline{\alpha}}$ X-radiation
Wavelength (λ, Å)	1.0462(1)	0.71073
Temperature (K)	15	293
Cooling Device	Displex	None
Crystal system	Orthorhombic	Monoclinic
Space Group	$P2_12_12_1$	$C2/c$
Number	19	15
Cell Parameters:		
$a(Å)$	8.664(1)	13.911(3)
b	14.047(2)	10.357(2)
c	16.184(2)	28.782(6)
$\beta(°)$		102.87(2)
Cell determination		
No. of reflections used	32	25
in 2θ ranges	$49 \leq 2\theta \leq 53$	$20 \leq 2\theta \leq 30$
Z	4	4

Table 2.3: Crystal and instrument details for Experiments 1 and 2.

	Experiment 1	Experiment 2
Scan type	$\theta - 2\theta$	ω profile
Scan speed	monitor count ~1.7s per step	variable 2-8°min^{-1}
Scan width	for $\sin\theta/\lambda \leq 0.44\AA^{-1}$ 2.8°	$\Delta\omega = (0.89 + 0.30tan\theta)°$
	70 steps	
	for $\sin\theta/\lambda \geq 0.44\AA^{-1}$	
	variable scan width:-	
	$\Delta 2\theta = (1.488 + 2.51tan\theta)°$	
	minimum 59 steps	
$\sin\theta_{max}/\lambda$ (Å^{-1})	0.8	0.65
No. of Data collected	4689	5222
Check reflections	2 10 $\bar{6}$	1 $\bar{1}$ 2
	2 6 12	4 4 $\bar{7}$
		4 0 $\bar{4}$

Table 2.4: Crystal and instrument details for Experiments 1 and 2 (cont'd).

Data were measured in the opposite hemisphere $h \pm k \pm l$ under the same conditions as before, except that the crystal had been remounted. This shell of data was started at $\theta = 20°$ to provide some overlap with the previous shell.

Due to certain mechanical problems the crystal had to be allowed to warm to room temperature before a third and final period of data collection. A new peak search had to be made and the crystal recooled. This restart was effected without further difficulty. Data were collected to a final θ-value of 40° ($sin\theta_{max}/\lambda = 0.62\AA^{-1}$). A shell of data, $3 \leq \theta \leq 20°$, was measured in the hemisphere $h \pm k \pm l$; equivalent reflections to those first measured.

Experiment 5

The aim of this experiment was to collect an extensive data set suitable for an experimental charge density study. This type of study demands that every effort is made to minimise errors by careful setting-up of the experiment.

A first crystal was selected and mounted on a glass fibre using epoxy resin.

	Experiment 3	Experiment 4
Formula	$C_{16}H_9Cl_9$	$C_{16}H_9Cl_9$
Crystal size (mm^3)	8.0	34
Colour	Clear,colourless	clear, colourless
Radiation	neutron	neutron
Wavelength (λ Å)	1.0462(1)	1.0466
Temperature (K)	123	123
Cooling Device	Displex	Displex
Crystal system	Monoclinic	Triclinic
Space Group	$P2_1/c$	$P\bar{1}$
Number	14	2
Cell Parameters:		
a (Å)	13.642(3)	8.600(4)
b	8.163(2)	8.767(8)
c	16.864(2)	14.06(1)
$\alpha(°)$	90	89.13(6)
β	92.84(1)	85.08(5)
γ	90	60.88(4)
Cell determination		
No. of reflections used	32	36
in 2θ ranges	$48 \leq 2\theta \leq 57$	$24 \leq 2\theta \leq 57$
Z	4	2

Table 2.5: Crystal and instrument details for Experiments 3 and 4.

	Experiment 3	Experiment 4
Scan type	$\theta - 2\theta$	$\theta - 2\theta$
Scan speed	monitor count	monitor count
Scan width	3.0° for $\sin\theta/\lambda \leq 0.44\AA^{-1}$	variable scan width
	75 steps	using resolution curve
	for $\sin\theta/\lambda$ $0.44\AA^{-1}$	50 steps
	variable scan width:-	
	$\Delta 2\theta = (1.718 + 2.758tan\theta)°$	
	minimum 59 steps	
$\sin\theta_{max}/\lambda$ ($\AA^{-1}$)	0.8	0.62
No. of Data collected	6496	4577
Check reflections	2 3 $\overline{12}$	
	8 $\overline{4}$ $\overline{5}$	

Table 2.6: Crystal and instrument details for Experiments 3 and 4 (cont'd).

An initial peak search was made and the orientation matrix determined. A shell of data to $\theta = 15°$ was measured to assess the quality of the crystal. Although it was planned to cool the crystal at this point the Cryostream cooling device was not working satisfactorily, so data were collected at room temperature to $\theta = 30°$. The crystal appeared to be stable and of good quality, with good agreement between equivalent reflections.

It was then cooled to 123K at a rate of $2Kmin^{-1}$ whilst several reflections were repeatedly centred. The orientation matrix was then re-determined. Once the scan parameters had been chosen the data collection was started.

Unfortunately the first crystal was lost after 3 days of data collection and a second crystal was selected and mounted in a capillary. The initial checks and determination of the orientation matrix were then repeated. A complete shell of 1004 data was collected to $\theta = 13°$ at room temperature and the crystal appeared to be acceptable.

The faces of the crystal were indexed using an optical goniometer. The

necessary cutting of the crystal resulted in some non-natural faces which were approximated by natural ones.

The crystal was cooled at $2Kmin^{-1}$ to 123K and a new, low temperature orientation matrix determined. The scan parameters were chosen and the data collection started.

All data were measured as $\theta/2\theta$-scans and the full profile recorded. A variable scan width was used, calculated as $\Delta\omega = (0.8 + 0.35tan\theta)°$. The scan speeds were determined from an initial prescan, measured at $5°(\omega)$ min^{-1}, up to a maximum time of 120 seconds per scan with a specified precision of $\sigma(I)/I$ ratio of 0.030.

Intensity and orientational check reflections were remeasured at regular intervals. The intensity standard reflections were measured every 2 hours. The data collection was set to be automatically interupted if a 10% drop was observed. Orientational checks were measured every 200 reflections with a tolerance of 0.10°.

A complete sphere of data was collected although, as the Laue symmetry was $\bar{1}$, this gave only two sets of equivalent reflections. These data were collected in shells as given in Table 2.7.

For hemisphere $\pm h \; -k \pm l$

θ-range (°)	0-30	30-50
prescan cut-off	final scan	final scan
	for all data	for all data
scan method	zig-zag	list driven
		for reflections with
		$I \geq 4\sigma(I)$ calculated

for hemisphere $\pm h \; +k \pm l$

θ-range (°)	0-30	30-45	45-50
prescan cut-off	$I \leq 1\sigma(I)$	$I \leq 1\sigma(I)$	$I \leq 1\sigma(I)$
scan method	zig-zag	zig-zag	zig-zag

Table 2.7: Details of data collection shells in Experiment 5.

Bibliography

[1] The following texts were used in the preparation of Chapter 2:

International Tables for Crystallography, Vol. C (1992). Edited by A.J.C. Wilson. Kluwer Academic Publishers.

C. Giacovazzo, H.L. Monaco, D. Viterbo, F. Scordari, G. Gilli, G. Zanotti and M. Catti (1992). *Fundamentals of Crystallography*, edited by C. Giacovazzo. IUCr Texts on Crystallography, OUP.

U.W. Arndt and B.T.M. Willis (1966). *Single Crystal Diffractometry* Cambridge University Press.

Accurate Molecular Structures: Their determination and Importance (1992). Edited by A. Domenicano and I. Hargittai. IUCr Monographs on Crystallography, OUP.

G.E. Bacon (1963). *Neutron Diffraction.* OUP.

[2] J. Cosier and A.M. Glazer (1986). *J. Appl. Cryst.* **19**, 105-107.

[3] R.J. Nelmes, Z. Tun and W.F. Kuhs (1987). *Ferroelectrics* **71**, 125-141.

[4] F.K. Larsen (1991) in *The Application of Charge Density Research to Chemistry and Drug Design*, edited by G.A. Jeffrey and J.F. Piniella. Plenum Press.

[5] J. Hornstra and H. Vossers (1974). *Philips Tech. Rundschau* **33**, 65-78.

[6] W.C. Hamilton (1974). *International Tables for X-ray Crystallography* Vol IV, p 278, edited by J.A. Ibers and W.C. Hamilton. England: The Kynoch Press.

[7] L.E. Alexander and G.S. Smith (1962). *Acta Cryst.* **15**, 983-1004.

[8] H.W. Wyckoff (1985). In *Methods of Enzymology* **114**, 330-386. Edited by H.W. Wyckoff, C.H.W. Hirs and S.N. Timasheff, Orlando: Academic.

[9] A. McL. Mathieson (1982). *Acta Cryst.* **A38**, 378-387.

[10] Texsan Structure Analysis Software, Molecular Structure Corporation.

[11] CAD4 software, Enraf-Nonius, Delft.

[12] H.D. Flack and D. Schwarzenbach (1992). *J. Appl. Cryst.* **25**, 455-459.

Chapter 3

Data Processing and Refinements

3.1 Data Processing

The raw data measured on the diffractometer consist of the Bragg peak superimposed on some background intensity. The first step in data reduction is the calculation of the integrated peak intensity with the background subtracted out. The structure factor amplitudes, $|F(\mathbf{h})|_{obs}$, can then be obtained by applying a number of corrections.

Peak Integration

Two methods of obtaining the integrated intensities were used when processing the data for Experiments 1 to 5 and are outlined below.

The simplest method is the background-peak-background (BPB) method. The outermost points of the scan are taken as being due to background; usually around 10% of the scan points on each side or sometimes one point at a certain offset from the peak centre is used. The mean value is then used to estimate a linear background to be subtracted from the sum of the counts in the scan. The resulting value is the integrated intensity, $I(\mathbf{h})$. The esd, $\sigma(I(\mathbf{h}))$, is calculated assuming Poisson statistics.

To ensure that the outermost points are indeed only background, the scan needs to be wider than its optimum width. This is to allow for peaks which are off centre and some variation in peak width. The additional width in turn affects the esd of the intensity, $\sigma(I(\mathbf{h}))$, as background points may be included in the peak.

Other methods of peak integration have been developed which aim to improve the ratio of $I(\mathbf{h})$ to $\sigma(I(\mathbf{h}))$ by determining the peak limits more accurately. One of these is the Lehmann-Larsen method [1] which uses the fact that the peak limits are near to where the ratio $\sigma(I(\mathbf{h}))$ / $I(\mathbf{h})$ is at a minimum. This method requires that the complete step-scan profiles have been recorded. Another advantage of recording the full peak profile is that it allows any irregular peaks to be re-examined.

Peaks which are weak or which have a high background, possibly due to overlap with neighbouring peaks, are generally not processed in the first pass of the Lehmann-Larsen programs. Instead, parameters determined from reflections which satisfy a number of tests are used to estimate the peak widths of the weak reflections. The peak limits are determined separately for each side of the peak as the profiles are not necessarily symmetrical. Outside these limits, the background is estimated by a least-squares fit of a straight line to the two sets of background points.

Corrections to the Data

The derived integrated intensities, $I(\mathbf{h})$, require a number of corrections to be made in order to convert them to the squares of the structure factor amplitudes, $|F(\mathbf{h})|^2$. Geometrical corrections, such as those for Lorentz and polarisation effects, depend on the experimental configuration used to collect the data. Other corrections are needed to account for limitations in the kinematic theory used, *e.g.* absorption and extinction corrections.

The two quantities, $I(\mathbf{h})$ and $|F(\mathbf{h})|$, are related as below.

For neutrons

$$I(\mathbf{h}) = \left(\frac{\lambda^3 V}{V_c^2}\right)\frac{1}{\varpi}\mathrm{LATE}|F(\mathbf{h})|^2 \tag{3.1}$$

and for X-rays

$$I(\mathbf{h}) = \left(\frac{\lambda^3 r_o^2 V}{V_c^2}\right)\frac{1}{\varpi}\mathrm{LPATE}|F(\mathbf{h})|^2 \tag{3.2}$$

where λ is the wavelength, V the crystal volume, V_c the unit cell volume, r_o the classical electron radius and ϖ the angular scanning velocity. L is the Lorentz factor, P the polarisation factor, A the absorption correction, T the correction for thermal diffuse scattering (TDS) and E the extinction correction.

The Lorentz factor, (L), is needed to correct for the fact that the time required for a reciprocal lattice point to cross the Ewald sphere is not the same for all the reciprocal lattice points. The correction takes the form $1/\sin(2\theta)$ for the equatorial geometry used in the experiments reported herein.

Polarisation (P), in the case of neutrons, only affects magnetic scattering measurements and so does not need to be considered for Experiments 1, 3 and 4. The radiation emitted by a conventional X-ray tube is randomly polarised and can be considered as two equal parts, half with the electric vector in the plane of scattering and half perpendicular to it. This gives rise to the polarisation factor of:-

$$\frac{1}{2}(1 + cos^2 2\theta) \tag{3.3}$$

However, if a single crystal monochromator is used the beam is partially polarised. One of two situations is usually assumed; the crystal is either a perfect or an ideally imperfect one. The correction then needs modifying to take this into account. The modified correction is:-

$$(1 + A cos^2 2\theta)(1 + A)^{-1} \tag{3.4}$$

where $A = cos^2 2\theta_M$ for a ideally imperfect crystal and $A = cos 2\theta_M$ for a perfect crystal, θ_M is the monochromator Bragg angle or 'take-off' angle. In reality, it is usually somewhere between the two situations and should be checked experimentally.

An absorption correction must be made to account for the attenuation of the beam as it passes through the crystal. The transmission factor, A, is given by:-

$$A = \frac{1}{V} \int \exp(-\mu t) dV \tag{3.5}$$

where V(Å^3) is the crystal volume, μ(mm^{-1}) is the linear absorption coefficient and t(mm) is the mean pathlength through the crystal. The correction to be made is therefore 1/A.

The linear absorption coefficient, μ, is calculated as

$$\mu = \frac{1}{V_c} \sum_{n}^{N_n} \sigma_n \tag{3.6}$$

where σ_n are the attenuation cross-sections for each of the N_n contributors in the unit cell of volume V_c. Normally, an acceptable approximation is used to calculate μ which does not fully take into account all the processes which attenuate the beam and assumes that the absorption is not sensitive to the arrangement of the atoms in the unit cell.

The beam attenuation is due to two main processes; true absorption and scattering, both coherent and incoherent. True absorption in the case of X-rays is due to the photoelectric effect where absorption of photons promotes or ejects an electron. For neutrons, it is nuclear capture processes which count as true absorption.

The integral in Equation 3.5 can be solved analytically for certain shapes such as cylinders and spheres. For crystals with regular faces, it can also be solved by dividing the crystal into Howells polyhedra and then ultimately into tetrahedra [2]. The contribution made by each tetrahedron can be calculated analytically and then summed over all the tetrahedra to give a total transmission factor.

The calculation of this integral, as described above, becomes very time consuming for more complex shapes of crystal and a numerical correction can

then be made. The crystal is divided into a non-isometric grid and the contributions made by the grid points can be summed to approximate the integral Equation 3.5. For each grid point the incident and diffracted path lengths are calculated, weighted by Gaussian constants as they do not represent equal volumes of crystal, and then, for each of the grid points, used to calculate the transmission factor.

As mentioned in the previous chapter, it is not always possible to describe the crystal faces. In this case, an empirical correction can be made provided azimuthal (ψ) scans have been made. The values of each of the points in the scans are then used to give a table of the relative transmission factor,T, as a function of the diffractometer angle ϕ. This table is then used to calculate relative transmission factors for all the data.

$$T = \frac{I(\phi)}{I_{max}(\phi)} \tag{3.7}$$

Extinction corrections are made to correct the observations for which the intensities are lower than that predicted by kinematic theory for an ideally imperfect crystal. The attenuation of the beam in this case is caused by scattering of the beam as it passes through the crystal, which is assumed not to occur by kinematic theory. This effect is especially pronounced for intense, low angle reflections.

In the Darwin mosaic model the crystal consists of crystalline blocks slightly misaligned with respect to one another. Using this model two extreme situations can be envisaged. The first situation, primary extinction, is caused by interactions between the diffracted beam from successive planes and the incident beam.This interaction occurs within the individual blocks. These beams are coherent within a single block and the necessary corrections involve the dynamical theory of scattering. The second situation, secondary extinction, is more common. It is concerned with the effective shielding of correctly aligned blocks deeper within the crystal by blocks with the same alignment which the

incident beam has already encountered. In this case the blocks are considered to scatter incoherently and corrections are based on kinematic theory. If the blocks are sufficiently misoriented they will not scatter together and so will not experience this shielding.

The degree of misorientation is quantified by the mosaic spread, (g) and the size of the blocks is given by the domain radius, (ϱ). The Becker and Coppens formalism [3] used to correct data employs a further division of secondary extinction into that of Type I and Type II crystals depending on which of the two quantities, g or ϱ, dominates. If the natural width of a reflection is far narrower than its mosaic spread then it is a Type I crystal.

The correction takes the form $y = y_p y_s$ where y_p and y_s are the corrections for primary and secondary extinction respectively. It is applied as $\mathrm{F}(\mathbf{h})_{obs} = \mathrm{yF}(\mathbf{h})_{calc}$ where for both cases y has the following form:-

$$y_i = (1 + 2x + \text{ higher order terms in x})^{-\frac{1}{2}} \tag{3.8}$$

For secondary extinction

$$2x = 2\left(\frac{\overline{T}\lambda^3}{V^2 sin^2\theta}\right) g^* \mathrm{F}(\mathbf{h})^2 \tag{3.9}$$

where $\overline{T}$ is the absorption weighted mean path length for that reflection and g^* is the extinction parameter related to the mosaic spread and the domain radius.

Unfortunately, neither of the latter quantities, the mosaic spread or domain radius, are usually known for the crystals studied and the extinction parameter is often refined as part of the least-squares refinements. For the neutron experiments reported herein the extinction corrections were made using the Becker and Coppens formalism for secondary extinction [3] in a Type I crystal with the distribution of the mosaic blocks taken to obey an isotropic Lorentzian distribution. $\overline{T}$ was calculated as part of the absorption corrections.

Another systematic error for which it is difficult to correct is thermal diffuse

scattering, TDS, or inelastic phonon scattering. TDS shows a maximum at the same position as the Bragg peak and so, unlike the incoherent scattering which is more uniform, it is not removed when the background is subtracted. In general, it can only be removed by calculations involving the elastic constants and these are very rarely available for molecular crystals. Although some methods of correction are available [5] based on information contained in the observed peaks themselves, no corrections were applied to the experiments reported herein. The effect of ignoring TDS is the overestimation of peak intensities, especially at higher scattering angles, so causing underestimation of the thermal parameters.

It is common that a decay correction is made to account for variation in the measured intensities as a function of time. This correction is necessary if there is decay due to radiation damage and also in some cases where the data collection has been made over a long period of time. The correction is usually based on the repeated measurements of the standard reflections. If the variation in the intensities of the standard reflections is well behaved, it can be fitted by a polynomial function to generate decay factors for all the data. Statistical tests can be employed to decide which order of polynomial function should be used. The *TEXSAN* [4] processing program calculates an R-factor for each order up to fifth order so allowing the best fit to be chosen. The *DREAM* package [5] uses the F-test to calculate if the addition of an extra term produces a significant improvement.

Since the decay corrections are based on the standard reflection measurements it is obviously important that these reflections represent the data set as a whole. A very strong, low angle reflection which is affected by extinction may increase in intensity as the mosaic character of a crystal changes but this will not be true of the rest of the data and so would be a poor choice of standard.

Sometimes a data set may consist of one or more subsets of data. This may be because data were collected on more than one crystal or that some other

change in the experimental set-up has occurred. In order to put the data on a common scale, inter-layer scale factors must be calculated which requires some reflections common to the subsets of data. In general, the standard reflections fulfil this requirement, although, obviously there may also be other common reflections. The *DREAM* program *SORTAV* [5] uses the least squares method of Hamilton, Rollett and Sparks [6] to calculate the inter-batch scale factors and normalises them such that the scale factor for the largest subset is unity.

In many cases, replicate and symmetry equivalent reflections are averaged. Corrections which depend on the time of measurement, such as decay, or on the orientation of the crystal when the reflection was measured, such as absorption and in some cases extinction, should be made first.

There are various choices made about how this averaging of observations is carried out but in general, a weighted average is calculated, the esd is modified in some way to take into account the scatter of the values observed and some tests are made in order to exclude outliers.

The following equations are as used in the *DREAM* data processing package but are typical of such programs. The mean value of the square of the structure factor amplitude is given by

$$\langle|\mathrm{F(h)}|^2\rangle = \frac{\sum_{\mathrm{i}=1}^{\mathrm{n}}(\mathrm{w_i}|\mathrm{F(h)}|_\mathrm{i}^2)}{\sum \mathrm{w_i}} \tag{3.10}$$

where the weight of the i^{th} of n observations is $w_i = 1/\sigma^2(|\mathrm{F(h)}|_\mathrm{i}^2)$. Two estimates of the standard deviation are calculated, one based on counting statistics and the other on the scatter of the values observed for a given reflection. The esd based on counting statistics and errors propagated through the data processing is given by $\sqrt{(n/\sum w_i)}$. The root mean square deviation ($rmsd$) is given as

$$rmsd = \sqrt{\frac{\frac{n}{(n-1)}\sum_i w_i(|\mathrm{F(h)}|_\mathrm{i}^2 - \langle|\mathrm{F(h)}|^2\rangle)^2}{\sum_\mathrm{i} \mathrm{w_i}}} \tag{3.11}$$

Depending on the program the error output with the averaged data may be the larger of the two of these values or may be the esd.

Outliers are usually rejected or downweighted on the basis of a predefined test; often the tests are as a function of a cut-off, c, such as

$$||\mathrm{F(h)}|_i^2 - \langle|\mathrm{F(h)}|^2\rangle| \geq c\sigma$$

For Experiment 5 outliers were down-weighted according to their calculated relative normal probabilities. In this case the mean, esd and rmsd were all recalculated using new weights

$$w_i = p_i/\sigma^2(|\mathrm{F(h)}|_i^2) \tag{3.12}$$

where

$$p_i = \exp\left[-0.5\left(\frac{|\mathrm{F(h)}|_i^2 - \langle|\mathrm{F(h)}|^2\rangle}{\sigma}\right)\right] \tag{3.13}$$

and σ is the maximum of the esd and the rmsd.

A further modification often made to σ uses 'p', the proportionality constant [7], sometimes called an ignorance factor or instability constant. Although intensity data are expected to follow Poisson statistics the variances of observations of a reflection are often much larger than this would predict. The proportionality constant is estimated by examining the scatter of repeated measurements of intense reflections, usually the standard reflections, above the scatter expected from Poisson statistics. The 'p' factor calculated should account for any fluctuations in the source, crystal or detector as well errors in the scaling factor. It is normally a value of around 0.01 to 0.05 and for a stable crystal has a characteristic value for a particular diffractometer.

The scaled variance as calculated in the *DREAM* package is

$$\sigma^2(|\mathrm{F(h)}|_{\mathrm{corr}}^2) = \frac{(\sigma^2(|\mathrm{F(h)}|^2) + \mathrm{p}^2[|\mathrm{F(h)}|^2]^2)}{\mathrm{K}^2} + \left(\frac{[|\mathrm{F(h)}|^2]^2}{\mathrm{K}^2}\right)\sigma^2(\mathrm{K}) \tag{3.14}$$

where K is the weighted average inverse scaling factor and

$$p^2 = \frac{\{\sum(|\mathrm{F(h)}|_{\mathrm{meas}}^2 - |\mathrm{F(h)}|_{\mathrm{calc}}^2(\mathrm{t}))^2 - \sum\sigma^2(|\mathrm{F(h)}|_{\mathrm{meas}}^2)\}}{\sum[|\mathrm{F(h)}|_{\mathrm{meas}}^2]^2} \tag{3.15}$$

3.2 Structure Solution

Once obtained, the set of corrected structure amplitudes $|F(\mathbf{h})|$ or their squares, $|F(\mathbf{h})|^2$, can be used to confirm the space group. Although the space group will have been determined long before this stage, it may have been ambiguous. The confirmation uses a number of criteria; the Laue symmetry, the Bravais lattice type, the cell constants and the systematic absences.

Systematic absences are reflections for which the calculated structure factors are zero and occur in certain classes of reflection due to conditions imposed by translational symmetry, such as screw axes, glide planes and also lattice centering.

The normalised structure factor, $E(\mathbf{h})$, is used in statistical analyses to remove the effects of atomic shape which causes the drop off in intensity with increasing $\sin\theta/\lambda$. This is calculated as:-

$$|E(\mathbf{h})| = \frac{|F(\mathbf{h})|}{\sqrt{\langle |F(\mathbf{h})|^2 \rangle}} = \frac{|F(\mathbf{h})|}{\sqrt{\epsilon \Sigma}} \tag{3.16}$$

which should have the mean value of $|E(\mathbf{h})|^2 = 1$ for all values of $\sin\theta$.

$$\Sigma = \sum_{j=1}^{N} f_j^2 \tag{3.17}$$

and $\sqrt{\langle |F(\mathbf{h})|^2 \rangle}$ is the expected value of $|F(\mathbf{h})|$ and should be the spherical average of the observed values. ϵ depends on the lattice symmetry and takes into account the effects of symmetry elements on the mean intensities of certain groups of reflections. It is equal to 1 for general reflections.

One of the commonest uses of these normalised structure factors is to examine if the space group is centrosymmetric. The theoretical probability distribution of $|F(\mathbf{h})|$ varies in form depending on whether the distribution is centric or acentric. Typically for a centric distribution $\langle |E(\mathbf{h})|^2 - 1 \rangle$, calculated for all the data, tends to a value of 0.97 and for an acentric distribution tends to 0.74.

Intensities are usually measured on a relative scale and not an absolute one. Although the scale factor which puts the data on an absolute scale is experimentally measurable, the relative scale factor is usually estimated. Before structure solution, an approximate scale factor is calculated using statistical analysis of the intensity data. The method used in Shelxtl-Plus [21] is that of Karle, Hauptman and Christ [8]. Data are divided into intervals of $\sin\theta/\lambda$ (s) and K is calculated for each of the intervals.

$$K = \frac{\sum(\epsilon\Sigma)}{\sum|\mathrm{F(h)}|^2_{\mathrm{obs}}} \tag{3.18}$$

Then, from a plot of K against s, data can be put on an approximate scale as $|\mathrm{F(h)}|^2 = |\mathrm{F(h)}|^2_{\mathrm{obs}}\mathrm{K(s)}$. Once the structure has been solved, a relative scale factor is usually refined as part of the least squares refinements. This refined scale factor puts the calculated structure factors, which are on an absolute scale, and the observed ones on the same scale. The scale factor refined (denoted by G as in Equation 3.21) is actually the reciprocal of K so as to leave the observed structure factor amplitudes unaltered.

The structures of three of the compounds under investigation KM5, KM22 and KM25, had been solved previously. The structure of KM9 was not known and was solved in this study from the data collected in Experiment 2.

As pointed out in Chapter 2, the structure factor amplitudes can be measured but their phase cannot. Unfortunately, it is the phases rather than the magnitudes which give the atomic positions, or at least the peaks, in the electron density map. Fortunately, we have some information about the electron density and so the two quantities, the phases and the magnitudes of the structure factors, are not independent. The situation is greatly simplified for centrosymmetric structures where the phase angles are restricted to values of 0 and 180°.

Direct methods of structure solution use the relationship between the phases and the magnitudes to derive the structure factor phases mathematically from

the measured X-ray intensities. The information about the electron density is used in the form of two important constraints applied to $\rho(x)$:-

1. The electron density must be everywhere positive, $\rho(x) \geq 0$.
2. It is composed of discrete atoms such that $\rho(x)$ is close to zero everywhere apart from approximately spherical peaks at the atomic positions.

Normalised structure factors, E(**h**), are used because the the effect of the atomic shape has been removed and so just such spherical peaks are produced in an E map. Reflections with large values of E(**h**) are used in the initial stages of the phase determination. The phase assignment with the best figure of merit can then be used to calculate an E map from which the structure may be picked out.

The model structure at this stage is often incomplete. The standard method of locating the 'missing' atoms is Fourier synthesis, most commonly difference Fourier synthesis.

$$\Delta\rho(\mathbf{r}) = \rho_{\text{obs}}(\mathbf{r}) - \rho_{\text{calc}}(\mathbf{r}) = \frac{1}{V}\sum_{\mathbf{h}} [\mathrm{F}(\mathbf{h})_{\text{obs}} - \mathrm{F}(\mathbf{h})_{\text{calc}}] \exp(-2\pi i \mathbf{h}.\mathbf{r}) \quad (3.19)$$

As the true phases of the observed structure factors are unknown the calculated phases from the incomplete model are used as an approximation. Thus Equation 3.19 becomes:-

$$\Delta\rho(\mathbf{r}) = \frac{1}{V}\sum_{\mathbf{h}} [|\mathrm{F}(\mathbf{h})|_{\text{obs}} - |\mathrm{F}(\mathbf{h})|_{\text{calc}}] \exp(-2\pi i \mathbf{h}.\mathbf{r} + i\phi(\mathbf{h})_{\text{calc}}) \quad (3.20)$$

This should result in positive peaks in the observed density which are not matched by one in the model. A difference Fourier has the important advantage that it is not susceptible to series truncation errors.

The more or less complete model, at this stage excluding any hydrogen atoms, is still only approximate and the next stage is to refine the structure. The treatment of hydrogen atoms differs considerably between X-ray and neutron studies; one of the main reasons for the neutron studies here. Neutron

diffraction data allow the hydrogen atomic parameters to be at least as well determined as all other atoms. Consequently, positional and anisotropic atomic displacement parameters may be refined for hydrogen atoms. Their positions are generally easily located in neutron Fourier difference maps as negative 'holes', due to the negative scattering length of hydrogen.

Compounds are often deuterated for neutron studies to reduce the problems caused by the considerable incoherent scattering cross-section of hydrogen. Deuterium, which has a very small incoherent scattering cross-section, is also a stronger scatterer than hydrogen. The deuteration of KM5 in Experiment 1 was a useful result of kinetic isotope effect studies carried out by K. Mackenzie.

The situation is somewhat different for X-rays as hydrogen has only one electron and so is a very weak scatterer. Added to this, such electron density as there is, is usually spread out asymmetrically and is not centred at the nuclear position, as well as having larger than average vibrational amplitudes. Even when hydrogen atom positions can be located in difference maps, within a sound structural model, it may not be possible to refine the hydrogen atom parameters satisfactorily.

The hydrogen atoms in the two X-ray studies reported in this Chapter were treated slightly differently. Those of Experiment 2 were located from the difference Fourier maps after the rest of the model had been refined satisfactorily and their atomic coordinates were refined, although all of them were assigned a fixed isotropic atomic displacement parameter, U_{iso}(H), of 0.08Å^2. In the X-ray study of KM25 (Experiment 5), since a neutron study of the same compound (Experiment 4) had been carried out at the same temperature as Experiment 5, the atomic coordinates and anisotropic adps for all the hydrogen atoms were fixed at the values from the neutron study. Other methods of treating hydrogen atoms are discussed in Chapter 6.

3.3 Structure Refinement

The most commonly used method of structure refinement is that of least-squares. This method is used to find the best fit of a particular model to a set of experimental data. This best fit is achieved by minimising the sum of the square of the deviations between the experimental observations and the equivalent calculated quantities. Therefore, given a set of experimental observations and the equivalent calculated quantities computed using a theoretical model with initial trial values of the parameters, the values of these parameters which give the best fit can be determined and an estimate of their accuracy can be made.

In the case of structure refinements, the experimental observations are the structure factor amplitudes, $|\mathrm{F}(\mathbf{h})|_{\mathrm{obs}}$, or their squares $|\mathrm{F}(\mathbf{h})|^2_{\mathrm{obs}}$. The 'model' is the structural model from which the calculated structure factor amplitudes $|\mathrm{F}(\mathbf{h})|_{\mathrm{calc}}$ can be computed using Equation 3.21. The 'parameters' are the scale factor, the atomic positions and some related parameters for describing the thermal motion of the individual atoms, their site occupancy and less commonly, an extinction parameter.

The quantity most usually minimised is:-

$$Q = \sum_{\mathbf{h}} w(|\mathrm{F}(\mathbf{h})|_{\mathrm{obs}} - \mathrm{G}|\mathrm{F}(\mathbf{h})|_{\mathrm{calc}})^2 \qquad (3.21)$$

where the summation is over all independent reflections, $\mathbf{h}$, w is the weight for each term and G is the reciprocal of the scale factor K for $|\mathrm{F}(\mathbf{h})|_{\mathrm{obs}}$.

This minimisation corresponds to differentiating partially with respect to the variables in $|\mathrm{F}(\mathbf{h})|_{\mathrm{calc}}$ denoted by p_j whose values are to be refined and equating the derivatives to zero. Then the normal equations are:-

$$\frac{\partial Q}{\partial p_j} = 0$$

or

$$\sum_{\mathbf{h}} w\Delta \frac{\partial |\mathrm{F}(\mathbf{h})|_{\mathrm{calc}}}{\partial \mathrm{p_j}} = 0 \tag{3.22}$$

where Δ is $|\mathrm{F}(\mathbf{h})|_{\mathrm{obs}} - |\mathrm{F}(\mathbf{h})|_{\mathrm{calc}}$.

However, the structure factor amplitudes are not linearly related to the aforementioned parameters and consequently there are a number of local minima in the residual Q. Provided that the trial structure is reasonably close to the true structure, a set of linear equations can be derived from the shifts (x_i) from the initial trial parameters (p_i) rather than the parameters themselves. This is achieved by expanding each of the $|\mathrm{F}(\mathbf{h})|_{\mathrm{calc}}$ into a Taylor series in which, because the trial structure is assumed to be sufficiently close to the best fit, terms higher than the first partial derivative may be neglected. Δ then becomes:-

$$\Delta(\mathbf{p}+\mathbf{x}) = \Delta(\mathbf{p}) - \sum_{\mathrm{i=1}}^{\mathrm{n}} \mathrm{x_i} \frac{\partial |\mathrm{F}(\mathbf{h})|_{\mathrm{calc}}}{\partial \mathrm{p_i}} \tag{3.23}$$

$\mathbf{p}$ and $\mathbf{x}$ represent the complete set of parameters and shifts. This leads to the normal equations:-

$$\sum_{i=1}^{n} \left[\sum_{\mathbf{h}} w \frac{\partial |F(\mathbf{h})|_{\mathrm{calc}}}{\partial \mathrm{p_i}} \frac{\partial |F(\mathbf{h})|_{\mathrm{calc}}}{\partial \mathrm{p_j}} \right] x_i = \sum_{\mathbf{h}} w\Delta \frac{\partial |F(\mathbf{h})|_{\mathrm{calc}}}{\partial \mathrm{p_j}} \tag{3.24}$$

The solution of which gives the correction terms or shifts which are then applied to the initial trial parameters. This process is repeated until the refinement can be said to have converged, that is, the shifts are zero or very small.

The weighting, $w(\mathbf{h})$, of each reflection is important and should reflect the precision of the individual measurements. $w(\mathbf{h})$ is often taken as $1/\sigma^2(|\mathrm{F}|_{\mathrm{obs}})$ so that measurements which are considered to be unreliable have a small influence on the refinement. Unfortunately, it is not easy to obtain an accurate estimate of the error in the measurement. Factors such as the proportionality constant (p) given on Page 83 have been introduced to give a truer estimate of the error. A weighting scheme which modifies the esds in some way is often used, based on an analysis of the variance when data are divided into subgroups in some way; *e.g.* intensity or $\sin\theta/\lambda$ intervals are commonly used.

Least squares refinements may be made using either the structure factor amplitudes, $|F(\mathbf{h})|$ or their squares $|F(\mathbf{h})|^2$ and there has been considerable discussion about the relative merits of the two approaches [9]. The conversion from $|F(\mathbf{h})|^2$ to $|F(\mathbf{h})|$ presents certain problems; the main ones being those of taking the square root of a negative number for those weak reflections which have a net negative intensity and the estimation of $\sigma(F(\mathbf{h})_{obs})$ from $\sigma(F(\mathbf{h})^2_{obs})$ which is complicated for weak and negative reflections. It is therefore impossible to use all the data in a refinement against $|F(\mathbf{h})|$. The data which are excluded are the weak data hence producing a bias towards higher values of $|F(\mathbf{h})|_{calc}$ which generally affects the thermal parameters and the scale factor. The common practice of omitting data on the basis of some cut-off criterion, for example all data where $|F(\mathbf{h})| < 3\sigma$ are excluded, is a further extension of this type of bias.

The main motivation for omitting data in this way is a cosmetic one and there is no statistical basis for it, however, if properly weighted, the least accurate data have little effect on the refinements so there is consequently little effect on the final parameters obtained [10, 11]. It is advocated to set reflections with negative intensities to zero since these intensities are not real but result from poor integration and no model will be able to reproduce these reflections correctly.

The model

The structure factor, $F(\mathbf{h})$, for X-rays is calculated as:-

$$F(\mathbf{h}) = \sum^{N} f_j \exp(2\pi i \mathbf{r}_j.\mathbf{h}) \tag{3.25}$$

where the summation is over all N atoms in the cell, $\mathbf{r_j}$ is the position of the j^{th} atom relative to the origin, $\mathbf{h}$ the scattering vector and f_j the atomic scattering factor for X-rays which is replaced by b_j, the atomic scattering length, for neutrons. It is modified by the thermal motion of the atoms as given in Equation 2.4.

The adjustable parameters in this model are, in general, the atomic positions and those describing the thermal motion of the atoms. Parameters for the occupancy of a particular site may also be refined if the structure is statistically disordered in some way. Neutron scattering lengths may also be refined but this is not generally the case. However, in Experiment 1, the scattering lengths for the hydrogen type atoms were refined in order to determine the level of deuteration, as discussed in Chapter 4.

The thermal motion of each of the atoms is considered to be mutually independent, although not really the case, and to be an oscillation about a position of minimum energy. The atomic oscillations due to thermal motion modify the electron density. The experimental data therefore give a time-averaged description of the atomic distributions with respect to their equilibrium position. This motion may be included in the structural model in the following way.

The probability of finding the centre of one atom at the position $\mathbf{r}'$, $p(\mathbf{r}')$, can be converted, by Fourier transform, to give a description of the thermal motion of an atom in reciprocal space, $q(\mathbf{r}^*)$, which is known as the Debye-Waller factor:-

$$q(\mathbf{r}^*) = \int p(\mathbf{r}') \exp(2\pi i \mathbf{r}'.\mathbf{r}^*) d\mathbf{r}' \tag{3.26}$$

If the thermal motion of the atom is assumed to be isotropic then it takes the form:-

$$q(\mathbf{r}^*) = \exp(-B\sin^2\theta/\lambda^2) \tag{3.27}$$

where $B = 8\pi^2\langle U^2\rangle$ (Å^2) and $\langle U^2\rangle$ is the mean square displacement of the atom with respect to the equilibrium position. In general, the thermal motion is not isotropic and the probability, $p(\mathbf{r}')$ is often assumed to have a 3-dimensional Gaussian distribution centred on the mean atomic position. Six parameters, the anisotropic temperature factors, U_{ij}, are then used to characterise the thermal motion. $q(\mathbf{r}^*)$ is then given by:-

$$q(\mathbf{r}^*) = \exp[-2\pi^2(U^*_{11}x^{*2} + U^*_{22}y^{*2} + U^*_{33}z^{*2} + 2U^*_{12}x^*y^* + 2U^*_{13}x^*z^* + 2U^*_{23}y^*z^*)] \tag{3.28}$$

The orientation of the thermal ellipsoid with respect to the crystallographic axes and its size, given by the lengths of its three principal axes are given by the six U_{ij} parameters.

For an atom assumed to have isotropic motion, there are generally four parameters per atom, three positional (xyz) and one atomic displacement parameter, (U_{iso}), and for an atom assumed to exhibit anisotropic motion there are five additional adps (U_{ij}s).

The X-ray atomic scattering factors used for most routine structure determinations assume the atoms are independent of one another and are spherically symmetrical. An alternative atomic model is used in the refinements discussed in Chapter 5.

The scattering factor for a static atomic electron density distribution is given below:-

$$f_o = \int_0^\infty U(\mathbf{r}) \frac{\sin(\mathbf{kr})}{\mathbf{kr}} \mathbf{dr} \tag{3.29}$$

where $k = 4\pi(sin\theta/\lambda)$ and the radial distribution of the static density, U($\mathbf{r}$), equals $4\pi\mathbf{r}^2\rho(\mathbf{r})$. The electron density is related to the wavefunction, ψ, as $\rho(\mathbf{r})$ can be replaced by $|\Psi|^2$. The atomic scattering factors are calculated using atomic wavefunctions from Hartree-Fock type calculations for most lighter atoms, Z<38, and from calculations using the Thomas-Fermi approximation for heavier atoms, Z$\geq$38.

Each alteration made to the model should be assessed in terms of its fit to the experimental data and its chemical sense. A measure of the fit of the model to the observed data is given by the agreement factors, generally several R-factors and a goodness of fit parameter. The formulae for these agreement factors are given in the glossary.

A difference Fourier synthesis should be calculated to show the extent of the residual density which has not been accounted for. The derived bond lengths and angles also provide a check of the model as unusual structural features

may indicate an anomaly in the model.

3.4 The Details

The different programs and methods used are detailed below.

Experiments 1 and 3

Experiments 1 and 3 were carried out at Brookhaven National Laboratories and data were processed using in-house programs in both cases.

Integrated intensities were obtained by the BPB method, with the outer 10% of the scan points on each side taken as background. Data were corrected for the Lorentz factor. No decay correction was required. An analytical absorption correction was made [2], the attenuation factor, μ, for which was calculated for all non-hydrogen elements using mass attenuation coefficients (μ/ρ) from International Tables [12]. The mass attenuation coefficient for hydrogen was taken from the experimental value determined by McMullan and Koetzle [13]:

$$\frac{\mu_H}{\rho} = 10.055 + 14.117\lambda \tag{3.30}$$

which is in close agreement with similar measurements made by Howard *et al* [14]. The total attenuation factor, μ, is calculated as

$$\mu_{tot} = \sum f_i \left(\frac{\mu}{\rho}\right)_i \tag{3.31}$$

over each of the i elements present where f_i is the mass fraction of the element in the crystal.

Intensity standard deviations were estimated using counting statistics except for those reflections where replicate or symmetry equivalent observations were merged. In such cases the esd was modified to give an estimated standard

Experiment	1	3
Chemical Formula	$C_{16}H_2D_6Cl_{10}$	$C_{16}H_9Cl_9$
No. of measured data	4689	6525
No. of unique data	4472	6022
R_{merge}	0.0219	0.0320
R_σ	0.0183	0.0134
μ_n (mm^{-1})	0.563	1.169
Transmission		
min	0.88	0.76
max	0.94	0.88
Crystal volume (mm^3)	6.6	7.95

Table 3.1: Data processing details for Experiments 1 and 3.

deviation of the mean as

$$\sigma(\langle|\mathrm{F(h)}|^2\rangle) = \frac{\sqrt{(\mathrm{n}-1)^{-1}\left(\langle|\mathrm{F(h)}|^2\rangle - |\mathrm{F(h)}|_\mathrm{i}^2\right)^2}}{\sqrt{\mathrm{n}}} \tag{3.32}$$

Further refinement details are given in Table 3.1.

Experiment 2

5222 profile scans were integrated using the Lehmann-Larsen method in Experiment 2. These data were also corrected for Lorentz and polarisation effects [4]. An empirical absorption correction was made based on azimuthal (ψ) scans of three reflections, 0 $\bar{4}$ 5, 0 $\bar{4}$ 4 and 0 $\bar{2}$ 5. The minimum and maximum relative transmission factors were 0.7977 and 1.0. Replicate and symmetry equivalent measurements were averaged to give 4643 unique data, $R_{int} = 0.032$, $R_{sigma} = 0.0575$.

Experiment 4

Experiment 4 was carried out in three parts (see Section 2.4) and consequently the data were treated in three separate blocks. The blocks were not merged after data processing since an extinction correction was included in the refinements. Data were processed using a combination of College 5 (ILL),

Block	1	2	3
θ range (°)	3-25	24.5-28.5	28.5-40 and 3-21
region	$-h \pm k \pm l$	$h \pm k \pm l$	$h \pm k \pm l$
N°. of data	1177	881	2689
N°. of unique data	994	715	2518
Transmission			
min	0.693	0.684	0.660
max	0.785	0.782	0.780

Table 3.2: Data processing details for Experiment 4.

S.U.N.Y/Buffalo and Risø software. Integrated intensities and esds were obtained by the Lehmann-Larsen method and a Lorentz correction applied. A numerical absorption correction was made using a 14 × 14 × 14 grid and a μ of 1.299mm^{-1}. The incoherent scattering cross-section for hydrogen, σ_H, was taken as 41.25 barns from a study made at ILL [15].

Experiment 5

The data from Experiment 5 were all processed using the *DREAM* [5] group of programs. Data were treated in four blocks as outlined below. The Lehmann-Larsen method of integration was used and Lorentz and polarisation corrections were applied. Data within each block were scaled according to the measurements of the standard reflections, however, little decay was observed. A proportionality factor was also calculated from analyses of the variation of the standards and included in the esds. An absorption correction, by Gaussian integration, was made using an $8 \times 8 \times 8$ grid. The linear absorption coefficient, μ, was 1.37mm^{-1} and the crystal volume 0.08mm^3. A correction was also made for absorption by the glass capillary (0.5mm diameter, 0.1mm thickness) using the program *ABSORB* [16].

The four blocks of data, in total 30571 observations, were put on a common scale with the following inter-batch scale factors:

Block	1	2	3	4
θ range (°)	0 - 30	0 - 30	30-45	45-50
	list driven 30-50			
Hemisphere	-ve k	+ve k	+ve k	+ve k
N°. of data	9727	5892	10541	4411
with F^2 $2\sigma(F^2)$	9151	5484	7158	2008
Scaling factors				
minimum	0.9987	0.980	0.969	0.988
maximum	1.012	1.004	1.018	1.009
Crystal transmission				
min	0.682	0.685	0.724	0.740
max	0.854	0.854	0.838	0.840
Capillary transmission				
min	0.966	0.973	0.967	0.964
max	0.978	0.978	0.978	0.977
Total transmission				
min	0.667	0.670	0.707	0.723
max	0.834	0.834	0.816	0.812

Table 3.3: Data processing details for Experiment 5.

Data Block	1	2	3	4
Scale factor	0.951(2)	1.047(2)	1.00	1.060(3)

and after averaging gave a total of 19228 unique data with a merging R of 0.0283.

Least-squares refinements

Experiments 1, 3 and 4

For the neutron diffraction experiments, Experiments 1, 3 and 4, the structure refinements were initiated from the preliminary room temperature X-ray derived models of the non-hydrogen atoms [18, 19]. In Experiment 1 the hydrogen atoms were located from difference Fourier maps. In Experiments 3 and 4 the initial hydrogen atomic positions were calculated by extending the C-H bond length to 1.1Å along the X-ray determined bond vector. Coherent neutron-scattering lengths (fm) for H (−3.7409), D (6.674), C (6.6484) and Cl (9.5792) were taken from the tabulation of Koester [3]. The refinements were carried out by full-matrix least-squares methods using the program *UPALS* [20]. The residual

$$\sum w[|\mathrm{F}(\mathbf{h})|^2_{\mathrm{obs}} - |\mathrm{F}(\mathbf{h})|^2_{\mathrm{calc}}]^2 \tag{3.33}$$

was minimized with weights

$$w = [\sigma(|\mathrm{F}(\mathbf{h})|^2_{\mathrm{obs}}) + (0.02|\mathrm{F}(\mathbf{h})|^2_{\mathrm{obs}})^2]^{-1} \tag{3.34}$$

in all three cases. An extinction correction was applied using the Becker and Coppens formalism for a Type I crystal with an isotropic Lorentzian distribution of mosaic blocks.

The variable parameters refined were as follows:- The atomic coordinates and anisotropic adps for all atoms and an extinction parameter were refined in all three cases. A single scale factor was refined for Experiments 1 and 3 and three separate scale factors and extinction parameters were refined for each of the three blocks of data in Experiment 3. In addition, the scattering lengths

	Experiment 1	Experiment 3	Experiment 4
N°. of Reflections	4374	5575	3989
Reflections deleted:			
due Al powder line contamination	38	0	30
due to Extinction	4	0	9
correction >	$1.45\times\|F(\mathbf{h})\|^2_{obs}$		$1.30\times\|F(\mathbf{h})\|^2_{obs}$
Agreement Factors:			
$R(F^2)$	0.0516	0.0596	0.0624
$wR(F^2)$	0.0616	0.0649	0.0835
S	1.114	1.044	2.110

Table 3.4: Refinement details for Experiments 1, 3 and 4.

at the 8 H/D atom sites were refined for the selectively deuterated sample studied in Experiment 1.

The refinements converged ($\Delta p_i/\sigma(p_i) < 0.002$) with agreement factors as given in Table 3.4. Further details of the refinements for these three experiments are also given in Table 3.4. In the final difference Fourier maps, the largest $|\Delta\rho|$ errors were $\sim 1.16\%$ and $< 1\%$ of the peak maximum of a chlorine atom in the ρ_o map for Experiments 1 and 3 respectively.

Experiment 2

The structure was solved by direct methods using the Shelxtl-Plus [21] package. Full-matrix least-squares refinement on $|F(\mathbf{h})|$ of 268 parameters against 2824, observed data $F(\mathbf{h}) \geq 2\sigma(F(\mathbf{h}))$, was also carried out using Shelxtl-Plus. Positional parameters were refined for all atoms, anisotropic adps were refined for all non-hydrogen atoms. A fixed isotropic adp, $U_{iso} = 0.08\mathring{A}^2$, was assigned to the hydrogen atoms, located from difference Fourier maps. An extinction correction was also made, of the form:-

$$F(\mathbf{h})^* = F(\mathbf{h})\sqrt[4]{\frac{1+0.002\chi F(\mathbf{h})2}{\sin(2\theta)}} \tag{3.35}$$

where $\chi = 0.00015(1)$.

The refinement converged with agreement factors R_w(F) 0.0381, R(F) 0.0501 and S of 1.27. The weighting scheme was of the form

$$w = \frac{1}{\sigma^2(\mathrm{F}(\mathbf{h})) + 0.0001\mathrm{F}(\mathbf{h})^2} \tag{3.36}$$

The minimum and maximum residual electron densities were -0.39eÅ^{-3} and 0.33eÅ^{-3}.

Experiment 5

Due to the extensive nature of this data set, $\sin\theta_{max}/\lambda = 1.08$Å^{-1}, a number of refinements, using different sections of the data, could be carried out. All refinements reported in this chapter were made using a spherical atom model with the program *UPALS*[20]. Atomic scattering factors for the carbon and chlorine atoms were taken from Doyle and Turner [22] while for the hydrogen atoms, the values of Cromer and Mann were used [23]. Anomalous dispersion contributions were from Cromer and Liberman [24]. Positional coordinates and anisotropic adps were refined for all non-hydrogen atoms. Hydrogen atom positions and thermal parameters were taken from the neutron study, also carried out at 123K (Experiment 4). Three sets of refinements, details of which are given in Table 3.5, were performed:-

1. Against all data with $|\mathrm{F}(\mathbf{h})|^2_{\mathrm{obs}} > 0$, which will be referred to as FULL.
2. Against all data satisfying the same criterion and with $\sin\theta/\lambda < 0.8$Å^{-1}, which will be referred to as LO (Low Order).
3. Against all data, again with $|\mathrm{F}(\mathbf{h})|^2_{\mathrm{obs}} > 0$ and $\sin\theta/\lambda > 0.8$Å^{-1} referred to as HO (High Order).

Results from all these refinements are given in the form of tables of atomic coordinates, atomic displacement parameters, bond lengths and angles in Appendix A.

Refinement	FULL	HO	LO
$\sin\theta/\lambda$ range (Å^{-1})	0-1.08	0.8-1.08	0-0.8
No. of data	19228	11322	7906
$R(F^2)$	0.0658	0.1038	0.055
$wR(F^2)$	0.0973	0.1119	0.0789
S	1.3817	1.2729	1.3919

Table 3.5: Details of the refinements using the X-ray data from Experiment 5.

Bibliography

[1] M.S. Lehmann and F.K. Larsen (1974). *Acta Cryst.* **A30**, 580-584.

[2] J. De Meulenaer and H. Tompa (1965). *Acta Cryst.* **19**, 1014-1018.

[3] P.J. Becker and P. Coppens (1974). *Acta Cryst.* **A30**, 129-147.

[4] Texsan Structure Analysis Software, Molecular Structure Corporation.

[5] R.H. Blessing (1987). *Cryst. Rev.* **1**, 3-58.

[6] W.C. Hamilton, J.S. Rollett and R.A. Sparks (1965). *Acta Cryst.* **18**, 129-130.

[7] L.E. McCandlish, G.H. Stout and L.C. Andrews (1975). *Acta Cryst.* **A31**, 245-249.

[8] Karle, Hauptman and Christ (1958). *Acta Cryst.* **11**, 757.

[9] D. Schwarzenbach, S.C. Abrahams, H.D. Flack, W. Gonschorek, Th. Hahn, K. Huml, R.E. Marsh, E. Prince, B.E. Robertson, J.S. Rollett and A.J.C. Wilson (1989). *Acta Cryst.* **A45**, 63-75.

[10] P. Seiler (1992). in *Accurate Molecular Structures: Their determination and importance*, edited by A. Domenicano and I. Hargittai, IUCr Monographs on Crystallography, OUP.

[11] F.L. Hirshfeld and D. Rabinovich (1973). *Acta Cryst.* **A29**, 510-513.

[12] *International Tables for X-ray Crystallography*, Vol III, (1968). edited by C.H. MacGillavry and G.R. Rieck. England:Kynoch Press.

[13] T.F. Koetzle and R.K. McMullan (1980). *Research Memo C-4*, Brookhaven National Laboratory.

[14] J.A.K. Howard, O. Johnson, A.J. Schultz and A.M. Stringer (1987). *J. Appl. Cryst.* **20**, 120-122.

[15] C. Frost. Stagiaires report, ILL, Grenoble.

[16] G.T. DeTitta (1985) *J. Appl. Cryst.* **18**, 75-79.

[17] L. Koester (1977) *Springer Tracts in Modern Physics,* **80**, Neutron Physics, edited by G. Höhler, Berlin: Springer.

[18] K. MacKenzie, J.A.K. Howard, E.C. Gravett, K.B. Astin, Liu Shi-Xiong, A.S. Batsanov, D. Vlaovic, J.P. Maher, M. Murray, D. Kendrew, C. Wilson, R.E. Johnson, T. Preiβ and R. Gregory (1993). *J. Chem. Soc. Perkin. Trans.* 2, 1211-1228.

[19] A.S. Batsanov (1992). Personal Communication.

[20] J.O. Lundgren (1982). *UPALS; A Full-Matrix Least-Squares Refinement Program.* Report UUICB13-4-05, Institute of Chemistry, University of Uppsala, Uppsala, Sweden.

[21] G.M. Sheldrick (1986). SHELXTL-Plus, Program for Crystal Structure Determination, University of Gottingen.

[22] P.A. Doyle and P.S. Turner (1968). *Acta Cryst.* **A24**, 390-399.

[23] D.T. Cromer and J.B. Mann (1968). *Acta Cryst.* **A24**, 321-324.

[24] D.T. Cromer and D. Liberman (1970).*J. Chem. Phys.* **53**, 1891-1898.

Chapter 4

Structural Results and Discussion

This chapter contains a report of the results of the neutron studies of KM5, KM22 and KM25 (Experiments 1, 3 and 4), the X-ray study of KM9 (Experiment 2) and some of the refinements made using the X-ray data for KM25 (Experiment 5). The details for all these refinements were given in Chapter 3. All the refinements converged without particular difficulty and there was no structural disorder, although this has been observed in certain of the pyrazoline structures [1].

The discussion is organised in the following manner. The first section, Section 4.1, discusses and compares the results of the studies of KM5 and KM9. These compounds form a pair of isomers. However, there are important differences between the experimental data sets for the two compounds which will be discussed below.

The following section, Section 4.2, describes the structural changes accompanying the rearrangement. The rearrangement clearly may be seen to have taken place from comparisons of the structures of the starting isomers, KM5 and KM22 with the rearranged products, KM9 and KM25.

Section 4.3 moves the discussion from individual pairs of isomers onto

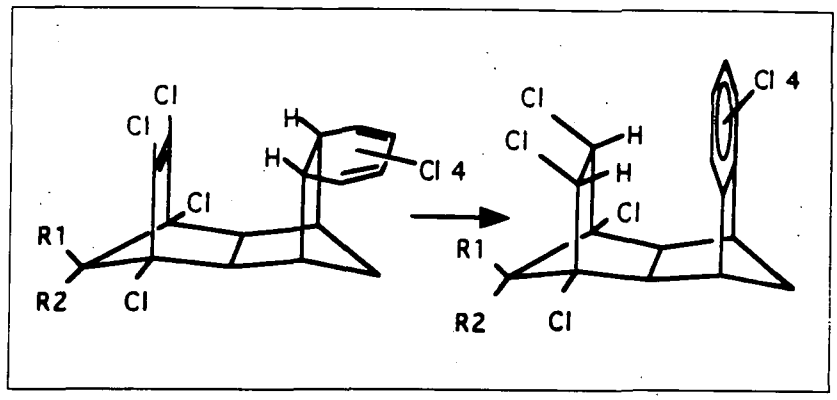

Figure 4.1: The compounds under discussion: KM5:KM9 where $R^1 = R^2 = Cl$, KM22:KM25 where $R^1 = H$, $R^2 = Cl$, and KM24:KM27 where $R^1 = R^2 = H$.

trends across the series of trienes and Section 4.4 discusses some of the thermochemical factors involved.

The final section of the chapter, Section 4.5, contains a detailed discussion of the structure of KM25 as determined by neutron and X-ray studies, both made at 123K (Experiments 4 and 5). The X-ray data set was collected to a much higher $\sin\theta/\lambda$ limit (of $1.08 Å^{-1}$) than is customary for most standard structural studies. This extended data set was collected in order to carry out a charge density study which will be discussed in Chapter 5. However, as well as the refinements discussed therein several refinements were made using a conventional Independent Atom Model (as described in Chapter 3) and different subsets of the data. The results from these refinements are discussed and compared, both with one another and with the results from the neutron study of the same compound.

4.1 Studies of KM5 and KM9.

It is the first time that data have been measured for these two compounds. However, although they form a pair of isomers, there are important differences

in the two sets of experimental data which should be taken into consideration when comparing the two structures. KM5 was studied at 15K using neutron diffraction data whereas KM9 was studied at room temperature using X-rays. The differences are particularly evident in the parameters for the hydrogen atoms and in all the atomic displacement parameters.

The effect of the temperature differences on the adps is illustrated by Figure 4.2. The atomic displacement parameters averaged over U_{11}, U_{22} and U_{33} are 9.6 times larger for KM9 at room temperature for the chlorine atoms and 7.8 times larger for the carbon atoms. For example, the value of the atomic displacement U_{33} for Cl(7) is 0.0660(9)Å^2 in KM9 at room temperature and 0.0066(3)Å^2 for KM5 at 15K.

In general, the chlorine atoms show greater thermal motion than the carbon atoms which is not usually the case for heavier atoms (1.54 times greater on average for KM9 and 1.24 for KM5). However, all the carbon atoms are involved in a very rigid framework whereas the chlorine atoms are terminally bound. A larger difference is seen for the hydrogen atoms where the average of the vibrational amplitudes is 2.7 times larger than those of the ligated carbon atoms in KM5 at 15K. No comparable data are available for KM9 as the hydrogen atoms were all constrained to have a U_{iso} of 0.08Å^2.

There are some differences between the two experiments in the precision of the refined parameters for the non-hydrogen atoms. For the chlorine atoms, the esds on the positional parameters from the two refinements are about equal but those of the adps are a factor of three larger for KM9. For carbon, the positional parameter esds are typically a factor of three larger for KM9 while those on the adps are around seven times greater. However, as expected, a far bigger difference is seen for the hydrogen atom coordinates where the ratio of esds(KM9:KM5) is approximately eighteen.

Other differences are also observed in the hydrogen positional parameters.

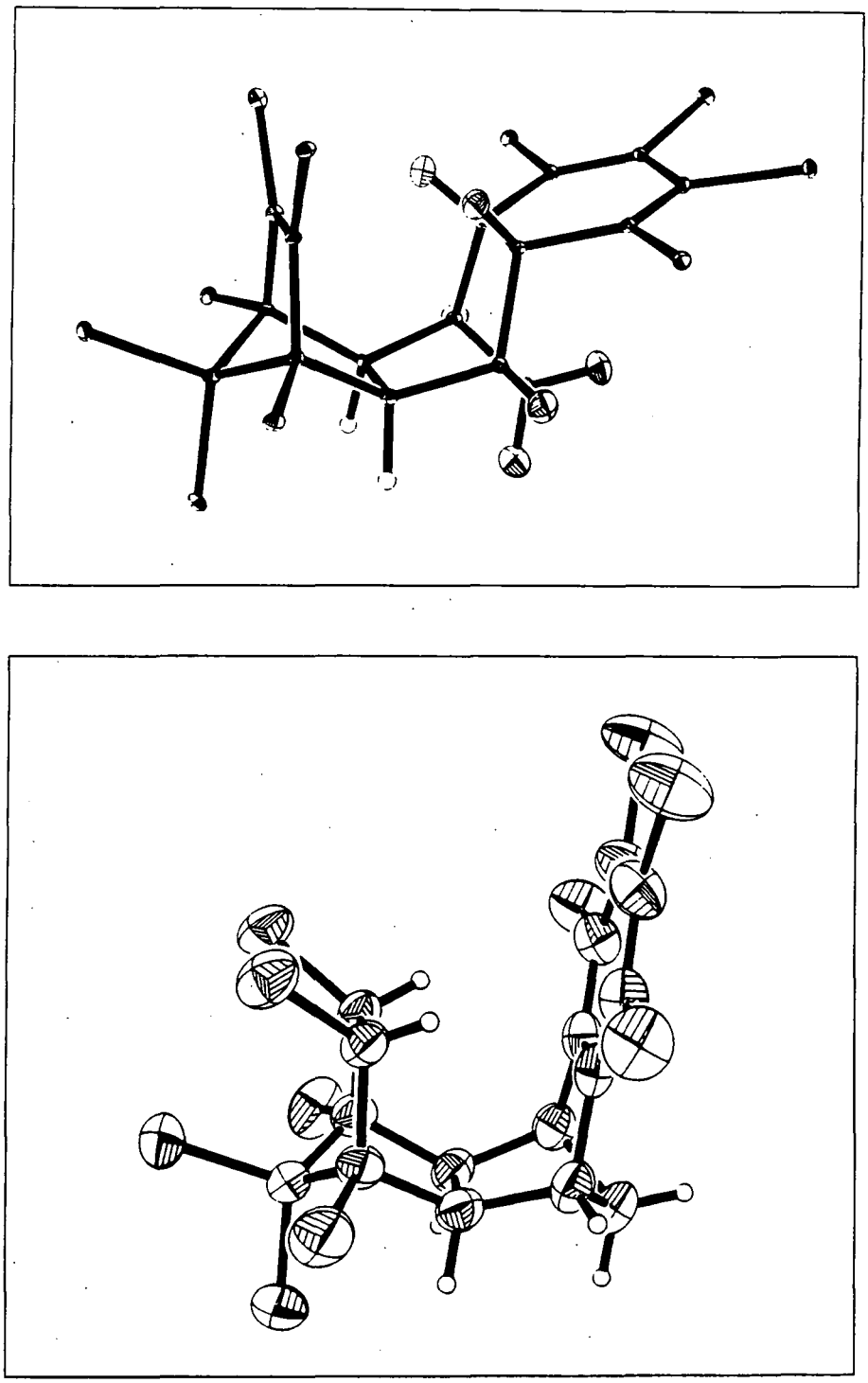

Figure 4.2: Thermal ellipsoid plots of KM5 and KM9 drawn at 50% probability level.

These differences are due to the displacement of the centroid of the electron density around the hydrogen atom from the nuclear position towards the ligated carbon. This results in shorter C–H bond lengths being observed in X-ray studies than in neutron work; average value of C–H bond length in Experiment 2 is 0.99(4)Å and 1.094(4)Å in Experiment 1.

The sample of KM5 used in Experiment 1 was selectively deuterated. The difference between hydrogen and deuterium cannot be seen by X-rays in terms of different scattering power. An attempt was made to distinguish the two isotopes using X-ray data by Seiler *et al* [2] on the basis of the different vibrational behaviour of the two hydrogen isotopes. This study showed that the data were just on the limit of the precision needed for such detailed comparisons. However, the neutron scattering lengths are very different for the two hydrogen isotopes [3] , $b_H = -3.7409$fm for H and $b_D = 6.674$fm for D and hence they can be distinguished easily. By assuming the occupancy to be 1.0 at each of the hydrogen atomic sites and refining the scattering length as part of the least-squares refinements, the degree of deuteration was calculated at each of the sites. The following relationship was used to convert the refined values, b_{ref}, of the scattering lengths for each of the i sites to the percentage deuteration,x :

$$x = \frac{b_{ref}(i) - b_H}{b_D - b_H} \times 100$$

The results are given in Table 4.1.

4.2 Structural Changes associated with the Rearrangement

As stated above, the compounds KM5 and KM9 form a pair of isomers, as do the compounds KM22 and KM25. Comparisons between this latter pair of isomers are rendered somewhat simpler as neutron data were measured for both isomers at the same temperature, 123K. This is the first time that neutron data have been collected for a pair of these dyotropic isomers at the

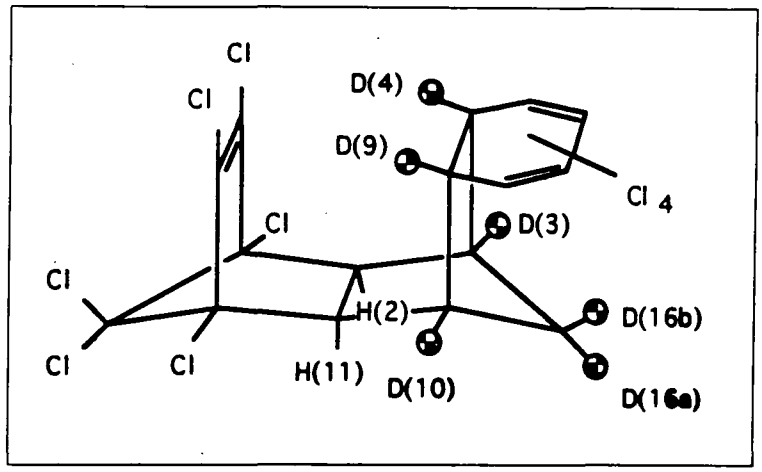

Atomic Site	b_{ref}	% deuteration from	
		Experiment 1	nmr study
D(3)	0.606(6)	94(1)	96.7
D(4)	0.649(6)	98(1)	97.6
D(9)	0.633(6)	97(1)	97.6
D(10)	0.586(6)	92(1)	96.7
D(16a)	0.593(6)	93(1)	95.8
D(16b)	0.584(6)	92(1)	96.6
H(2)	-0.365(6)	9(1)	
H(11)	-0.372(6)	2(1)	

Table 4.1: Percentage deuteration for KM5. Deuterated sites marked by patterned circles.

same temperature. Hitherto, neutron data have been collected for both isomers of only one other pair, that of KM24 and KM27; measured at 15K and 120K respectively. Although both X-ray and neutron data are available for the compound KM25 the results from the neutron study, Experiment 4, are used exclusively in this part of the discussion.

The gross structural changes predicted to be associated with the rearrangement can be seen to have taken place. The hydrogen atoms of the starting isomer have transferred from the H(4), H(9) positions (or D(4), D(9) positions in KM5) to those of H(13) and H(14) in the rearranged isomer. Changes have also occured in the geometry around the C(4)–C(9) and C(13)–C(14) bonds. The C(13)–C(14) separation has increased from that of a typical C=C bond in KM5 and KM22 to that of a C–C bond in isomers KM9 and KM25 (see Table 4.2). A parallel decrease can be seen in the C(4)–C(9) separation as it changes from a single C–C bond to an aromatic C–C bond.

Similarly, the bond lengths around the 6-membered ring (atoms C(4) to C(9)) alter with its aromatisation. In each of the starting isomers, KM5 and KM22, there are two significantly shorter bonds in the ring, C(5)–C(6) and C(7)–C(8), corresponding to the two C=C bonds, see Figure 4.3. As expected for an aromatic ring, the bond lengths become far more homogeneous in the rearranged isomers.

However, the largest positional changes due to the rearrangement are not those made by the two hydrogen atoms transferring, nor the changes described above but those of the 6-membered ring and the attached chlorine atoms. The program *OFIT* [4] was used to fit, by least-squares, specified atoms from one model to those of the other isomer in order to calculate the distance 'moved' by the atoms during the rearrangement. In all cases only the frame carbon atoms C(1) to C(4) and C(9) to C(14) were involved in the fitting. The largest changes in position are those of the chlorine atoms Cl(6) and Cl(7) which move 4.23Å and 3.75Å respectively for the pair of isomers KM5:KM9, and 3.71Å and

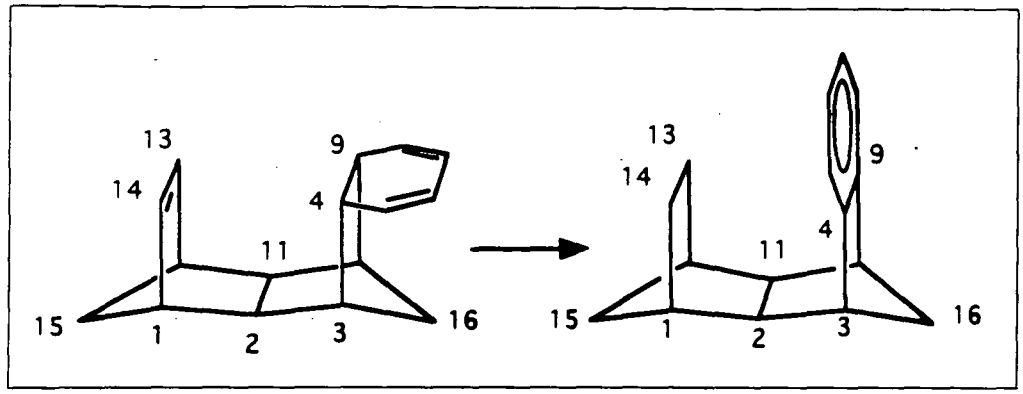

Compound	$d_{C(13)-C(14)}$	$d_{C(4)-C(9)}$	∠C(12)–C(13)–Cl(13)	∠C(1)–C(14)–Cl(14)
KM5	1.341(2)	1.569(2)	125.0(1)	124.6(1)
KM9	1.570(5)	1.397(5)	115.8(3)	114.9(3)
KM22	1.343(2)	1.572(1)	124.91(8)	124.92(8)
KM25	1.579(2)	1.397(2)	110.6(1)	112.6(1)
KM24	1.367	1.590	125.0	125.2
KM27	1.579	1.404	110.9	110.7

Table 4.2: Selected bond lengths (Å) with esds from least squares refinement given in parentheses. Values for KM25 taken from the neutron study at 123K (Experiment 4), those for KM24 and KM27 [17] are included for comparison.

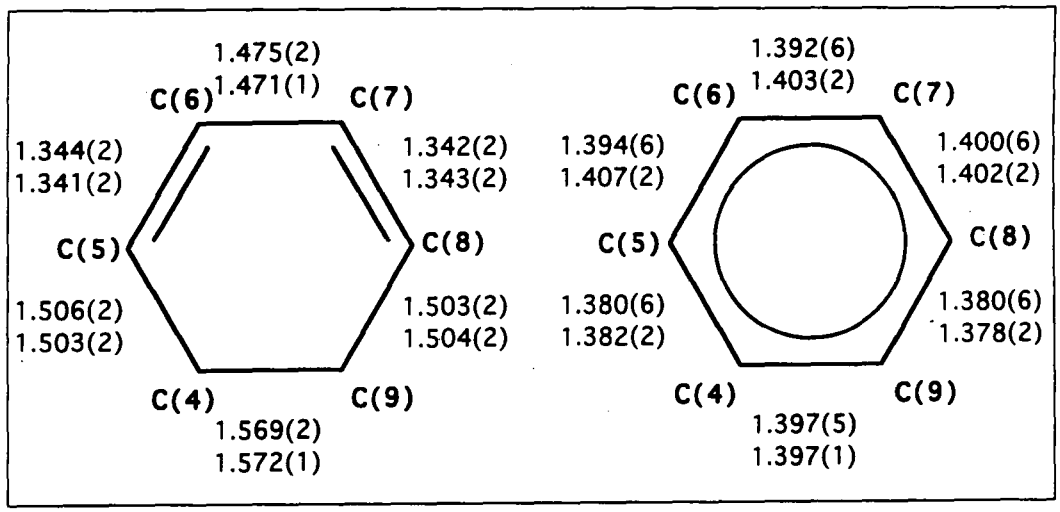

Figure 4.3: Bond lengths around the ring C(4) to C(9) for diene isomers KM5 and KM22 (below) on the left and for aromatic isomers KM9 and KM25 (below) on the right. All distances in Å with esds in parentheses.

3.51Å for the pair KM22:KM25. Other distances similarly calculated are given in Table 4.3.

Structural differences between the two isomers are also reflected in the relative orientations of certain planes. The values given were calculated using the program *MPLN* [4] which calculates the best least-squares plane through the specified atoms. From the fitted pairs of isomers the angle between the planes A and A′ is 60.9° for the KM5:KM9 pair and 55.4° for the pair KM22:KM25. Similarly for planes C and C′ the interplanar angles are 49.4° and 56.6° for KM5:KM9 and KM22:KM25 respectively.

The changes in the hybridisation of the carbon atoms, C(13) and C(14), from sp^2 to sp^3 are also indicated by the bond angles in the two pairs of compounds (see Table 4.2). In both cases the bond angles are slightly larger than the ideal angles of 120° and 109.5° (for sp^2 and sp^3 hybridisation). These deviations are predominantly due to ring strain, although they are in part caused by the inequivalence of the groups around the carbon atoms C(13) and C(14).

Another feature of interest shown by the *MPLN* results is the coplanarity of planes A′ and B in the rearranged aromatic isomers and of planes C and D in the starting isomers. The root mean square deviation from the plane for the eight atoms contained in planes A′ and B is 0.0049Å for KM9 and a little larger at 0.0331Å for KM25. For the starting isomers KM5 and KM22 the deviation from a plane fitted to the six atoms in planes C and D is 0.0174Å and 0.0132Å.

However, careful interpretation of the interplanar angles calculated by *MPLN* is required as the plane is fitted to the defining atoms in each case and the angle is not between the two planes hinged along the C(4)–C(9) or C(13)–C(14) internuclear vectors as might be imagined. Planes C and D both lie midway between atoms C(13) and C(14); C(13) and C(14) lie 0.0018Å to

Atom	KM5→KM9	KM22→KM25
H(4)–H(14)	†1.401	1.422
H(9)–H(13)	†1.254	1.411
C(5)–C(5a)	1.376	1.265
C(6)–C(6a)	2.551	2.307
C(7)–C(7a)	2.386	2.240
C(8)–C(8a)	1.148	1.162
Cl(6)–Cl(6a)	4.233	3.714
Cl(7)–Cl(7a)	3.748	3.509
Cl(13)–Cl(13a)	1.173	1.395
Cl(14)–Cl(14a)	1.328	1.443

Table 4.3: Calculated separations (Å) between selected atoms and their equivalents in the rearranged isomer. Values for KM22 and KM25 are taken from the neutron refinements (Experiments 3 and 4). † Hydrogen atom positions for KM9 were extended along the bond vector (as determined from the X-ray study) to a C-H bond length of 1.1Å. The shaded planes in the Figure below correspond to those of the diene.

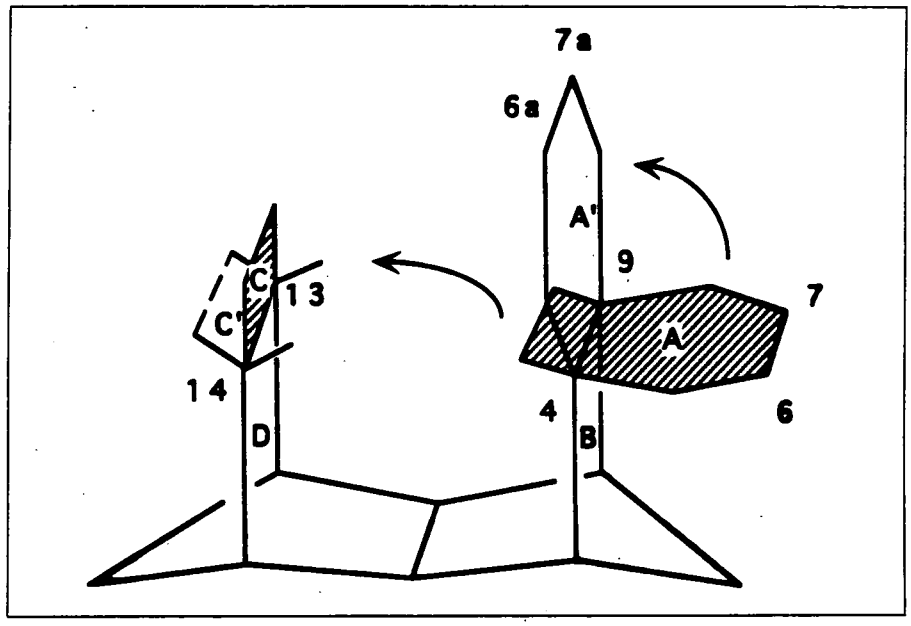

Compound	Atom		rms deviation atoms in plane D
	Cl(13)	Cl(14)	
KM5	-0.088	-0.063	0.0014
KM22	-0.070	-0.008	0.0022
KM24	+0.031	+0.055	0.0012
	Atom		rms deviation atoms in plane A′
	C(3)	C(10)	
KM9	-0.0134	-0.0034	0.0051
KM25	+0.117	+0.125	0.0122
KM27	+0.099	+0.110	0.0086

Table 4.4: Deviation out of plane (Å) for certain atoms. + signifies out of plane to the side of C(16).

opposite sides of Plane D and 0.0026Å to Plane C in KM5. Perhaps a more informative figure than the interplanar angle is the deviation of the two Cl atoms, Cl(13) and Cl(14), from plane D and of the atoms C(3) and C(10) from the plane of the aromatic ring plane A′ in the other isomers, (see Table 4.4).

The degree of tilt of Cl(13) and Cl(14) and its direction, *i.e.* towards or away from the reaction cavity, have been discussed previously [17] with reference to its implications on the π-density in the reaction zone. However, as pointed out above, these angles may be misleading and the deviations are relatively small when compared with the mean deviations from the plane of the atoms defining it.

4.3 The Trienes as a series

The comparisons made between the pairs of isomers given above clearly show the rearrangement to have taken place with the expected structural changes. They also show that different members of this series of compounds have very similar structures. The carbon skeleton, C(1) to C(4) and C(9) to C(14), has

a very rigid and effectively constant structure. The fit of these parts of the molecule is very close between pairs of isomers where the two isomers have different types of C(13)–C(14) and C(4)–C(9) bonds (root mean square deviation 0.0773Å and 0.0832Å for KM5:KM9 and KM22:KM25 respectively) and is even closer for two starting isomers, *e.g.* 0.0253Å for KM5 and KM22 fitted by the program *OFIT* [4]. This series of compounds therefore provides a system in which rather small structural changes can be investigated, particularly in relation to their rates of rearrangement.

One of the features which has been suggested to have a key effect on the rate of rearrangment is the separation, d_{CC}, across the reaction cavity of the donor and acceptor carbon atoms, and that between the transferring hydrogen atoms and the acceptor carbons, d_{CH}.

A series of syn-sesquinorbornene disulphones with various substituents, studied by Paquette [5], undergo a similar dyotropic rearrangement (see Figure 4.4). A close correlation was originally found between the separations d_{CC} and d_{CH}, as determined by X-ray crystallography, and the rate of rearrangement. The interpretation of the d_{CH} distances is somewhat optimistic given that all the data are from room temperature X-ray studies in which hydrogen positions are only poorly determined and one of these compounds (where X=CHMe) even showed some structural disorder. However, the d_{CC} distances do appear to follow a similar trend. Paquette stated that "modulation on the order of 0.1Å in the size of the intracavity gap is reflected in a rate spread greater than 10^4" [5]. A similar correlation is not observed for the trienes of our series either with the carbon-carbon separations d_{CC} (see Figure 4.5), or with the precise carbon-hydrogen separations d_{CH} determined from neutron diffraction data.

A further ambiguity in these distances is caused by the marked inequivalence of the two values of d_{CC} and d_{CH} in any given compound. This inequivalence is observed in both the trienes and the syn-sesquinorbonene disulphones.

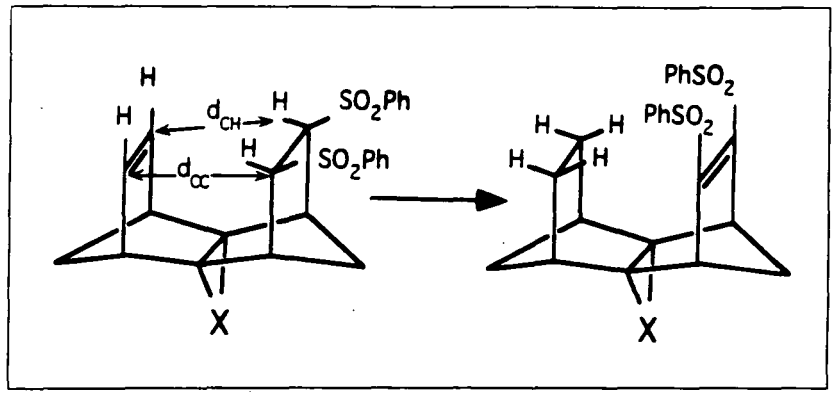

Figure 4.4: Syn-sesquinorbornene disulphones; another example of compounds which undergo a dyotropic rearrangement.

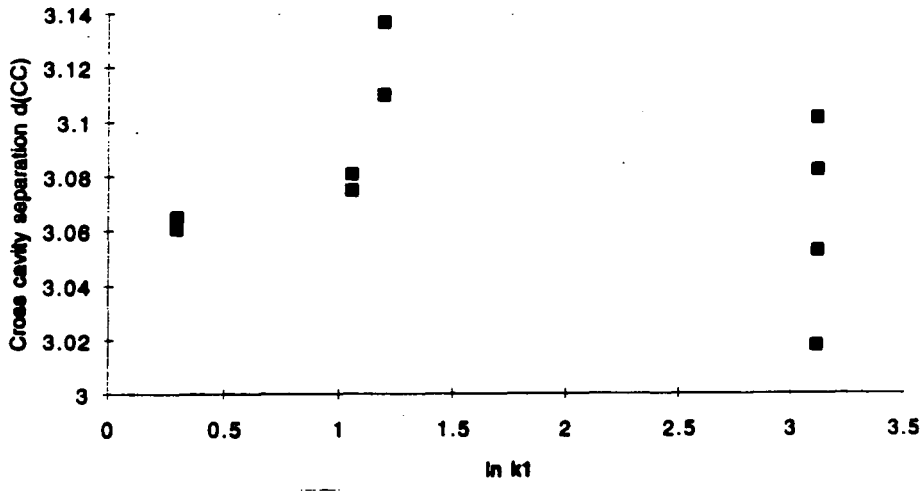

Figure 4.5: Plot of cross-cavity separations d_{CC} against $\ln k_1$ for trienes the trienes.

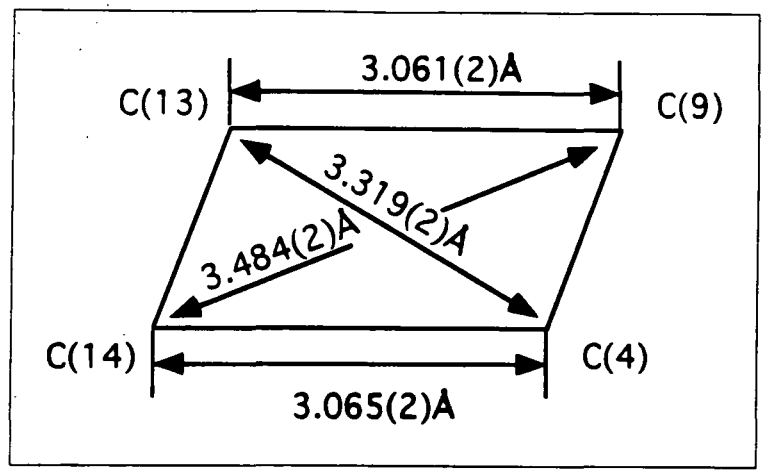

Figure 4.6: Separations across the reaction cavity of KM25 illustrating the asymmetry.

A-B-C	∠ A-B-C	A-B-C	∠ A-B-C
C(9)-C(4)-C(14)	95.3(1)	C(9)-C(13)-C(14)	91.61(9)
C(4)-C(9)-C(13)	87.95(9)	C(4)-C(14)-C(13)	84.83(9)

Table 4.5: Selected distances and angles within the reaction cavity of KM25.

From the symmetrical appearance of these compounds they might be expected to have a plane of symmetry bisecting the molecule lengthways, midway between C(13) and C(14), C(2) and C(11), C(4) and C(9) and passing through C(15) and C(16). This is not the case; there is neither chemical nor crystallographic symmetry in the solid state in any of these compounds. Even for compounds such as KM25 where the two d_{CC} values, 3.061(2)Å and 3.065(2)Å, are not significantly different there is no such mirror, as illustrated below in Figure 4.6.

Paquette ignores the inequivalence of the two cross-cavity separations and uses the average value for each compound in his discussion. However, in some cases the differences between the two values for a given compound are of the same order as those attributed to a 10^4 factor rate change, *e.g.* for the compound where X=O the d_{CH} separations are 2.60Å and 2.46Å.

In later work the situation appeared to be less clear [6]. Previously it had been thought that electronic effects would not be particularly important since the substituents were not directly attached to the acceptor/donor sites. However it was subsequently concluded that other effects played an important role in determining the rate of reaction, such as π-electronic effects, differences in strain energies and the energy required to stretch the key C–H bonds.

The most recent report [7] states that proximity of the two reacting groups is not the sole contributor to the differing rates of reaction. It suggests that steric interactions within the disulphones, although not necessarily affecting the cross-cavity separations, may alter the stability of the ground state and hence the rate. Several compression zones were defined but as the discussion is purely qualitative, it is difficult to make any meaningful comparison with the trienes under discussion here.

4.4 Energetic considerations and MM Calculations

MM (Molecular Mechanics) calculations were made on a number of compounds in the series of trienes. These calculations were made to investigate some of the thermochemical quantities which are expected to correlate with the rate, for example, the reactant strain energy, E_S, and the reactant-product π-energy differences, ΔE_π.

The dyotropic rearrangement of these trienes is markedly exothermic as suggested by the irreversible nature of the rearrangement and the fact that the reactions go to completion. Experimental results also provide evidence of the exothermic nature of these compounds; *e.g.* the experimentally determined enthalpy change of -22.63 kcal for KM24 and the sudden rise in temperature of the sample observed as the rearrangement takes place. The exothermicity is largely due to the release of resonance energy as the aromatic ring is formed.

The aromatisation is one reason for the generally higher activity of the trienes relative to the syn-sesquinorbornene disulphones.

In addition to the aromatisation there is also a contribution to the overall energy gain by the saturation of the π-acceptor bond, C(13)–C(14). Hence changes in the substituents on and around this bond affect the overall exothermicity of the reaction. Electron withdrawing substituents cause a drop in the π-energy, E_π, and consequently in the exothermicity and rate.

Across a family of compounds, changes in the rate are expected to reflect changes in the difference between the reactant and product π-energy, ΔE_π. A convincing linear relationship between ΔE_π and $\ln k_1$, is not observed except over a very narrow range of compounds [1] (see Figure 4.7). The narrow range in this example is over compounds KM5, KM23 and KM24. KM22 deviates significantly from this limited linear relationship. It was suggested that this deviation might have been due to the exceptionally long d_{CH} separations (2.587Å) across the reaction cavity which was determined by X-ray crystallography. However, with the benefit of the neutron diffraction derived values from Experiment 3 of 2.376(3)Å and 2.393(3)Å, it can be seen that the separation are well within the normal range of values (2.25-2.46Å).

Exothermic reactions are believed to have reactant-like transition states since very little structural change is needed to reach the transition state. Correlation of the reactant strain energy, E_s, with $\ln k_1$ is also expected; the more strained the molecule the easier it is to reach the transition state, the lower the activation energy and the faster the rate. The product strain energy does not affect the rate of reaction in exothermic rearrangements. The strain energy has a much smaller effect than the π-energy on the rate. Again a linear relationship is not observed except over the same narrow range, see Figure 4.8, and other trienes in the series, especially the very reactive KM17, show no such correlation.

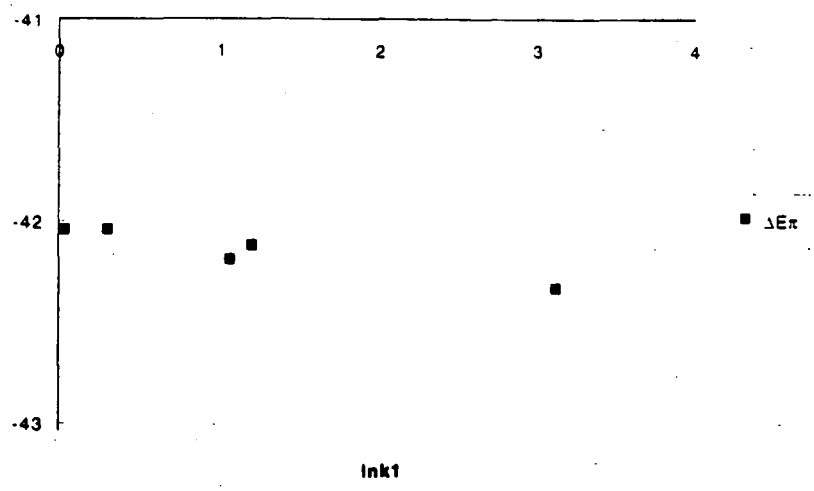

Figure 4.7: Plot of ΔE_π against $\ln k_1$ for the trienes.

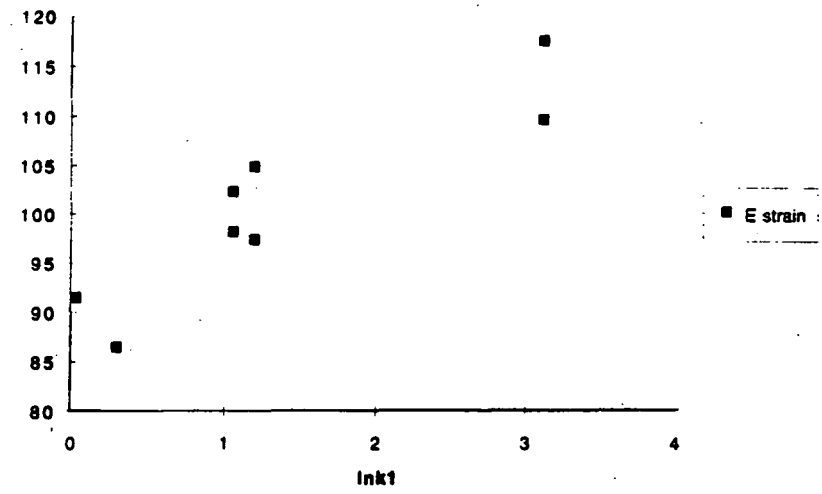

Figure 4.8: Plot showing E_s against $\ln k_1$ for the trienes.

The correlation between the rate and the strain and π-energy may indeed be as outlined above and the apparent lack of a linear relationship due to shortcomings of the MM calculations. The intracavity distances d_{CH} and d_{CC} do not agree closely with the experimental values from the crystallographic studies nor do they follow the same trends. Figure 4.9 clearly shows that the correlation between the MM calculated separations and the experimentally determined values is far from perfect. Furthermore, the observed inequivalence of the d_{CC} and d_{CH} distances in a given compound is not modelled by the MM calculations for the trienes. Recent calculations on compounds which are asymmetrically substituted (see Figure 4.10) show asymmetry but experimentally observed asymmetry in symmetrically substituted compounds is not reflected in the calculated values. Calculations based on models which agree more closely with the experimentally determined structures may show clearer correlations.

4.5 Conventional refinements of the structure of KM25

The apparent lack of a simple relationship between the structure of these compounds and their reactivity, combined with the greater emphasis on their electronic properties has prompted a new programme of more detailed studies of the trienes. The first of these studies has been made of KM25.

An extensive X-ray and a neutron data set have been collected at 123K (Experiments 4 and 5) and have been used to investigate the electron density distribution in KM25. A more sophisticated model has been used in this study, details of which are given in Chapter 5.

Refinements have also been carried out using a more conventional independent atom model, IAM. Several refinements were made against subsets of the X-ray data as well as the full X-ray data set and against the neutron data (see

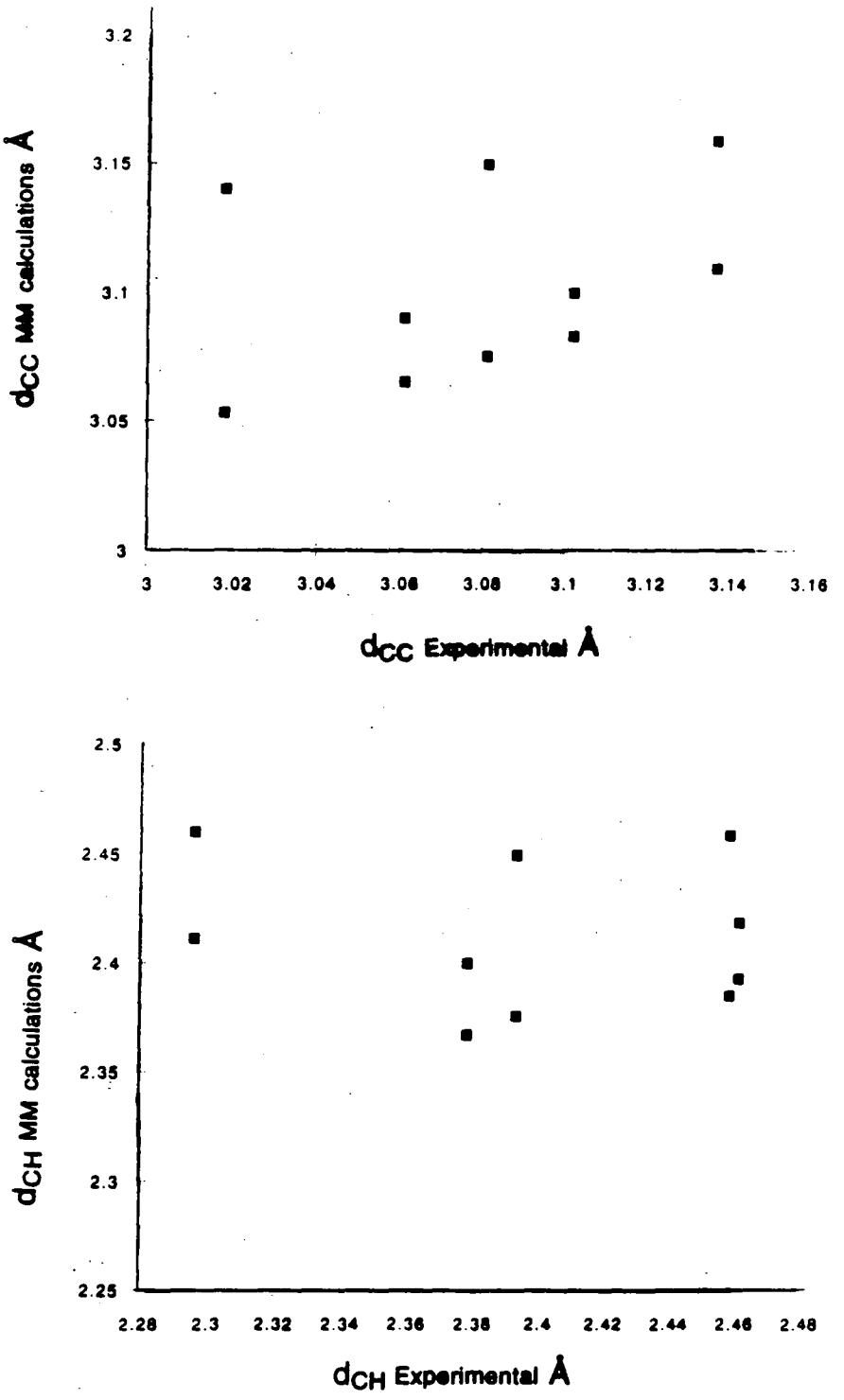

Figure 4.9: Plots of d_{CC} and d_{CH} from crystallographic studies versus those from MM calculations.

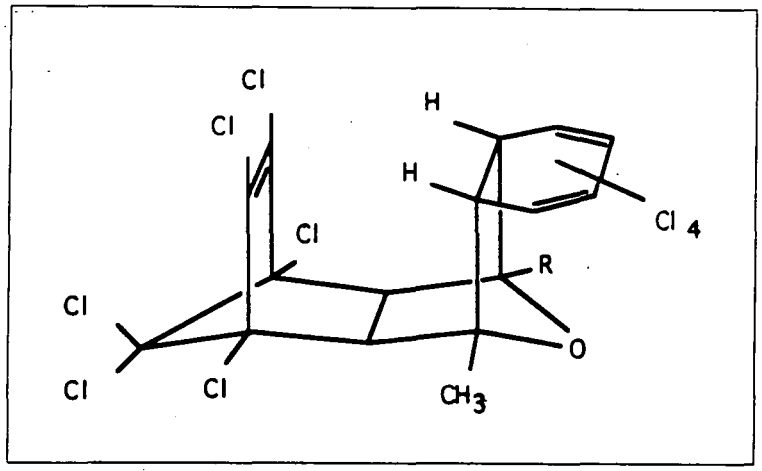

Figure 4.10: Asymmetrically substituted compounds. R = H, CH_3

Table 4.6). The results are discussed below.

Refinement	RT	LO	HO	FULL	N
Radiation λ (Å)	Mo K_α X-radiation 0.7107				neutron 1.04
Temperature (K)	298	123			
$\sin\theta/\lambda$ range ($Å^{-1}$)	0-0.65	0-0.8	0.8-1.08	0-1.08	0-0.62
Number of data	3852	7906	11322	19228	3989 *
$R(F^2)$	0.0335 †	0.055	0.1038	0.0658	0.0624
$wR(F^2)$	0.0397	0.0789	0.1119	0.0973	0.0835
S	2.102	1.3919	1.2729	1.3817	2.110

Table 4.6: Details of refinements made for KM25. †Refinement made against $|F|$ not $|F|^2$ therefore the agreement factor given is R(F) not $R(F^2)$. Formulas of agreement factors are given in the glossary. * not unique data.

As a result of chemical bonding the electron density distribution is deformed relative to a spherical distribution of electrons around the atomic nuclei. The atomic positions obtained from X-ray studies correspond to the centroids of the electron density peaks and will be biased by such a redistribution. The adps will also be biased as they often absorb some of the deviations from sphericity that these peaks show. This bias on positional and thermal parameters has

important consequences in studies of the charge density (see Chapter 5).

There are two main approaches to reducing the aforementioned bias. The first is to use neutron data. Atomic positions derived from neutron experimental data are unbiased by the electron distribution and so truly correspond to the nuclear positions. The adps are also closer to the atomic vibrations than those from standard X-ray refinements. Therefore, as well as the essential use of neutrons to obtain accurate information on the critical hydrogen atoms, neutron studies have an important role to play in the investigation of electron densities when combined with X-ray data.

However, the combined use of data sets from separate experiments presents certain difficulties in ensuring that they are compatible. Neutron studies demand much larger samples than X-ray work (see Chapter 2), so the experiments are not carried out on the same crystal. Equally, ensuring that the temperature is identical in both experiments can be problematic. There is also the added problem of obtaining beam time for neutron experiments which are necessarily made at central facilities.

In an attempt to avoid some of these difficulties an alternative approach has been developed to obtain unbiased atomic positions and adps solely from X-ray data. This approach uses only the high order data to refine the structural model and such refinements are often called high order refinements (HO in Table 4.6). These refinements rely on the assumption that the valence electrons of many atoms do not contribute significantly to X-ray scattering at high values of $\sin\theta/\lambda$.

Examination of the scattering factors of Cromer and Waber [8], which are partitioned into those of core and valence electrons, shows the valence scattering of the chlorine atom to be less than 10% of its maximum value at $\sin\theta/\lambda$ of 0.3Å^{-1}. Provided that the core electrons are not affected significantly by bonding and that bonding features do not contribute to high order scattering,

then the results of a high order refinement should be free of the bias caused by deviations from sphericity in the electron distribution.

The lower limit of such 'high order' refinements is somewhat arbitrary and has been steadily rising in recent years. The rise in cut-off value is partly due to improved experimental conditions allowing collection of a greater quantity of more precise high angle data and partly due to evidence in a number of studies that sharp deformation density features may scatter to high $\sin\theta/\lambda$ values. In the study of KM25 a lower limit of 0.8Å^{-1} was chosen since it gave an acceptable refinement and no residual features indicating asphericity were found in the difference Fourier maps (see Figure 4.13).

Since X-ray and neutron data collected at the same temperature were available for KM25 both approaches could be tried and compared. In the following discussion all comparisons were made only between non-hydrogen atoms, as the parameters resulting from the neutron refinement were used in all the X-ray refinements. Differences quoted as being significant are those where the difference, Δ, was greater than $3\sigma_c$ where

$$\sigma_c = \sqrt{\sigma^2(p_i) + \sigma^2(p_j)} \tag{4.1}$$

and $\sigma(p_i)$ and $\sigma(p_j)$ are the esds from the least-squares refinements i and j on parameter p.

Bond lengths and angles from all the refinements (HO, LO, FULL and N) agree well, even those from the RT refinement only disagree significantly with the HO values for the C(1)–C(15) bond; RT value 1.547(2)Å and HO 1.556(1)Å. The bond lengths cited here and in Table 4.7 are from the neutron study, although all the bond lengths from the HO refinement agree within three esds (see Figure 4.11). The asymmetry observed in the d_{CC} distances (see above) is also observed in the rest of the structure, in all the refinements; bond lengths C(1)–C(14) and C(12)–C(13) differ significantly at 1.541(2)Å and 1.553(2)Å. Other bond lengths illustrating this lack of symmetry in the solid

state are given in Table 4.7. Such close agreement in the bond lengths from the various refinements suggests that the positional parameters do not differ greatly.

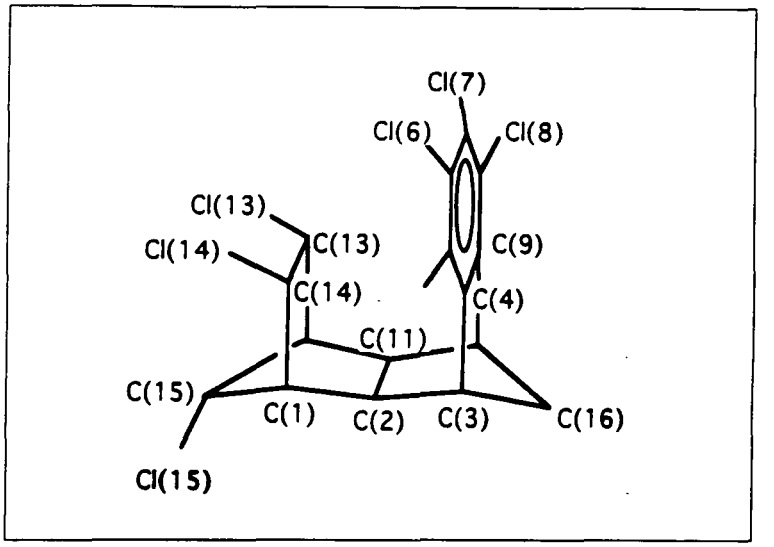

A-B	d_{AB}	A-B	d_{AB}
C(1)-C(2)	1.541(2)	C(11)-C(12)	1.548(2)
C(2)-C(3)	1.565(2)	C(10)-C(11)	1.555(2)
C(3)-C(4)	1.517(2)	C(9)-C(10)	1.498(2)
C(1)-C(14)	1.541(2)	C(12)-C(13)	1.553(2)

Table 4.7: Selected bond lengths for KM25 taken from the neutron study, refinement N; esds from the least-squares refinement given in parentheses.

Comparison of neutron and X-ray results

An initial comparison of the positional parameters, x,y and z, was made by examining the ratio $\Delta/\sigma(\Delta)$. Δ is the difference between a particular parameter, p_i, from the two refinements HO and N

$$\Delta = p_i(N) - p_i(HO)$$

and $\sigma(\Delta)$ is the error on Δ calculated as

$$\sigma(\Delta) = \sqrt{\sigma^2(p)_N + \sigma^2(p)_{HO}}$$

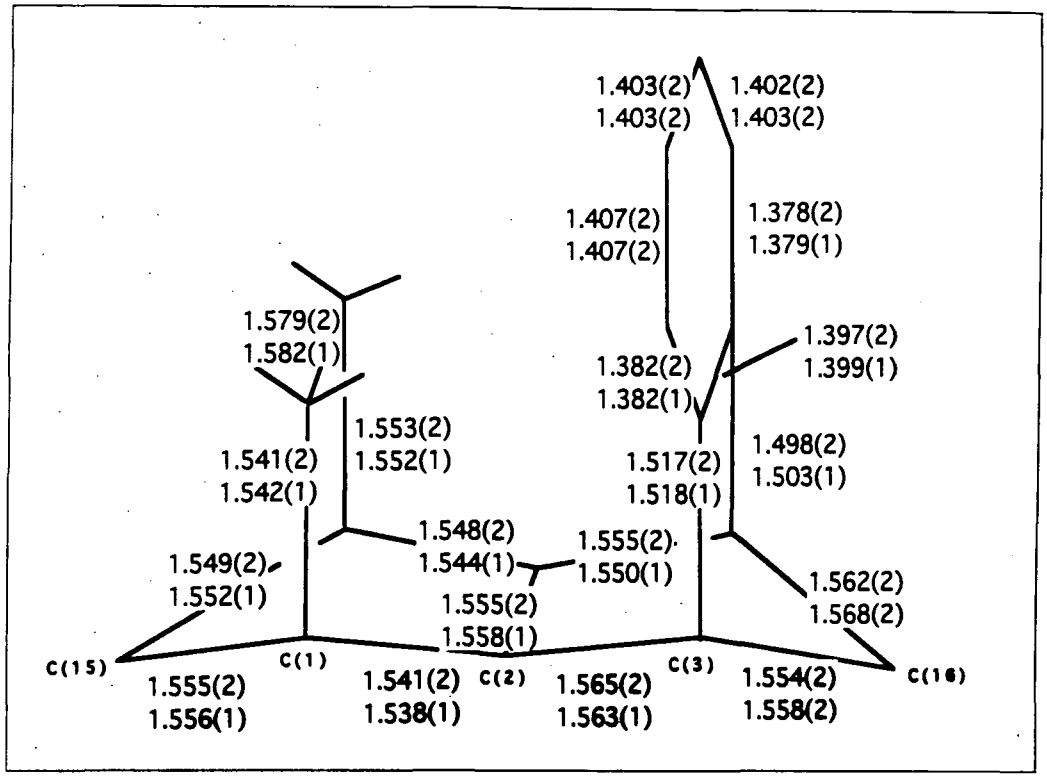

Figure 4.11: Carbon–Carbon bond lengths (Å) from N and HO (values given below) refinements with least squares esds in parentheses.

This showed that all the positional parameters for the carbon atoms, C(1) to C(16), from the two sets agree within 3σ except for the fractional coordinate z of C(13) where $\Delta/\sigma(\Delta)$ is 3.2.

The ratio $p_i(N)/p_i(HO)$ is very uniform over the positional parameters. The mean value of this ratio is 1.000(2) where the value given in parentheses is the variance. The variance gives an indication of the spread of values and in this case is of approximately the same order as the least-squares derived esds on the coordinates themselves. As might be expected the agreement between the parameters from the separate X-ray refinements is even closer, with a mean ratio $x(HO)/x(LO)$ of 1.0001(8).

However, as has been seen in a number of studies comparing neutron and X-ray results, such good agreement is not seen when comparing the adps from

these refinements. Comparisons were made using the parameters β_{ij} from the least-squares refinements. The β_{ij}s are dimensionless anisotropic temperature factor coefficients defined with respect to the crystal axis system. They must then be transformed to an orthogonal systen to obtain the U_{ij} values which have dimensions of $Å^2$ and were discussed in Chapter 3. Not only do the ratios $\beta_{ii}(N)/\beta_{ii}(HO)$ deviate significantly from unity (see Table 4.8) but there is also a much greater spread of ratios for the individual parameters than was observed in the positional parameters.

	carbon	chlorine	All non-H
β_{11}	0.84(6)	0.94(5)	0.88(7)
β_{22}	0.97(5)	0.99(4)	0.98(5)
β_{33}	1.03(5)	1.07(2)	1.04(5)

Table 4.8: Ratio of adps N:HO refinements.

The adps will differ if the two experiments (Experiments 4 and 5) were carried out at different temperatures. Such temperature differences should be reflected in the unit cell parameters. Impressive agreement was found for the parameters a and b (see Table 4.9). However, significant differences were found for the interaxial angle β. This problem has been noted in several other studies. Klooster *et al* [9] made considerable efforts to match the cell parameters from the X-ray and neutron studies of 1-methyluracil, even recollecting the X-ray data and still found significant differences in the cell parameters.

With the disagreement as it stands, the relatively small changes (for example, in γ on cooling from room temperature to 123K) and the precision of the cell parameters it is unfortunately impossible to rule out some difference in temperature. The parameter differences suggest that it is the neutron experiment which was carried out at the higher temperature. This seems unlikely as although flow type cooling devices often show temperature variations, Displex cryorefrigerators are generally very stable. In addition, both cooling devices had been calibrated carefully.

	a	b	c	α	β	γ
RT X-ray 293K	8.664(1)	8.8134(6)	14.261(1)	89.768(6)	84.232(8)	61.138(8)
LT X-ray 123K	8.601(3)	8.767(2)	14.081(3)	89.29(2)	85.32(2)	60.99(2)
Neutron 123K	8.600(4)	8.767(8)	14.063(10)	89.13(6)	85.09(5)	60.88(4)
$\Delta(RT-LT)$	0.063	0.046	0.121	0.477	-1.09	0.14
no. of esds	23	27	51	25	47	6.5
$\Delta(RT-N_{123})$	0.064	0.046	0.198	0.642	-0.854	0.262
no. of esds	15	6	20	11	18	6
$\Delta(LT-N)$	0.0004	0.0002	0.0177	0.165	0.236	0.122
no. of esds	0.08	0.02	1.7	5	5	3

Table 4.9: Cell parameters and differences of KM25 at 293 and 123K.

There are possible explanations for the observed differences in the adps from the two refinements other than small differences in experimental temperature.

The tendancy of adps derived from X-ray refinements to contain some of the valence density as well as actual atomic vibrations can result in the X-ray derived values being systematically larger than those from neutron studies. High order refinements should be less susceptible to this problem.

The differences observed in KM25 are not, however, consistently in this sense of the X-ray derived adps being greater than those from the neutron studies. A very similar range of ratios was found in the study of p-nitropyridine N-oxide made using both X-ray and neutron data measured at 30K [10]. The ratios for neutron over high order X-ray values of U_{ii} averaged over all atoms were found to be 0.82 for $i = 1$, 0.96 for $i = 2$ and 1.07 for $i = 3$. No indication of temperature differences was given in this study.

A more subtle and harder to resolve explanation, may be that the discrepancies between the two sets of parameters are due to some uncorrected systematic errors in one or both data sets. Effects, such as extinction and absorption and also TDS, which have not been properly corrected for will affect the adps. TDS was not corrected for in either data set and may not affect the

two experiments to the same extent. In a comparison of adps from X-ray and neutron studies of several compounds [11] it was suggested that a considerable part of the differences could be attributed to differences in TDS and that pronounced anisotropy and contributions of more than 20% to high angle data have been observed. Coppens and Lehmann concluded that it was impossible to draw any conclusions concerning any systematic bias in either of their two data sets. Unsatisfactorily this appears often to be the case. The IUCr commission project to compare the structural parameters of oxalic acid dihydrate [12] also found significant differences, even between results from studies which showed no temperature differences.

Comparison between the X-ray refinements

In addition to the differences between the results from the HO and the neutron refinements, there are systematic differences between the refinements HO, LO and FULL all of which use the X-ray data from Experiment 5. Most of the very strong reflections in the data set are found at low $\sin\theta/\lambda$ (see Figure 4.12). The R-factor is dominated by the agreement between F_{obs} and F_{calc} of these reflections. As a greater proportion of weaker, less precise data are introduced into the refinement, the R-factor increases (see Table 4.6).

The esds from the least-squares refinements are not influenced in the same way as the R-factors but depend on the number of data in the refinement. As more data are included the esds are reduced, provided of course that the model is in agreement with the data. Esds on the positional parameters of the carbon atoms from refinement HO are typically 75% of those from the LO refinement. Similarly the average ratio σ(FULL):σ(HO) though closer to unity for the carbon atom positional parameters is still less at 0.82 and is 0.7 for the chlorine atoms. A similar trend is observed for the esds of the adps where the average ratio σ(LO):σ(HO) is 0.5 for the carbon atoms and the ratio FULL:HO is 0.9 for the carbon atoms and 0.73 for the chlorine atoms. The ratio between HO and LO chlorine positional parameter esds is less consistent

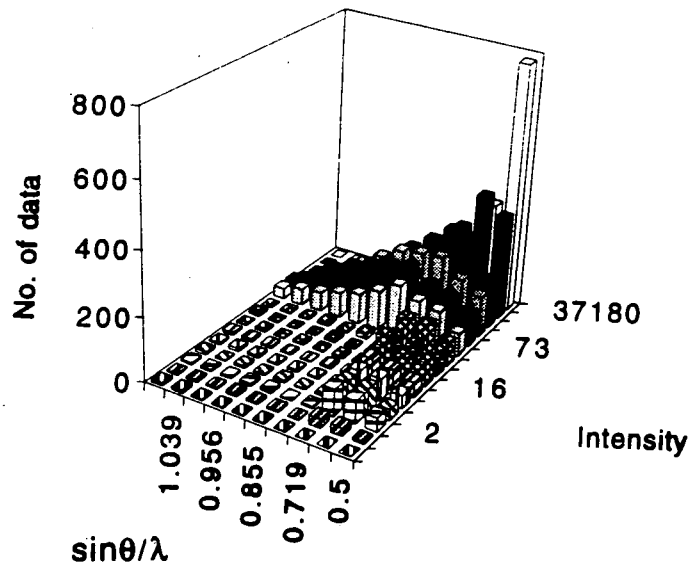

Figure 4.12: Plot showing the number of data as a function of $\sin\theta/\lambda$ (Å^{-1}) and intensity.

at 1.1(1) with a far larger spread of values. This is perhaps a consequence of the greater thermal motion of the chlorine atoms relative to the carbon atoms which reduces the intensity and precision of the high angle data.

Some disagreement between the positional and thermal parameters from the refinements HO and LO is to be expected if the low order data are indeed biased by the deformation density. There is only one significant difference between the positional parameters for the carbon atoms from the two refinements, that on the coordinate x for C(13) where the difference is 0.0055Å. More significant differences are seen in the positional parameters of the chlorine atoms, including a difference of 0.0063Å in the coordinate z of Cl(1) corresponding to 10σ.

The differences are smaller between the HO and FULL refinements. There are no significant differences for the carbon atom positional parameters, the

majority of which are less than one esd. This agreement is even better considering that the esds are lower in these refinements than in refinement LO. Again there are more differences in the chlorine atom parameters, the largest of which is 0.0035Å for Cl(5).

As was seen with the HO and neutron comparisons the largest differences from the various X-ray refinements are between the adps. Between the refinements HO and LO there are many significant differences. The overall ratios averaged over all atoms are β_{11} 1.03(4), β_{22} 1.01(4) and β_{33} 1.02(3), *i.e.* all the adps from the HO refinement are larger than those from LO. This is not consistent with the inclusion of diffuse electron density in the adps in the LO refinement. The difference may be due to a systematic underestimation of the thermal motion as a consequence of the number of strong reflections with large weights included in the LO refinement.

A similarly systematic difference is seen between the adps of the FULL and HO refinements where the ratios HO/FULL are 1.048(20), 1.049(17) and 1.052(10) for the adps β_{11}, β_{22} and β_{33} respectively, averaged over all non-hydrogen atoms. This again may be due to the strong influence of the intense reflections on the model.

Overall, all the refinements proceeded normally and show the data to be of good quality although the poor agreement between the X-ray and neutron derived adps is somewhat disappointing.

Figure 4.13 is included as a final note to illustrate the contribution the valence density makes to the low order data. This Figure shows two difference Fourier maps of the section through the aromatic ring containing atoms C(4) to C(9). The $F(\mathbf{h})_{calc}$ values are from the refinements FULL which used the whole data set. The difference between the two maps is the top map, Figure 4.13(a), is calculated using reflections with $\sin\theta/\lambda < 0.8\mathring{A}^{-1}$ and Figure 4.13(b), the lower map, uses data with $\sin\theta/\lambda > 0.8\mathring{A}^{-1}$.

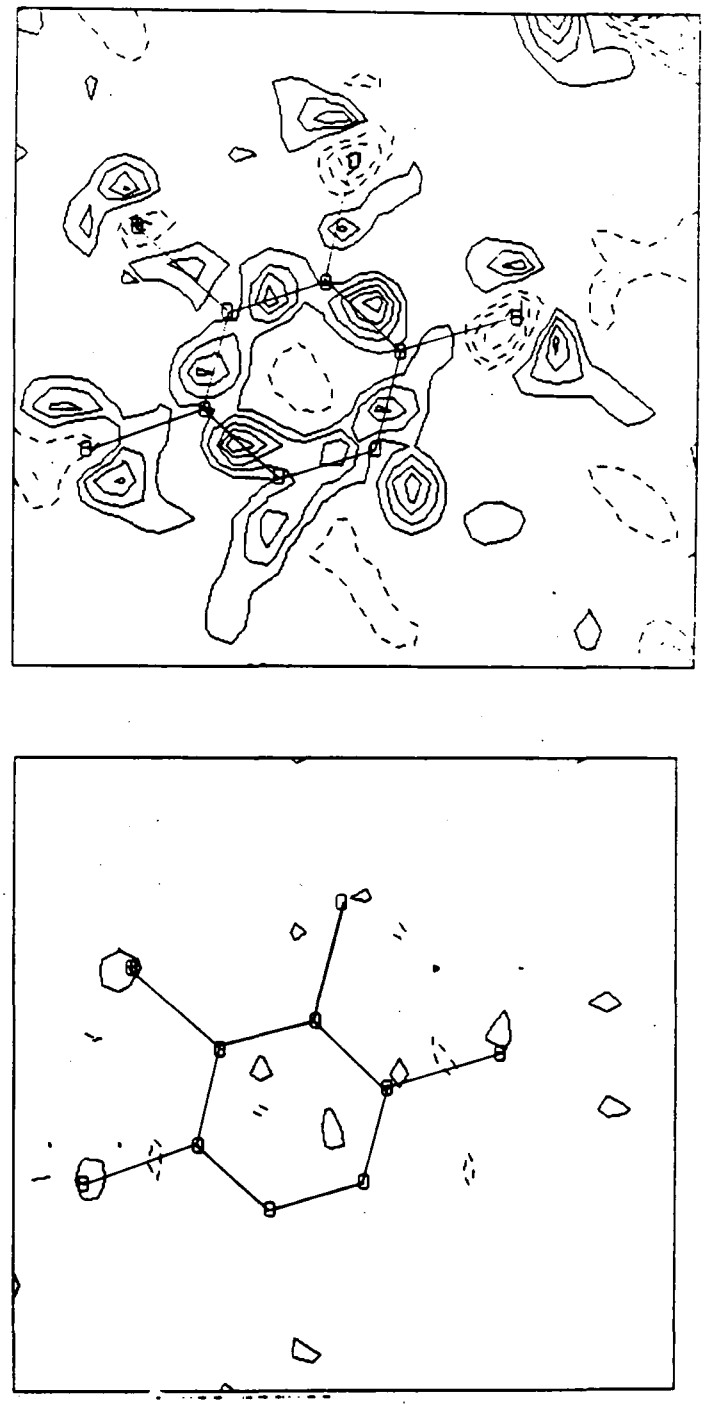

Figure 4.13: Difference Fourier maps in the plane of the aromatic ring C(4) to C(9). (a) above for data with $\sin\theta/\lambda < 0.8\text{Å}^{-1}$ and (b) below with $\sin\theta/\lambda < 0.8\text{Å}^{-1}$. Contours marked at 0.1eÅ^{-3} intervals.

Figure 4.13(a) is almost featureless showing that the high order data are well modelled by the Independent Atom Model, (IAM). This is to be expected since these data contain information on the core electrons. The residual density in Figure 4.13(b) is far from featureless, clearly showing density in the regions between the bonded atomic nuclei and also in the region of the chlorine atom lone pair electrons. This is consistent with the concept of the high order refinements and gives an indication of the deformation of the density caused by bonding. It is this density which has been modelled using a more sophisticated model in the charge density study; the results of which are presented in the following chapter, Chapter 5.

Bibliography

[1] K. MacKenzie, J.A.K. Howard, E.C. Gravett, K.B. Astin, Liu Shi-Xiong, A.S. Batsanov, D. Vlaovic, J.P. Maher, M. Murray, D. Kendrew, C. Wilson, R.E. Johnson, T. Preiβ, and R. Gregory (1993). *J. Chem. Soc. Perkin. Trans.* 2, 1211-1228.

[2] P. Seiler, B. Martinoni and J.D. Dunitz (1984). *Nature* **309**, 435-438.

[3] L. Koester (1977). *Springer Tracts in Modern Physics* **80**, Neutron Physics, edited by G. Höhler, Berlin: Springer.

[4] G.M. Sheldrick (1986). Shelxtl-Plus - Program for Crystal Structure Determination, University of Gottingen.

[5] L.A. Paquette, M.A. Kesselmayer, and R.D. Rogers (1990). *J. Am. Chem. Soc.* **112**, 284-291.

[6] L.A. Paquette, G.A. O'Doherty and R.D. Rogers (1991). *J. Am. Chem. Soc.* **113**, 7761-7762.

[7] G.A. O'Doherty, R.D. Rogers and L.A. Paquette (1994). *J. Am. Chem. Soc.* **116**, 10883-10894.

[8] D.T. Cromer and J.T. Waber (1974). *International Tables for X-ray Crystallography* Vol IV, edited by J.A. Ibers and W.C. Hamilton, 103-147.

[9] W.T. Klooster, S. Swaminathan, R. Nanni and B.M. Craven (1992). *Acta Cryst.* **B48**, 217-227.

[10] P. Coppens and M.S. Lehmann (1976). *Acta Cryst.* **B32**, 1777-1784.

[11] H. Fuess (1992) in *The Application of Charge Density Research to Chemistry and Drug Design*, edited by G.A. Jeffrey and J.F. Piniella, Plenum Press.

[12] J. Dam, S. Harkema, D. Feil, R. Feld, M.S. Lehmann, R. Goddard, C. Krüger, E. Hellner, H. Johansen, F.K. Larsen, T.F. Koetzle, R.K. McMullan, E.N. Maslen, E.D. Stevens and P. Coppens (1984). *Acta Cryst.* **A40**, 184-195.

Chapter 5

Charge Density Study of km25.

5.1 Introduction

The X-ray refinements discussed in the previous chapter were all made using the conventional *Independent Atom Model*, (IAM); a model which assumes that the atoms are neutral and of spherical shape with a radial dependence equal to that of free atoms in the gas phase. Such a model is used in the majority of X-ray crystallographic structural studies. However, refinements using the IAM ignore a great deal of information contained in the measured Bragg intensities.

For almost as long as X-ray diffraction by crystals has been known about, it has been recognised that X-ray data contain information on electronic structure in the crystals. Debye stated in 1915 that he thought it should be possible to determine the arrangement of the electrons in the atoms from the scattered radiation. However, despite this early recognition and some pioneering work over subsequent decades (notably on the structure of diamond and sodium chloride), there was little confidence in the feasibility of the technique.

A number of technical breakthroughs over the past 30 years have meant that charge densities are now being made on a wide range of compounds al-

though not a large number of them.

One of the important technical breakthroughs was the use of neutron diffraction. Results from neutron studies demonstrated the bias in the structural parameters obtained from IAM refinements against X-ray data caused by their tendency to account for bonding features in the density. The combination of neutron and X-ray diffraction studies allowed bonding and lone pair electron densities to be observed [1, 2].

Other advances in X-ray studies such as computer controlled diffractometers and the use of scintillation counters as detectors have improved the ease and precision of data collection. The increasingly routine use of low temperature techniques has also improved the precision and accessibility of high resolution data. The availability of powerful computing has made the use of sophisticated models and the handling of large data sets practicable.

Despite these advances, experimental charge density studies are still far from being routine. The bonding effects of interest form only a small proportion of the total electron density and these are often diffuse in nature. To have any confidence in the results of the study, especially on a quantitative level, requires very accurate and extensive data.

Due to its diffuse nature, much of the information on the bonding density is contained in the low order data. However, accurate and extensive high order data are required for the determination of the nuclear positions and displacement parameters. The fall-off in scattering power with increasing Bragg angle is one of the reasons for adopting low temperature techniques. TDS, which also affects high order data is reduced by lowering of the temperature.

5.2 Investigating the bonding density

There are several strategies which have been developed to investigate the electron density distribution (see for example Reference [3]).

A Fourier synthesis of the structure factor amplitudes derived from the experimentally measured intensities gives the thermally averaged electron density provided that a suitable estimate of the phases has been made. The majority of the phases from the IAM will be assigned correctly for a centrosymmetric crystal, such as KM25, where the choice is limited to values of 0 or π. More serious errors will occur for a non-centrosymmetric structure. However, such a Fourier map will provide little information on the effects of chemical bonding on the electron density as it will be dominated by the core electrons.

A more informative representation is a difference map of the density calculated for the IAM subtracted from the total experimental density (using the model phases). This type of map, the equation for which is shown below, is often called a deformation map. Care should be taken with this term as it is used for a number of maps which show the non-spherical density, some of which involve experimental data and some of which are entirely model densities.

$$\Delta\rho = \frac{1}{V}\sum(\mathrm{F_{obs}}(\mathbf{h}) - \mathrm{F_{calc,IAM}}(\mathbf{h})\exp(-2\pi i\mathbf{h}.\mathbf{r}) \qquad (5.1)$$

The use of a difference density shows the bonding density more clearly than the does the total density and additionally avoids the problem of series termination.

Deformation maps show the electronic redistribution to form bound atoms in the crystal relative to a promolecule density. The IAM is generally the model used to provide this reference or promolecule density of non-interacting isolated atoms although other promolecule densities have been proposed, *e.g.* the Oriented Atom Model [4].

Despite the wide acceptance of the IAM density as the promolecule density,

its use presents some problems. The assumptions contained in the IAM (neutral, spherical atoms) produce biased parameters which consequently means that the promolecule density is not that of the reference model desired. The least-squares refinement process tends to minimise the residual density and so produce structural parameters which attempt to compensate for the deviations from sphericity. For example, in order to best fit the electron density which has been drawn into the region of the covalent bond, hydrogen atom positions are usually displaced, relative to their true nuclear position, towards the ligated atom. Lone pair density may also be modelled by the IAM as anisotropic thermal displacements. The promolecule density will therefore contain some of the bonding density and as a consequence the deformation density maps will be smoother than they are really.

As mentioned in the previous chapter, refinements and the combination of neutron data with X-ray refinements can be used to reduce this bias. However, both of these solutions present some problems. High order refinements present problems in being sure that no bonding features scatter to high angles and the neutron experiments present problems in ensuring their compatibility with the X-ray data. Rather than having the worrying uncertainty of whether the promolecule density contains any of the bonding density, extra atomic parameters can be included in the model to describe explicitly the effects of the chemical bonding.

One of the simplest such models is that used in the Kappa refinement [5] which retains the spherical shape but allows both the variation of the population of the valence shell and its expansion or contraction. The latter expansion or contraction is a consideration which is in agreement with Slater's rules of nuclear screening. There are therefore two extra parameters per atom, the valence population $P_{valence}$ and κ, an expansion/contraction factor.

The expression for the perturbed valence density, $\rho'_{valence}$, as related to the

free-atom ground state density, $\rho_{valence}$, is then:

$$\rho'_{valence}(\mathbf{r}) = \mathbf{P}_{\mathrm{valence}}\kappa^3\rho_{\mathrm{valence}}(\kappa\mathbf{r}) \tag{5.2}$$

The structure factor expression then becomes:

$$\mathrm{F}(\mathbf{h}) = \sum_{\mathrm{j=1}}^{\mathrm{Na}}[\mathrm{f_{j,core}}(\mathbf{h}) + \mathrm{P_{j,valence}f_{j,valence}}(\kappa_\mathrm{j}, \mathbf{h})]\mathrm{T_j}(\mathbf{h})\exp(2\pi\mathrm{i}\mathbf{h}.\mathbf{r_j}) \tag{5.3}$$

where T_j is the atomic temperature factor and P_j the population parameters of atom j at $\mathbf{r}_j$. A κ parameter larger than one signifies that the valence density at $\mathbf{r}$ is equal to that of the free-atom valence density at a point further from the nucleus, *i.e.* the atom is contracted relative to the free atom.

The above formalism (Equation 5.3) has been called the poor man's charge density refinement as it is very computer efficient. The great availability of powerful computers nowadays means that there are not so many 'poor men' about, nonetheless, the method gives a better estimate of the net atomic charges than the multipole models.

Several more flexible and more sophisticated models have been developed [6, 7, 8] which allow explicitly for the description of non-spherical electron density features. The rigid pseudoatom model of Stewart [6], on which Hansen and Coppens [7] have based their formalism, contains two important assumptions:

- that the total electron density in the molecule or crystal may be divided into pseudoatoms (atoms deformed due to their crystal environment) which are centred on the nuclei.
- that these atomic fragments rigidly follow the thermal vibrations of the appropriate nucleus.

If the second of these assumptions is indeed valid then we can calculate static electron density maps using experimental data (see below).

Order	Symbol Y_{lm}	Cartesian Coordinates	Spherical Coordinates
0	Y_{00}	1	1
1	Y_{11}	x	$\sin\theta\cos\phi$
	Y_{11-}	y	$\sin\theta\sin\phi$
	Y_{10}	z	$\cos\theta$
2	Y_{20}	$(3z^2-1)$	$3\cos^2\theta$-1
	Y_{21}	xz	$\sin\theta\cos\theta\cos\phi$
	Y_{21-}	yz	$\sin\theta\cos\theta\sin\phi$
	Y_{22}	x^2-y^2	$\sin^2\theta\cos2\phi$
	Y_{22-}	$2xy$	$\sin^2\theta\sin2\phi$
3	Y_{30}	$(5z^2-3)z$	$\cos\theta(5\cos^2\theta-3)$
	Y_{31}	$(5z^2-1)x$	$\sin\theta(5\cos^2\theta$-1$)\cos\phi$
	Y_{31-}	$(5z^2-1)y$	$\sin\theta(5\cos^2\theta$-1$)\sin\phi$
	Y_{32}	$(x^2-y^2)z$	$\sin^2\theta\cos\theta\cos2\phi$
	Y_{32-}	xyz	$\frac{1}{2}\sin^2\theta\cos\theta\sin2\phi$
	Y_{33}	$(x^2-3y^2)x$	$\sin^3\theta\cos3\phi$
	Y_{33-}	$(3x^2-y^2)y$	$\sin^3\theta\sin3\phi$

Table 5.1: Real spherical harmonic functions up to the order of 3.

In general, the models consist of an invariant spherical core electron density much like that of the IAM, the nucleus as described by its coordinates and thermal displacement parameters, and a third component which is the deformation functions. The last component, the deformation functions, is usually expressed in polar coordinates (r, θ, ϕ) and the functions are centred on the nucleus, although this is not a prerequisite. The deformation terms are then further separated into a radial and an angular part and are given an associated weight or population parameter which is usually refined in the least-squares fitting.

The angular parts in both the Stewart and the Hansen and Coppens models are spherical harmonic functions, $Y_{lm}(\theta, \phi)$. Some of the spherical harmonic functions are shown in Figure 5.1 and more information given in Table 5.1. It is these terms which are often referred to as 'multipoles'. The functions are normalised such that for a population constant of unity ($P_{lm} = 1.0$), one

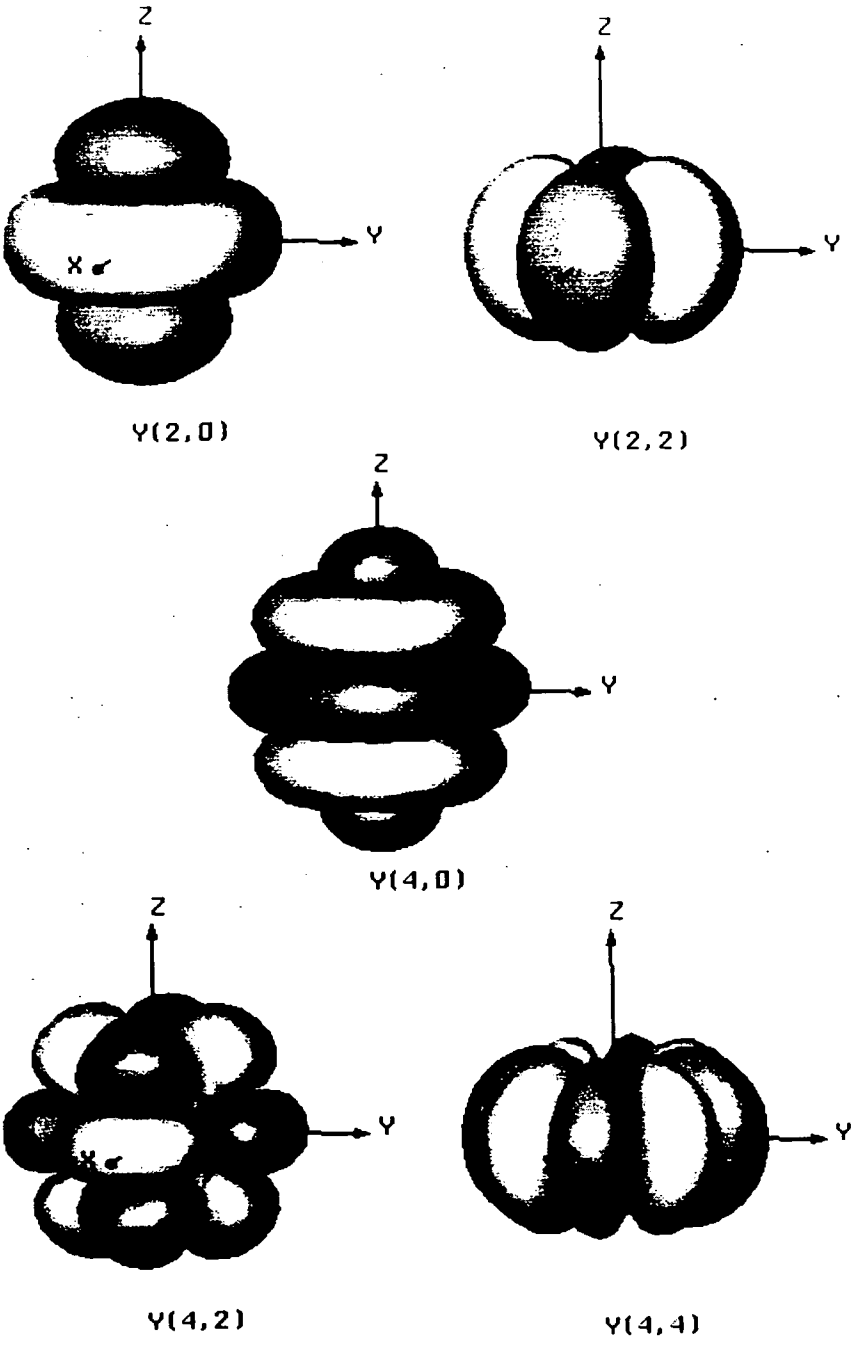

Figure 5.1: Representation of selected Spherical Harmonic functions.

electron has moved from the negative to the positive lobes of the deformation functions (for those functions with l greater than one). For the spherically symmetric function, a population constant, P_{00}, of 1.0 implies that the function is populated with one electron. The normalisation constants used in the refinements are given in reference [7]. P_{00} is the only function which confers any net charge, the higher poles cause the aspherical distribution.

The angular functions are not necessarily spherical harmonics. The formalism developed by Hirshfeld [8] uses cosine functions of the form $cos^n\theta_k$ where θ_k is the angle between the radius vector, **r**, and a specified polar axis. There are up to 35 non-orthogonal deformation functions allowed per atomic centre in this model. Refinements made using the various models have been shown to reproduce the bonding density equally well although differences in other regions of the density and in the derived charges have been noted [3].

5.3 Static versus dynamic densities

The electron density described by the deformation density is a static one. Static densities have several advantages over dynamic ones. The effect of the thermal motion smears the electron density and so some of the sharper features in the density may be lost. There may also be some confusion between thermal effects and the bonding density. This makes static densities intrinsically more informative.

In order to make comparisons between theoretical and experimental densities the thermal effects in the experimental density must be taken into consideration; either the thermal effects must be removed from the experimental density or the theoretical one must be thermally smeared. It is also important when comparing experimentally determined charge distributions as they may not be affected to the same degree nor measured at the same temperature.

Vibrational motion in the crystal causes several problems. The reduction in intensity due to thermal motion particularly affects the high order data and so limits resolution. TDS also contributes to the high angle data. Cooling of the sample during data collection alleviates these difficulties to some extent, nevertheless the experimentally determined density will always be the time average over the thermal motion of the crystal. It is therefore of interest to deconvolute the thermal motion and so obtain a static distribution from the experiment.

The convolution approximation is used to deconvolute the thermal motion from the experimentally determined density by assuming that the charge density rigidly (*i.e.* without changing its shape) follows the nucleus and so can be convoluted with the vibrational motion of that nucleus. This raises the question of how to partition the continuous electron density into atomic fragments assigned to a particular nucleus, especially for density between atomic nuclei. The method of partitioning becomes a more important factor if the nuclear displacements of neighbouring atoms differ greatly. In the case of the multipole models, each set of functions is centred on a particular nucleus and so are convoluted with the nuclear motion of that nucleus. This does not present particular difficulties in terms of the total density but makes any attempts to look at an atomic density somewhat complex.

An alternative method of dividing the total density has been proposed by Hirshfeld, the Stockholder Principle [9]. In general terms this proposes that the contribution, $\delta\rho_i$, from a given atom, i, to the total deformation density, $\delta\rho_{total}$ at a particular point $\mathbf{r}$, is in direct proportion to the contribution from that same atom's spherical density, $\rho_{spherical,i}$ to the total procrystal density at that point such that:

$$\delta\rho_i(\mathbf{r}) = w_i(\mathbf{r}).\delta\rho_{\text{total}}(\mathbf{r}) \tag{5.4}$$

where w_i gives the relative share in the promolecule density of the atom i at $\mathbf{r}$

and is given below:

$$w_i = \frac{\rho_{spherical,i}(\mathbf{r})}{\sum_{j=1}^{atoms} \rho_{spherical,j}(\mathbf{r})} \tag{5.5}$$

The work of Coulson and Thomas [10], which examined the effect of stretching vibrations on the charge density using both a convolution model and a full Born-Oppenheimer study of H_2^+ and H_2, suggests that the convolution approximation is an acceptable one. This is particularly encouraging given that hydrogen is such a light atom and therefore subject to much larger vibrational amplitudes than heavier atoms.

However, as well as doubts as to the validity of the approximation itself there are also some doubts concerning the reliability of the experimentally determined vibrational amplitudes and the type of model used to describe them. In many studies, including this one, an anisotropic harmonic probability density function is used.

A test of the thermal motion model has been proposed by Hirshfeld [11]. It uses the experimentally determined adps and depends on the idea that for a pair of bonded atoms, A and B, the mean square vibrational amplitudes along their mutual bond should be equal, *i.e.* if $z^2_{A,B}$ denotes the mean square displacement of atom A along the vector to atom B then:-

$$\Delta_{A,B} = z^2_{A,B} - z^2_{B,A} = 0 \tag{5.6}$$

For atoms at least as heavy as carbon Hirshfeld proposed that the rigid-bond test should hold to within 0.001Å. If this is the case then it should give some confidence in the refined adps and if it does not hold it indicates some bias in the model or refinement. However parameters which are affected by a systematic error will also satisfy this test.

5.4 Fitting the model

The specific model used in the refinements reported herein was that of Hansen and Coppens [7]. In direct space the atomic density is represented by Equation 5.7:-

$$\rho_{atomic}(\mathbf{r}) = \mathrm{P_c}\rho_{\mathrm{core}} + \mathrm{P_v}(\kappa')^3\rho_{\mathrm{valence}}(\kappa'\mathrm{r}) + \sum_{\mathrm{l=0}}^{4}(\kappa'')^3\mathrm{R_l}(\kappa''\mathrm{r})\sum_{\mathrm{m=-l}}^{\mathrm{l}}\mathrm{P_{lm}y_{lm}}(\mathbf{r}/\mathrm{r}) \tag{5.7}$$

P_c, P_v and P_{lm} are population coefficients. ρ_{core} and $\rho_{valence}$ are Hartree-Fock densities of the free atoms normalised to one electron, although the valence function is allowed to expand or contract by adjustment of κ'. The radial function is of the form:

$$R_l(r) = \frac{\zeta^{n_l+3}}{(n_l+2)!}r^{n_l}\exp(-\zeta_l r) \tag{5.8}$$

where ζ is modified by the variable parameter κ'' and values for n_l were taken from reference [7] and for the optimised Slater exponent, ζ_l, taken from self-consistent field calculations of Clementi and Raimondi [12].

However, as with the IAM, the actual fitting is carried out in reciprocal space by a least squares minimisation of the differences between the observed and calculated structure factor amplitudes. In the case of the multipole model the calculated structure factor expression is as given below in Equation 5.9:

$$F(\mathbf{h}) = \sum_{k}^{atoms}\sum_{p}^{symm}\left[P_c f_{core}(h) + P_v f_{valence}(h/\kappa') + \sum_{l=0}^{4}\Phi_{kl}(h/\kappa''\sum_{m=-l}^{l}P_{klm}y_{lm}^{k}(\mathbf{h_p}/\mathrm{h})\right]$$

$$\times\exp(2\pi i\mathbf{h}.\mathbf{r_{kp}}\mathrm{T_k}(\mathbf{h}) \tag{5.9}$$

f_{core} and $\mathrm{f}_{valence}$ are the Fourier transforms of ρ_{core} and $\rho_{valence}$ respectively, Φ_{kl} is the Fourier-Bessel transform of R_{kl}, T_k the temperature factor and $\mathbf{h}_p$ and $\mathbf{r}_{lp}$ the scattering and position vectors. One of the advantages of using spherical harmonic functions is that their Fourier transforms are also spherical harmonic functions.

The parameters which are refined are the positional and atomic displacement parameters, the radial parameters κ' and κ'' and the population coefficients P_v and P_{klm}. The total charge is constrained so that the crystal remains neutral.

The use of a least-squares refinement has certain advantages. It allows: (i) the structure factor amplitudes to be assigned statistical weights from those estimated on the intensities, (ii) the calculation of estimated standard deviations on the refined parameters and (iii) statistical measures of the fit between the experimental and model values to be calculated so checking the fit of the model.

The use of a more flexible model than the IAM reduces the errors in the phase assignment and generally introduces less bias into the refined parameters. The explicit separation of the parameters for both static spherical and deformation densities from the thermal motion allows the calculation of the static density from experimental data, provided that the convolution approximation is valid.

The use of a model density also has the advantage of being free from experimental noise. It gives a quantitative description of the deformation density and allows the calculation of a number of electrostatic properties.

One problem with the static densities obtained from multipole models is that they imply infinite resolution. However, there is an experimental limit to the data available of $1/\lambda$ and in general data are not collected as far as this limit. The model density close to the nuclei, which is not accessible to X-ray diffraction, is therefore totally model dependent.

5.5 Topological Analyses

The topology of the electron distribution may used to describe some of the chemical properties of the molecule [13]. The following section is a brief introduction to the terms which will be further discussed later in the text.

The topological properties of the electronic distribution can be described concisely by certain values at the points where the first derivative of the density vanishes, *i.e.* where

$$\nabla\rho(\mathbf{r}_c) = \mathbf{i}\frac{\partial\rho}{\partial \mathrm{x}} + \mathbf{j}\frac{\partial\rho}{\partial \mathrm{y}} + \mathbf{k}\frac{\partial\rho}{\partial \mathrm{z}} = 0 \qquad (5.10)$$

These points are known as critical points and their position is denoted by the position vector $\mathbf{r}_c$.

The location and classification of critical points and the determination of certain quantities at these points allows the formal definition of such concepts as nuclear positions and bonds in topological terms. This permits a range of chemical concepts to be related to the total electronic charge density, ρ and so quantitative comparisons may be made both within studies and with care, between studies.

To decide if these stationary points are maxima, minima or saddle points the second derivative must be examined. For an arbitrary choice of coordinate axes, nine values of the form $\partial^2\rho/\partial x\partial y$ will be obtained, the ordered 3×3 array of which is the Hessian matrix of ρ. This matrix can be diagonalised and the eigenvectors and eigenvalues correspond to the principal axes and the corresponding curvatures at the critical point.

Critical points are characterised by two quantities; their rank, ω and their signature, σ and are labelled as (ω, σ). The rank is the number of non-zero eigenvalues or curvatures of ρ at the critical point and the signature is the algebraic sum of the signs of the eigenvalues.

Almost all stable critical points are of rank three for which there are four possible signature values:

- (3,-3) critical points are local maxima in the electronic density, ρ, where all curvatures are negative. These correspond to nuclear positions.
- (3,-1) critical points, known as bond critical points (bcp), are of most interest to this study and will be discussed in more detail below.
- (3,+1) are critical points where two curvatures are positive. ρ is a minimum at $\mathbf{r}_c$ in the plane of these two curvatures and a maximum at $\mathbf{r}_c$ along the third axis perpendicular to the previous plane. These critical points are associated with rings.
- (3,+3) are local minima in ρ as all curvatures are positive and are linked to the presence of cages.

(3,-1) critical points are saddle points which lie between every pair of nuclei linked by a chemical bond. Along the line of maximum charge density linking the two bound nuclei, called the bond path, the critical point lies at a minimum in the density. By convention, the principal axes in the direction of the bond path, which is not necessarily coincident with the internuclear vector, is taken as z and the corresponding curvature or eigenvalue is denoted by λ_3. The curvatures perpendicular to the bond path, the x and y components are denoted by λ_1 and λ_2 respectively. At a bond critical point these two curvatures are both negative, showing an accumulation of electron density between the two nuclei.

The relative magnitudes of the eigenvalues λ_1 and λ_2 indicate the extent to which electronic charge has accumulated preferentially in a given plane along the bond path, for example in bonds which contain a π-component. Where electron density has accumulated the density will drop away less steeply from the bond critical point and so the curvature will be smaller. A measure of this

charge accumulation is given by the bond ellipticity, ε defined in Equation 5.11.

$$\varepsilon = \left(\frac{\lambda_1 - \lambda_2}{\lambda_2}\right) \tag{5.11}$$

Therefore if λ_1 is equal to λ_2 the density has axial symmetry at the critical point and the ellipticity is zero.

Bader and co-workers have published a series of papers discussing certain concepts in topological terms for the theoretical electron densities of a series of hydrocarbons. For example, the characterisation of bond orders in terms of the value of electron density at the bond critical point, bond ellipticities as a quantitive measure of the π-character of C-C bonds [14, 15] and strain energies from examination of the bond paths and their deviation from the internuclear vector [16], have been discussed. Some of these factors will be further discussed in this chapter with reference to the results of the charge density study of KM25.

Topological considerations of the charge density can provide a useful means of quantifying and characterising chemical concepts such as atoms and bonds in terms of the measurable electron density in molecular systems. However, there are no features which correspond to the concepts of localised electron pairs, either in bonds or as non-bonding lone pairs. This model of Lewis pairs appears in the topology of the Laplacian of ρ, $\nabla^2\rho(\mathbf{r})$ as defined below in Equation 5.12.

$$\nabla^2\rho(\mathbf{r}) = \frac{\partial^2\rho}{\partial \mathrm{x}^2} + \frac{\partial^2\rho}{\partial \mathrm{y}^2} + \frac{\partial^2\rho}{\partial \mathrm{z}^2} \tag{5.12}$$

The Laplacian of ρ represents local concentrations and depletions of the charge density where $\nabla^2\rho(\mathbf{r}) < 0$ and $\nabla^2\rho(\mathbf{r}) > 0$ respectively. The distribution of the Laplacian shows maxima, minima and saddle points which correspond to our ideas of localised pairs of electrons. These features in the Laplacian can be used to show the local charge depletion associated with electrophiles and conversely local charge concentrations associated with nucleophiles, thus locating possible sites of reactivity.

The electronic charge density used in this study was the model density from the multipole refinements which has the advantage of being free from experimental noise. Provided that the model is a good fit to the data, this model density will introduce very little in the way of model dependent bias. Topological analyses thus provide a relatively objective way of investigating and comparing bonds and factors such as strain in the molecule.

5.6 Choice of a system to study

Given the considerable amount of time and effort demanded for a charge density study it is important to consider carefully the suitability of the study to be undertaken.

Some of the obvious considerations are the reason for studying the electron density of a particular molecule, what information it is hoped will be obtained and whether a charge density study can provide this information. As discussed in the previous chapter (Chapter 4), it has become increasingly obvious that electronic factors play an important role in the dyotropic rearrangement. Some structural parameters such as bond lengths and angles around certain atomic sites have been cited as indicating different electronic properties. For example, the degree of tilt of the chlorine atoms at the C(13) and C(14) sites in the starting isomer has been suggested to indicate the degree of pyrimidalisation [17]. The aim of the charge density studies was therefore to investigate the electronic structure of these compounds directly rather than from such indications. This chapter contains a report of the results of the first of the charge density studies made of one of these compounds.

KM25 was chosen as the initial subject of study for several reasons. One of the main interests in this work is to compare the density distributions in a pair of isomers. It is therefore important that both isomers of the pair should

be suitable for such studies.

The chemical interest is equally important for each of the three pairs of isomers which have been studied, KM5:KM9, KM22:KM25 and KM24:KM27. Such general criteria as Coppens' suitability factor [18] are also equivalent for all three pairs. This suitability factor quantifies the degree to which the bonding effects are dominated by the core scattering. The trienes give typical values for organic compounds of around 3.5-4.0. The smaller values generally obtained for metals indicate that to obtain a given precision in the bonding density requires that the intensities are measured to a higher relative precision. The decision was therefore made on the basis of practical considerations as discussed below.

As has been stated previously, charge density studies require extensive and accurate data sets measured at low temperature. This requires high quality crystals which are stable enough to allow long data collection periods (of many weeks in this case), give good quality data and are stable at low temperature. In general, the trienes crystallise to give high quality crystals which satisfy these conditions. Both in combination with X-ray data for charge density studies and in their own right, neutron experiments form an important part of this work. It is therefore desirable to study compounds of which large crystals can be grown (see Chapter 2). These criteria do not rule out any of the three pairs of isomers.

Although these compounds crystallise in a variety of space groups, see Table 1.1 and Tables 1.2 and 1.3 in Chapter 1, the amount of unique data does not vary very much from compound to compound, provided that there is only one molecule in the asymmetric unit. In some ways a higher symmetry crystal is better 'value' as there are more possibilities for collecting symmetry equivalents. However, there may be a price to pay in terms of the resolution of the reflections since many of the higher symmetry compounds have a cell axis of approximately 30Å in length.

One of the most important factors is the choice of a centrosymmetric structure. Although the phases may be better approximated by the use of a more sophisticated and flexible model, such as the multipole models used, the situation is simplified enormously in the case of centrosymmetric crystals. This therefore ruled out the study of KM5. Also, the neutron data were collected at 15K (Experiment 1) and this temperature could not be matched with X-ray data at the time. An additional point against the study of this pair of isomers was that, in a preliminary study, KM9, its isomer, showed some instability at low temperatures.

Both isomers of the pair KM24:KM27 crystallise in centrosymmetric space groups and both have been studied using neutron diffraction but at differing temperatures, 120K and 15K.

KM25 was therefore chosen as both isomers satisfy all the above criteria and in addition the neutron and X-ray experiments could be made at the same temperature for both isomers and for both types of experiment, X-ray and neutron.

5.7 The refinements

All the refinements were made using the *XD* package of programs [19] which is currently under development. It contains a least-squares refinement program for multipole model refinements, programs for calculating Fourier syntheses and one-electron properties for the refined model. The overall aim of the project is the provision of a comprehensive multipole refinement and analysis source code which is updated and supported. It therefore contains some new features as well as some well established ones. I have been using these programs by kind permission of P.R. Mallinson.

The multipole model formalism used in the refinements was that of Hansen

and Coppens [7], as described above. The scattering factors used were calculated from the ground state Slater-type orbital Hartree-Fock atomic wavefunctions of Clementi and Roetti [20]. The radial functions of the valence deformation density are of single Slater-type and the parameters for these functions n(l) and $\zeta(l)$ are obtained from the single-zeta wavefunctions [20]. The thermal motion was described by an anisotropic harmonic model.

All the refinements were made using all the X-ray data, collected to a $\sin\theta/\lambda$ limit of 1.08Å^{-1}, which satisfied the condition F> 2σ(F). The weighting scheme used was $w = \sigma^{-2}$. No correction for extinction was made.

Local coordinate systems were defined for all atoms. However, these local coordinate systems are usually used to apply symmetry constraints. These are not appropriate to KM25. The only constraint applied was that of electroneutrality, such that the contents of the asymmetric unit were neutral.

A number of refinements were made using a variety of combinations of X-ray and neutron derived parameters. The use of neutron data in charge density studies is well established. As discussed in Chapter 4 the nuclear positional and atomic displacement parameters derived from neutron experiments are free from any bias arising from the electron density distribution. Several methods have been proposed to utilise this freedom from bias. Coppens reported the use of X-N deformation maps to investigate the bonding density in s-Triazine in 1967 [1]. The IAM promolecule density uses the positional and atomic displacement parameters derived from the neutron study and the deformation maps are the difference maps between the total electron density, as measured by the X-ray study, and the neutron based IAM density. All the deviations are assumed to be due to bonding effects.

Joint refinement of parameters using the neutron and X-ray data for a compound simultaneously have been proposed by Duckworth, Willis and Pawley [2] and also by Coppens and co-workers [21]. These refinements are denoted

as X+N refinements. It is prudent first to run refinements using the two sets of diffraction data separately.

In most combined neutron and X-ray charge density studies, the results of the separate neutron structural refinement are used as constrained parameters in the X-ray refinements rather than refining the model against the two data sets together. It was hoped originally that the results from the neutron experiment, Experiment 4, carried out on KM25 could be used in this way. Unfortunately, as discussed in Chapter 4, important differences were found between the neutron and X-ray refinement results, not all of which are caused by the bias in the X-ray derived parameters.

The first model which was tried was an Independent Atom Model in which the parameters were all constrained to the values derived from the neutron study and only a scale factor was refined against the X-ray data. This did not result in a satisfactory refinement and gave an unacceptably poor fit of the data with the deformation density showing a number of features more consistent with incorrect adps than with bonding density. This was probably only to be expected given the differences discussed in Chapter 4.

It was decided therefore that in future refinements all hydrogen atom positional and atomic displacement parameters would be constrained to their neutron derived values, but for all non-hydrogen atoms these parameters would be refined against the X-ray data.

A further set of refinements using the IAM were run against the X-ray data with the parameters refined as above. These refinements will be referred to henceforth as SPH. Within the XD least squares program, this was effected by fixing the monopole populations to the number of valence electrons; four for carbon, seven for chlorine and one for hydrogen and the expansion/contraction parameter κ' to 1.0 for the carbon and chlorine atoms. The κ' and κ'' parameters for hydrogen were fixed to a value of 1.2 in all refinements. This value

gives a scattering factor curve which corresponds to the Stewart, Davidson and Simpson curve [22] normally used in conventional refinements.

After the examination of several sets of refinements, a final multipole model was chosen and will be referred to as MULT. The data used in the refinement and the treatment of the positional and atomic displacement parameters were as described above. Population parameters of multipole functions of up to third order (octapoles), were refined for all carbon atoms and up to fourth order (hexadecapoles), for the chlorine atoms. First order (dipole) populations were refined for the hydrogen atoms. Four groups of atoms were assigned common expansion/contraction factors, two for each group, one for the spherical valence density and one for the aspherical functions, κ' and κ'' respectively. The four groups of atoms were:-

Group 1	sp^3 hybridised carbon atoms:	C(1) to C(3) and C(10) to C(16)
Group 2	sp^2 hybridised carbon atoms:	C(4) to C(9)
Group 3	the chlorine atoms.	
Group 4	the hydrogen atoms.	

As for the IAM refinement, both these κ-parameters were fixed at a value of 1.2 for the hydrogen atoms. The κ' parameters for the other three groups were all allowed to refine, as were the κ'' parameters for the two different groups of carbon atoms. The κ'' parameter for the chlorine atoms refined to an unusually high value of 1.62(2). This did not result in a noticeable improvement in the fit of the model to the experimental data nor did the model deformation density resemble more closely the residual density from the IAM model. It was therefore decided to constrain the κ'' parameter for the chlorine atoms to a value of 1.0.

The IAM refinement was made purely as a reference for the multipole refinement. Perfectly satisfactory refinements of a spherical atom model had

	SPH	MULT
No. of Parameters refined	226	748
No. of data used	13662	13662
Criterion for observed data	F> σ(F)	F> σ(F)
Scale Factor	0.8534(6)	0.8379(8)
R(F)	0.0401	0.0307
wR(F)	0.0474	0.0385
Goodness of Fit	1.576	1.299
Min/Max Shift/esd	0.0014, 0.52	0.0001, 0.086
Min/Max Residual Density (eÅ^{-3})	-0.741, 1.024	-0.527, 0.299
κ' and κ'' values for		
Group 1	1.0, 1.0	1.011(6), 0.79(2)
Group 2	1.0, 1.0	1.013(8), 0.80(3)
Group 3	1.0, 1.0	1.030(3), 1.0
Group 4	1.2, 1.2	1.2, 1.2

Table 5.2: Some details of the refinements SPH and MULT.

already been made using the program *UPALS*, the results from which were discussed in Chapter 4. The results of the refinement using XD showed no significant differences from these previous results.

Some of the details of the two refinements, SPH and MULT, are given in Table 5.2.

The results of the refinement MULT are discussed below. Some of the general results are discussed first and then each of the bond types; aromatic C-C, single C-C, C-H and C-Cl bonds are discussed in turn.

As a test of the refined atomic displacement parameters (adps), Hirshfeld's rigid bond test [11] was applied to both the adps from the SPH and MULT refinements. The largest differences found in the root mean square displacement amplitudes were 0.0006Å^2 in the SPH refinement (for the bonds C(5)-C(6) and C(6)-Cl(6)) and 0.0007Å^2 in the bonds C(5)-C(6) and C(7)-Cl(7) in refinement MULT. Both of these results are well within the 0.001Å^2 limit suggested by

Hirshfeld.

The statistical agreement factors, R(F), wR(F) and the goodness of fit all showed satisfactory agreement. The multipole model agreement factors indicate that data are fitted more closely by this model which is unsurprising given the far greater number of refined parameters.

An additional, and more informative, method of checking the model is the calculation and examination of difference Fourier maps. These are expected to differ for the two models. The residual maps $\rho_{obs} - \rho_{calc,IAM}$ should reveal the features of the density which result from the deformation of the density caused by bonding. The residual maps from the multipole refinement should be flat and featureless as the aim of using these models is to reproduce all of the density.

For the carbon and hydrogen atoms of KM25 this is indeed the result, as illustrated by Figures 5.2 and 5.4 for example. Clear bonding features can be seen in the $\rho_{obs} - \rho_{calc,SPH}$ maps and the $\rho_{obs} - \rho_{calc,MULT}$ maps are indeed clean and featureless. This suggests that these atoms are well modelled by the refined multipole model. The chlorine atoms are less well modelled and on first inspection do not show the expected accumulation of charge in the region between the bonded nuclei. This will be discussed below.

The positional parameters agree very closely from the two refinements. The adps are consistently larger from the IAM refinement which is to be expected if these include some of the deformation density.

Of the multipole population parameters refined it is only the monopole populations P_{00} which account for any transfer of charge between the atoms. Monopole populations greater than that of a the neutral atom (4.0 for carbon, 7.0 for chlorine and 1.0 for hydrogen) show an increase in electronic charge. The higher multipole terms have no effect on the net charge but whereas the monopole terms have spherical symmetry the higher poles cause aspherical

Atom	Charge	Atom	Charge	Atom	Charge	Atom	Charge
C(1)	0.0(1)	C(10)	-0.1(1)	Cl(1)	-0.2(1)	H(2)	+0.15(8)
C(2)	-0.1(1)	C(11)	+0.1(1)	Cl(5)	-0.1(1)	H(3)	+0.29(9)
C(3)	0.0(1)	C(12)	+0.3(1)	Cl(6)	-0.2(1)	H(10)	+0.11(9)
C(4)	0.0(2)	C(13)	+0.1(1)	Cl(7)	-0.4(1)	H(11)	+0.14(8)
C(5)	+0.2(2)	C(14)	-0.1(1)	Cl(8)	-0.5(1)	H(13)	+0.23(8)
C(6)	+0.2(2)	C(15)	0.0(1)	Cl(12)	-0.2(1)	H(14)	+0.22(8)
C(7)	0.0(2)	C(16)	-0.2(1)	Cl(13)	-0.1(1)	H(15)	+0.24(8)
C(8)	-0.2(2)			Cl(14)	-0.3(1)	H(16a)	+0.32(9)
C(9)	0.0(2)			Cl(15)	-0.1(1)	H(16b)	+0.22(9)

Table 5.3: Atomic charges from multipole model refinement MULT.

deformations.

The refined monopole populations are consistent with simple ideas of electronegativity, *i.e.* all the chlorine atoms have a small negative charge and the hydrogens a small positive one, see Table 5.3

The aromatic ring: C(4) to C(9)

The atoms C(4) to C(9) form a six membered planar ring. The results from the neutron study (see Chapter 4) show the bond angles within the ring to all be 120° ± 1.2°, the ideal angle for sp^2 hybridised carbon atoms. These structural features suggest that the ring is an aromatic ring without angular strain. It is therefore interesting to examine the electron density and see if it is compatible with such a structure.

Figure 5.2 shows the difference density $\rho_{obs} - \rho_{calc,SPH}$ in the plane of the aromatic ring, where $\rho_{calc,SPH}$ is the calculated density for the refined IAM of the SPH refinement. This residual density map shows electron density accumulation between the pairs of bonded nuclei. Figure 5.3 shows map of the multipole density in the same plane and shows how this density has been modelled in refinement MULT. The increased density shown in this plot, relative to that in Figure 5.2, is due to the effect of thermal smearing which is present

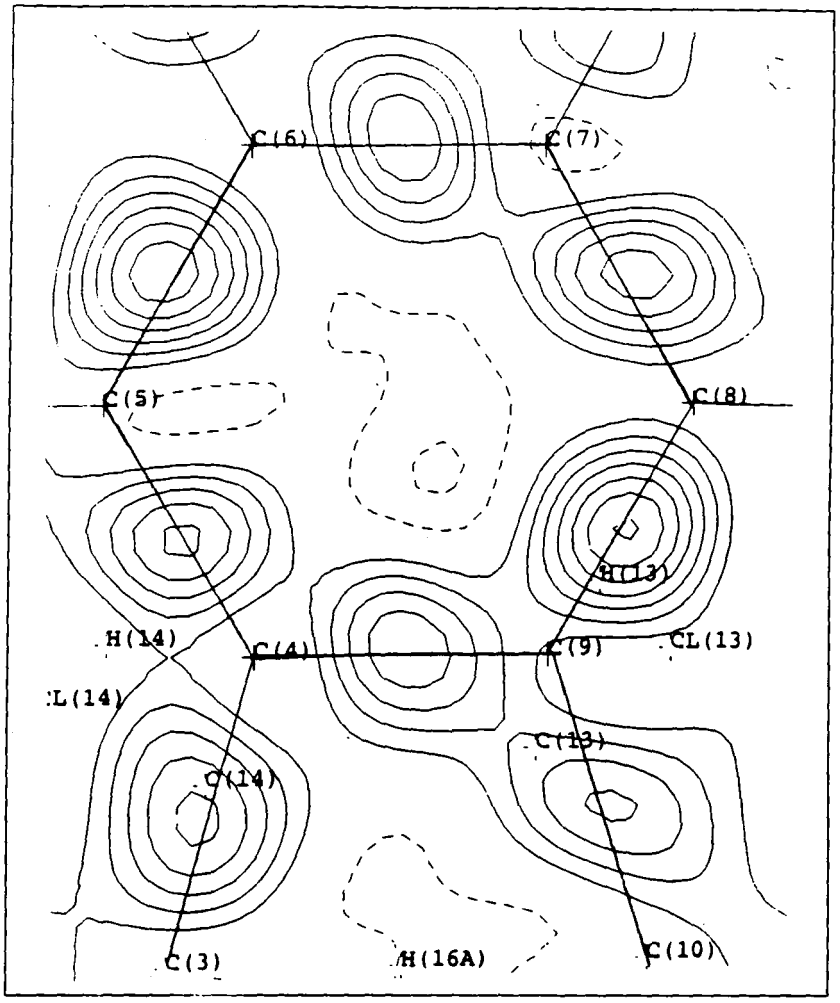

Figure 5.2: Difference Fourier of the plane of the aromatic ring C(4) to C(9). $\rho_{obs} - \rho_{calc,SPH}$ for all data to $\sin\theta/\lambda$ 0.7Å^{-1}. Contours drawn at 0.1eÅ^{-3} intervals.

in the dynamic difference map but not in the dynamic model map shown in Figure 5.3. The clean, featureless residual density for the MULT refinement, shown in Figure 5.4, demonstrates that this model has successfully taken into account all the electron density in this plane.

The results from the topological analysis are compatible with the multiple bonds expected of an aromatic structure. (3,-1) critical points were located between all pairs of nuclei which, from the interatomic separations, are considered to be bonded. The electron density at these points, $\rho(\mathbf{r}_c)$, is higher,

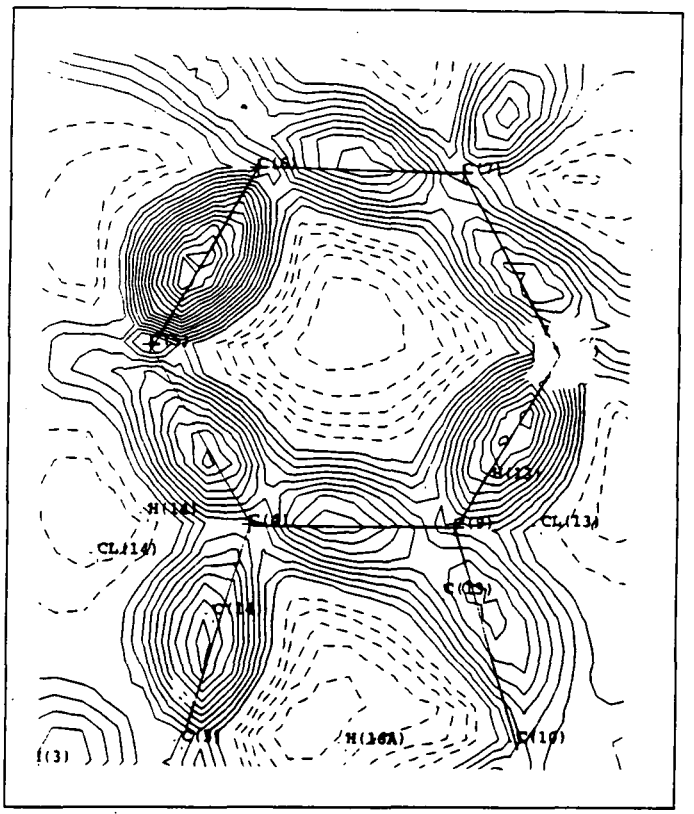

Figure 5.3: Static deformation density map in the plane of the aromatic ring C(4) to C(9) for data to $\sin\theta/\lambda$ of 1.08Å^{-1}. Contours drawn at 0.1eÅ^{-3} intervals.

Bond	λ_1	λ_2	λ_3	$\rho(\mathbf{r}_c)$	$\nabla^2\rho(\mathbf{r}_c)$	ε	R_{ij}	d_1	d_2
C(4)-C(5)	-24.02	-17.51	7.58	2.562	-33.951	0.37	1.39	0.782	0.610
C(4)-C(9)	-19.50	-17.05	8.73	2.467	-27.823	0.14	1.40	0.758	0.646
C(5)-C(6)	-28.39	-20.60	7.00	3.032	-41.992	0.38	1.41	0.781	0.625
C(6)-C(7)	-22.20	-15.47	8.13	2.475	-29.538	0.43	1.41	0.701	0.705
C(7)-C(8)	-21.41	-13.33	10.06	2.295	-24.678	0.61	1.40	0.657	0.746
C(8)-C(9)	-23.94	-16.81	9.16	2.764	-31.586	0.42	1.38	0.737	0.642

Table 5.4: Details of the bond critical points in the aromatic ring, C(4) to C(9). For an explanation of the column headings see Page 148

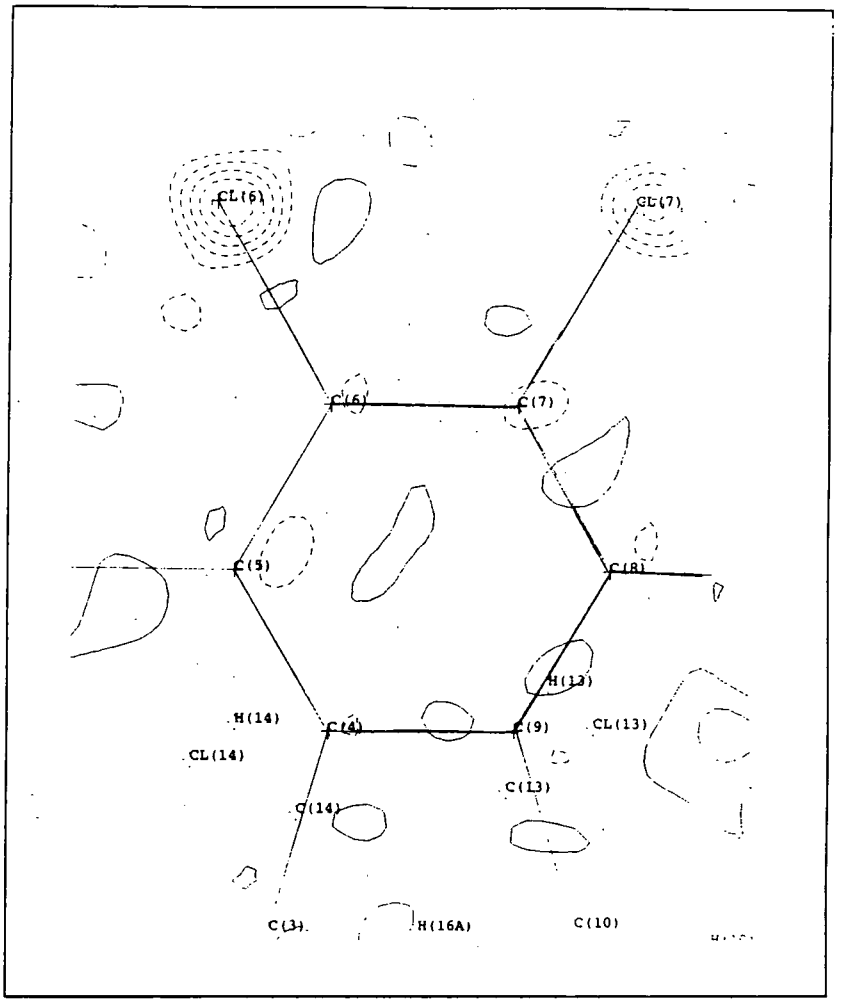

Figure 5.4: Difference Fourier of the plane of the aromatic ring C(4) to C(9). $\rho_{obs} - \rho_{calc,MULT}$ for all data to $\sin\theta/\lambda$ 0.7Å^{-1}. Contours drawn at 0.1eÅ^{-3} intervals.

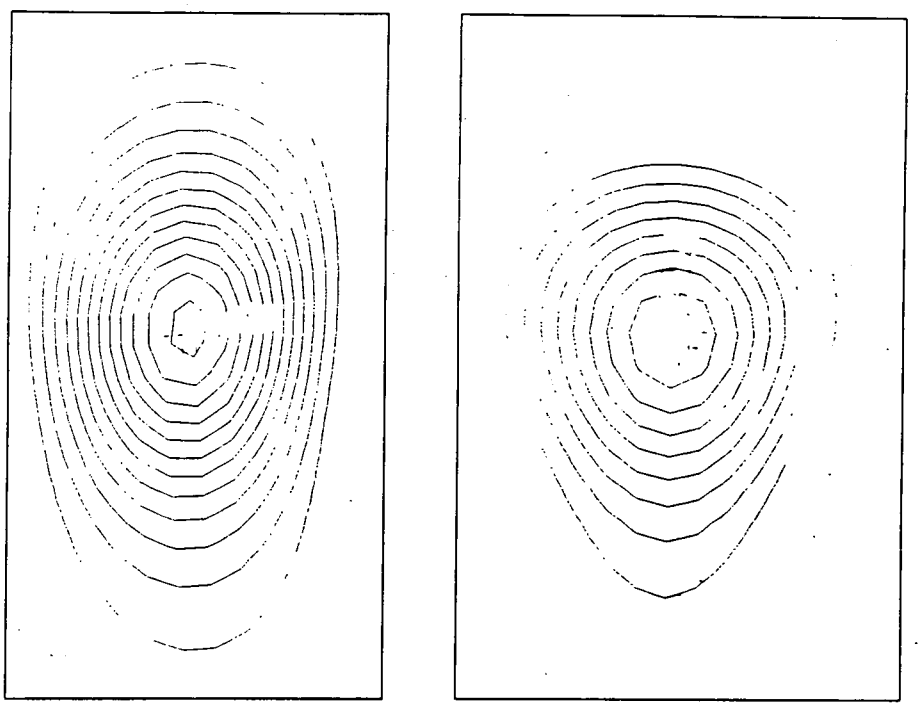

Figure 5.5: Sections of the static model deformation density through the C(8)-C(9) and C(2)-C(11) bonds, illustrating the difference in their axial symmetry.

on average, than that in the other C-C bonds in the structure; average density 2.6eÅ^{-3} compared to 2.0eÅ^{-3} for the single C-C bonds. See Table 5.4 for details of the individual bond critical point in the aromatic ring.

The C-C bonds in phenyl rings contain a significant π-contribution. This should be reflected in the ellipticity of the bond. The ellipticity at the bond critical points of the ring has an average value of 0.4(1) which is larger than the maximum value found for the other C-C bonds and is significantly non-zero. The deviation from axial symmetry in these bonds is also illustrated by the two sections of the model density shown in Figure 5.5.

C-C single bonds

All carbon-carbon bonds other than the aromatic bonds discussed above, are single bonds. Figures 5.6 to 5.8 are composite maps of four non-coplanar

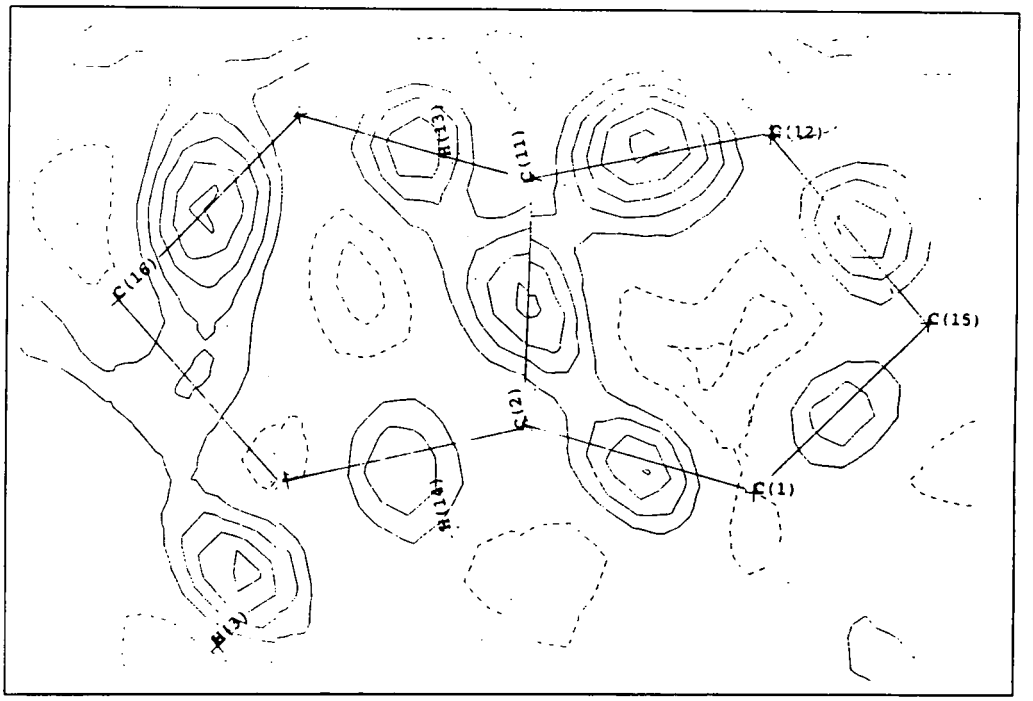

Figure 5.6: Composite difference Fourier map $\rho_{obs} - \rho_{calc,SPH}$. Contours drawn at 0.1eÅ^{-3} intervals.

sections; the sections are (a) that containing the C(1), C(12) and C(15) nuclei, (b) containing the C(1), C(2), C(11) and C(12) nuclei, (c) containing the C(2), C(3), C(10) and C(11) nuclei and (d) containing the C(3), C(10) and C(16) nuclei. The four sections are joined along their common internuclear vectors.

The experimental deformation map Figure 5.6 and the static model deformation map Figure 5.7 both show an accumulation of charge density in the region between the bonded nuclei. The Laplacian of the electron density, shown in Figures 5.9 and 5.11, highlights these regions of local concentration in the electron density between the bonded nuclei.

Similarly, an accumulation of charge is also seen in the remaining C-C single bonds as illustrated for the C(13)-C(14) bridgehead bonds in Figure 5.10 and for the C(3)-C(4) and C(9)-C(10) bonds shown in Figures 5.2 and 5.3.

Table 5.5 gives the values of certain properties, including the electron den-

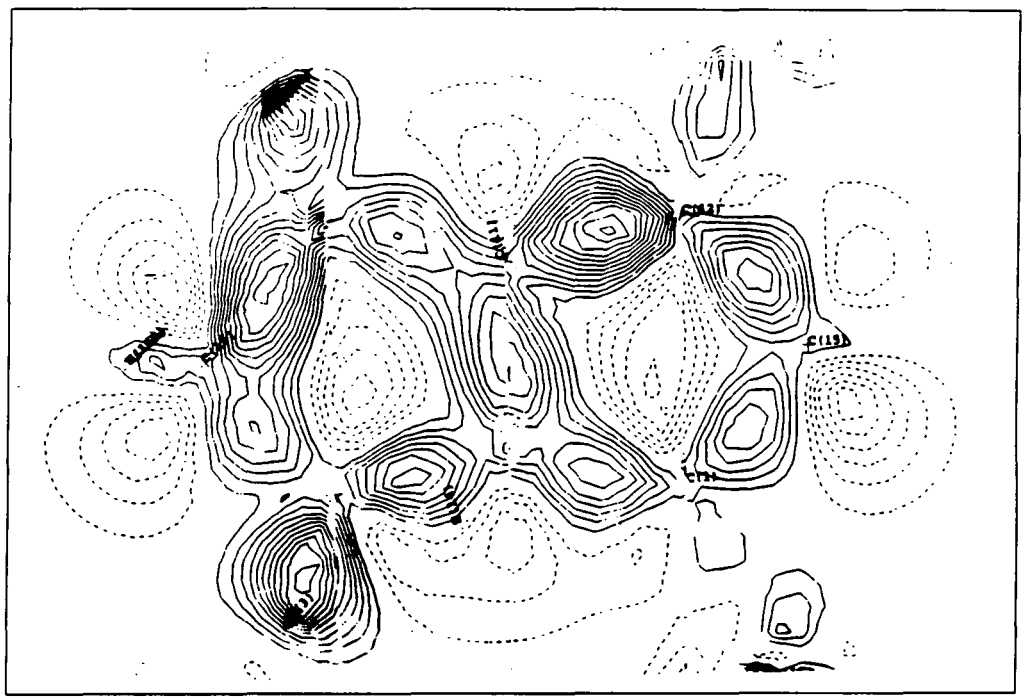

Figure 5.7: Composite static deformation density from refinement MULT. Contours drawn at $0.1e\text{Å}^{-3}$ intervals.

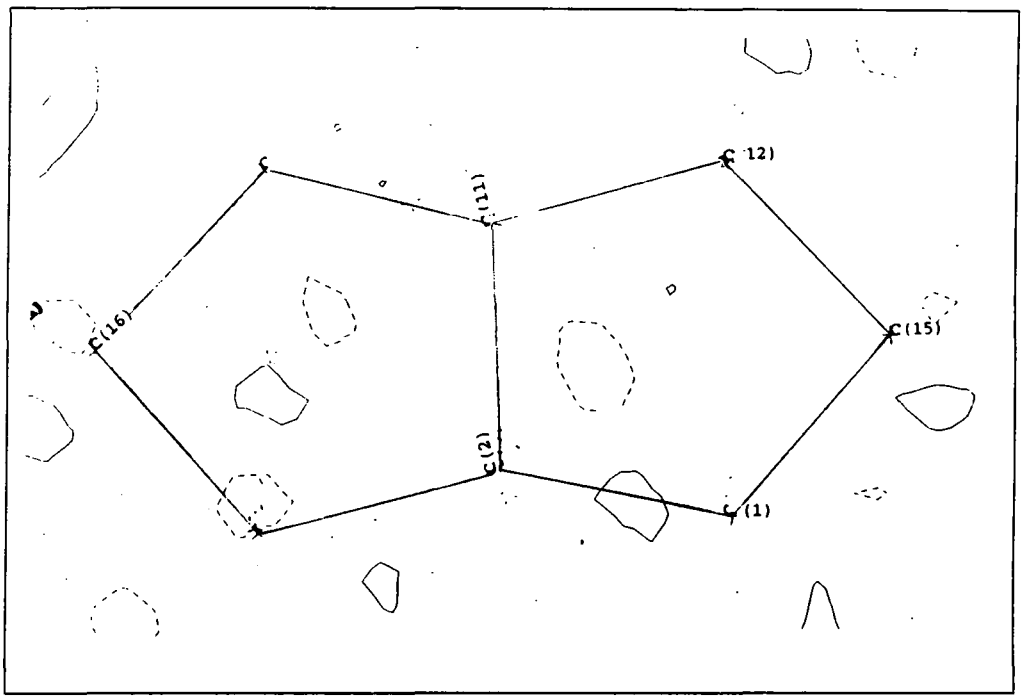

Figure 5.8: Composite residual map $\rho_{obs} - \rho_{calc,MULT}$ Contours drawn at 0.1eÅ^{-3} intervals.

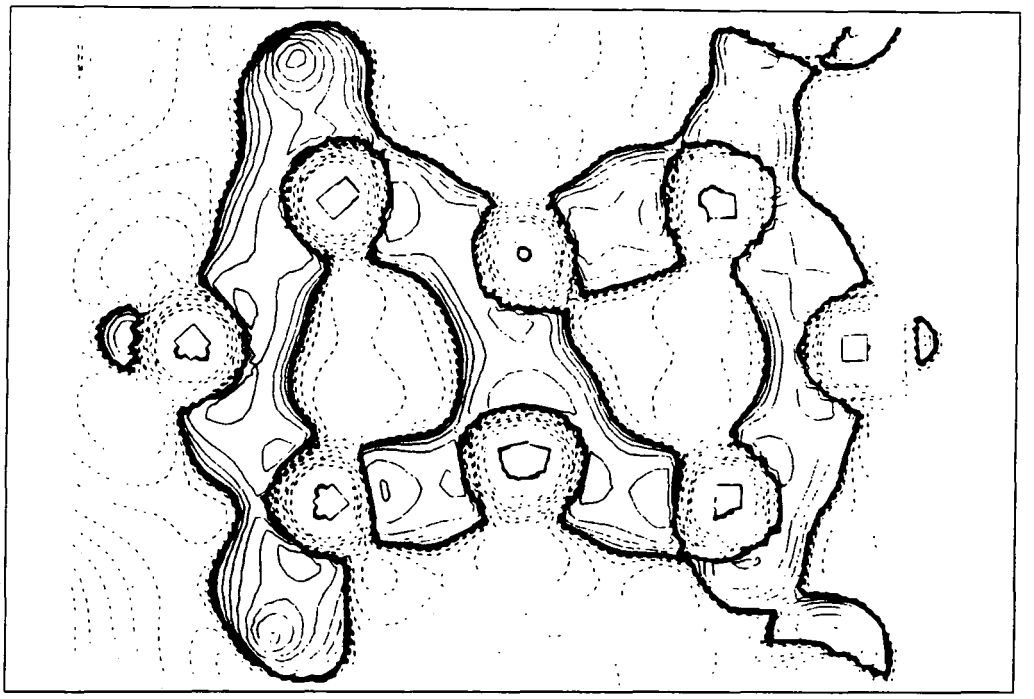

Figure 5.9: Composite plot of the Laplacian of ρ.

sity, at the bond critical points. (3,-1) critical points were located between all pairs of carbon nuclei considered to be bonded. As expected the electron density at the critical points in the single C-C bonds is generally lower than that in the aromatic C-C bonds. Table 5.5 gives the ellipticity of each of the bonds, which are lower than those of the aromatic C-C bonds. The greater axial symmetry is illustrated by Figure 5.5.

In many of the single carbon-carbon bonds the peak of the density lies off the internuclear vector to the outer side of the rings. Such bent bonds are a means of easing the angular strain in these rings, such that the electron density is not as strained as the nuclear positions would suggest. Bent bonds have been noted in many structures, particularly those compounds which contain small cyclic groups such as cyclopropyl groups, see for example, the review article of Tsirelson and Ozerov [23].

Angular strain is particularly evident around the atom C(15). The bond

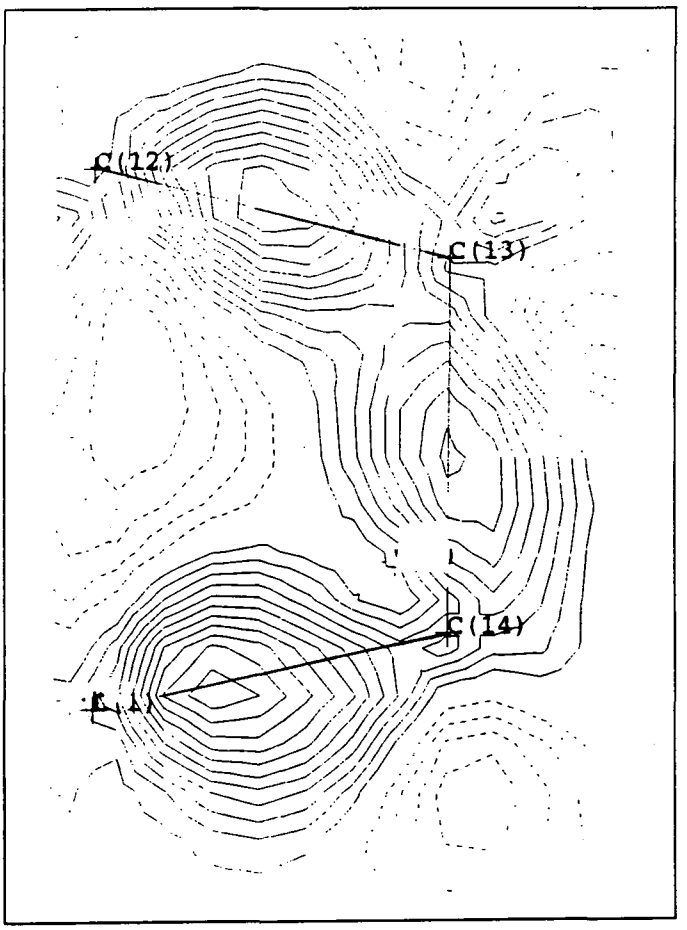

Figure 5.10: Static deformation density from the refinement MULT in the section containing the C(1), C(12),C(13) and C(14) nuclei. Contours drawn at 0.1e$Å^{-3}$ intervals.

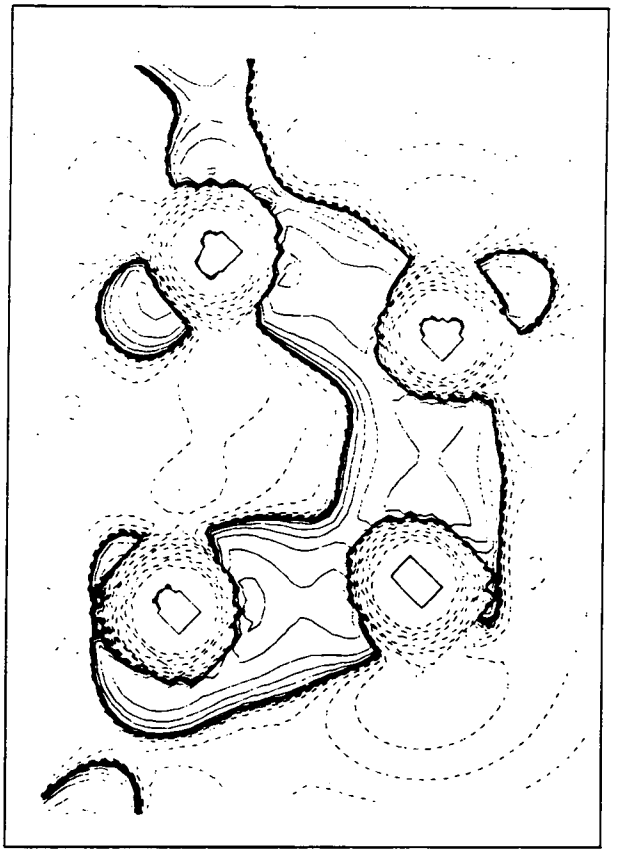

Figure 5.11: Laplacian of ρ in the plane of the C(1), C(12), C(13) and C(14) nuclei.

Bond	λ_1	λ_2	λ_3	$\rho(\mathbf{r}_c)$	$\nabla^2\rho(\mathbf{r}_c)$	ε	R_{ij}	d_1	d_2
C(1)-C(2)	-15.11	-13.52	8.92	1.878	-19.710	0.12	1.54	0.761	0.784
C(1)-C(14)	-17.18	-14.99	10.27	2.167	-21.900	0.15	1.55	0.858	0.689
C(1)-C(15)	-14.42	-11.68	9.64	1.743	-16.451	0.23	1.56	0.793	0.769
C(2)-C(3)	-14.74	-12.17	8.46	1.843	-18.446	0.21	1.56	0.704	0.861
C(2)-C(11)	-14.59	-13.56	11.51	2.038	-16.645	0.08	1.56	0.794	0.766
C(3)-C(4)	-18.52	-15.16	9.90	2.264	-23.782	0.22	1.52	0.802	0.719
C(3)-C(16)	-14.09	-11.00	8.86	1.735	-16.221	0.28	1.56	0.740	0.822
C(9)-C(10)	-15.45	-11.51	10.76	1.974	-16.206	0.34	1.51	0.779	0.728
C(10)-C(11)	-13.77	-11.76	10.61	1.862	-14.926	0.17	1.55	0.802	0.753
C(10)-C(16)	-17.47	-16.63	10.50	2.311	-23.608	0.05	1.56	0.784	0.780
C(11)-C(12)	-18.22	-15.29	8.99	2.323	-24.519	0.19	1.55	0.698	0.848
C(12)-C(13)	-17.85	-16.78	7.57	2.271	-27.066	0.06	1.55	0.796	0.757
C(12)-C(15)	-16.02	-13.18	8.74	1.940	-20.468	0.22	1.55	0.766	0.788
C(13)-C(14)	-15.76	-13.54	8.72	1.925	-20.588	0.16	1.58	0.771	0.810

Table 5.5: Details of the C-C single bond critical points. For an explanation of the column headings see Table 5.4.

angle ∠C(1)-C(15)-C(12) is 93.3(1)°. This significant deviation from the ideal tetrahedral angle of 109°28′ for an sp^3 hybridised carbon atom is the largest in this structure. Figure 5.12 shows the model deformation density in the section of the C(1), C(12) and C(15) nuclei and the peaks in the bond density can clearly be seen to lie outside the internuclear vector. This bending of the bonding density is also indicated by the length of the bond path relative to the internuclear separation. For example, the C(1)-C(15) bond length is 1.555(2)Å compared to the bond path length at 1.578Å, and similarly for C(12)-C(15), the bond length is 1.549(2)Å and the bond path length 1.576Å.

The bond angle ∠C(3)-C(16)-C(10) of 94.5(1)° also indicates considerable angular strain. Again, the bond density peaks lie outside the internuclear vectors. However, the C(3)-C(16) bond appears to have a slightly unusual density distribution. Examination of the experimental deformation maps (see Figure 5.13) shows there to be very little density in this bond, although the

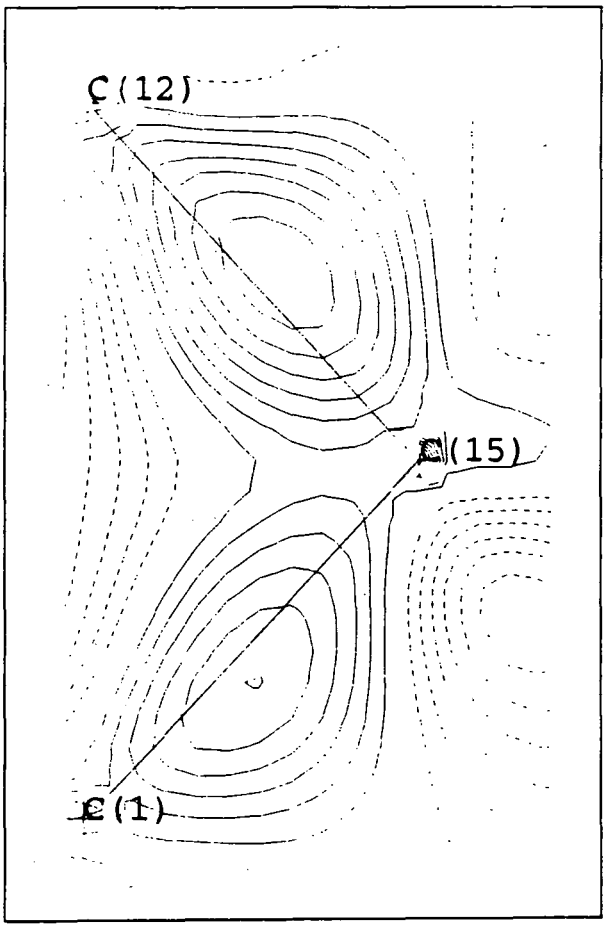

Figure 5.12: Static deformation density in the C(1), C(12), C(15) section. Contours drawn at $0.1e\text{Å}^{-3}$ intervals.

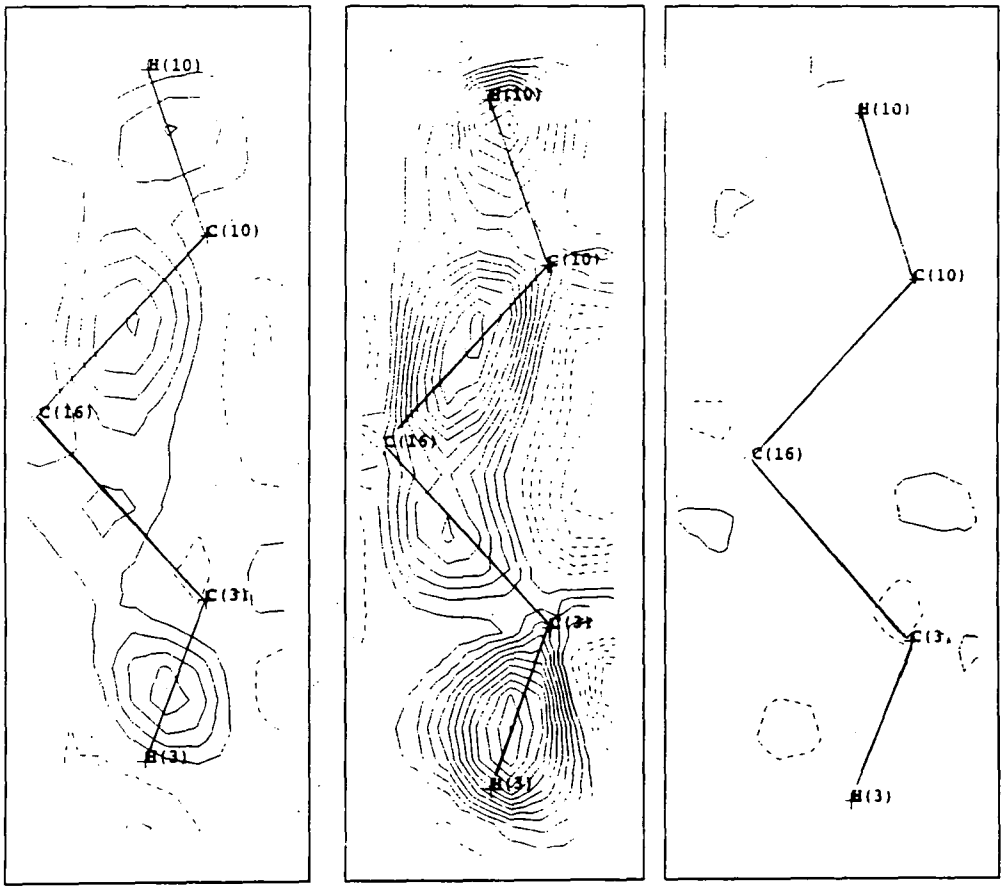

Figure 5.13: Three densities for the section containing the nuclei C(3), C(10) and C(16). From left to right:- difference Fourier density $\rho_{obs} - \rho_{calc,SPH}$, static model deformation density and the residual density $\rho_{obs} - \rho_{calc,MULT}$. Contours drawn at intervals of 0.1eÅ^{-3}.

bond length of 1.554(2)Å indicates a standard C-C single bond. The model density (see Figure 5.13) at the bond critical point, $\rho(\mathbf{r}_c)$, is the lowest of any of the C-C bond critical points at 1.74eÅ^{-3}. However, the residual map, shown in Figure 5.13, does not indicate any unmodelled density nor is the low density correlated in any way to a long or apparently weak bond.

Bond	λ_1	λ_2	λ_3	$\rho(\mathbf{r}_c)$	$\nabla^2\rho(\mathbf{r}_c)$	ε	R_{ij}	d_1	d_2
C(2)-H(2)	-21.34	-20.27	19.38	2.188	-22.226	0.05	1.10	0.767	0.330
C(3)-H(3)	-26.22	-23.71	13.71	2.429	-36.223	0.11	1.08	0.754	0.330
C(10)-H(10)	-18.05	-15.11	12.64	1.937	-20.532	0.19	1.10	0.656	0.440
C(11)-H(11)	-17.18	-15.47	15.07	1.886	-17.581	0.11	1.10	0.696	0.401
C(13)-H(13)	-21.38	-20.61	14.79	2.219	-27.197	0.04	1.09	0.745	0.348
C(14)-H(14)	-23.83	-19.36	16.27	2.249	-26.917	0.23	1.09	0.755	0.338
C(15)-H(15)	-22.42	-21.44	15.72	2.229	-28.135	0.05	1.10	0.761	0.338
C(16)-H(16a)	-20.03	-18.94	14.48	1.970	-24.484	0.06	1.10	0.766	0.335
C(16)-H(16b)	-22.37	-21.59	15.56	2.236	-28.392	0.04	1.10	0.755	0.344

Table 5.6: Details of C-H bond critical points. See Table 5.4 for details of the column headings.

C-H bonds

As with the C-C bonds discussed above, an accumulation of charge density is also observed in the region between the hydrogen atoms and the ligated carbon atoms. This density is of about the same order as in the C-C single bonds with a slightly higher average density ($2.15 e\text{Å}^{-3}$) at $\mathbf{r}_c$. This is probably due to the shorter C-H separation making for somewhat denser bonds.

Figure 5.14 shows the static model deformation density in the plane containing the C(16), H(16a) and H(16b) nuclei. This Figure clearly shows the displacement of the centroid of the electron density relative to the nuclear position, as derived from neutron diffraction data. This illustrates the cause of the systematic difference between the C-H bond lengths determined by X-ray and neutron studies. This is also true of the density of the hydrogen atoms attached to carbons C(13) and C(14), also shown in Figure 5.14. Table 5.6 gives details of the bond critical points located in the C-H bonds.

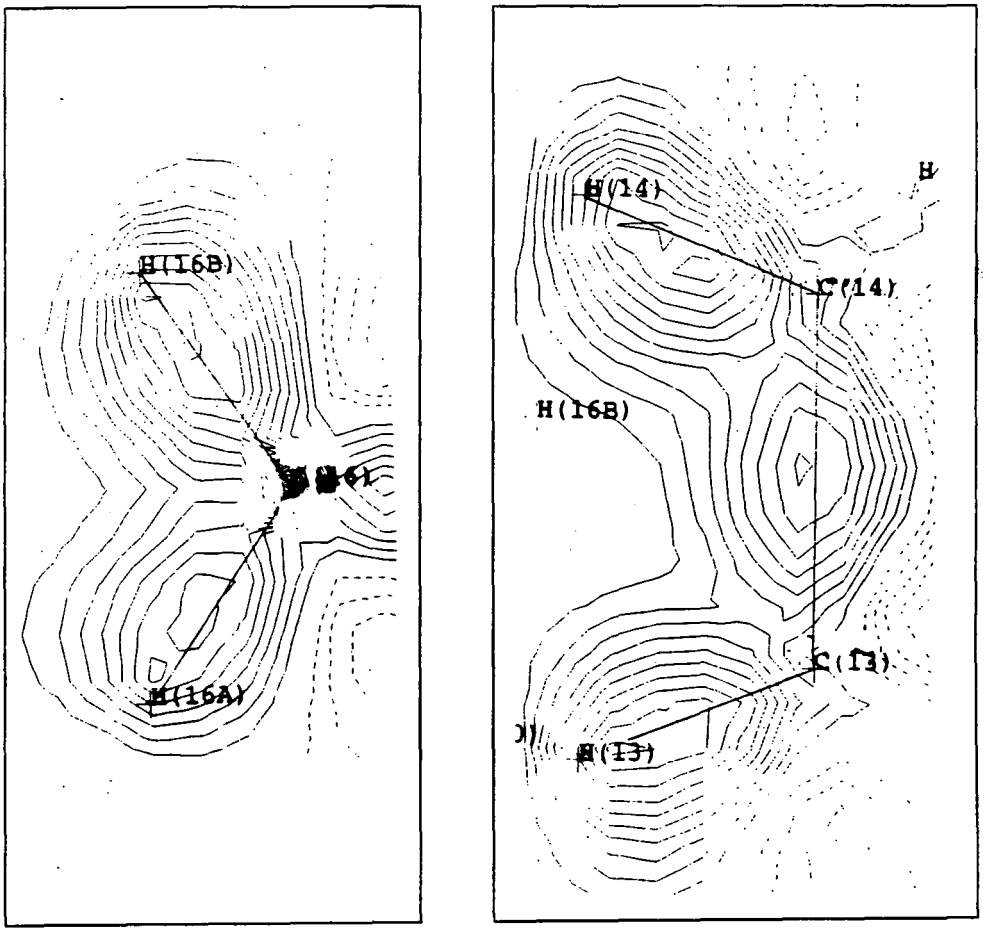

Figure 5.14: Sections of the static model deformation density containing the C(16),H(16a) and C(16b) nuclei on the left and C(14),C(13),H(14) and H(13) nuclei on the right. Contours are drawn at 0.1e$Å^{-3}$ intervals.

C-Cl bonds

Unlike the C-C and C-H bonds discussed above, examination of the experimental deformation maps does not systematically show an accumulation of charge density in the region between the chlorine atoms and their ligated carbon atoms. In the bonds where some accumulation is observed it is very much lower than that seen in the C-C and C-H bonds.

Figure 5.15 shows some density in the C(6)-Cl(6) and C(7)-Cl(7) bonds and very little density in the C(5)-Cl(5) and C(8)-Cl(8) bonds. This density has been modelled as shown in Figure 5.16. Difference Fourier maps of other sections containing C-Cl bonds show a similar lack of density in the bonding region, see Figure 5.17 for example.

Although the apparent lack of bonding density in the C-Cl bonds may appear to be contrary to expectation it is not without precedent. One of the best known examples, reported by Dunitz and co-workers [24] and further investigated by Hirshfeld [25], is that of tetrafluoroterephthalonitrile, (TFT). They observed very little bonding density in the C-F bond in both the dynamic experimental deformation maps and in the static model deformation maps from Hirshfeld's study.

A similar situation has been observed in a number of structures containing chlorine. No C-Cl bond density was observed in the study of 2-amino-5-chloropyridine [26] nor in that of 2-(2-chlorobenzoylimino)-1,3-thiazoline [27].

Several papers have been published [28, 29, 30] which offer possible explanations of this lack of accumulation in what otherwise appear to be covalent bonds, not only in carbon-halogen bonds but also in bonds between other electronegative atoms, such as O-O bonds in peroxides and in C-N and C-O bonds in other compounds [31].

These works suggest that the use of the IAM may not be the most ap-

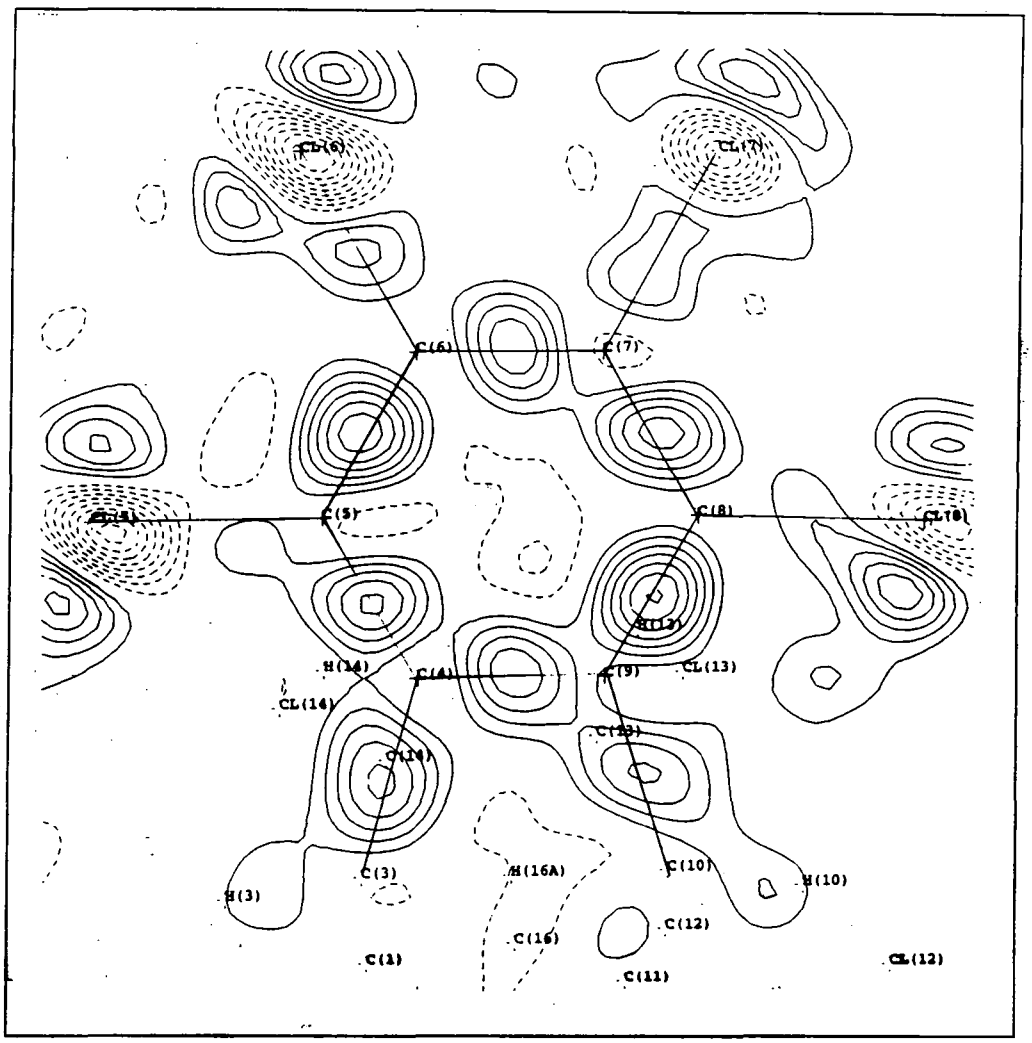

Figure 5.15: **Difference Fourier map in the plane of the aromatic ring.** $\rho_{obs} - \rho_{calc,SPH}$ **for all data to** $\sin\theta/\lambda$ 0.7Å^{-1}. **Contours drawn at** 0.1eÅ^{-3} **intervals.**

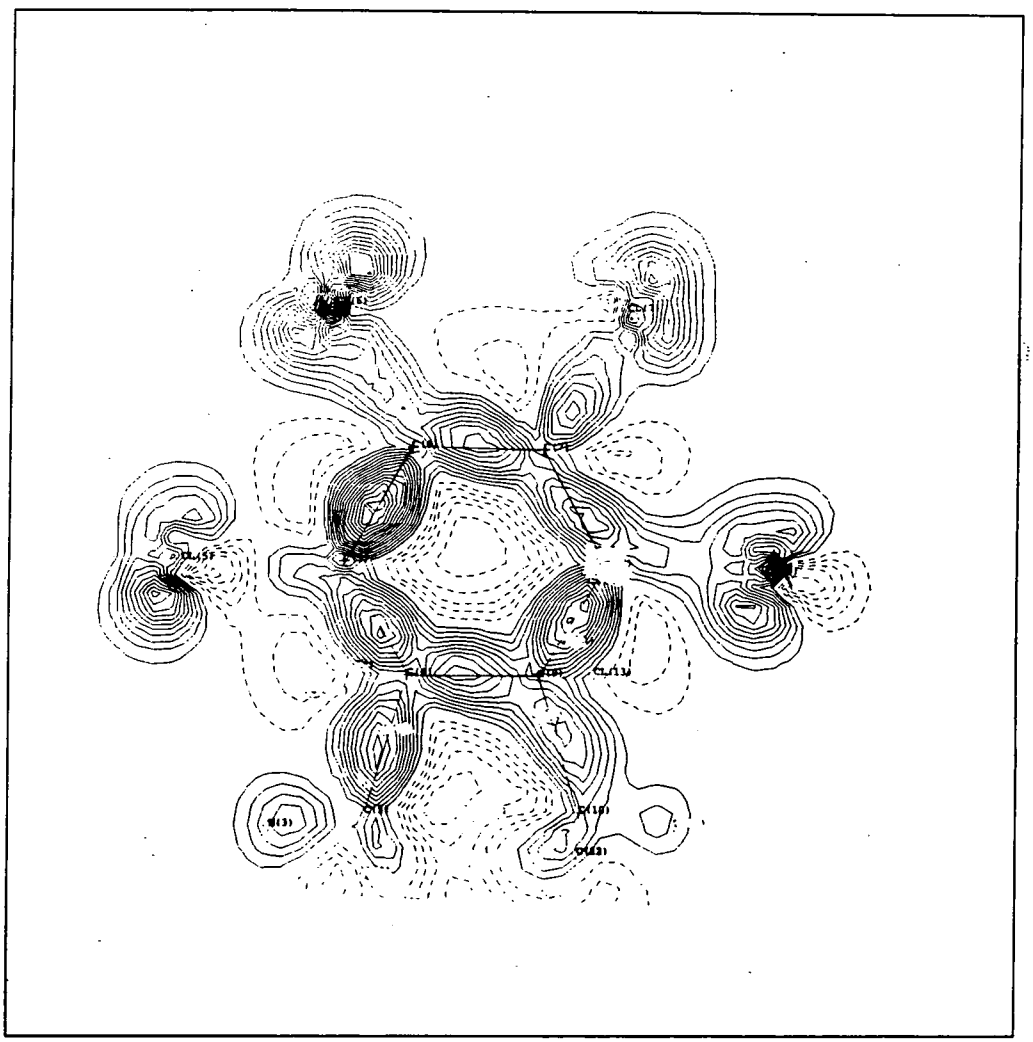

Figure 5.16: Static model deformation density in the plane of the aromatic ring. $\rho_{calc,MULT}$ for all data to $\sin\theta/\lambda$ 0.7Å^{-1}. Contours drawn at 0.1eÅ^{-3} intervals.

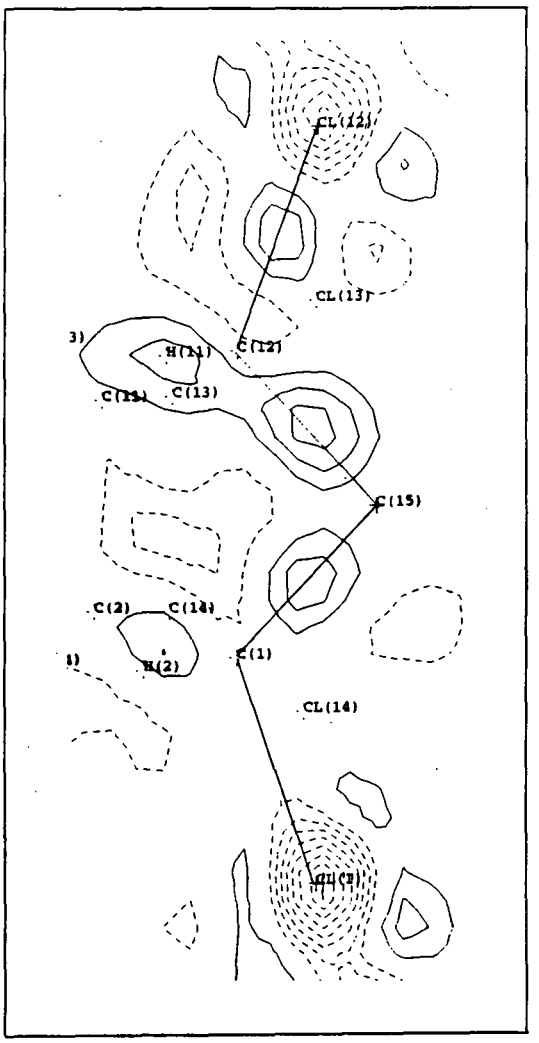

Figure 5.17: Difference Fourier map in the plane containing the C(1),C(12) and ligated chlorine nuclei. $\rho_{obs} - \rho_{calc,SPH}$ for all data to $\sin\theta/\lambda$ 0.7Å^{-1}. Contours drawn at 0.1eÅ^{-3} intervals.

propriate reference model to use to investigate the bonding in all bonds. For example, Kunze and Hall [28] describe the situation of fluorine in F_2. For the electronic configuration $2s^22p^5$ a spherical atom model will distribute the 5 electrons evenly over the three p orbitals and so $1\frac{5}{3}$ electrons will be removed from the direction along the bond. However, if there are in fact two filled p orbitals and one electron in the orbital lying in the direction of the bond, then the extra $\frac{2}{3}$ of an electron removed will compensate considerably for any accumulation of charge which results from bonding.

The suggestion has been made that, in order to investigate the bonding density in such situations, 'prepared' atoms may be more appropriate as a reference state. These prepared atoms have already taken into account orientation, polarisation and hybridisation effects. A second stage of deformation, due to the formation of a covalent bond, may then be investigated.

Such a model was proposed called the Oriented-Atom Model or OAM [4]. This model has been used in the study of a series of chlorobenzene derivatives [32]. In the initial experimental deformation maps using a conventional IAM as the reference density, very little accumulation of charge was observed in the C-Cl bonds. Such models account for the lone pair density explicitly and reveal the bonding density.

Features consistent with lone pair electron densities can be seen in the difference Fourier map shown in Figure 5.15 and in the model electron density shown in Figure 5.16. Figure 5.18 shows a section of the static deformation density through the Cl(8) nucleus perpendicular to the C(8)-Cl(8) internuclear vector. This map shows lobes of electron density suggestive of lone pair electron density, as do many of the other chlorine atoms in this structure. The orientation of these lobes of density appears to vary with respect to the C-Cl internuclear vectors but this is not perhaps surprising since all the chlorine atoms form terminal bonds to the ligated carbon atoms.

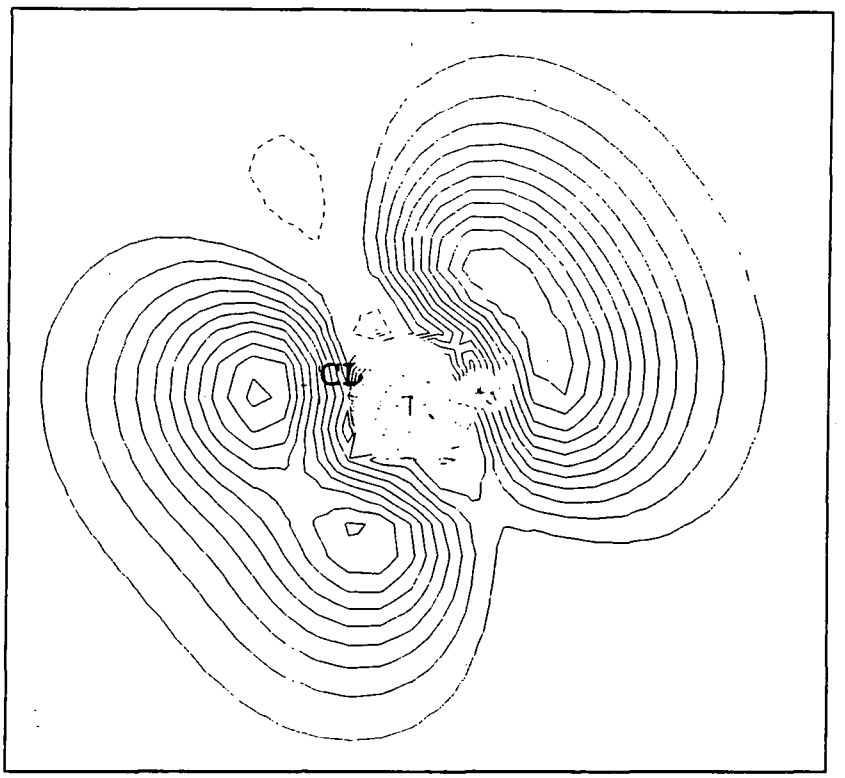

Figure 5.18: Static deformation density in a section through the Cl(8) nucleus perpendicular to the C(8)-Cl(8) internuclear vector. Contours are drawn at 0.1e$Å^{-3}$ intervals.

Bond	λ_1	λ_2	λ_3	$\rho(\mathbf{r}_c)$	$\nabla^2\rho(\mathbf{r}_c)$	ε	R_{ij}	d_1	d_2
C(1)-Cl(1)	-7.46	-5.14	11.02	1.194	-1.584	0.45	1.77	0.837	0.931
C(5)-Cl(5)	-9.25	-7.90	12.16	1.352	-4.988	0.17	1.72	0.820	0.901
C(6)-Cl(6)	-14.94	-10.99	13.57	1.748	-12.357	0.36	1.71	0.751	0.962
C(7)-Cl(7)	-12.29	-8.43	13.88	1.781	-6.845	0.46	1.71	0.823	0.891
C(8)-Cl(8)	-12.61	-8.91	14.26	1.568	-7.260	0.41	1.72	0.786	0.933
C(12)-Cl(12)	-10.81	-10.28	11.20	1.451	-9.901	0.05	1.77	0.775	0.996
C(13)-Cl(13)	-11.02	-8.58	13.22	1.541	-6.383	0.28	1.77	0.768	1.006
C(14)-Cl(14)	-13.92	-7.72	14.98	1.453	-6.653	0.80	1.78	0.832	0.951
C(15)-Cl(15)	-11.94	-9.65	13.33	1.648	-8.262	0.24	1.77	0.807	0.964

Table 5.7: Details of the C-Cl bond critical points.

Topological analysis of the electron density is free of the problems associated with the use of the IAM as the promolecule density as it uses the total electron density. Bond critical points were located between each of the bonded carbon and chlorine nuclei. The electron density at these bcps is somewhat lower than for the other types of bond. The values of $\rho(\mathbf{r}_c)$ at the carbon-chlorine bond critical points are given in Table 5.5. However, the same argument as that used to explain the higher densities in the C-H bonds suggests that this may be a consequence of the longer internuclear separations of the C-Cl bonds.

The Laplacian of ρ, $\nabla^2\rho(\mathbf{r})$, is also free of the problems associated with the IAM promolecule density. Local charge concentrations can indeed been seen in between the bonded carbon and chlorine nuclei, see Figure 5.19.

The atomic shell structure is also revealed by the Laplacian of ρ. Figure 5.20 shows the $\nabla^2\rho(\mathbf{r})$ in the section containing the C(15), Cl(15) and H(15) nuclei. Two shells are visible for the chlorine atom, one for the carbon and none for the hydrogen atom which has no core electrons.

The chlorine atoms are the least well modelled in the structure, with negative 'peaks' of electron density in the residual maps $\rho_{obs} - \rho_{calc,mult}$ of up to

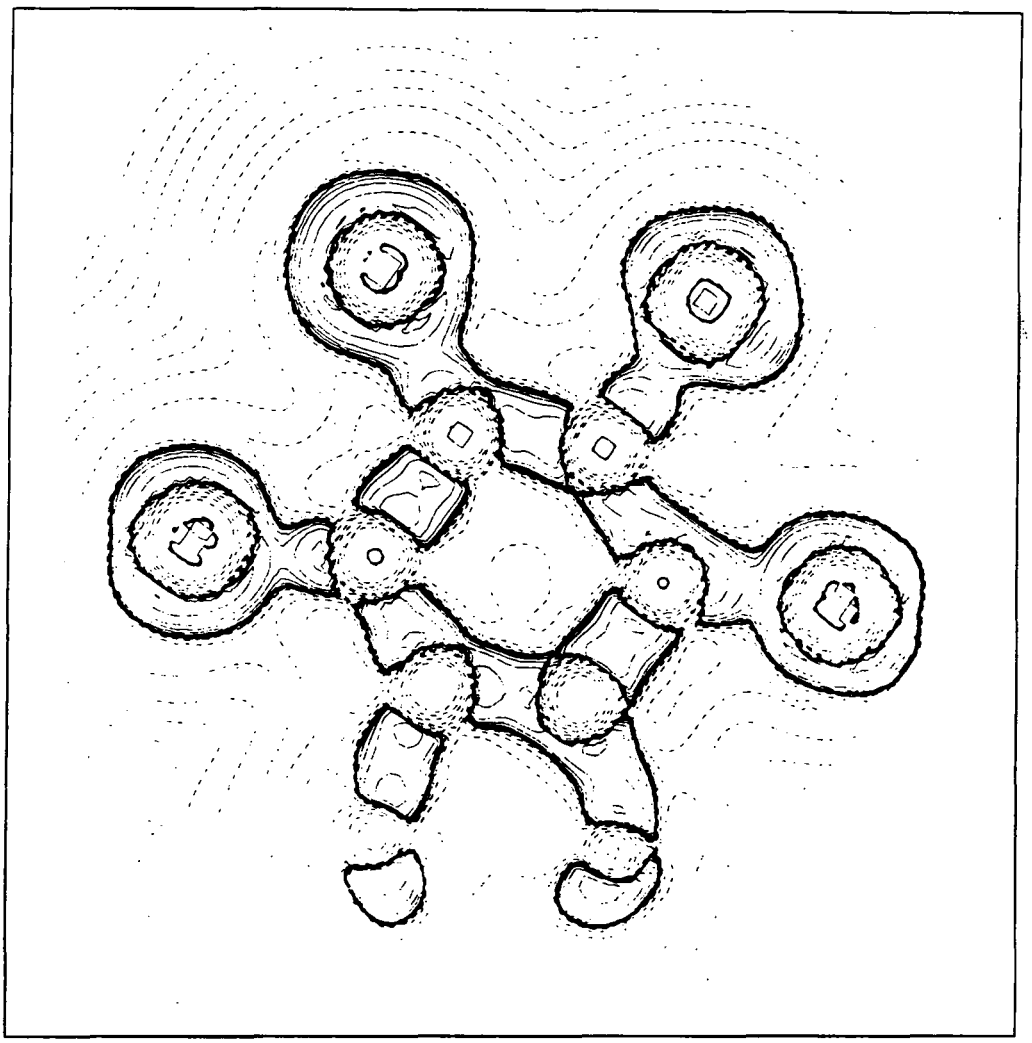

Figure 5.19: Laplacian of ρ ($\nabla^2\rho(\mathbf{r})$) in the plane of the aromatic ring.

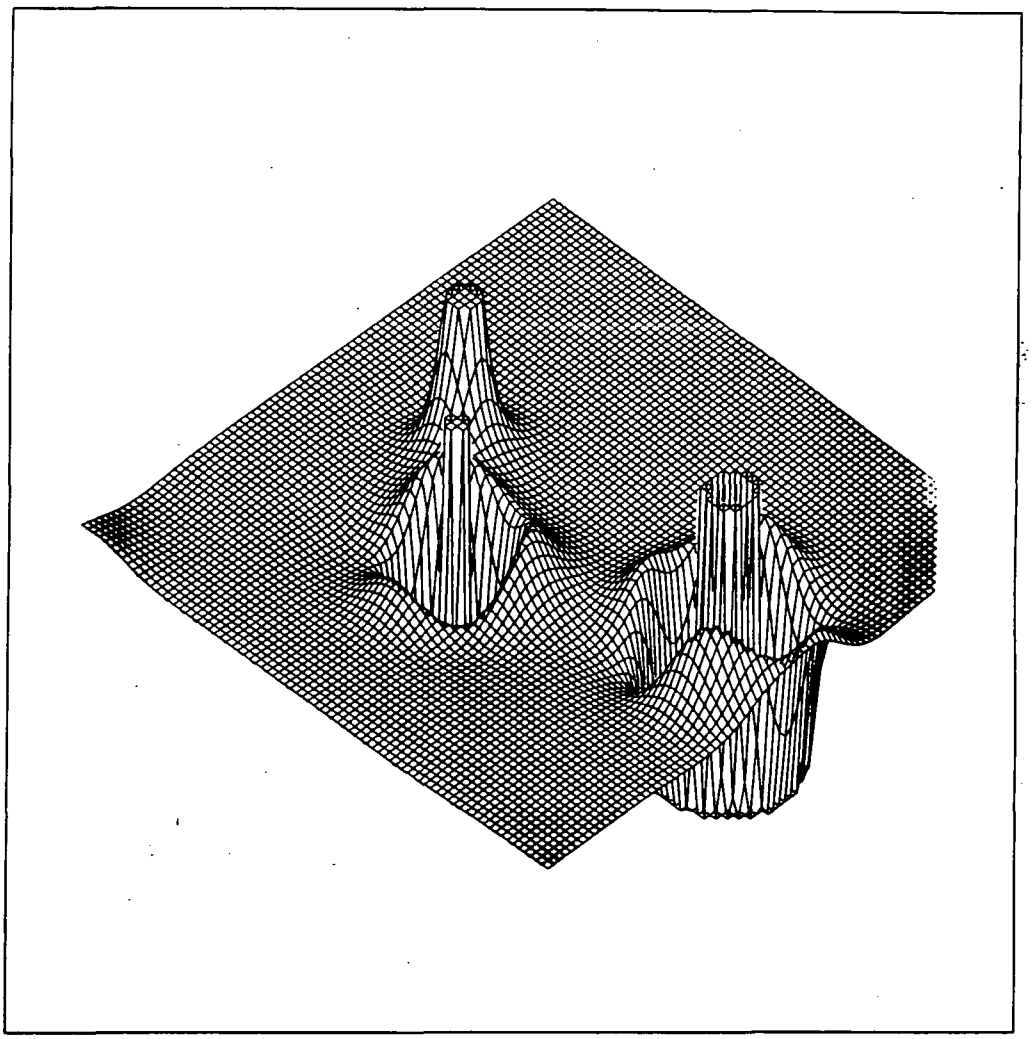

Figure 5.20: Relief plot of the Laplacian of ρ ($\nabla^2\rho(\mathbf{r})$) in the section containing the C(15), Cl(15) and H(15) nuclei.

around $0.5e\text{Å}^{-3}$ at the nuclear positions. However, the effect of any systematic errors in the data will tend to accumulate at the atomic positions, particularly at those of the heavier atoms. Such differences form a very small percentage of the total electron density of these atoms.

In general terms, the multipole model has successfully modelled the observed electron density in KM25 , especially for the carbon and hydrogen atoms. This study therefore shows that such studies of these compounds are feasible and can give credible results.

The results of this study provide an important reference density for comparison with other compounds in the series. However, the conclusions which can be drawn from this study in isolation are limited. A charge density study of the starting isomer, KM22, which rearranges to form KM25 may be more informative in terms of the compounds reactivity. Studies of more than one starting isomer with differing rates of rearrangement would be particularly interesting. There may also be scope for examining such densities in terms of reactivity using Bader's topological analysis of the electron density.

Bibliography

[1] P. Coppens (1967). *Science* **158**, 1577-1579.

[2] J.A.K. Duckworth, B.T.M. Willis and G.S. Pawley (1969). *Acta Cryst.* **A25**, 482-484.

[3] C. Lecomte (1990). In *The Application of Charge Density Research to Chemistry and Drug Design*, edited by G.A. Jeffrey and J.F. Piniella. New York:Plenum.

[4] W.H.E Schwarz, P. Valtazanos and K. Ruedenberg (1985). *Theor. Chim. Acta.* **68**, 471-506.

[5] P. Coppens, T.N. Guru Row, P. Leung, E.D. Stevens, P.J. Becker and Y.W. Yang (1979). *Acta Cryst.* **A35**, 63-72.

[6] R.F. Stewart (1976). *Acta Cryst.* **A32**, 565-574.

[7] N.K Hansen and P. Coppens (1978). *Acta Cryst.* **A34**, 909-921.

[8] F.L. Hirshfeld (1971). *Acta Cryst.* **B27**, 769-781.

[9] F.L. Hirshfeld (1977). *Theoret. Chim. Acta* **44**, 129-138.

[10] C.A. Coulson and M.W. Thomas (1971). *Acta Cryst.* **B27**, 1354-1359.

[11] F.L. Hirshfeld (1976). *Acta Cryst.* **A32**, 239-244.

[12] E. Clementi and D.L. Raimondi (1963). *J. Chem. Phys.* **38**, 2686-2689.

[13] R.F.W. Bader and K.F. Laidig (1990). *Transactions ACA* **26**, 1-21.

[14] R.F.W. Bader and H. Essén (1984). *J. Chem. Phys.* **80**, 1943-1960.

[15] K.B. Wiberg, R.F.W. Bader and C.D.H. Lau (1987). *J. Am. Chem. Soc.* **109**, 985-1001.

[16] K.B. Wiberg, R.F.W. Bader and C.D.H. Lau (1987). *J. Am. Chem. Soc.* **109**, 1001-1012.

[17] K. MacKenzie, J.A.K. Howard, E.C. Gravett, K.B. Astin, Liu Shi-Xiong, A.S. Batsanov, D. Vlaovic, J.P. Maher, M. Murray, D. Kendrew, C. Wilson, R.E. Johnson, T. Preiβ and R. Gregory (1993). *J. Chem. Soc. Perkin. Trans.* 2, 1211-1228.

[18] P. Coppens (1977). *Isr. J. of Chem.* **16**, 144-148.

[19] T. Koritsanszky, S.T. Howard, Z. Su, P.R. Mallinson, N.K. Hansen, and T. Richter (1994). *XD-* Package for multipole analysis of experimental electron densities.

[20] E. Clementi and C. Roetti (1974). *Atomic and Nuclear Data Tables* **14**, 177.

[21] P. Coppens, R. Boehme, P.F. Price and E.D. Stevens (1981). *Acta Cryst.* **A37**, 857-863.

[22] R.F. Stewart, E.R. Davidson and W.T. Simpson (1965). *J. Chem. Phys.* **42**, 3175-3187.

[23] V.G. Tsirelson and R.P. Ozerov (1992). *J. Mol. Struct. (Theochem)* **255**, 335-392.

[24] J.D. Dunitz, W.B. Schweizer and P. Seiler (1982). *Helv. Chim. Acta* **66**, 123-133.

[25] F.L. Hirshfeld (1984). *Acta Cryst* **B40**, 484-492.

[26] A. Kvick, R. Thomas and T.F. Koetzle (1976). *Acta Cryst.* **B32**, 224-231.

[27] C. Cohen-Addad, J.-M. Savariault and M.S. Lehmann (1981). *Acta Cryst.* **B37**, 1703-1706.

[28] K.L. Kunze and M.B. Hall (1986). *J. Am. Chem. Soc.* **108**, 5122-5127.

[29] K.L. Kunze and M.B. Hall (1987). *J. Am. Chem. Soc.* **109**, 7617-7623.

[30] M.A. Spackman and E.N. Maslen (1985). *Acta Cryst.* **A41**, 347-353.

[31] J.D. Dunitz and P. Seiler (1983). *J. Am. Chem. Soc.* **105**, 7056-7058.

[32] H. Takazawa, S. Ohba and Y. Saito (1989). *Acta Cryst.* **B45**, 432-437.

Chapter 6

Structural Studies of Four Coordinate Nb Half-Sandwich Imido and Mo Bis(imido) Bent Metallocene Analogues

6.1 Introduction

This chapter contains details of the structure determination of several organometallic complexes synthesised by the group of Prof. V.C. Gibson of the Department of Chemistry, University of Durham. This work has been published in References [1, 2] and [3] and details of the syntheses and other characterisation of the samples is given in the Ph.D. theses of A.D. Poole, M. Jolly and P.W. Dyer [4, 5, 6]

These compounds can be considered as analogues of the bent Group 4 metallocenes [Cp_2ML_2], where M=Ti, Zr. Complexes containing the bent metallocene fragment have been found to be important reagents in organic syntheses

[7] and as catalysts for polymerisation reactions, for example as Ziegler Natta catalysts [8].

In comparison to the highly symmetrical 'normal' metallocenes, such as ferrocene, the metallocenes of early transition metals are electron deficient. However, they may achieve an 18-electron configuration by coordinating additional ligands which, in turn, causes the $[Cp_2M]$ fragment to adopt a bent geometry. Lauher and Hoffman [9] have examined the frontier orbitals of a bent $[Cp_2M]$ fragment using Extended Hückel Molecular Orbital calculations on a model of $[Cp_2Ti]^{2+}$. They have computed that there are three empty, low-lying molecular orbitals (one b_2 and two a_1) which may bind additional ligands. All three of these molecular orbitals lie in the yz plane as shown in Figure 6.1. The b_2 orbital is mainly d_{yz} in character, whereas both a_1 orbitals contain some contribution from the s and p as well as the $d_{x^2-y^2}$ and d_{z^2} orbitals. The $1a_1$ is strongly directed along the y-axis and the $2a_1$ is hybridised along the z-axis.

Gibson *et al* [10] have carried out Fenske-Hall calculations (using a consistent set of coordinate axes) investigating the bonding in Group 5 half-sandwich imido complexes such as $[CpNb(NMe)Cl_2]$ and some other related cyclopentadienyl compounds. The accessible frontier orbitals available for ligand coordination in these compounds were found to be very similar (in energy and orientation) to those of the bent metallocenes. From a consideration of the bonding of both cyclopentadienyl, Cp^-, and imido, NR^{2-}, closed shell anions it can been seen that both form $(2\pi + 1\sigma)$ type interactions with a transition metal. The Cp group in Cp_2ZrX_2 forms a strong π-type interaction with the metal d_{xz} and d_{yz} and a σ-type interaction with the s and p_z orbitals. For the later transition metals, the two unfilled δ^*-symmetry orbitals of the Cp ligand are another important difference as $\delta - \delta^*$ back-bonding from filled

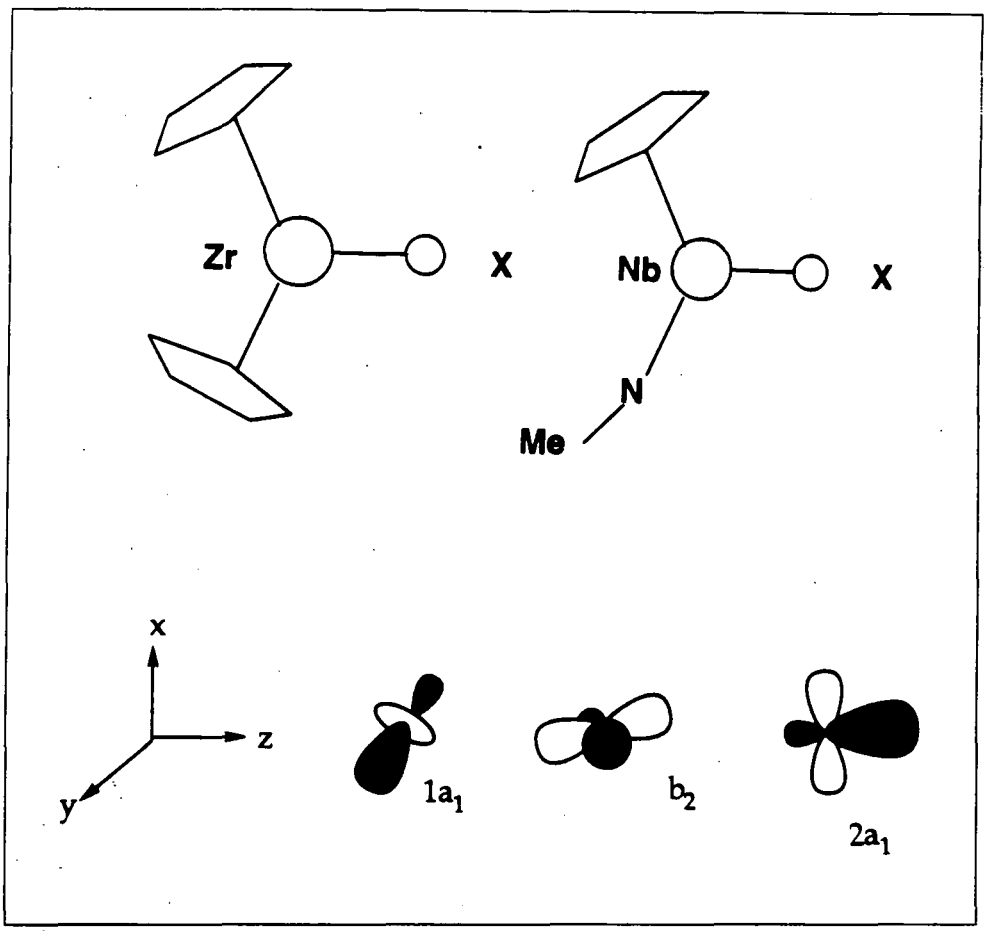

Figure 6.1: Axial framework for MO calculations and representations of the three low lying Molecular Orbitals.

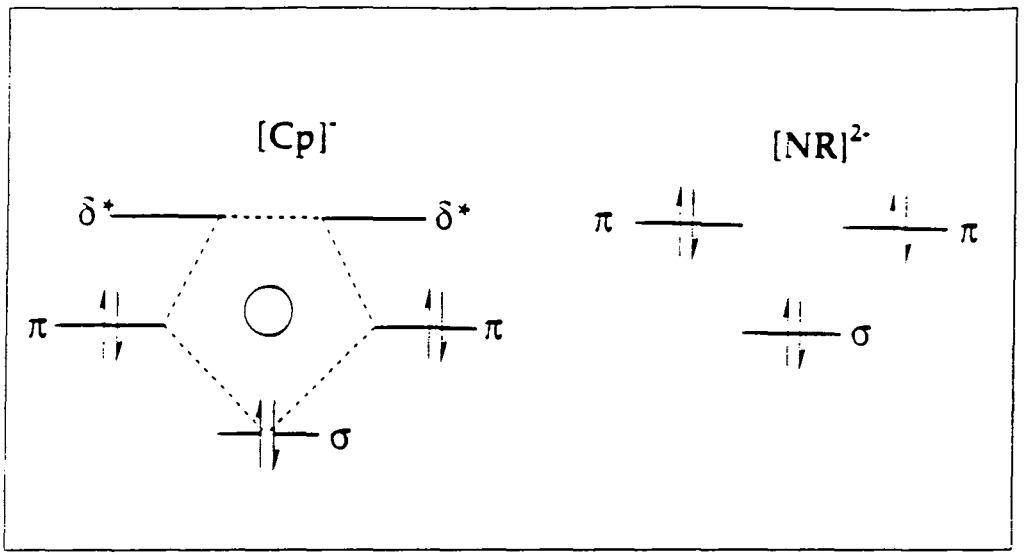

Figure 6.2: Representation of the energies of the $[Cp]^-$ and $[NR]^{2-}$ fragment frontier orbitals.

metal d-orbitals of suitable symmetry is possible.

The linear imido group, NR, formally donates four electrons, one less electron than the η^5-C_5H_5 group, to the metal electron count. This suggests that half-sandwich imido Group 5 complexes can be considered to be valence isoelectronic and isolobal to the Group 4 metallocenes. By analogy this relationship may be extended to the bis(imido) complexes of Group 6 metals, see Figure 6.3

Imido ligands have the useful ability to act as both two and four electron donors to transition metals as shown in Figure 6.4. The linear, four electron donor implies a triple M-N bond where an *sp* hybridised nitrogen forms one σ and two π bonds to the metal. In the bent bonding mode the imido acts as a two electron donor retaining its lone pair on the nitrogen. The variation in bonding mode allows the stabilisation of the metals in their highest oxidation states yet the imido ligand can also act as a two electron donor on reduction of the metal centre [11]. The two electron donating mode of bonding usually occurs when there is only one metal orbital of π-symmetry available or where the metal d-orbitals are filled. The use of a bulky organo substituent can also

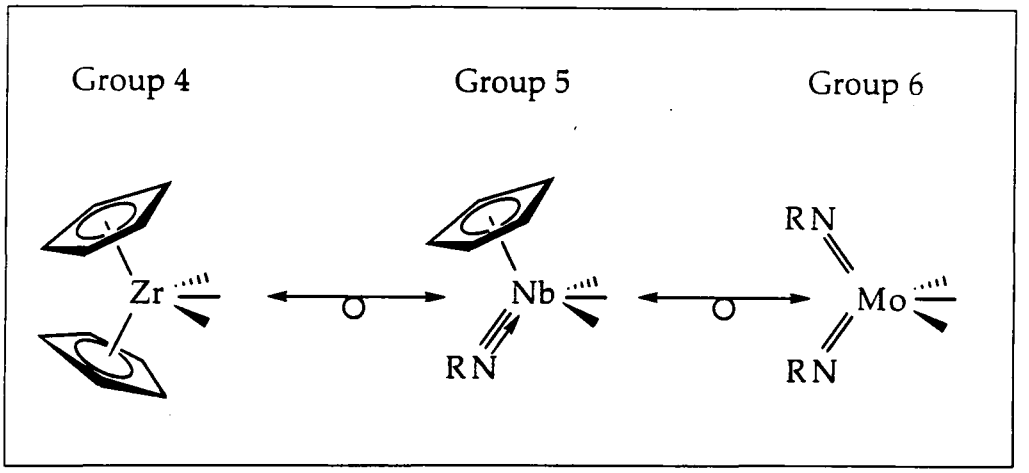

Figure 6.3: Isolobal 14 electron fragments of Group 4, 5 and 6 metals.

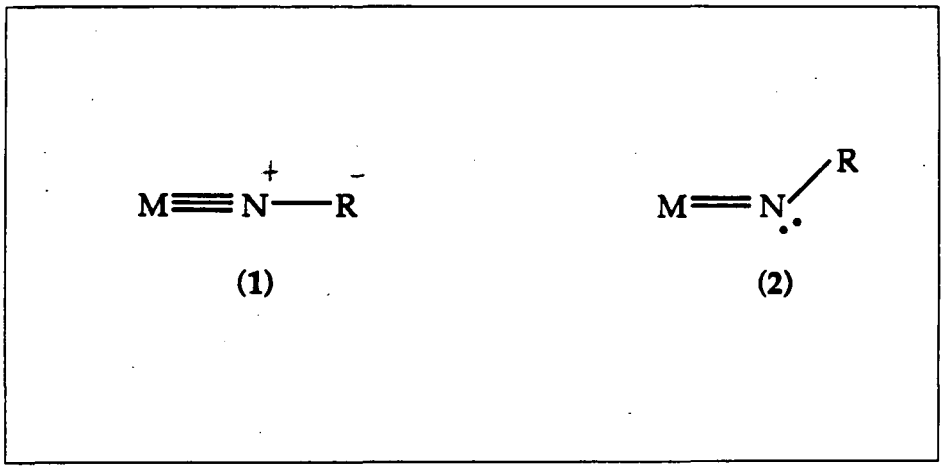

Figure 6.4: Two of the possible bonding modes of the imido group NR^{2-}.

be employed to stabilise low coordinate, highly reactive metal centres and thus imido ligands can provide a means of tailoring both the steric and electronic properties of the complex.

Although the strength of the M-L multiple bond may provide an important stabilising effect in catalytic cycles it is still an unsaturated bond and as such remains a possible reactive site. However, these ligands are increasingly being used as ancillary ligands, much as cyclopentadienyl groups are commonly used.

The isolobal and valence isoelectronic relationship of the Group 4 and 5 complexes to the Group 4 metallocenes, the chemistry of which is very well documented, allows the geometry and chemistry of these compounds to be predicted to a certain degree. A large number of these Group 4 and 5 compounds, with chemistry related to the Group 4 metallocenes, have been synthesised and their chemistry investigated. Single crystal X-ray diffraction studies on six of these compounds have been made, the results of which are reported herein. These studies allow the detailed geometry of these molecules as determined experimentally to be compared to that predicted using this 'isolobal' relationship.

6.2 Experimental

The six compounds discussed herein and the numbering scheme used for the complexes are shown in Figure 6.5. For atom labelling schemes see Figures 6.9 to 6.18 later in this chapter.

All six compounds were sensitive to air and to moisture and so were mounted in capillaries under N_2 using dried Apiezon grease. In all cases data were collected on an automated 4-circle Rigaku AFC6S diffractometer using graphite monochromated Mo-K_α X-radiation. Data were collected at room

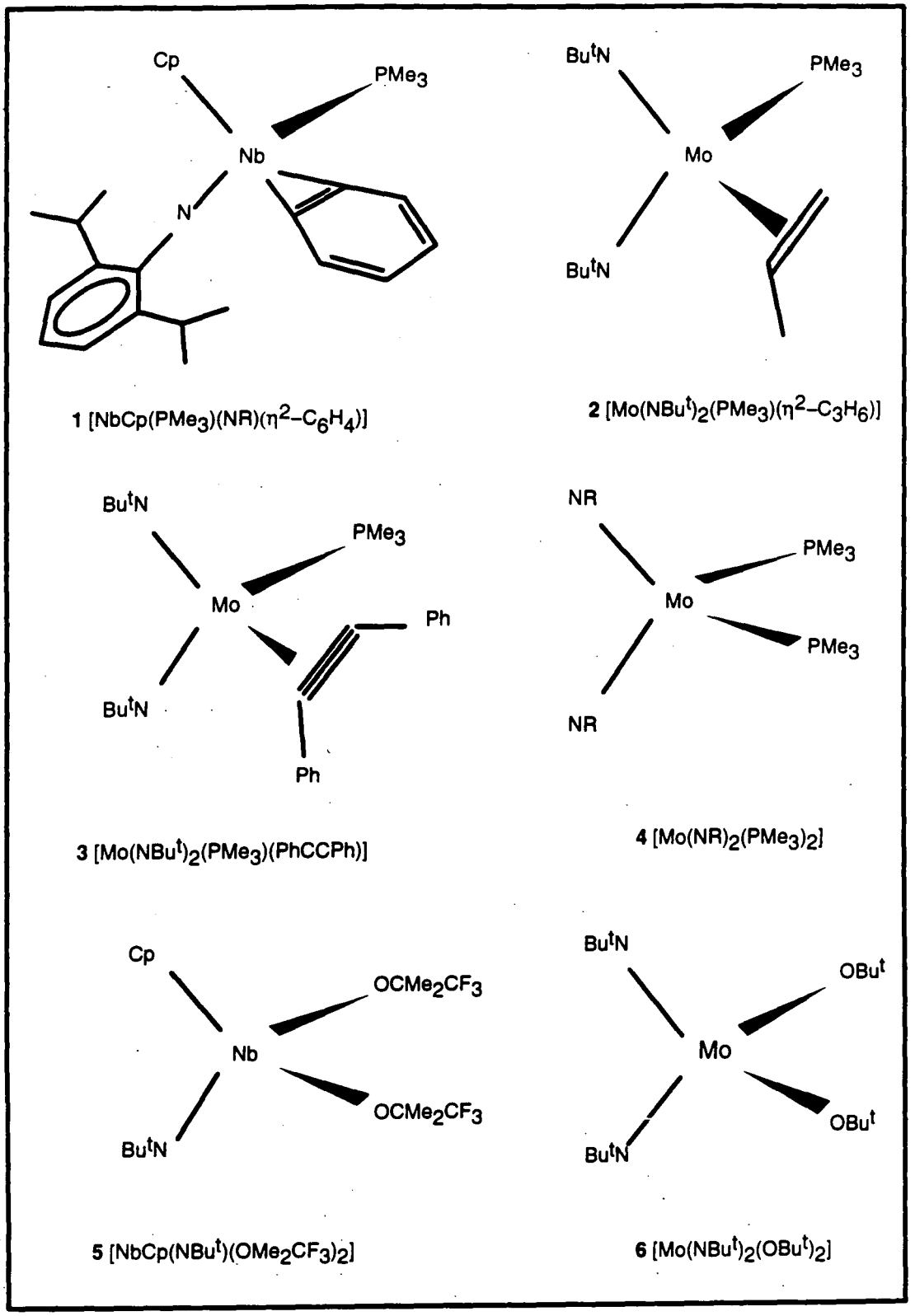

Figure 6.5: Numbering scheme for the organometallic compounds. R=2,6-$^{i}Pr_2C_6H_3$.

temperature for **1** and **2** and also for **4** as cooling was not satisfactory for this compound. **3** was measured at 120K and **5** and **6** were necessarily measured at low temperatures as both compounds had low melting points. Cooling was effected using a Cryostream [12] N_2 gas stream device. Details of data collection are given in Tables 6.1 to 6.4.

Net intensities, corrected for Lorentz-polarisation effects, were calculated from the raw X-ray data by the *PROCESS* program; part of the *TEXSAN* [13] package. Data for all compounds were corrected for absorption by means of an empirical correction using the ψ-scan measurements.

All refinements were made using the *SHELXTL*-Plus [14] package by full matrix least-squares minimisation of

$$\sum w[|\mathrm{F(h)}|_{\mathrm{obs}} - |\mathrm{F(h)}|_{\mathrm{calc}}]^2$$

where

$$w^{-1} = \sigma^2(F(\mathbf{h})) + \mathrm{gF(h)}^2$$

Hydrogen atoms were placed in calculated positions using the positions of other relevant atoms at a C-H separation, d_{CH}, of 0.96Å. The positional parameters of the hydrogens were constrained to ride on the ligated carbon atoms, *i.e.* calculated shifts in x, y and z for a given carbon atom were applied to the attached H atom. Due to large thermal vibrations in several of the compounds other constraints and restraints were applied as detailed below.

1 [Nb(η^2-C_6H_4)Cp(N-2,6-$^i Pr_2C_6H_4$)(PMe_3)] and **3** [Mo(NBu^t)$_2$(PMe_3)(PhC≡CPh)]

Positional parameters and anisotropic adps were refined for all non-hydrogen atoms. All hydrogen atoms were given fixed isotropic adps, $U_{iso} = 0.08$.

2 [Mo(NBu^t)$_2$(PMe_3)(CH_2=$CHCH_3$)]

Apart from the carbon atoms, C(9), C(10) and C(11) for which a common isotropic adp was refined, anisotropic adps were refined for all other non-

hydrogen atoms and positional parameters were refined for all non-hydrogen atoms. The tertiary butyl group containing the above carbon atoms showed large thermal vibrations and was restrained to form a regular tetrahedron with a refined C-C bond length of 1.482(8)Å. The hydrogen atoms were treated as before with a fixed U_{iso} of 0.08Å^2.

4 [Mo(N-2,6-^{i}Pr$_2$C$_6$H$_3$)$_2$(PMe$_3$)$_2$]

This compound crystallised with one full molecule and two half molecules in the asymmetric unit. The two half molecules are situated on the 2-fold axes with the Mo atoms constrained to be on the special positions 0.5, y, 0.25 and 0, y, 0.25 and their anisotropic thermal factors constrained to be consistent with the 2-fold symmetry. The identical length of the cell dimensions a and b prompted a thorough search for higher symmetry to be made although none was found and the monoclinic symmetry was confirmed by the satisfactory refinement.

The isopropyl groups showed large thermal motion so the distances d_{C-C} from carbon (a) as labelled in Figure 6.6 to carbon (b) in each 'molecule' or part molecule were restrained to a refined common bonded C-C separation of 1.50(2)Å.

Of the non-hydrogen atoms the thermal parameters of the Mo, P, N and methyl carbons of the PMe$_3$ groups were refined anisotropically while all carbon atoms of the 2,6-diisopropylphenylimido ligands were refined isotropically. Individual isotropic adps were refined for the phenyl carbon atoms marked (c) in Figure 6.6. Common isotropic adps were refined for the carbon atoms (a) and for carbon atoms (b) in each of the 'molecules'. The hydrogen atoms were divided into four groups; methyl hydrogens of the PMe$_3$ ligands and phenyl hydrogens (each group with a common refined isotropic adp) and the hydrogens of the isopropyl groups attached to atoms (a) and (b) were assigned isotropic adps 1.2 times that of the ligated carbon atoms.

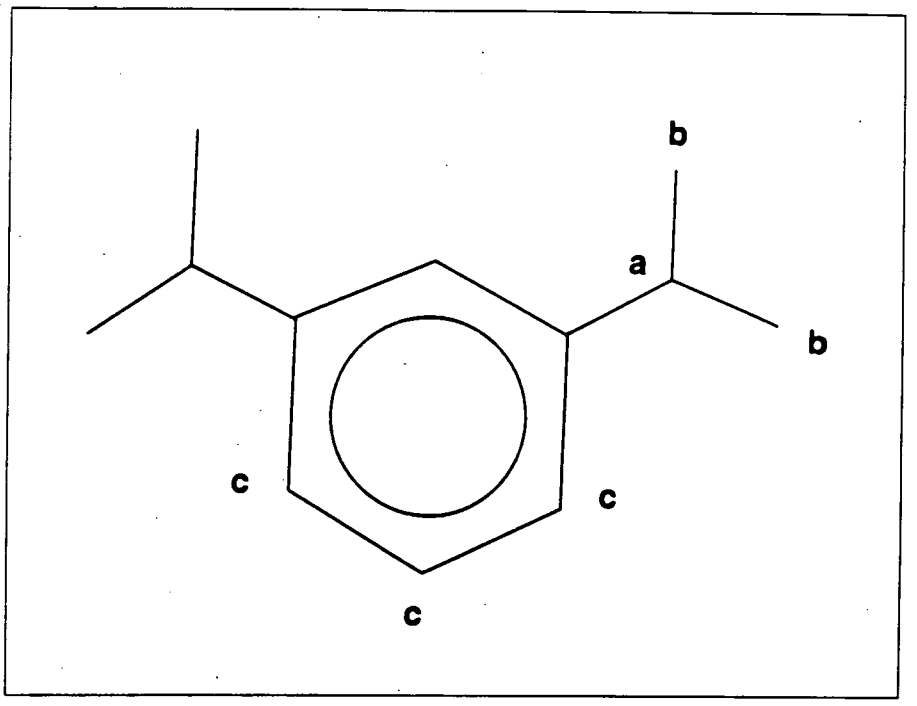

Figure 6.6: 2,6-diisopropylphenyl imido ligand with labelling for discussion.

5 [$NbCp(NBu^t)(OCMe_2CF_3)_2$]

This compound showed considerable disorder which was modelled as follows. The cyclopentadienyl group was modelled as two rings; C(1) to C(5) and C(1A) to C(5A) with occupancies of 0.55 and 0.45. These rings were constrained to be regular pentagons with a C-C separation of 1.42Å and were refined as a rigid group with a common isotropic adp. Hydrogen atoms also formed part of the rigid group and were assigned isotropic adps 1.2 times that of the carbon atoms.

Both the CF_3 and butyl carbon frame of the trifluorobutoxide ligands were restrained to the geometry of a regular tetrahedron, C-F and C-C separations were refined in each ligand. As for the cyclopentadienyl ring, these were also modelled as two sites C(11), C(12) C(13) with 0.7 occupancy and the second sites, C(11A), C(12A) C(13A), with an occupancy of 0.3. Similarly for the group attached to C(14) where the occupancy was 0.5 for each site.

Anisotropic adps were refined for the atoms Nb(1), the non-hydrogen atoms of the imido ligand and the oxygen atoms of the alkoxide ligands. Positional parameters were refined for all non-hydrogen atoms apart from those of the constrained Cp rings. Isotropic adps were refined for C(10) and C(14). Common isotropic adps were refined for the fluorine and for the carbon atoms in each butoxide ligand. Hydrogen atoms were assigned isotropic adps 1.2 times those of the ligated carbon atoms, apart from those of the imido ligand which were fixed at 0.08Å^2.

6 [$Mo(NBu^t)_2(OBu^t)_2$]

This compound also showed some disorder although to a far lesser degree. The tertiary butyl group of one imido ligand, that of N(2), was modelled as two sites with occupancies 0.6 and 0.4. Individual isotropic adps were refined for the carbon atoms C(14), C(15) and C(16) and their second site equivalents C(14A), C(15A) and C(16A). Anistropic adps were refined for all other non-hydrogen atoms and hydrogen atoms were refined an isotropic adp of 0.08Å^2. Positional parameters were refined for all non-hydrogen atoms.

6.3 Results and Discussion

This discussion is organised such that the initial part contains details relevant to all or several of the compounds. A slightly more detailed discussion of the individual structures then follows. The results of the studies of **1** to **4** have been published see references [1, 2] and [3].

All the compounds studied, **1** to **6**, can be considered as four coordinate at the metal and to have approximately tetrahedral geometry. **1** and **4** are half-sandwich niobium imido complexes, *i.e.* niobium complexes with an η^5-cyclopentadienyl ring and one imido group. The remaining four compounds, **2**, **3**, **5** and **6**, are bis-imido molybdenum complexes.

Compound	**1**	**2**	**3**
Formula	$NbNPC_{26}H_{35}$	$MoN_2PC_{14}H_{33}$	$MoPC_{25}N_2H_{37}$
Molecular Weight	485.4	356.3	492.5
D_{calc} gcm^{-3}	1.276	1.192	1.221
Cell Parameters			
a($\AA$)	16.140(2)	9.312(2)	13.980(3)
b($\AA$)	16.919(2)	9.723(2)	15.332(6)
c($\AA$)	18.511(4)	11.203(2)	24.988(9)
α°	90.0	78.85(2)	90.0
β°	90.0	88.23(2)	90.0
γ°	90.0	85.94(2)	90.0
Volume($\AA^3$)	5054.5(1)	992.5(4)	5356(3)
Temperature (K)	293	293	120
Z	8	2	8
Crystal System	Orthorhombic	Triclinic	Orthorhombic
Space Group	P*bca*	$P\bar{1}$	P*bca*
Crystal description	prism	prism	needle
Colour	orange	orange	yellow
Dimensions(mm)	0.3 × 0.15 × 0.35	0.25 × 0.35 × 0.5	1.0 × 0.2 × 0.2
Absorption			
μ (mm^{-1})	0.55	0.73	0.56
min/max transmission	0.89/1.00	0.908/1.00	0.92/1.00

Table 6.1: Details of Data Collection for **1**, **2** and **3**.

Compound	**1**	**2**	**3**
Formula	$NbNPC_{26}H_{35}$	$MoN_2PC_{14}H_{33}$	$MoPC_{25}N_2H_{37}$
$2\theta°$ range for	20-28	6-13	18-21
Cell parameters			
$2\theta°$ range data collection	5-55	5-55	5-55
Scan width A,B	1.52 0.3	1.37 0.3	0.945 0.4
(A + Btanθ °)			
Scan Speed $(\omega)°min^{-1}$	2.0-8.0	1.0-4.0	0.8-8.0
No.of data measured	6544	4945	8099
No.of unique data	5799	4555	4722
No.of observed data	2350	3839	2344
(σ(F) cut-off)	3	4	2
R_{int}	0.0061	0.0115	0.0656
No. of parameters refined	262	149	262
Final R	0.0559	0.0456	0.0585
Final R_w	0.0452	0.0644	0.0673
Goof	1.289	1.553	1.08
weighting (g)	0.0001	0.001	0.0015
$(\Delta\rho)_{min}(e\AA^{-3})$	-0.49	-0.65	-1.07
$(\Delta\rho)_{max}(e\AA^{-3})$	0.48	0.92	0.72

Table 6.2: Details of Data Collection (cont'd) for **1**, **2** and **3**.

Compound	**4**	**5**	**6**
Formula	$MoP_2N_2C_{30}H_{52}$	$NbC_{14}H_{26}NO_2F_6$	$MoN_2O_2C_{16}H_{36}$
Molecular Weight	598.6	483.3	384.4
D_{calc} gcm^{-3}	1.171	1.49	1.16
Cell Parameters			
a($\AA$)	25.848(6)	25.90(1)	17.969(4)
b($\AA$)	25.848(3)	10.214(5)	7.885(2)
c($\AA$)	21.340(3)	16.377(5)	17.881(4)
α°	90.0	90.0	90.0
β°	107.72(2)	96.04(3)	119.64(3)
γ°	90.0	90.0	90.0
Volume($\AA^3$)	13581(4)	4309(3)	2201.9(9)
Temperature (K)	293	150	200
Z	16	8	4
Crystal System	Monoclinic	Monoclinic	Monoclinic
Space Group	$C2/c$	$C2/c$	$P2_1/c$
Crystal description	prism	cube	prism
Colour	dark green	colourless	pale yellow
Dimensions(mm)	0.6 × 0.4 × 0.2	0.4 × 0.4 × 0.4	0.3 × 0.3 × 0.2
Absorption			
μ (mm^{-1})	0.499	0.619	0.601
min/max transmission	0.936/1.00	0.954/1.00	0.83/1.00

Table 6.3: Details of Data Collection for **4**, **5** and **6**.

Compound	**4**	**5**	**6**
Formula	$MoP_2N_2C_{30}H_{52}$	$NbC_{14}H_{26}NO_2F_6$	$MoN_2O_2C_{16}H_{36}$
$2\theta°$ range for lattice parameters	20-24	20-24	24-30
$2\theta°$ range data collection	5-45	5-50	5-50
Scan width A,B (A + Btanθ °)	1.26 0.35	1.37 0.3	1.31 0.3
Scan Speed $(\omega)°min^{-1}$	2.0-16.0	1.1-8.0	1.0-8.0
No.of data measured	9344	4225	4449
No.of unique data	8874	3792	3887
No.of observed data	4121	2702	2965
(σ(F) cut-off)	2	4	4
R_{int}	0.016	0.020	0.018
No. of parameters refined	382	172	187
Final R	0.0603	0.0754	0.0429
Final R_w	0.0668	0.1014	0.0486
Goof	1.71	2.29	2.04
weighting (g)	0.0002	0.0008	0.0001
$(\Delta\rho)_{min}(e\AA^{-3})$	-0.36	-0.98	-0.42
$(\Delta\rho)_{max}(e\AA^{-3})$	0.66	1.04	0.58

Table 6.4: Details of Data Collection (cont'd) and Structure Refinement.

The tetrahedral geometry can be illustrated by certain bond and interplanar angles. For example the bond angles around the Mo atom in **3** range from 100.7(2)° to 117.6(3)°. The use of the centroid of the Cp rings, X, and the midpoint, Y, of the coordinated C-C bond of the acetylenes and olefins of **1**, **2** and **3** facilitates this demonstration.

Examination of the angle between the plane defined by the Cp centroid, imido N atom and the metal for the half-sandwich imido complexes or the two imido N atoms and the metal for the bis-imido ligands and a second plane containing the ligated atoms of the remaining ligands, *e.g.* C(1), C(2) and P(1) for **3**, also illustrates the tetrahedral geometry.

Figures 6.9 and 6.11 to 6.18 show the molecular structure and labelling scheme for each of the complexes and selected bond lengths and angles are given in Tables 6.5 to 6.10. Full lists of atomic coordinates, adps, bond lengths and angles are given in Appendix A.

	Atoms defining		Interplanar
Compound	Plane 1	Plane 2	angle (°)
1	X, N(1), Nb	C(1), C(2), P, Nb	95.9
2	N(1), N(2), Mo(1)	C(1), C(2), P(1), Mo(1)	89.4
3	N(1), N(2), Mo	C(1), C(2), P(1), Mo	90.4
4	N(31), N(32), Mo(3)	P(31), P(32), Mo(3)	82.8
5	X, N(1), Nb(1)	O(1), O(2), Nb(1)	89.4
6	N(1), N(2), Mo(1)	O(1), O(2), Mo(1)	90.4

However, as well as illustrating the tetrahedral geometry these angles are also important to the discussion of the pseudo-isolobal relationship between these compounds and the Group 4 bent metallocenes. If the pseudo-isolobal relationship, as discussed in the introduction to this chapter, is valid, then the coordinated acetylenic carbon atoms of **1** and **3** and olefinic carbons of **2** are expected to be coplanar with the phosphorous atom of the phosphine ligand and the metal.

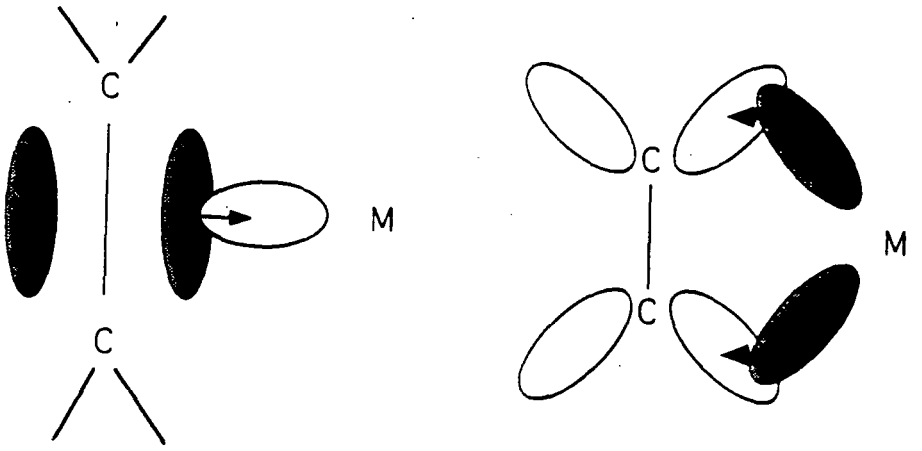

Figure 6.7: Diagram showing an MO view of olefin-metal bonding. σ interaction shown on the left, π backbonding on the right. Shading indicates filled orbitals.

Compound	Atoms defining plane	Mean deviation from plane (Å)
1	C(1), C(2), P, Nb	0.0292
2	C(1), C(2), P(1), Mo(1)	0.0381
3	C(1), C(2), P, Mo	0.0172

These atoms are clearly coplanar and show the geometry predicted for bent metallocene analogues, thus lending support to the pseudo-isolobal relationship.

In general terms the propene, the benzyne and the diphenylacetylene, interact with the metal in a similar manner. The interaction between the olefin and the metal has both a σ and π component; the σ component comes from the donation of C=C π-electrons to an unfilled d orbital on the metal, the π-component comes from the back donation from a filled metal *d* orbital into the vacant C=C π^* orbital, as shown in Figure 6.7. This back donation results in the lengthening of the C=C bond and in the extreme case the system may be viewed as a metallacyclopropane. The situation is similar for the alkynes but there are two sets of filled orthogonal π-orbitals available. Alkynes can therefore act as either two or four electron donors in which there is either a σ type donation or both σ and π donation.

The structure of complex **2** is consistent with this model of the bonding.

The C-C bond length for C(1)-C(2) of 1.431(7) is significantly longer than that of a free C=C suggesting that there is considerable back bonding from the metal to the C=C π^* antibonding orbital.

Similarly, the C-C separations in **1** and **3** are also longer at 1.34(1) and 1.306(12)Å than for a free C≡C bond (1.18Å) as given in Reference [15]. For these two compounds there is the added possibility of the alkynes acting as four electron donors, through the two mutually orthogonal π-systems. Templeton [16] has reported an empirical correlation of the number of electrons formally donated by the alkyne and the chemical shift of the bound acetylene nuclei in ^{13}C NMR spectra. The chemical shifts for the two acetylene carbon nuclei of **3** lie somewhere between the values for two and four electron donors. This intermediate value has been attributed to only partial donation from the second filled π-system of the alkyne due to competition for the available metal π-symmetry orbitals from the imido ligands [6].

The two bonding modes are expected to be reflected in structural changes in the acetylene and benzyne ligands. Churchill and Youngs [17] observed a marked alternation of bond lengths around the benzyne ring in Schrock's $[Ta(\eta^2\text{-}C_6H_4)(\eta^5C_5H_5)Me_2]$ complex. The alternating bond-lengths are consistent with the benzyne acting as a four electron donor, that is, electron pair donation from both filled π-orbitals of the benzyne. Such an alternation in these bond lengths is not seen in **1**. All bonds lengths in the benzyne ring, except the C≡C bond C(1)-C(2) at 1.340(10)Å, are equivalent within experimental error. The C-C separation in **3** is shorter than in both the Zr and Ta [18, 17] benzyne compounds (1.364Å in both cases).

Structural changes are also observed in the diphenylacetylene ligand when it binds to the molybdenum. There is considerable bending at the acetylenic carbon atoms, shown by the bond angles ∠C(1)-C(2)-C(201) and ∠C(2)-C(1)-C(101) which are 138.4(9) and 142.0(9)°. This bending at the acetylenic carbons and the elongated C-C bond length suggest that there is considerable

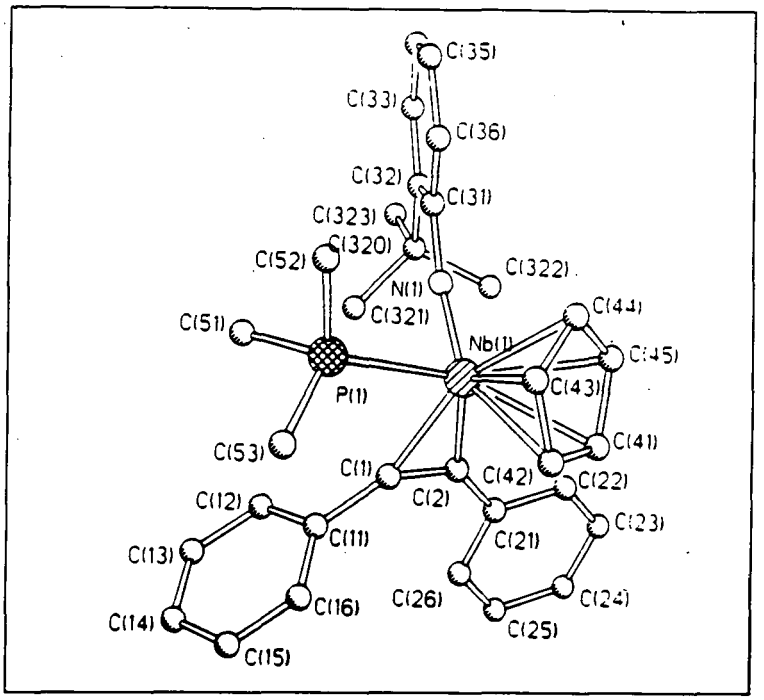

Figure 6.8: Molecular structure and labelling of [NbCp(N-2-Bu^{t}C$_6$H$_3$)(PhC≡CPh)(PMe$_3$)].

back-bonding from the metal to the π^*-orbitals of the acetylene. The closely related complex [NbCp(N-2-Bu^{t}C$_6$H$_3$)(PhC≡CPh)(PMe$_3$)], the structure of which has been determined at 150K by C.W. Lehmann [19], shows very similar geometry around the acetylenic carbon atoms; comparable bond angles are ∠C(11)-C(1)-C(2) 137.7(3) and ∠C(1)-C(2)-C(21) 136.0(3)° and a short C-C separation of 1.309(5)Å. See Figure 6.8.

The greater electronegativity of the alkyne ligands relative to the alkenes is reflected in the shorter M-C separations for **1** (2.139(7), 2.194(7) Å) and **3** (2.081(8), 2.158(9)Å) compared to those of **2** (2.238(4), 2.188(4)Å). Shorter separations are also observed in the Nb diphenylacetylene compound discussed above (2.200(3), 2.144(3)Å). The difference is especially marked given that Nb has a larger ionic radius.

As well as the overall tetrahedral geometry another feature common to

all six complexes is the presence of the imido ligands. As discussed in the introduction to this chapter, there are two main types of bonding for these ligands applicable to these complexes, linear and bent, shown in Figure 6.4. All the imido ligands in these compounds can be considered as linear from examination of the the bond angles ∠M-N-C. These angles are all greater than 160° (except for in the Mo bis-imido complex **6** where one of the angles is 169.5(6)° and the other 157.1(5)°). Such bond angles are thought to indicate linear M≡N triple bonds with the imido unit acting as an sp hybridised four-electron donor forming two π-bonds to the metal centre. However there are insufficient metal π-bonding orbitals available for two such ligands in a tetrahedral arrangement and it has been suggested that this might result in one bent two electron donating imido ligand and one linear four electron donor. From examination of the structures of these complexes the situation does not appear to be clear. For example, in the bis-imido **4** two imido ligands attached to two of the metal centres are not independent but are related by symmetry and so are necessarily equivalent.

1 [NbCp(N-2,6-^{i}Pr$_2$C$_6$H$_3$)(PMe$_3$)(η^2-C$_6$H$_4$)]

1 is a rare example of a niobium benzyne. The only other structurally characterised [Nb(η^2-C$_6$H$_4$)] complex is an unusual lithiated species [20]. The [Nb(η^2-C$_6$H$_4$)Cp(N-2,6-Pr$^i_2$C$_6$H$_4$)PMe$_3$] structure reported here shows a very similar metallocene-type geometry to that reported by Buchwald [18] for [Zr(η^5-C$_5$H$_5$)$_2$(η^2-C$_6$H$_4$)PMe$_3$].

The orientation of the benzyne ligand in the Ta complex [17] is very different from that of **1**, as shown in Figure 6.10. The Nb benzyne has the η^2-C$_6$H$_4$, Nb, P plane at an angle of 38.2° to the plane of the cyclopentadienyl ring, atoms C(19) to C(23), whereas in the Ta complex the benzyne ring is at an angle of 85.3° to the plane of the Cp ring and at 85.84° to the plane defined by the Ta atom and the two Me groups coordinated to it.

The benzyne ring of **1** is itself planar with a rms deviation of 0.0062Å .

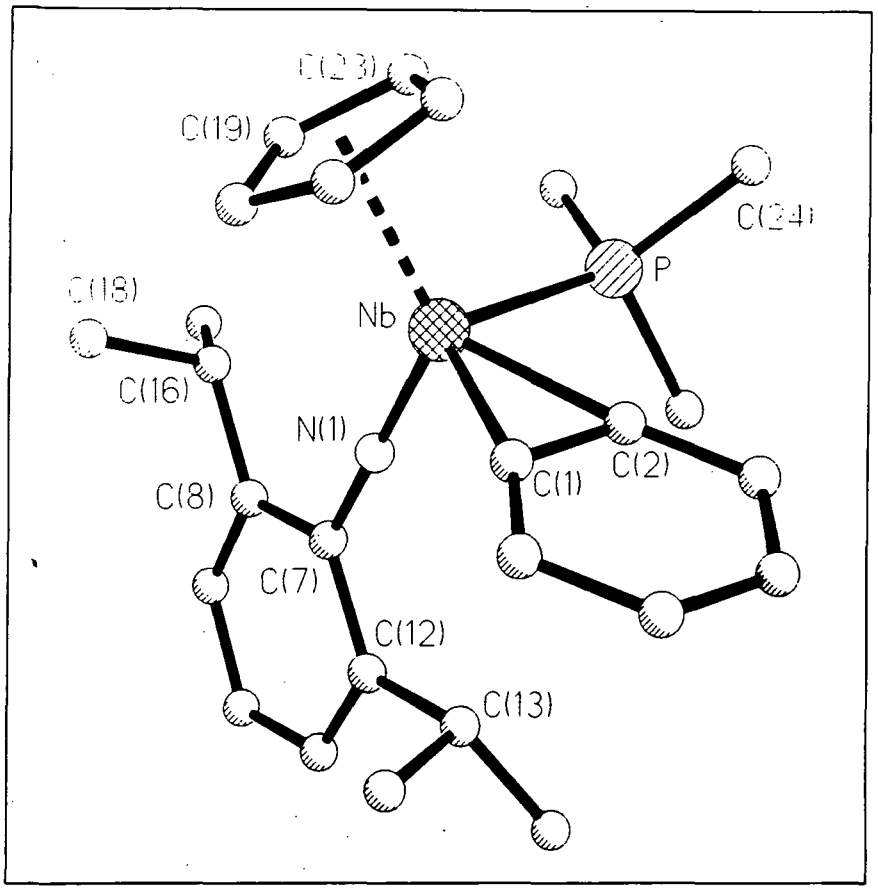

Figure 6.9: Molecular structure and labelling scheme for **1**.

A-B	d_{AB} (Å)
Nb-C(1)	2.139(7)
Nb-C(2)	2.194(7)
Nb-Y	2.060
Nb-N(1)	1.805(5)
Nb-X	2.161
Nb-P	2.528(2)
C(1)-C(2)	1.340(10)

A-B-C	∠ A-B-C (°)
N(1)-Nb-X	129.1
N(1)-Nb-Y	105.9
P-Nb-X	109.7
P-Nb-Y	95.7
X-Nb-Y	117.2
N(1)-Nb-P	90.7(2)

Table 6.5: Selected bond lengths and angles for **1**. X is the centroid of the Cp ring and Y is the centroid of the benzyne ring.

Figure 6.10: Projections of the Ta and Nb benzynes onto the plane of the Cp rings, showing the different relative orientations of the the Cp and benzyne rings.

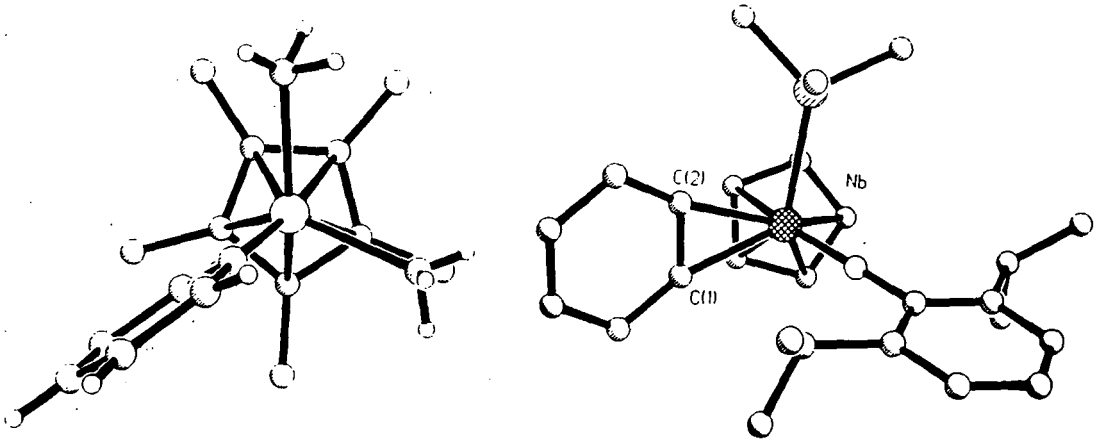

The bond lengths Nb-C(1) and Nb-C(2) are not equivalent, at 2.139(7) and 2.194(7)Å respectively, which may be a consequence of the asymmetry of their environment. The longer Nb-C(2) bond length is probably due to steric crowding by the bulky PMe_3 ligand. This asymmetry is also seen in Buchwald's Zr-benzyne complex [18] where the Zr-C bond lengths are 2.267(5) and 2.228(5)Å and again the longer bond length corresponds to the carbon atom closest to the PMe_3 group.

2 [Mo(NBu^t)$_2$(CH=CHMe)(PMe$_3$)]

The choice of [NBu^t] as the imido group rather than [N-2,6-Pr$^i_2$C$_6$H$_3$] was made in an attempt to form the 4-coordinate species rather than the 5-coordinate complex, [Mo(NAr)$_2$(PMe$_3$)$_2$(C$_2$H$_4$)]. The anisotropy of the aryl substituent allows it to orient such that the steric crowding around the metal centre is reduced, giving access to the 5-coordinate species.

There are two possible orientations of the propene whilst maintaining the metallocene-like geometry. The Me substituent may either be oriented towards

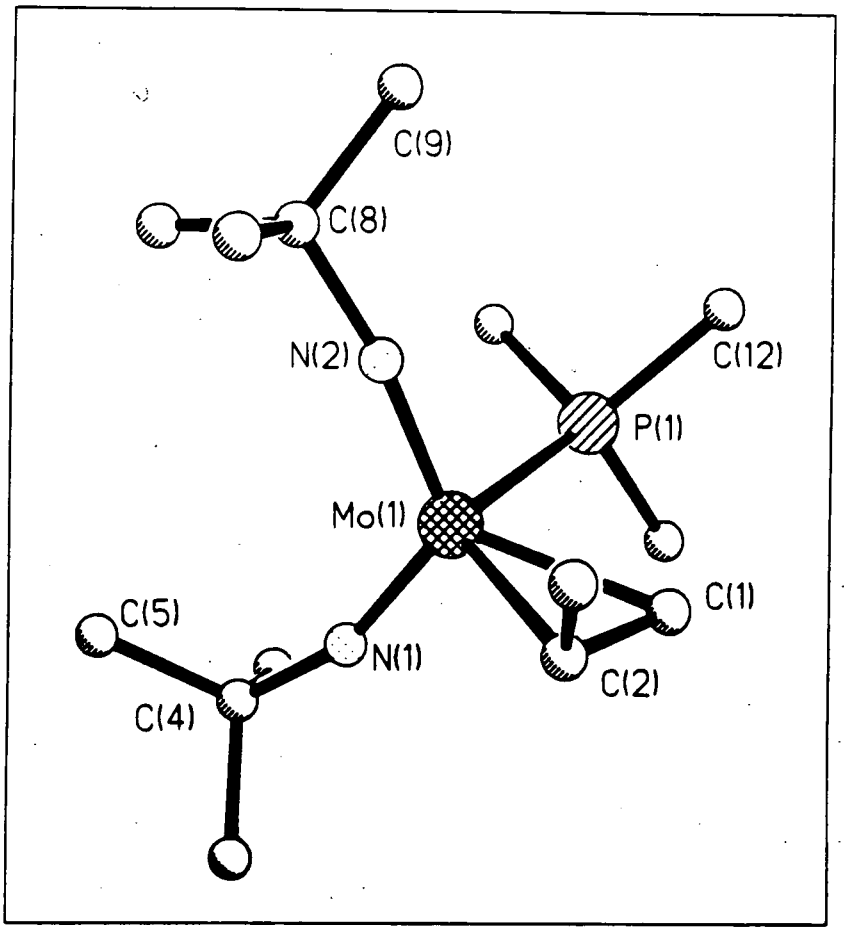

Figure 6.11: Molecular structure and labelling scheme for **2**.

A-B	d_{AB}(Å)
Mo(1)-C(1)	2.238(4)
Mo(1)-C(2)	2.188(4)
Mo(1)-X	2.094
Mo(1)-P(1)	2.446(1)
Mo(1)-N(1)	1.771(3)
Mo(1)-N(2)	1.772(4)
C(1)-C(2)	1.431(7)
C(2)-C(3)	1.517(8)

A-B-C	∠A-B-C (°)
P(1)-Mo(1)-X	99.6
N(1)-Mo(1)-X	113.3
N(2)-Mo(1)-X	114.2
P(1)-Mo(1)-N(1)	101.9(1)
P(1)-Mo(1)-N(2)	99.4(1)
N(1)-Mo(1)-N(2)	123.0(2)
Mo(1)-N(1)-C(4)	162.9(3)
Mo(1)-N(2)-C(8)	168.2(3)
C(1)-C(2)-C(3)	119.0(4)

Table 6.6: Selected bond lengths and angles for **2**. Y is the midpoint of C(1) and C(2).

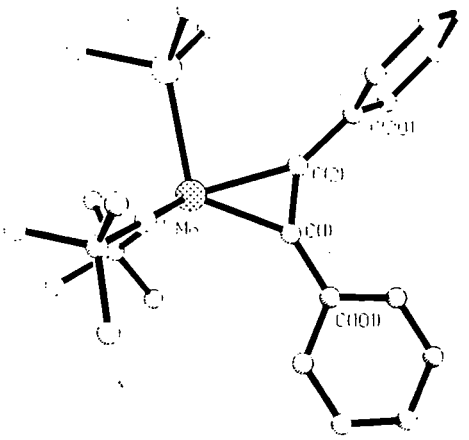

Figure 6.12: A view of **3** projected onto the plane of the Mo, P, C(1) and C(2) atoms, showing the tilt of the phenyl rings.

or away from the PMe_3 ligand. In this case it is oriented away from it, the *exo* isomer. This preferred orientation (supported by solution NMR data) probably results from this being the least sterically demanding arrangement of the Me substituent.

3 [$Mo(PMe_3)(NBu^t)_2(PhC{\equiv}CPh)$]

3 is an example of a transition metal complex of an alkyne. As discussed above, the PhC≡CPh group is in a plane with the Mo and P atoms which deviates 0.0172Å from planarity. The *ipso*-carbon atoms of the phenyl substituents also lie in this plane, the rms deviation from the plane defined by atoms C(1), C(2), C(101) and C(201) is 0.0015Å and 0.0099Å if the Mo atom is included in the definition of the plane. However the phenyl rings are tilted out of this plane; the ring containing C(101) to C(106) by 24.1° and the other, containing C(201) to C(206,) by 103.45° (see Figure 6.12). This is presumed to be for steric reasons as the second ring, C(201) to C(206), is closer to the bulky PMe_3 ligand. This effect is also reflected in the Mo-C bond lengths of 2.081(8) and 2.158(9)Å for Mo-C(1) and Mo-C(2) respectively.

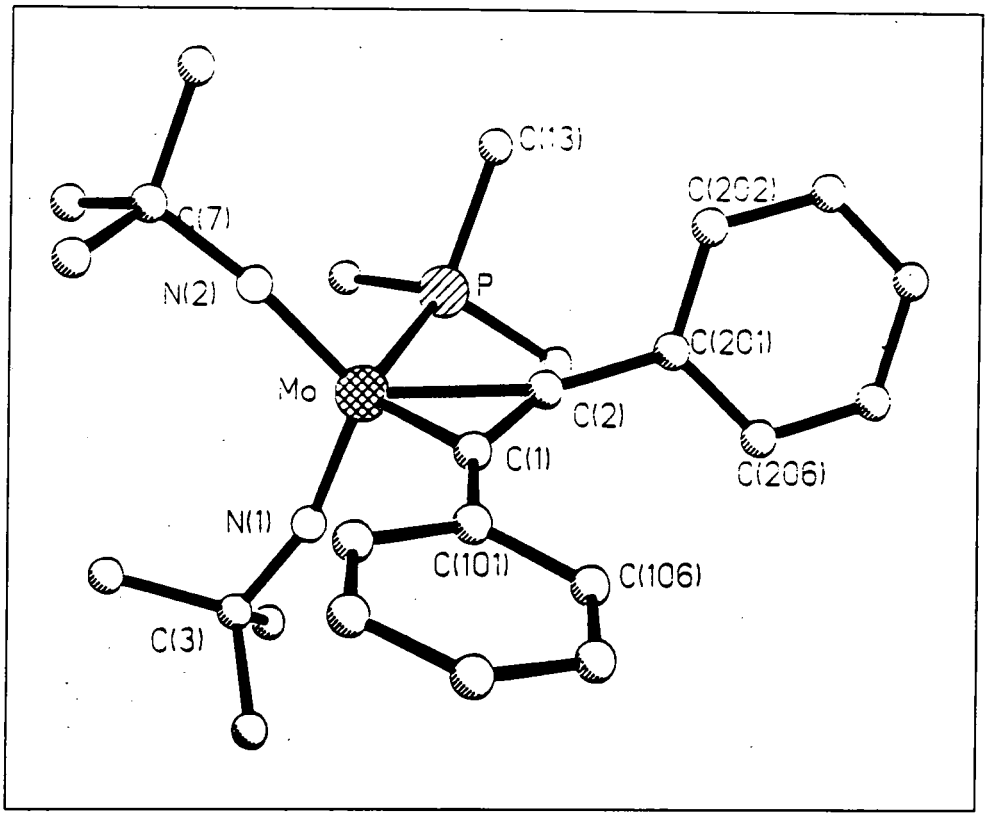

Figure 6.13: Molecular structure and labelling scheme for **3**.

A-B	d_{AB} (Å)
Mo-C(1)	2.081(8)
Mo-C(2)	2.158(9)
Mo-Y	2.017
Mo-N(1)	1.759(7)
Mo-N(2)	1.761(7)
Mo-P	2.465(3)
C(1)-C(2)	1.306(12)

A-B-C	∠ A-B-C (°)
N(1)-Mo-N(2)	117.6(3)
N(1)-Mo-P	100.7(2)
N(2)-Mo-P	100.7(3)
Mo-N(1)-C(3)	162.8(6)
Mo-N(2)-C(7)	171.6(7)
N(1)-Mo-Y	115.0
N(2)-Mo-Y	115.4
P-Mo-Y	103.6

Table 6.7: Selected bond lengths and angles for **3**. Y is the midpoint of C(1) and C(2).

Schwartz [7] comments on the possible usefulness of the inequivalence of the two substituents of the acetylene ligand. By using an asymmetrically substituted acetylene with one bulky substituent one particular orientation is expected to be favoured, as was observed in the structure of **2**. This would hence allow the selection of the products of certain reactions, for example, of protonation.

The overall geometry is again pseudo-tetrahedral, as shown by the bond lengths and angles around the metal centre given in Table 6.7. The molecular structure of **3**, see Figure 6.13, is similar to that reported by Floriani and co-workers of $[Ti(Cp)_2(CO)(PhC{\equiv}CPh)]$ [21]. The carbonyl ligand however is a much less bulky ligand than PMe_3 and the tilting of the phenyl rings is reduced relative to the plane containing the metal atom, the CO ligand and the acetylenic carbon atoms. The two rings form angles of 23.9° and 47.4° with the plane described above, the two M-C bond lengths are still significantly different at 2.107(7) and 2.230(7)Å.

The structure of an analogous $[Cp_2Zr(PhC{\equiv}CPh)PMe_3]$ complex has also been reported by Takahashi *et al* [22] which appears to have the same geometry as **3** but their structure is of poor quality.

A criterion given for an imido ligand to be considered as linear [11] is that the bond angle ∠M-N-C should be greater than 161°. Both the Mo-N-C bond angles are therefore acceptable for a linear imido group with the Mo-N(1)-C(3) of 162.8(6) and the Mo-N(2)-C(7) of 171.6(7). The two Mo-N bond lengths are identical within one esd at 1.759(7) and 1.761(7)Å for Mo-N(1) and Mo-N(2) respectively which are equivalent to the bond length quoted for an M≡N triple bond [11].

4 $[Mo(2,6\text{-}^{i}Pr_2C_6H_3)_2(PMe_3)_2]$

This compound crystallised with one full molecule on a general position and two half molecules with the Mo atoms on special positions with 2-fold symme-

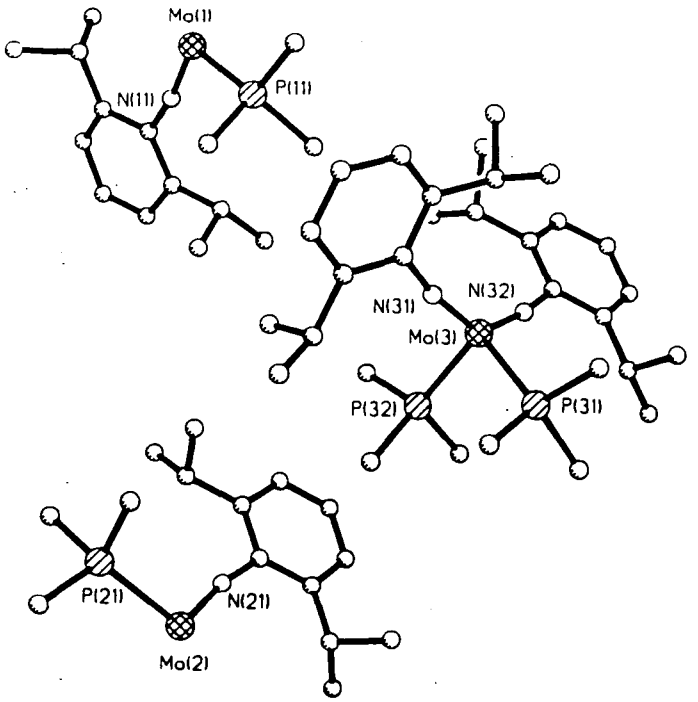

Figure 6.14: Contents of the asymmetric unit for **4**.

try. $[TiCp_2(PMe_3]$ [23] shows a similar pattern with one molecule in a general position and another on a 2-fold symmetry site in the space group F*dd*2. The contents of the asymmetric unit are shown in Figure 6.14, selected bond lengths and angles for the molecule in a general position centred on Mo(3) are given in Table 6.8 and Figure 6.15 shows the molecular structure and labelling scheme.

This complex has similar geometry to the the other compounds and as such can be considered as pseudo-tetrahedral, with the angle between the N(31), N(32) and Mo(3) plane and the Mo(3), P(31) and P(32) plane of 82.8°. However the ∠N(31)-Mo(3)-N(32) of 137.1(5) is greatly distorted from a tetrahedral angle.

The two imido ligands are approximately linear, with Mo(3)-N(31)-C(311) and Mo(3)-N(32)-C(321) bond angles of 169.8(9)° and 172.3(9)° respectively, as expected for a linear M≡NR bond.

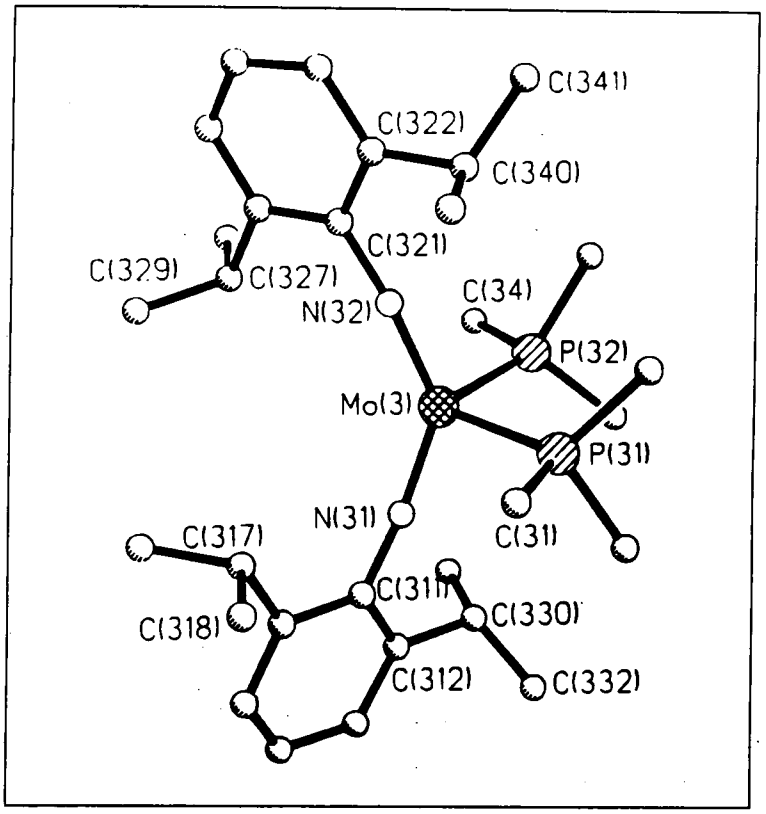

Figure 6.15: Molecular structure and labelling scheme for **4**.

A-B	d_{AB}(Å)
Mo(3)-P(31)	2.400(4)
Mo(3)-P(32)	2.405(5)
Mo(3)-N(31)	1.805(13)
Mo(3)-N(32)	1.797(10)

A-B-C	∠A-B-C (°)
P(31)-Mo(3)-P(32)	96.9(2)
P(31)-Mo(3)-N(31)	98.9(3)
P(32)-Mo(3)-N(31)	109.0(4)
N(31)-Mo(3)-N(32)	137.1(5)
Mo(3)-N(31)-C(311)	169.8(9)
Mo(3)-N(32)-C(321)	172.3(9)

Table 6.8: Selected bond lengths and angles for molecule of Mo(3) for **4**.

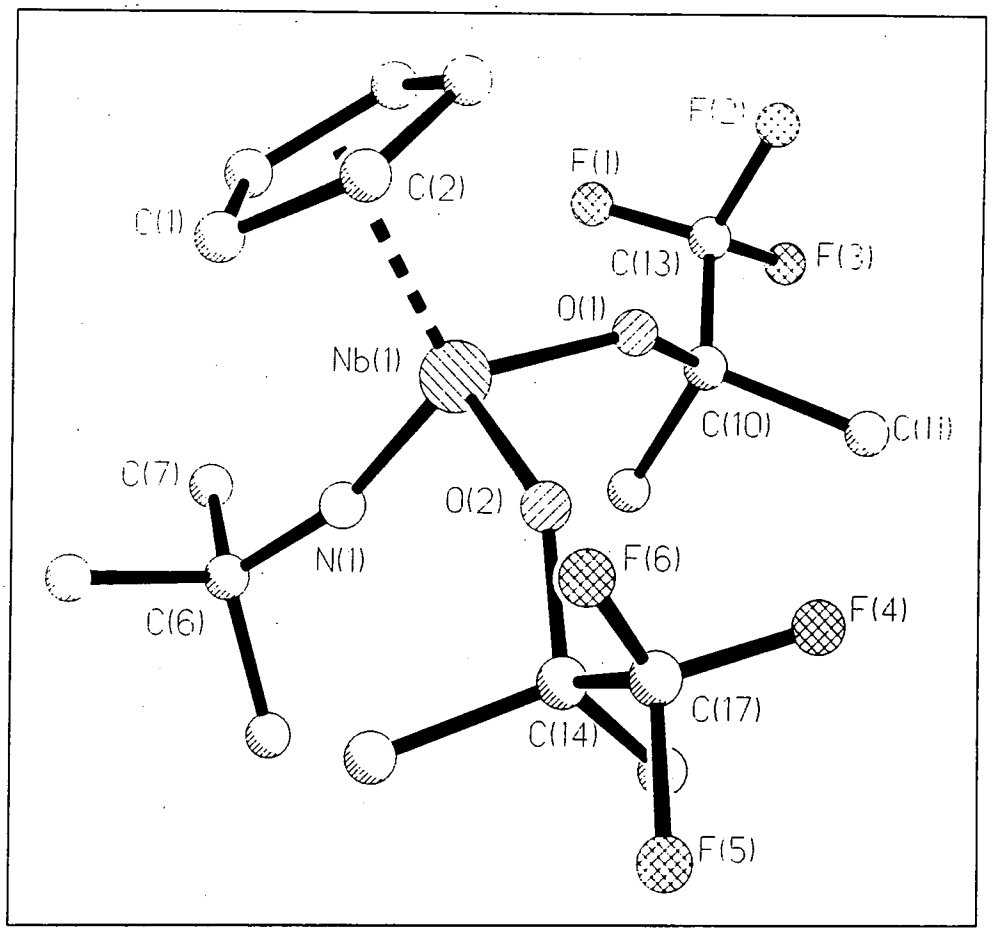

Figure 6.16: Molecular structure and labelling scheme for **5**. Second sites modelling disorder are omitted for clarity.

5 [$NbCp(NBu^t)(OMe_2CF_3)_2$]

This complex is a further example of a niobium half-sandwich imido with the predicted metallocene analogue structure. The angles around the niobium atom show the geometry to be approximately tetrahedral. Selected bond lengths and angles are given in Table 6.9 and, as for the other compounds, a full list of coordinates, bond lengths and angles is given in Appendix A.

The relative orientation of the trifluoro groups is, as one would expect from steric considerations, that they are oriented away from one another, as shown in Figure 6.17

A-B	d_{AB}(Å)
Nb(1)-O(1)	1.930(6)
Nb(1)-O(2)	1.936(6)
Nb(1)-N(1)	1.773(7)
Nb(1)-X	2.169
N(1)-C(6)	1.447(12)

A-B-C	∠A-B-C (°)
O(1)-Nb(1)-O(2)	102.1(3)
O(1)-Nb(1)-N(1)	106.1(3)
O(2)-Nb(1)-N(1)	106.9(3)
O(1)-Nb(1)-X	112.1
O(2)-Nb(1)-X	111.0
N(1)-Nb(1)-X	117.3
Nb(1)-N(1)-C(6)	165.6(7)

Table 6.9: Selected bond lengths and angles for **5**. X is the centroid of the Cp ring C(1) to C(5).

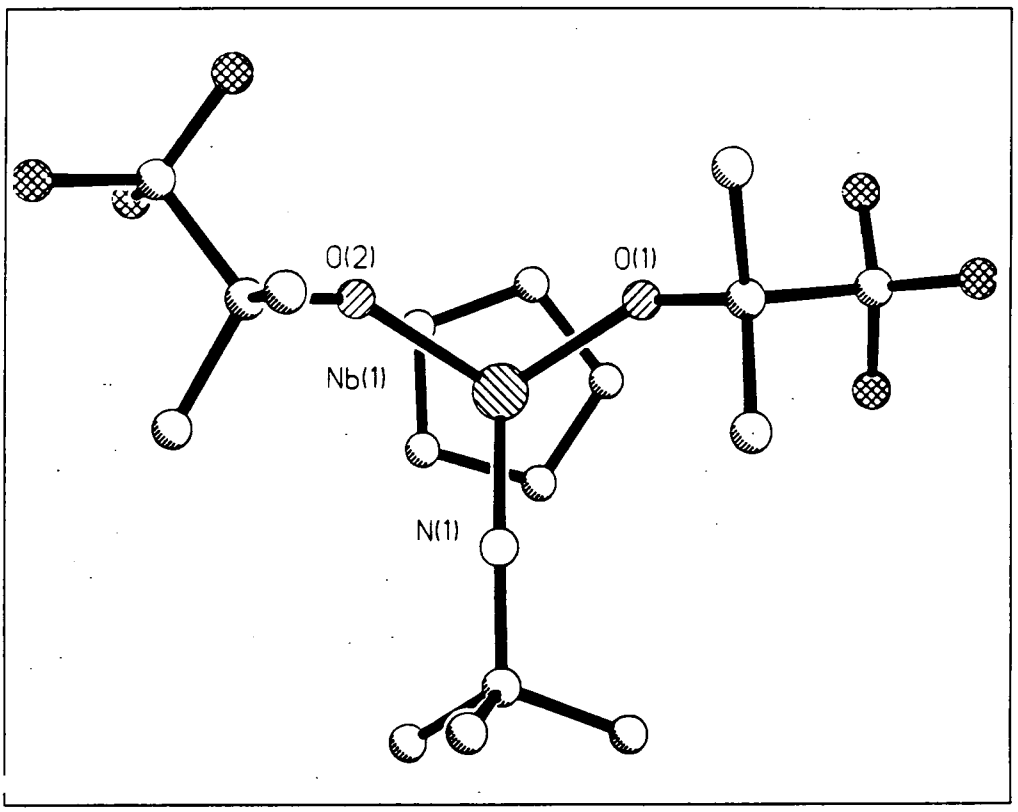

Figure 6.17: **5** showing the relative orientations of the CF_3 groups.

A-B	d_{AB}(Å)
Mo(1)-O(1)	1.862(4)
Mo(1)-O(2)	1.877(3)
Mo(1)-N(1)	1.716(5)
Mo(1)-N(2)	1.777(6)
N(1)-C(9)	1.471(7)
N(2)-C(13)	1.442(10)

A-B-C	∠A-B-C (°)
O(1)-Mo(1)-O(2)	107.9(2)
O(1)-Mo(1)-N(1)	110.1(3)
O(2)-Mo(1)-N(1)	109.6(2)
O(1)-Mo(1)-N(2)	108.2(2)
O(2)-Mo(1)-N(2)	108.8(2)
N(1)-Mo(1)-N(2)	112.2(3)
Mo(1)-N(1)-C(9)	169.5(6)
Mo(1)-N(2)-C(13)	157.1(5)

Table 6.10: Selected bond lengths and angles for **6**.

6 $[Mo(NBu^t)_2(OBu^t)_2]$

This compound very clearly has a tetrahedral arrangement of ligands around the molybdenum with a very narrow range of bond angles around the metal from 107.9(2)° to 112.2(3)° (see Table 6.10). The angle between the plane containing the atoms Mo(1), O(1) and O(2) and a second plane also containing Mo(1) and the two imido nitrogen atoms, N(1) and N(2) is 90.4°

The two imido ligands are significantly different and are consistent with the proposal of there being one bent and one linear imido to ease the competition for certain metal orbitals. This arrangement suggests that the bent imido ligand acts as a two electron donor and as such has a weaker interaction, reflected in the longer bond length (Mo(1)-N(2) 1.777(6)Å) relative to the four electron donating linear imido (Mo(1)-N(1) 1.716(5) Å). However, it is not clear that this is indeed the situation nor why it is not also the case for **4**.

All the six compounds have been found to have approximately tetrahedral geometry around the metal atoms. For the compounds which contain coordinated alkene and alkyne groups, **1,2** and **3**, these groups have been found to lie in the orientation which one would predict using their proposed isolobal relationship with the Group 4 metallocenes. Where there is more than one possible orientation consistent with the metallocene-like structure then steric effects appear to play an important role. These structural features are in

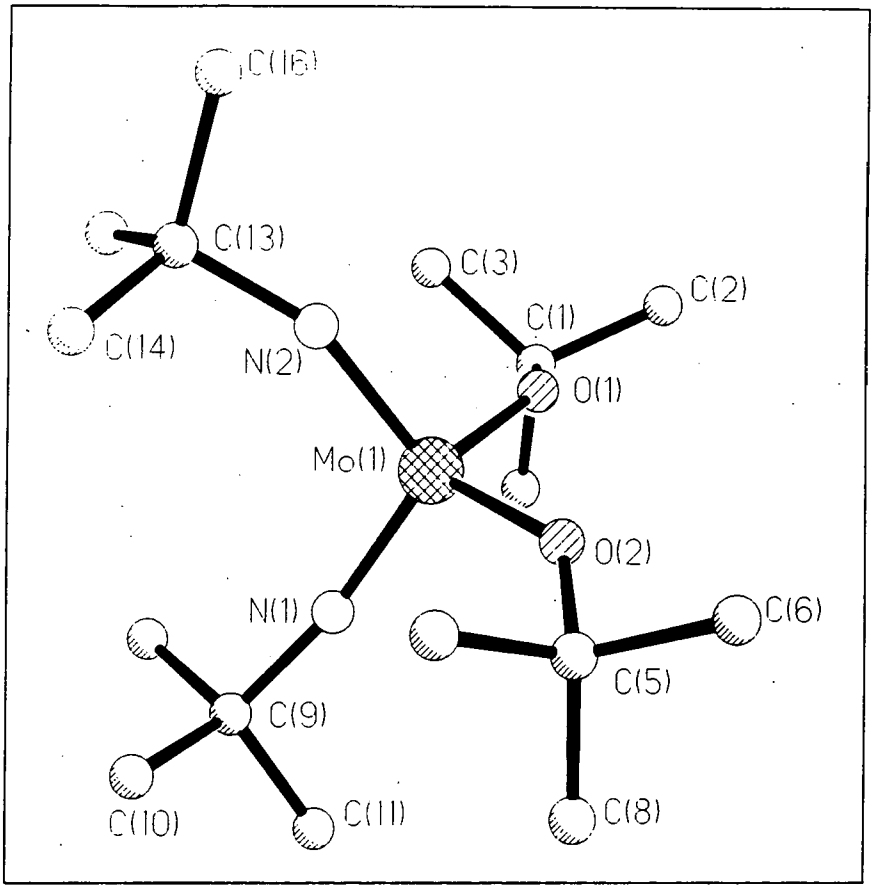

Figure 6.18: Molecular structure and labelling scheme for **6**.

agreement with the results of the calculations discussed in the introduction to this chapter. Hence, in conclusion, the structures of the compounds reported herein lend considerable support for the pseudo-isolobal relationship between the Group 4 bent metallocenes and these Group 5 half-sandwich imido and Group 6 bis-imido compounds.

Bibliography

[1] J.K. Cockcroft, V.C. Gibson, J.A.K. Howard, A.D. Poole, U. Siemeling and C. Wilson (1992). *J. Chem. Soc., Chem. Commun.*, 1668-1670.

[2] P.W. Dyer, V.C. Gibson, J.A.K. Howard, B. Whittle and C. Wilson (1995). *Polyhedron* **14**, 103-111.

[3] P.W. Dyer, V.C. Gibson, J.A.K. Howard and C. Wilson (1993). *J. Organomet. Chem.* **462**, C15-C17.

[4] A.D. Poole (1992). PhD thesis, University of Durham, UK.

[5] M. Jolly (1994). PhD thesis, University of Durham, UK.

[6] P.W. Dyer (1994). PhD thesis, University of Durham, UK.

[7] G. Schwartz and J.A. Labinger (1976). *Angew. Chem. Int. Ed. Engl.* **15**, 333.

[8] W. Kaminsky, K. Kulper, H.H. Brintzinger and F.R.W.P. Wild (1985). *Angew. Chem. Int. Ed. Engl.* **24**, 507.

[9] J.W. Lauher and R. Hoffmann (1976). *J. Am. Chem. Soc.* **98**, 1729.

[10] D.N. Williams, J.P. Mitchell, A.D. Poole, U. Siemeling, W. Clegg, D.C.R. Hockless, P.A. O'Neil and V.C. Gibson (1992). *J. Chem. Soc. Dalton Trans.* 739.

[11] W.A. Nugent and J.M. Mayer (1988) *Metal-Ligand Multiple Bonds,* Wiley-Interscience, New York.

[12] J. Cosier and A.M. Glazer (1986). *J. Appl. Cryst.* **19**, 105-107.

[13] Texsan Structure Analysis Software, Molecular Structure Corporation.

[14] G.M. Sheldrick (1986). SHELXTL-Plus, Program for Crystal Structure Determination, University of Gottingen.

[15] F.H. Allen, O.Kennard, G.D. Watson, L. Brammer, A.G. Orpen and R. Taylor (1992). in *International Tables for Crystallography,*Vol C, edited by A.J.C. Wilson. Kluwer Academic : The Netherlands.

[16] J.L. Templeton and B.C Ward (1980). *J. Am. Chem. Soc.* **102**, 3288-3290.

[17] M.R. Churchill and W.J. Youngs (1979). *Inorg. Chem.* **18**, 1697-1702.

[18] S.L. Buchwald, B.T. Watson and J.C. Huffman (1986). *J. Am. Chem. Soc.* **108**, 7411-7413.

[19] C.W. Lehmann (1994). Personal Communication.

[20] R.A. Bartlett, P.P. Power and S.C. Shoner (1988). *J. Am. Chem. Soc.* **110**, 1966-1968.

[21] G. Fachinetti, C. Floriani, F. Marchetti and M. Mellini (1978). *J. Chem. Soc. Dalton Trans.*, 1399-1403.

[22] T. Takahashi, D.R. Swanson and E. Negishi (1987). *Chem. Letters,* 623-626.

[23] L.B. Kool, M.D. Rausch, H.G. Alt, M. Herberhold, U. Thewalt and B. Wolf (1985). *Angew. Chem. Int. Ed. Engl.* **24**, 394-402.

[24] D.S. Williams, M.H. Schofield, J.T. Anhaus and R.R. Schrock (1990). *J. Am. Chem. Soc.* **112**, 6729-6731.

Chapter 7

Concluding Remarks

The investigation of the the dyotropic rearrangement which occurs in the Isodrin derivatives discussed in this thesis, involves and links several important areas of chemistry; organic synthesis, kinetic studies, theoretical work, such as the Molecular Mechanics calculations which have been made, and of course, crystallographic studies. It is also a project with a great deal of scope for future work.

The compounds provide a useful system in which to study a structure-reactivity relationship since a considerable number of compounds exist with many structural variations, both in terms of electronic and steric properties. The ongoing synthetic and kinetic studies of Kenneth Mackenzie in Bristol have recently opened up several new series of related compounds which show dyotropy. Therefore, in addition to the triene series, with which this thesis has been concerned primarily, and the pyrazoline/pyrazole pairs which have also been discussed, there are several new series to be investigated. The generally very high quality of the samples available for crystallographic studies make this a potentially very rewarding area for further X-ray and neutron studies.

The work reported in this thesis has contributed significantly to the study of the triene series. The number of data points is obviously an important factor

when investigating trends in a series. The addition of the structures of one pair of isomers which had not been studied previously (KM5 and KM9) and neutron data at the same temperature for a second pair (KM22 and KM25), for which X-ray data had been collected previously, is a most significant contribution to the project. This is especially true when one considers that neutron data have been collected for only one other pair of these dyotropic isomers; KM24 and KM27.

With these additional data it is possible to confirm conclusively that the expected gross structural changes which are predicted accompany the rearrangement do indeed take place.

The results from these studies have also confirmed the emerging view that the relationship between these compounds and their rates of reactivity is not a simple one. It is definitely not as straight forward a relationship as was originally proposed by Paquette and co-workers in Reference 5 of Chapter 4, which directly correlated the cross-cavity separations in the reactant isomers with the rates of reaction. The neutron studies of KM5, KM22 and KM25 have a particularly important role in this discussion as they have provided accurate hydrogen atomic positions. This is especially true of the study of KM22 since the X-ray derived hydrogen positions for this compound showed some anomalies.

The cross-cavity separation is not the the only steric factor involved in these reactions and the role of the electronic stucture also appears to be important. The MM calculations were made partly with the aim of quantifying these factors and hence allow the examination of any correlation of the calculated thermochemical quantities with the rates of reaction. The results from these calculations are slightly disappointing but may be a consequence of the limitations of such calculations. It would be very interesting to see if any greater degree of correlation is found with quantities derived from calculations based on the experimentally derived structural parameters, or at least using

calculations which show the same trends as the structural parameters from experiment. Increasingly, as the database of structural parameters is enlarged for these compounds it will become possible to eliminate some of the suggested causes of the rate variations and concentrate on fewer lines of investigation.

As well as the investigations of the trends in the series, opportunites exist for very detailed studies of one or a few compounds, such as the charge density study of KM25 reported herein. This study was prompted by the investigations of the series as a whole, highlighting the importance of the electronic effects. The study has given credible results and shown that such studies of these compounds are feasible. It provides an important reference density, however, its importance in isolation is limited. Features in the electron density of the starting isomers will be more informative in terms of the investigation of the reactivity of these compounds. I would very much like to see the charge density work completed, at the very least with a charge density study of the starting isomer KM22 which rearranges to form KM25. The neutron study of this compound at 123K has been reported in this thesis. It would be still more interesting to study the charge density for several starting isomers with very different rates of rearrangement.

Another possible area of future work involving detailed crystallographic work is the study of the rearrangement as it proceeds. These compounds have been observed to rearrange in the solid state as well as in solution. It may be possible to collect data at various stages of the reaction and so follow the rearrangement with a series of 'snapshot' structures. This, of course, depends on the crystal quality being maintained throughout the rearrangement and a system being chosen which rearranges at a suitable rate. This would require a feasibility study to be made prior to selection.

In conclusion, the work presented here is of significance to a much larger project which has great potential for further work.

Appendix A

Tables of results from all refinements.

The following Appendix contains full listings of the atomic coordinates, atomic displacement parameters, bond lengths and angles from the refinements discussed in Chapter 4:-

- Neutron study of KM5 at 15K, Experiment 1.
- X-ray study of KM9 at room temperature, Experiment 2.
- Neutron study of KM22 at 123K, Experiment 3.
- Neutron study of KM25 at 123K, Experiment 4.

and also the results from the following IAM refinements using the X-ray data for KM25 at 123K.

- FULL refinement using all the X-ray data with $|F(\mathbf{h})|^2_{obs} > 0$ and to a $\sin\theta/\lambda$(max) of 1.08Å^{-1}.
- HO refinement using all the X-ray data with $|F(\mathbf{h})|^2_{obs} > 0$ with $\sin\theta/\lambda >$ 0.8Å^{-1}.

- LO refinement using all the X-ray data with $|F(\mathbf{h})|^2_{obs} > 0$ and to a $\sin\theta/\lambda(\max)$ of 0.8Å^{-1}.

Values involving hydrogen atoms are not included in the tables from these three refinements, FULL, HO and LO, as the hydrogen atoms were constrained to their neutron derived positions and atomic displacements in these refinements.

Tables of atomic coordinates, anisotropic adps and the refined multipole populations from the refinement MULT, discussed in Chapter 5 are also included in this Appendix.

Full listings of atomic coordinates, bond lengths and angles (excluding hydrogen atoms), and atomic displacement parameters are also given for compounds **1** to **6** discussed in Chapter 6. Details of the treatment of the hydrogen atoms are given in the text of Chapter 6.

All atomic positions are given in fractional coordinates, all bond lengths in Å and all bond angles in degrees (°). The equivalent isotropic atomic displacement parameter, U_{eq} is defined as one third of the trace of the orthogonalised U_{ij} tensor and the anisotropic displacement factor exponent takes the form:-

$$-2\pi^2 \sum_i \sum_j h_i h_j a_i^* a_j^* U_{ij}$$

Esds from the least-squares refinements are given in parentheses.

Atom	x	y	z	U_{eq}
CL1	0.1051(1)	0.80336(6)	0.27487(6)	0.0065(2)
CL5	0.5407(1)	0.78625(6)	0.51187(6)	0.0071(2)
CL6	0.8182(1)	0.89455(6)	0.58910(5)	0.0061(2)
CL7	0.8605(1)	1.11181(6)	0.55606(5)	0.0066(2)
CL8	0.6720(1)	1.21159(6)	0.41598(6)	0.0073(2)
CL12	0.2664(1)	1.17101(6)	0.18454(5)	0.0072(2)
CL13	0.1583(1)	1.16996(6)	0.37935(5)	0.0073(2)
CL14	0.0630(1)	0.94397(7)	0.43441(5)	0.0064(2)
CL15	-0.0346(1)	1.01447(7)	0.19783(6)	0.0065(2)
CL25	0.2188(1)	0.94199(6)	0.10451(5)	0.0062(2)
C1	0.2013(1)	0.91314(9)	0.27676(8)	0.0050(3)
C2	0.3794(1)	0.90721(9)	0.26742(8)	0.0051(3)
C3	0.4966(1)	0.88361(9)	0.33637(8)	0.0054(3)
C4	0.4764(1)	0.94175(9)	0.41773(7)	0.0049(3)
C5	0.5809(1)	0.90129(9)	0.48327(7)	0.0054(3)
C6	0.6980(1)	0.94915(9)	0.51837(7)	0.0056(3)
C7	0.7262(1)	1.05012(9)	0.49859(7)	0.0055(3)
C8	0.6439(1)	1.09317(9)	0.43915(8)	0.0055(3)
C9	0.5180(1)	1.04570(9)	0.39035(8)	0.0054(3)
C10	0.5634(1)	1.03426(9)	0.29799(8)	0.0058(3)
C11	0.4250(1)	1.01109(9)	0.24112(8)	0.0053(3)
C12	0.2672(1)	1.06386(9)	0.23995(7)	0.0052(3)
C13	0.1929(1)	1.06834(9)	0.32552(8)	0.0052(3)
C14	0.1551(2)	0.97926(9)	0.34724(7)	0.0052(3)
C15	0.1624(1)	0.98263(9)	0.20350(7)	0.0052(3)
C16	0.6398(1)	0.93430(9)	0.29978(8)	0.0059(3)
D9	0.4179(2)	1.09246(12)	0.39762(10)	0.0132(4)
D16B	0.7411(2)	0.93121(14)	0.34027(11)	0.0148(5)
D16A	0.6719(2)	0.90823(13)	0.23833(11)	0.0156(5)
D10	0.6348(2)	1.09259(13)	0.27521(11)	0.0137(4)
D4	0.3591(2)	0.93740(12)	0.44215(10)	0.0133(4)
D3	0.5071(2)	0.80771(12)	0.34759(11)	0.0142(4)
H11	0.4675(3)	1.01149(22)	0.17707(17)	0.0158(8)
H2	0.4018(4)	0.85725(21)	0.21695(18)	0.0159(8)

Table A.1: Atomic coordinates and U_{eq} (Å^2) for KM5 from Experiment 1, neutron data measured at 15K. Esds given in parentheses.

Atom	U_{11}	U_{22}	U_{33}	U_{12}	U_{13}	U_{23}
CL1	0.0079(3)	0.0048(3)	0.0068(3)	-0.0011(3)	-0.0001(3)	0.0001(3)
CL5	0.0092(4)	0.0051(3)	0.0069(3)	-0.0017(3)	-0.0014(3)	0.0019(3)
CL6	0.0067(3)	0.0056(3)	0.0060(3)	0.0006(3)	-0.0013(3)	0.0006(3)
CL7	0.0070(3)	0.0061(3)	0.0066(3)	-0.0008(3)	-0.0013(3)	-0.0013(3)
CL8	0.0094(4)	0.0043(3)	0.0082(3)	-0.0009(3)	-0.0018(3)	0.0008(3)
CL12	0.0084(3)	0.0056(3)	0.0075(3)	0.0000(3)	-0.0003(3)	0.0022(3)
CL13	0.0089(4)	0.0053(3)	0.0077(3)	0.0011(3)	-0.0003(3)	-0.0016(3)
CL14	0.0067(3)	0.0071(3)	0.0054(3)	-0.0003(3)	0.0014(3)	0.0006(3)
CL15	0.0048(3)	0.0082(3)	0.0064(3)	0.0007(3)	-0.0006(3)	0.0004(3)
CL25	0.0070(3)	0.0076(3)	0.0040(3)	0.0003(3)	-0.0002(3)	-0.0005(3)
C1	0.0059(5)	0.0043(4)	0.0049(4)	-0.0002(4)	0.0001(4)	0.0003(4)
C2	0.0049(4)	0.0045(4)	0.0058(4)	-0.0003(4)	0.0002(4)	-0.0005(4)
C3	0.0050(5)	0.0055(5)	0.0056(4)	0.0001(4)	-0.0007(4)	-0.0005(4)
C4	0.0050(4)	0.0049(4)	0.0048(4)	-0.0009(4)	0.0007(4)	0.0005(4)
C5	0.0055(5)	0.0059(5)	0.0050(4)	-0.0007(4)	-0.0001(4)	0.0000(4)
C6	0.0067(5)	0.0049(4)	0.0052(4)	-0.0005(4)	-0.0009(4)	0.0002(4)
C7	0.0061(5)	0.0053(4)	0.0053(4)	-0.0012(4)	-0.0010(4)	0.0006(4)
C8	0.0066(5)	0.0041(4)	0.0058(4)	0.0002(4)	-0.0009(4)	0.0003(4)
C9	0.0054(5)	0.0048(4)	0.0061(4)	-0.0006(4)	-0.0008(4)	0.0000(4)
C10	0.0060(5)	0.0063(5)	0.0051(5)	-0.0004(4)	0.0006(4)	0.0006(4)
C11	0.0056(5)	0.0057(5)	0.0045(5)	-0.0001(4)	-0.0007(4)	0.0008(4)
C12	0.0062(5)	0.0047(4)	0.0045(4)	-0.0002(4)	-0.0003(4)	0.0006(4)
C13	0.0067(5)	0.0037(4)	0.0053(4)	0.0010(4)	0.0010(4)	0.0002(3)
C14	0.0062(5)	0.0055(4)	0.0040(4)	-0.0004(4)	0.0007(4)	0.0007(4)
C15	0.0056(5)	0.0054(4)	0.0047(4)	-0.0007(4)	0.0000(4)	0.0002(4)
C16	0.0054(5)	0.0063(5)	0.0059(4)	0.0014(4)	-0.0007(4)	-0.0001(4)
D9	0.0112(7)	0.0124(7)	0.0160(7)	0.0038(5)	-0.0003(5)	-0.0009(5)
D16B	0.0109(8)	0.0198(9)	0.0138(8)	0.0005(6)	-0.0044(6)	-0.0002(6)
D16A	0.0164(8)	0.0184(8)	0.0120(7)	0.0015(6)	0.0032(6)	-0.0032(6)
D10	0.0145(8)	0.0136(8)	0.0130(7)	-0.0045(6)	-0.0002(6)	0.0029(6)
D4	0.0095(7)	0.0166(7)	0.0139(7)	-0.0004(5)	0.0017(5)	0.0007(5)
D3	0.0171(8)	0.0097(7)	0.0157(8)	0.0005(5)	-0.0018(6)	0.0001(5)
H11	0.0164(14)	0.0196(14)	0.0115(12)	-0.0003(10)	0.0009(9)	0.0001(9)
H2	0.0187(14)	0.0154(13)	0.0137(13)	0.0015(10)	0.0010(10)	-0.0045(9)

Table A.2: Anisotropic atomic displacement parameters (Å^2) for KM5 from Experiment 1, neutron data measured at 15K. Esds given in parentheses.

A-B	d_{A-B}	A-B	d_{A-B}	A-B	d_{A-B}
CL1 –C1	1.754(2)	C2 –C3	1.545(2)	C11 –C12	1.556(2)
CL5 –C5	1.717(2)	C2 –C11	1.571(2)	C12 –C13	1.529(2)
CL6 –C6	1.727(2)	C3 –C4	1.560(2)	C12 –C15	1.573(2)
CL7 –C7	1.724(2)	C3 –C16	1.548(2)	C13 –C14	1.341(2)
CL8 –C8	1.723(2)	C4 –C5	1.506(2)	C2 –H2	1.095(3)
CL12 –C12	1.753(1)	C4 –C9	1.569(2)	C3 –D3	1.086(2)
CL13 –C13	1.699(2)	C5 –C6	1.344(2)	C4 –D4	1.092(2)
CL14 –C14	1.695(2)	C6 –C7	1.475(2)	C9 –D9	1.095(2)
CL15 –C15	1.766(2)	C7 –C8	1.342(2)	C10 –D10	1.091(2)
CL25 –C15	1.770(2)	C8 –C9	1.503(2)	C11 –H11	1.100(3)
C1 –C2	1.552(2)	C9 –C10	1.554(2)	C16 –D16A	1.096(2)
C1 –C14	1.525(2)	C10 –C11	1.546(2)	C16 –D16B	1.096(2)
C1 –C15	1.573(2)	C10 –C16	1.553(2)		

Table A.3: Bond lengths (Å) for KM5 from Experiment 1, neutron study at 15K. Esds given in parentheses.

A-B-C	∠A-B-C	A-B-C	∠A-B-C
CL1 –C1 –C2	115.1(1)	CL1 –C1 –C14	115.1(1)
CL1 –C1 –C15	115.5(1)	C2 –C1 –C14	111.5(1)
C2 –C1 –C15	100.0(1)	C14 –C1 –C15	97.4(1)
C1 –C2 –C3	126.5(1)	C1 –C2 –C11	103.1(1)
C3 –C2 –C11	103.3(1)	C1 –C2 –H2	106.5(2)
C3 –C2 –H2	106.5(2)	C11 –C2 –H2	110.4(2)
C2 –C3 –C4	115.1(1)	C2 –C3 –C16	98.7(1)
C4 –C3 –C16	99.9(1)	C2 –C3 –D3	112.7(1)
C4 –C3 –D3	112.5(1)	C16 –C3 –D3	116.7(2)
C3 –C4 –C5	109.2(1)	C3 –C4 –C9	102.9(1)
C5 –C4 –C9	114.3(1)	C3 –C4 –D4	112.4(1)
C5 –C4 –D4	106.5(1)	C9 –C4 –D4	111.6(1)
CL5 –C5 –C4	115.1(1)	CL5 –C5 –C6	120.7(1)
C4 –C5 –C6	124.3(1)	CL6 –C6 –C5	120.9(1)
CL6 –C6 –C7	118.2(1)	C5 –C6 –C7	121.0(1)
CL7 –C7 –C6	118.6(1)	CL7 –C7 –C8	121.3(1)
C6 –C7 –C8	120.1(1)	CL8 –C8 –C7	121.1(1)
CL8 –C8 –C9	114.6(1)	C7 –C8 –C9	124.2(1)
C4 –C9 –C8	115.6(1)	C4 –C9 –C10	103.5(1)
C8 –C9 –C10	111.6(1)	C4 –C9 –D9	110.3(1)
C8 –C9 –D9	104.6(1)	C10 –C9 –D9	111.5(1)

Table A.4: Bond angles (°) for KM5 from Experiment 1, neutron study at 15K. Esds given in parentheses.

A-B-C	∠A-B-C	A-B-C	∠A-B-C
C9 –C10 –C11	113.5(1)	C9 –C10 –C16	100.6(1)
C11 –C10 –C16	98.7(1)	C9 –C10 –D10	113.0(1)
C11 –C10 –D10	113.4(1)	C16 –C10 –D10	116.4(1)
C2 –C11 –C10	103.3(1)	C2 –C11 –C12	103.0(1)
C10 –C11 –C12	126.1(1)	C2 –C11 –H11	110.1(2)
C10 –C11 –H11	107.5(2)	C12 –C11 –H11	106.3(2)
CL12 –C12 –C11	114.8(1)	CL12 –C12 –C13	115.3(1)
CL12 –C12 –C15	115.4(1)	C11 –C12 –C13	112.3(1)
C11 –C12 –C15	99.6(1)	C13 –C12 –C15	97.3(1)
CL13 –C13 –C12	125.0(1)	CL13 –C13 –C14	127.4(1)
C12 –C13 –C14	107.6(1)	CL14 –C14 –C1	124.6(1)
CL14 –C14 –C13	127.3(1)	C1 –C14 –C13	108.0(1)
CL15 –C15 –CL25	107.6(1)	CL15 –C15 –C1	113.8(1)
CL15 –C15 –C12	113.2(1)	CL25 –C15 –C1	115.0(1)
CL25 –C15 –C12	114.5(1)	C1 –C15 –C12	92.5(1)
C3 –C16 –C10	94.7(1)	C3 –C16 –D16A	113.4(1)
C3 –C16 –D16B	113.2(1)	C10 –C16 –D16A	113.2(1)
C10 –C16 –D16B	112.8(1)	D16A –C16 –D16B	109.1(2)

Table A.5: Bond angles (°) for KM5 from Experiment 1, neutron study at 15K (cont'd). Esds given in parentheses.

Atom	x	y	z	U_{eq}
Cl(1)	4.8269(8)	-0.4429(12)	6.2857(5)	0.638(5)
Cl(5)	6.3374(8)	-1.2058(14)	4.9644(4)	0.652(5)
Cl(6)	7.8233(10)	0.5885(15)	4.5970(4)	0.823(6)
Cl(7)	9.7445(9)	1.5114(14)	5.2914(5)	0.776(6)
Cl(8)	10.2498(8)	0.5218(13)	6.3556(4)	0.622(5)
Cl(12)	8.3783(9)	1.2276(13)	7.4238(4)	0.654(5)
Cl(13)	7.5791(8)	3.1268(11)	6.5456(4)	0.552(4)
Cl(14)	5.5673(8)	2.2086(11)	5.9235(4)	0.534(4)
Cl(15)	5.9054(9)	2.0165(12)	7.0679(4)	0.602(5)
Cl(25)	6.2594(10)	-0.5130(13)	7.4257(4)	0.701(5)
C(1)	6.0869(28)	-0.0566(40)	6.4541(14)	0.402(15)
C(2)	6.7535(29)	-1.2845(40)	6.4998(14)	0.389(15)
C(3)	7.1094(29)	-2.0130(41)	6.0921(15)	0.404(16)
C(4)	7.6515(28)	-1.1509(38)	5.8085(15)	0.381(15)
C(5)	7.4337(28)	-0.7466(41)	5.3397(14)	0.426(16)
C(6)	8.0917(32)	0.0696(46)	5.1818(14)	0.516(18)
C(7)	8.9628(30)	0.4672(45)	5.4874(15)	0.499(17)
C(8)	9.1878(28)	0.0298(41)	5.9594(15)	0.421(15)
C(9)	8.5303(27)	-0.7681(38)	6.1157(14)	0.381(15)
C(10)	8.5485(29)	-1.3823(42)	6.5958(15)	0.417(15)
C(11)	7.7442(30)	-0.8247(41)	6.8333(14)	0.416(15)
C(12)	7.5315(28)	0.6103(40)	6.9202(13)	0.399(15)
C(13)	7.4480(30)	1.4276(39)	6.4606(14)	0.385(15)
C(14)	6.4394(28)	0.9750(39)	6.1397(14)	0.381(15)
C(15)	6.4425(30)	0.5216(41)	6.9654(14)	0.447(16)
C(16)	8.0256(34)	-2.6688(45)	6.4199(18)	0.498(18)

Table A.6: Atomic coordinates and U_{eq} ($Å^2$) for KM9 from Experiment 2. Esds given in parentheses.

Atom	U_{11}	U_{22}	U_{33}	U_{12}	U_{13}	U_{23}
Cl(1)	0.369(6)	0.588(8)	0.941(10)	-0.026(6)	0.108(6)	0.030(8)
Cl(5)	0.542(7)	0.875(10)	0.471(7)	-0.218(7)	-0.034(6)	-0.050(7)
Cl(6)	0.855(10)	1.168(13)	0.409(7)	-0.324(9)	0.063(7)	0.121(8)
Cl(7)	0.715(9)	0.966(12)	0.660(9)	-0.389(8)	0.180(7)	0.032(8)
Cl(8)	0.458(7)	0.691(9)	0.648(8)	-0.150(6)	-0.026(6)	-0.097(7)
Cl(12)	0.760(8)	0.652(8)	0.416(7)	0.117(7)	-0.156(6)	-0.101(6)
Cl(13)	0.657(8)	0.366(6)	0.565(7)	-0.043(6)	-0.011(6)	-0.009(6)
Cl(14)	0.541(7)	0.464(7)	0.510(7)	0.099(6)	-0.072(5)	0.088(6)
Cl(15)	0.713(8)	0.583(8)	0.531(7)	0.255(7)	0.183(6)	0.005(6)
Cl(25)	0.912(10)	0.720(9)	0.570(8)	0.204(8)	0.375(7)	0.243(7)
C(1)	0.341(22)	0.433(26)	0.429(25)	0.026(20)	0.080(19)	0.077(21)
C(2)	0.387(24)	0.331(25)	0.452(26)	0.041(20)	0.102(20)	0.052(21)
C(3)	0.412(25)	0.346(26)	0.447(26)	0.005(21)	0.080(21)	-0.021(21)
C(4)	0.369(23)	0.324(24)	0.458(26)	-0.023(20)	0.107(20)	-0.100(21)
C(5)	0.377(23)	0.510(29)	0.376(24)	-0.055(22)	0.054(20)	-0.097(22)
C(6)	0.517(28)	0.669(34)	0.346(24)	-0.082(25)	0.064(21)	-0.006(24)
C(7)	0.479(26)	0.570(31)	0.470(27)	-0.128(25)	0.153(22)	-0.080(25)
C(8)	0.348(23)	0.438(27)	0.454(26)	-0.035(20)	0.038(20)	-0.120(22)
C(9)	0.338(22)	0.360(25)	0.434(24)	0.048(20)	0.063(19)	-0.093(20)
C(10)	0.365(23)	0.408(26)	0.457(26)	0.071(21)	0.043(20)	-0.029(22)
C(11)	0.462(25)	0.399(27)	0.361(24)	0.056(21)	0.037(21)	0.039(21)
C(12)	0.437(24)	0.444(27)	0.267(21)	0.062(21)	-0.028(18)	-0.015(20)
C(13)	0.436(25)	0.322(24)	0.365(24)	0.020(20)	0.020(19)	-0.003(20)
C(14)	0.354(22)	0.381(26)	0.375(24)	0.063(20)	0.009(19)	0.001(21)
C(15)	0.553(28)	0.410(27)	0.401(24)	0.156(22)	0.154(21)	0.091(22)
C(16)	0.502(29)	0.391(29)	0.591(32)	0.111(23)	0.098(24)	0.030(24)

Table A.7: Anisotropic atomic displacement parameters ($Å^2$) for KM9 from Experiment 2. Esds given in parentheses.

Atom	x	y	z	U_{iso}
H(14)	0.6560(30)	0.0556(42)	0.5853(15)	0.080
H(11)	0.7826(31)	-0.1175(42)	0.7154(16)	0.080
H(10)	0.9225(30)	-0.1338(42)	0.6806(15)	0.080
H(13)	0.8003(31)	0.1246(44)	0.6323(16)	0.080
H(16B)	0.7864(31)	-0.3254(42)	0.6684(16)	0.080
H(3)	0.6598(31)	-0.2525(43)	0.5903(16)	0.080
H(2)	0.6332(30)	-0.1937(42)	0.6665(15)	0.080
H(16A)	0.8381(32)	-0.3174(44)	0.6230(16)	0.080

Table A.8: Atomic coordinates and U_{iso} (Å^2) for hydrogen atoms of KM9 from Experiment 2.

A-B	d_{AB}	A-B	d_{AB}	A-B	d_{AB}
Cl(1)-C(1)	1.757(4)	Cl(5)-C(5)	1.728(4)	Cl(6)-C(6)	1.727(4)
Cl(7)-C(7)	1.716(5)	Cl(8)-C(8)	1.730(4)	Cl(12)-C(12)	1.771(4)
Cl(13)-C(13)	1.781(4)	Cl(14)-C(14)	1.776(4)	Cl(15)-C(15)	1.772(4)
Cl(25)-C(15)	1.766(4)	C(1)-C(2)	1.562(6)	C(1)-C(14)	1.549(6)
C(1)-C(15)	1.564(5)	C(2)-C(3)	1.565(6)	C(2)-C(11)	1.568(5)
C(3)-C(4)	1.519(6)	C(3)-C(16)	1.562(6)	C(4)-C(5)	1.380(6)
C(4)-C(9)	1.397(5)	C(5)-C(6)	1.394(6)	C(6)-C(7)	1.392(6)
C(7)-C(8)	1.400(6)	C(8)-C(9)	1.380(6)	C(9)-C(10)	1.516(6)
C(10)-C(11)	1.547(6)	C(10)-C(16)	1.548(6)	C(11)-C(12)	1.547(6)
C(12)-C(13)	1.553(6)	C(12)-C(15)	1.552(6)	C(13)-C(14)	1.570(5)

Table A.9: Bond lengths (Å) for KM9 from Experiment 2. Esds given in parentheses.

A-B-C	∠A-B-C	A-B-C	∠A-B-C	A-B-C	∠A-B-C
Cl(1)-C(1)-C(2)	112.0(3)	Cl(1)-C(1)-C(14)	115.0(3)	C(2)-C(1)-C(14)	110.6(3)
Cl(1)-C(1)-C(15)	115.7(3)	C(2)-C(1)-C(15)	100.1(3)	C(14)-C(1)-C(15)	102.2(3)
C(1)-C(2)-C(3)	127.6(3)	C(1)-C(2)-C(11)	103.2(3)	C(3)-C(2)-C(11)	102.9(3)
C(2)-C(3)-C(4)	113.4(3)	C(2)-C(3)-C(16)	96.2(3)	C(4)-C(3)-C(16)	98.3(3)
C(3)-C(4)-C(5)	132.6(3)	C(3)-C(4)-C(9)	107.2(3)	C(5)-C(4)-C(9)	120.2(4)
Cl(5)-C(5)-C(4)	119.9(3)	Cl(5)-C(5)-C(6)	121.0(3)	C(4)-C(5)-C(6)	119.0(3)
Cl(6)-C(6)-C(5)	119.4(3)	Cl(6)-C(6)-C(7)	119.5(4)	C(5)-C(6)-C(7)	121.1(4)
Cl(7)-C(7)-C(6)	120.3(3)	Cl(7)-C(7)-C(8)	120.1(3)	C(6)-C(7)-C(8)	119.5(4)
Cl(8)-C(8)-C(7)	121.2(3)	Cl(8)-C(8)-C(9)	119.5(3)	C(7)-C(8)-C(9)	119.3(3)
C(4)-C(9)-C(8)	120.9(4)	C(4)-C(9)-C(10)	107.0(3)	C(8)-C(9)-C(10)	132.1(3)
C(9)-C(10)-C(11)	112.3(3)	C(9)-C(10)-C(16)	98.7(3)	C(11)-C(10)-C(16)	97.6(3)
C(2)-C(11)-C(10)	103.9(3)	C(2)-C(11)-C(12)	102.5(3)	C(10)-C(11)-C(12)	127.8(4)
Cl(12)-C(12)-C(11)	111.3(3)	Cl(12)-C(12)-C(13)	114.2(3)	C(11)-C(12)-C(13)	111.5(3)
Cl(12)-C(12)-C(15)	115.9(3)	C(11)-C(12)-C(15)	100.5(3)	C(13)-C(12)-C(15)	102.4(3)
Cl(13)-C(13)-C(12)	115.8(3)	Cl(13)-C(13)-C(14)	115.3(3)	C(12)-C(13)-C(14)	103.1(3)
Cl(14)-C(14)-C(1)	114.9(3)	Cl(14)-C(14)-C(13)	116.3(3)	C(1)-C(14)-C(13)	102.7(3)
Cl(15)-C(15)-Cl(25)	105.6(2)	Cl(15)-C(15)-C(1)	115.8(3)	Cl(25)-C(15)-C(1)	113.9(3)
Cl(15)-C(15)-C(12)	114.7(3)	Cl(25)-C(15)-C(12)	113.9(3)	C(1)-C(15)-C(12)	93.1(3)
C(3)-C(16)-C(10)	94.8(3)				

Table A.10: Bond angles (°) for KM9 from Experiment 2. Esds given in parentheses.

Atom	x	y	z	U_{eq}
CL1	0.87614(7)	0.81544(11)	0.79384(4)	0.0228(2)
CL5	0.56656(7)	0.43104(13)	0.74055(5)	0.0290(3)
CL6	0.45123(6)	0.21681(11)	0.61529(5)	0.0231(2)
CL7	0.50980(6)	0.20773(10)	0.44096(5)	0.0206(2)
CL8	0.68790(6)	0.41140(11)	0.38632(4)	0.0212(2)
CL12	0.96953(6)	0.80016(10)	0.47672(5)	0.0186(2)
CL13	0.74987(6)	0.95514(10)	0.49011(5)	0.0200(2)
CL14	0.68866(6)	0.95473(10)	0.68437(5)	0.0206(2)
CL15	1.07163(6)	0.75038(11)	0.67035(5)	0.0221(2)
C1	0.86744(8)	0.77155(13)	0.69175(6)	0.0146(3)
C2	0.86847(8)	0.58558(13)	0.67263(6)	0.0136(2)
C3	0.78067(8)	0.46675(13)	0.67326(6)	0.0140(2)
C4	0.68697(7)	0.52848(13)	0.62618(6)	0.0127(2)
C5	0.60012(8)	0.42364(14)	0.64384(6)	0.0154(3)
C6	0.55002(8)	0.33176(13)	0.58977(6)	0.0147(2)
C7	0.57823(8)	0.32699(13)	0.50676(6)	0.0139(3)
C8	0.65492(8)	0.41498(13)	0.48355(6)	0.0135(2)
C9	0.71738(7)	0.52352(12)	0.53752(6)	0.0120(2)
C10	0.82442(7)	0.45928(13)	0.54475(6)	0.0129(2)
C11	0.89714(7)	0.58241(13)	0.58396(6)	0.0129(2)
C12	0.90617(7)	0.76715(13)	0.56349(6)	0.0132(2)
C13	0.81046(8)	0.86296(13)	0.56817(6)	0.0138(2)
C14	0.78723(8)	0.86466(13)	0.64464(6)	0.0149(3)
C15	0.95493(8)	0.83310(13)	0.64292(6)	0.0152(3)
C16	0.81710(8)	0.33727(13)	0.61459(6)	0.0148(3)
H2	0.92793(17)	0.53269(32)	0.71090(14)	0.0279(6)
H3	0.76587(18)	0.42327(32)	0.73272(13)	0.0285(6)
H4	0.66735(17)	0.65336(29)	0.64337(14)	0.0260(6)
H9	0.71262(17)	0.64584(28)	0.51099(14)	0.0262(6)
H10	0.84927(17)	0.40804(30)	0.48926(13)	0.0258(6)
H11	0.97095(16)	0.53185(30)	0.57946(14)	0.0256(6)
H15	0.96166(18)	0.96653(30)	0.64343(15)	0.0293(6)
H16A	0.88809(18)	0.28359(31)	0.63429(15)	0.0305(7)
H16B	0.76343(18)	0.23942(30)	0.60177(14)	0.0290(6)

Table A.11: Atomic coordinates and U_{eq} for KM22 from the neutron study at 123K, Experiment 3. Esds given in parentheses.

Atom	U_{11}	U_{22}	U_{33}	U_{12}	U_{13}	U_{23}
CL1	0.0302(4)	0.0263(4)	0.0119(3)	-.0029(3)	0.0005(3)	-.0048(3)
CL5	0.0247(4)	0.0466(6)	0.0165(3)	-.0115(4)	0.0100(3)	-.0059(4)
CL6	0.0203(4)	0.0236(4)	0.0259(4)	-.0094(3)	0.0057(3)	0.0015(3)
CL7	0.0202(3)	0.0201(4)	0.0213(3)	-.0059(3)	-.0012(3)	-.0050(3)
CL8	0.0220(4)	0.0302(4)	0.0115(3)	-.0046(3)	0.0022(3)	-.0022(3)
CL12	0.0228(4)	0.0167(3)	0.0171(3)	-.0040(3)	0.0081(3)	-.0011(3)
CL13	0.0235(4)	0.0161(3)	0.0198(3)	0.0008(3)	-.0042(3)	0.0022(3)
CL14	0.0193(3)	0.0181(4)	0.0251(4)	0.0027(3)	0.0071(3)	-.0058(3)
CL15	0.0146(3)	0.0247(4)	0.0265(4)	-.0015(3)	-.0034(3)	-.0034(3)
C1	0.0158(4)	0.0160(5)	0.0120(4)	-.0007(4)	-.0002(3)	-.0034(4)
C2	0.0146(4)	0.0140(4)	0.0121(4)	0.0001(4)	0.0000(3)	-.0007(4)
C3	0.0148(4)	0.0152(4)	0.0121(4)	-.0009(4)	0.0017(3)	0.0012(4)
C4	0.0131(4)	0.0126(4)	0.0127(4)	-.0007(4)	0.0024(3)	-.0018(3)
C5	0.0143(4)	0.0178(5)	0.0144(4)	-.0018(4)	0.0045(3)	-.0011(4)
C6	0.0143(4)	0.0142(4)	0.0158(4)	-.0017(4)	0.0025(3)	0.0003(4)
C7	0.0151(4)	0.0121(4)	0.0146(4)	-.0015(4)	0.0008(3)	-.0005(4)
C8	0.0137(4)	0.0146(4)	0.0122(4)	-.0016(4)	0.0013(3)	-.0008(4)
C9	0.0123(4)	0.0116(4)	0.0123(4)	-.0009(4)	0.0015(3)	-.0002(3)
C10	0.0128(4)	0.0131(4)	0.0128(4)	-.0007(4)	0.0022(3)	-.0012(3)
C11	0.0126(4)	0.0124(4)	0.0137(4)	-.0002(4)	0.0015(3)	-.0011(4)
C12	0.0144(4)	0.0120(4)	0.0134(4)	-.0019(4)	0.0020(3)	-.0015(4)
C13	0.0148(4)	0.0126(4)	0.0141(4)	-.0002(4)	0.0015(3)	-.0013(3)
C14	0.0161(5)	0.0142(5)	0.0145(4)	0.0006(4)	0.0028(3)	-.0021(4)
C15	0.0142(4)	0.0155(5)	0.0158(4)	-.0019(4)	0.0000(3)	-.0023(4)
C16	0.0167(5)	0.0118(4)	0.0161(4)	0.0001(4)	0.0019(4)	0.0002(4)
H2	0.0252(10)	0.0310(12)	0.0269(10)	0.0026(10)	-.0056(8)	0.0026(9)
H3	0.0331(12)	0.0329(12)	0.0197(9)	-.0023(10)	0.0033(8)	0.0051(9)
H4	0.0262(10)	0.0217(10)	0.0305(11)	0.0017(9)	0.0049(9)	-.0042(9)
H9	0.0286(11)	0.0213(10)	0.0287(10)	-.0009(9)	0.0021(9)	0.0052(9)
H10	0.0260(10)	0.0288(11)	0.0233(9)	-.0013(9)	0.0062(8)	-.0072(9)
H11	0.0184(9)	0.0281(11)	0.0306(11)	0.0017(9)	0.0032(8)	-.0022(9)
H15	0.0317(12)	0.0214(10)	0.0347(12)	-.0059(10)	0.0005(9)	-.0051(9)
H16A	0.0246(10)	0.0287(12)	0.0379(12)	0.0064(10)	-.0006(9)	0.0021(10)
H16B	0.0306(11)	0.0228(11)	0.0335(11)	-.0067(9)	0.0017(9)	-.0017(9)

Table A.12: Anisotropic atomic displacement parameters (Å^2) for KM22 from the neutron study at 123K, Experiment 4. Esds given in parentheses.

A-B	d_{A-B}	A-B	d_{A-B}	A-B	d_{A-B}
Cl1 - C1	1.757(1)	Cl5 - C5	1.717(1)	Cl6 - C6	1.715(1)
Cl7 - C7	1.717(1)	Cl8 - C8	1.722(1)	Cl12 - C12	1.757(1)
Cl13 - C13	1.696(1)	Cl15 - C15	1.770(1)	C1 - C14	1.523(1)
C1 - C2	1.552(1)	C1 - C15	1.566(1)	C2 - C11	1.565(1)
C2 - C3	1.542(1)	C3 - C16	1.547(1)	C3 - C4	1.555(1)
C4 - C5	1.503(1)	C4 - C9	1.572(1)	C5 - C6	1.341(1)
C6 - C7	1.471(1)	C7 - C8	1.343(1)	C8 - C9	1.504(1)
C9 - C10	1.551(1)	C10 - C11	1.538(1)	C10 - C16	1.549(1)
C11 - C12	1.553(1)	C12 - C13	1.527(1)	C12 - C15	1.561(1)
C13 - C14	1.343(1)	H2 - C2	1.099(3)	H3 - C3	1.092(3)
H4 - C4	1.097(3)	H9 - C9	1.095(3)	H10 - C10	1.094(3)
H11 - C11	1.094(2)	H15 - C15	1.093(3)	H16A - C16	1.099(3)
H16B - C16	1.098(3)				

Table A.13: Bond lengths (Å) for KM22 from the neutron study at 123K, Experiment 3. Esds given in parentheses.

A-B-C	∠A-B-C	A-B-C	∠A-B-C
C2 - C1 - C15	100.93(8)	C14 - C1 - C15	96.44(8)
C1 - C2 - C3	126.79(9)	C1 - C2 - C11	102.71(8)
C3 - C2 - C11	103.13(8)	C2 - C3 - C4	114.32(9)
C2 - C3 - C16	98.70(8)	C4 - C3 - C16	100.19(8)
C3 - C4 - C5	110.51(9)	C3 - C4 - C9	103.20(8)
C5 - C4 - C9	114.93(8)	C4 - C5 - C6	124.31(9)
C5 - C6 - C7	120.89(16)	C6 - C7 - C8	120.50(9)
C7 - C8 - C9	124.38(9)	C4 - C9 - C10	103.05(8)
C8 - C9 - C10	110.57(8)	C9 - C10 - C11	113.42(8)
C9 - C10 - C16	100.45(8)	C11 - C10 - C16	99.08(8)
C2 - C11 - C10	103.60(8)	C2 - C11 - C12	102.86(8)
C10 - C11 - C12	126.54(8)	C11 - C12 - C13	114.09(8)
C11 - C12 - C15	100.33(8)	C13 - C12 - C15	96.21(8)
C12 - C13 - C14	107.33(9)	C1 - C14 - C13	107.34(9)
C1 - C15 - C12	92.13(8)	C3 - C16 - C10	94.69(8)
C2 - C1 - C14	113.16(8)		

Table A.14: Bond Angles (°) for KM22 from the neutron study at 123K, Experiment 3. Esds given in parentheses.

A-B-C	∠A-B-C	A-B-C	∠A-B-C
CL1 - C1 - C2	113.72(8)	CL1 - C1 - C14	114.92(8)
CL1 - C1 - C15	115.70(8)	CL5 - C5 - C4	114.72(8)
CL5 - C5 - C6	120.97(9)	CL6 - C6 - C5	121.05(9)
CL6 - C6 - C7	118.06(8)	CL7 - C7 - C6	118.08(8)
CL7 - C7 - C8	121.42(8)	CL8 - C8 - C7	120.82(8)
CL8 - C8 - C9	114.79(8)	CL12 - C12 - C11	112.44(7)
CL12 - C12 - C13	114.93(8)	CL12 - C12 - C15	117.09(8)
CL13 - C13 - C12	124.91(8)	CL13 - C13 - C14	127.71(9)
CL14 - C14 - C1	124.92(8)	CL14 - C14 - C13	127.74(9)
CL15 - C15 - C1	116.06(8)	CL15 - C15 - C12	115.60(8)
C1 - C2 - H2	106.03(16)	C3 - C2 - H2	107.44(16)
C11 - C2 - H2	110.02(16)	C2 - C3 - H3	112.95(16)
C4 - C3 - H3	112.93(16)	C16 - C3 - H3	116.44(16)
C3 - C4 - H4	111.81(16)	C5 - C4 - H4	105.76(16)
C9 - C4 - H4	110.78(16)	C4 - C9 - H9	110.62(15)
C8 - C9 - H9	105.64(15)	C10 - C9 - H9	112.16(15)
C9 - C10 - H10	113.12(15)	C11 - C10 - H10	113.38(15)
C16 - C10 - H10	116.02(16)	C2 - C11 - H11	110.29(15)
C10 - C11 - H11	107.45(15)	C12 - C11 - H11	105.51(15)
CL15 - C15 - H15	107.70(15)	C1 - C15 - H15	112.42(16)
C12 - C15 - H15	112.48(16)	C3 - C16 - H16A	112.66(16)
C3 - C16 - H16B	113.00(16)	C10 - C16 - H16A	113.40(16)
C10 - C16 - H16B	112.68(15)	H16A - C16 - H16B	109.78(20)
C16 - H16A - H16B	35.08(12)	C16 - H16B - H16A	35.13(13)

Table A.15: Bond Angles (°) for KM22 from the neutron study at 123K, Experiment 3 (cont'd). Esds given in parentheses.

Atom	x	y	z	U_{eq}
C1	0.3483(2)	-0.3241(2)	0.8383(1)	0.0188(6)
C2	0.5337(2)	-0.3636(2)	0.8659(1)	0.0168(6)
C3	0.7136(2)	-0.4501(2)	0.8010(1)	0.0182(6)
C4	0.7091(2)	-0.3522(2)	0.7108(1)	0.0188(6)
C5	0.7302(2)	-0.3971(2)	0.6150(1)	0.0217(6)
C6	0.7362(2)	-0.2810(2)	0.5469(1)	0.0253(6)
C7	0.7161(2)	-0.1197(2)	0.5763(1)	0.0236(6)
C8	0.6874(2)	-0.0729(2)	0.6736(1)	0.0205(6)
C9	0.6889(2)	-0.1911(2)	0.7393(1)	0.0197(6)
C10	0.6808(2)	-0.1854(2)	0.8460(1)	0.0220(6)
C11	0.5080(2)	-0.1806(2)	0.8922(1)	0.0199(6)
C12	0.3143(2)	-0.0568(2)	0.8685(1)	0.0173(6)
C13	0.2852(2)	-0.0532(2)	0.7608(1)	0.0174(6)
C14	0.3108(2)	-0.2409(2)	0.7399(1)	0.0190(6)
C15	0.2211(2)	-0.1627(2)	0.9039(1)	0.0184(6)
C16	0.8138(2)	-0.3823(2)	0.8601(1)	0.0230(6)
CL1	0.3165(2)	-0.5074(1)	0.8520(1)	0.0309(5)
CL5	0.7477(2)	-0.5920(1)	0.5800(1)	0.0363(5)
CL6	0.7671(2)	-0.3368(2)	0.4283(1)	0.0413(5)
CL7	0.7301(2)	0.0199(1)	0.4943(1)	0.0400(5)
CL8	0.6489(2)	0.1285(1)	0.7122(1)	0.0320(5)
CL12	0.2300(1)	0.1529(1)	0.9219(1)	0.0236(4)
CL13	0.0711(1)	0.1190(1)	0.7390(1)	0.0205(4)
CL14	0.1258(2)	-0.2410(2)	0.6935(1)	0.0360(5)
CL15	0.2231(1)	-0.2007(1)	1.0274(1)	0.0252(4)
H2	0.5574(4)	-0.4428(4)	0.9296(2)	0.0386(13)
H3	0.7731(4)	-0.5907(4)	0.7910(2)	0.0338(13)
H10	0.7101(5)	-0.0888(4)	0.8766(2)	0.0480(14)
H11	0.5068(4)	-0.1654(4)	0.9694(2)	0.0378(13)
H13	0.3801(4)	-0.0293(4)	0.7158(2)	0.0370(13)
H14	0.4230(4)	-0.3133(4)	0.6870(2)	0.0372(13)
H15	0.0813(4)	-0.1019(4)	0.8875(2)	0.0340(13)
H16A	0.9488(4)	-0.4213(5)	0.8280(3)	0.0465(15)
H16B	0.8175(5)	-0.4200(5)	0.9349(2)	0.0462(15)

Table A.16: Atomic coordinates and U_{eq} (Å^2) for KM25 from the neutron study at 123K, Experiment 4. Esds given in parentheses.

Atom	U_{11}	U_{22}	U_{33}	U_{12}	U_{13}	U_{23}
C1	0.0124(8)	0.0110(7)	0.0183(8)	-0.0081(6)	0.0006(6)	0.0017(6)
C2	0.0098(8)	0.0123(7)	0.0164(8)	-0.0059(6)	0.0005(6)	0.0038(6)
C3	0.0107(8)	0.0134(8)	0.0186(8)	-0.0053(6)	0.0013(6)	0.0025(6)
C4	0.0119(8)	0.0132(7)	0.0166(8)	-0.0079(6)	0.0015(6)	0.0020(6)
C5	0.0161(8)	0.0136(8)	0.0176(8)	-0.0095(7)	0.0023(6)	-0.0008(6)
C6	0.0190(9)	0.0184(8)	0.0156(8)	-0.0125(7)	0.0019(6)	0.0003(6)
C7	0.0174(9)	0.0173(8)	0.0147(8)	-0.0118(7)	0.0011(6)	0.0010(6)
C8	0.0129(8)	0.0149(8)	0.0160(8)	-0.0101(6)	0.0014(6)	0.0014(6)
C9	0.0122(8)	0.0152(8)	0.0140(7)	-0.0102(6)	0.0003(6)	0.0010(6)
C10	0.0130(8)	0.0184(8)	0.0158(8)	-0.0107(7)	-0.0017(6)	0.0016(6)
C11	0.0131(8)	0.0160(8)	0.0130(8)	-0.0099(6)	-0.0002(6)	0.0011(6)
C12	0.0134(8)	0.0118(7)	0.0117(7)	-0.0081(6)	0.0002(6)	0.0005(6)
C13	0.0123(8)	0.0130(7)	0.0126(7)	-0.0076(6)	0.0000(6)	0.0011(6)
C14	0.0112(8)	0.0151(8)	0.0164(8)	-0.0074(7)	0.0001(7)	-0.0018(6)
C15	0.0119(9)	0.0124(7)	0.0168(8)	-0.0073(7)	0.0015(6)	0.0014(6)
C16	0.0111(9)	0.0204(8)	0.0214(9)	-0.0083(7)	-0.0029(7)	0.0056(7)
CL1	0.0195(6)	0.0143(6)	0.0366(7)	-0.0123(5)	0.0033(5)	0.0009(5)
CL5	0.0344(7)	0.0179(6)	0.0241(6)	-0.0180(6)	0.0025(5)	-0.0029(5)
CL6	0.0387(8)	0.0291(7)	0.0159(6)	-0.0217(6)	0.0038(5)	-0.0033(5)
CL7	0.0384(8)	0.0241(6)	0.0193(6)	-0.0211(6)	0.0022(5)	0.0056(5)
CL8	0.0277(7)	0.0164(6)	0.0242(6)	-0.0160(5)	-0.0010(5)	0.0004(5)
CL12	0.0210(6)	0.0129(5)	0.0195(6)	-0.0088(5)	-0.0017(5)	-0.0023(4)
CL13	0.0129(6)	0.0175(6)	0.0188(6)	-0.0048(5)	-0.0025(4)	0.0033(4)
CL14	0.0210(7)	0.0286(7)	0.0307(7)	-0.0160(5)	-0.0082(5)	-0.0017(5)
CL15	0.0188(6)	0.0205(6)	0.0169(6)	-0.0084(5)	0.0038(5)	0.0045(4)
H2	0.0317(19)	0.0268(17)	0.0266(17)	-0.0155(15)	-0.0022(14)	0.0096(14)
H3	0.0266(18)	0.0180(17)	0.0386(19)	-0.0061(14)	0.0023(15)	0.0027(14)
H10	0.0347(20)	0.0358(19)	0.0304(18)	-0.0249(16)	-0.0033(15)	-0.0012(15)
H11	0.0304(19)	0.0316(18)	0.0202(17)	-0.0159(15)	-0.0036(14)	0.0034(13)
H13	0.0227(17)	0.0316(18)	0.0265(17)	-0.0155(15)	0.0020(14)	0.0053(13)
H14	0.0251(18)	0.0315(18)	0.0272(17)	-0.0126(15)	0.0050(15)	-0.0091(14)
H15	0.0190(18)	0.0291(17)	0.0315(18)	-0.0103(15)	-0.0011(14)	0.0003(14)
H16A	0.0188(19)	0.0453(21)	0.0418(20)	-0.0167(16)	0.0013(15)	0.0036(16)
H16B	0.0333(20)	0.0432(21)	0.0261(18)	-0.0178(17)	-0.0101(15)	0.0121(15)

Table A.17: Anisotropic atomic displacement parameters (Å^2) for KM25 from the neutron study at 123K, Experiment 4. Esds given in parentheses.

A-B	d_{A-B}	A-B	d_{A-B}	A-B	d_{A-B}
C1 - C14	1.541(2)	C1 - C2	1.541(2)	C1 - C15	1.555(2)
C2 - C11	1.555(2)	C2 - C3	1.565(2)	C3 - C4	1.517(2)
C3 - C16	1.554(2)	C4 - C5	1.382(2)	C4 - C9	1.397(2)
C5 - C6	1.407(2)	C6 - C7	1.403(2)	C7 - C8	1.402(2)
C8 - C9	1.378(2)	C9 - C10	1.498(2)	C10 - C11	1.555(2)
C10 - C16	1.562(2)	C11 - C12	1.548(2)	C12 - C15	1.549(2)
C12 - C13	1.553(2)	C13 - C14	1.579(2)	CL1 - C1	1.763(2)
CL5 - C5	1.716(2)	CL6 - C6	1.709(2)	CL7 - C7	1.712(2)
CL8 - C8	1.717(2)	CL12 - C12	1.767(2)	CL13 - C13	1.774(2)
CL14 - C14	1.770(2)	CL15 - C15	1.767(2)	H2 - C2	1.099(3)
H3 - C3	1.087(3)	H10 - C10	1.096(4)	H11 - C11	1.095(3)
H13 - C13	1.090(3)	H14 - C14	1.090(4)	H15 - C15	1.097(4)
H16A - C16	1.097(4)	H16B - C16	1.098(4)		

Table A.18: Bond lengths (Å) for KM25 from the neutron study at 123K, Experiment 4. Esds given in parentheses.

A-B-C	∠A-B-C	A-B-C	∠A-B-C
C2 - C1 - C14	111.5(1)	C2 - C1 - C15	102.3(1)
C1 - C2 - C3	127.2(1)	C1 - C2 - C11	103.5(1)
C3 - C2 - C11	103.6(1)	C2 - C3 - C4	113.6(1)
C2 - C3 - C16	96.6(1)	C4 - C3 - C16	97.9(1)
C3 - C4 - C5	132.9(1)	C3 - C4 - C9	106.7(1)
C5 - C4 - C9	120.3(1)	C4 - C5 - C6	119.2(1)
C5 - C6 - C7	120.1(1)	C6 - C7 - C8	120.1(1)
C7 - C8 - C9	119.0(1)	C4 - C9 - C8	121.3(1)
C4 - C9 - C10	107.7(1)	C8 - C9 - C10	130.9(1)
C9 - C10 - C11	111.7(1)	C9 - C10 - C16	98.0(1)
C11 - C10 - C16	98.4(1)	C2 - C11 - C12	102.7(1)
C10 - C11 - C12	127.0(1)	C2 - C11 - C10	103.6(1)
C14 - C1 - C15	100.1(1)	C11 - C12 - C13	114.4(1)
C11 - C12 - C15	100.9(1)	C13 - C12 - C15	99.1(1)
C12 - C13 - C14	103.0(1)	C1 - C14 - C13	102.3(1)
C1 - C15 - C12	93.3(1)	C3 - C16 - C10	94.5(1)

Table A.19: Bond Angles (°) for KM25 from the neutron study at 123K, Experiment 4. Esds given in parentheses.

A-B-C	∠A-B-C	A-B-C	∠A-B-C
C2 - C1 - CL1	111.5(1)	C14 - C1 - CL1	114.8(1)
C15 - C1 - CL1	115.6(1)	C4 - C5 - CL5	120.2(1)
C6 - C5 - CL5	120.5(1)	C5 - C6 - CL6	119.8(1)
C7 - C6 - CL6	120.2(1)	C6 - C7 - CL7	120.5(1)
C8 - C7 - CL7	119.5(1)	C7 - C8 - CL8	121.5(1)
C9 - C8 - CL8	119.5(1)	C11 - C12 - CL12	111.5(1)
C13 - C12 - CL12	113.5(1)	C15 - C12 - CL12	116.3(1)
C12 - C13 - CL13	110.6(1)	C14 - C13 - CL13	113.7(1)
C1 - C14 - CL14	112.6(1)	C13 - C14 - CL14	114.4(1)
C1 - C15 - CL15	115.4(1)	C12 - C15 - CL15	114.8(1)
C1 - C2 - H2	105.8(2)	C3 - C2 - H2	106.1(2)
C11 - C2 - H2	110.1(2)	C2 - C3 - H3	114.4(2)
C4 - C3 - H3	115.0(2)	C16 - C3 - H3	116.9(2)
C9 - C10 - H10	115.0(2)	C11 - C10 - H10	114.1(2)
C16 - C10 - H10	117.5(2)	C2 - C11 - H11	110.6(2)
C10 - C11 - H11	107.1(2)	C12 - C11 - H11	105.3(2)
C12 - C13 - H13	112.9(2)	C14 - C13 - H13	111.3(2)
CL13 - C13 - H13	105.6(2)	C1 - C14 - H14	111.4(2)
C13 - C14 - H14	111.1(2)	CL14 - C14 - H14	105.3(2)
C1 - C15 - H15	113.5(2)	C12 - C15 - H15	112.9(2)
CL15 - C15 - H15	106.8(2)	C3 - C16 - H16A	112.6(2)
C3 - C16 - H16B	112.7(2)	C10 - C16 - H16A	112.4(2)
C10 - C16 - H16B	113.4(2)	H16A - C16 - H16B	110.5(3)

Table A.20: Bond Angles (°) for KM25 from the neutron study at 123K, Experiment 4 (cont'd). Esds given in parentheses.

Atom	x	y	z	U_{eq}
C1	0.3484(1)	-0.3241(1)	0.83843(6)	0.0180(2)
C2	0.5337(1)	-0.3639(1)	0.86592(6)	0.0166(2)
C3	0.7131(1)	-0.4504(1)	0.80090(6)	0.0178(2)
C4	0.7091(1)	-0.3525(1)	0.71065(6)	0.0184(2)
C5	0.7302(1)	-0.3974(1)	0.61483(6)	0.0218(2)
C6	0.7364(1)	-0.2812(1)	0.54699(6)	0.0248(2)
C7	0.7162(1)	-0.1198(1)	0.57622(6)	0.0244(2)
C8	0.6880(1)	-0.0729(1)	0.67340(6)	0.0205(2)
C9	0.6893(1)	-0.1912(1)	0.73916(6)	0.0188(2)
C10	0.6803(1)	-0.1853(1)	0.84615(6)	0.0212(2)
C11	0.5080(1)	-0.1807(1)	0.89209(5)	0.0176(2)
C12	0.3146(1)	-0.0570(1)	0.86865(5)	0.0158(1)
C13	0.2855(1)	-0.0530(1)	0.76118(5)	0.0165(2)
C14	0.3110(1)	-0.2409(1)	0.73998(6)	0.0188(2)
C15	0.2211(1)	-0.1628(1)	0.90403(6)	0.0174(2)
C16	0.8136(1)	-0.3821(1)	0.86008(7)	0.0223(2)
CL1	0.3162(4)	-.50765(3)	0.85214(2)	0.0291(6)
CL5	0.7481(5)	-.59264(3)	0.57988(2)	0.0351(8)
CL6	0.7678(5)	-.33730(4)	0.42814(2)	0.0412(9)
CL7	0.7299(5)	0.02004(4)	0.49409(2)	0.0396(9)
CL8	0.6496(4)	0.12824(3)	0.71213(2)	0.0305(6)
CL12	0.2302(3)	0.15285(3)	0.92225(2)	0.0226(5)
CL13	0.0718(3)	0.11898(3)	0.73924(2)	0.0195(5)
CL14	0.1257(4)	-.24121(4)	0.69369(2)	0.0334(7)
CL15	0.2232(4)	-.20045(3)	1.02769(2)	0.0240(6)

Table A.21: Atomic coordinates and U_{eq} (Å^2) for KM25 from the refinement FULL, using X-ray data measured at 123K and to a $\sin\theta/\lambda$(max) of 1.08Å^{-1}.

Atom	U_{11}	U_{22}	U_{33}	U_{12}	U_{13}	U_{23}
C1	0.0127(2)	0.0112(2)	0.0178(2)	-0.0059(2)	0.0014(2)	-0.0004(2)
C2	0.0126(2)	0.0116(2)	0.0147(2)	-0.0047(2)	0.0002(2)	0.0019(2)
C3	0.0129(2)	0.0126(2)	0.0169(2)	-0.0044(2)	0.0006(2)	0.0018(2)
C4	0.0135(2)	0.0130(2)	0.0151(2)	-0.0065(2)	0.0013(2)	-0.0001(2)
C5	0.0183(3)	0.0142(2)	0.0156(2)	-0.0086(2)	0.0020(2)	-0.0015(2)
C6	0.0206(3)	0.0184(3)	0.0141(2)	-0.0109(2)	0.0023(2)	-0.0013(2)
C7	0.0204(3)	0.0169(3)	0.0146(2)	-0.0111(2)	0.0013(2)	0.0011(2)
C8	0.0154(3)	0.0143(2)	0.0152(2)	-0.0087(2)	0.0002(2)	0.0004(2)
C9	0.0133(2)	0.0145(2)	0.0137(2)	-0.0076(2)	-0.0001(2)	0.0004(2)
C10	0.0147(3)	0.0177(2)	0.0141(2)	-0.0090(2)	-0.0017(2)	0.0006(2)
C11	0.0137(2)	0.0136(2)	0.0121(2)	-0.0063(2)	-0.0013(2)	0.0010(2)
C12	0.0133(2)	0.0110(2)	0.0118(2)	-0.0053(2)	-0.0004(2)	0.0000(2)
C13	0.0124(2)	0.0135(2)	0.0119(2)	-0.0052(2)	-0.0006(2)	0.0006(2)
C14	0.0129(2)	0.0150(2)	0.0155(2)	-0.0059(2)	-0.0002(2)	-0.0029(2)
C15	0.0132(2)	0.0125(2)	0.0141(2)	-0.0054(2)	0.0018(2)	0.0003(2)
C16	0.0134(3)	0.0203(3)	0.0188(3)	-0.0064(2)	-0.0033(2)	0.0036(2)
CL1	0.01979(8)	0.01375(6)	0.03408(12)	-0.01019(6)	0.00258(8)	-0.00048(7)
CL5	0.03478(13)	0.01811(8)	0.02227(9)	-0.01585(9)	0.00282(8)	-0.00442(7)
CL6	0.04060(16)	0.02940(11)	0.01414(7)	-0.02054(11)	0.00399(8)	-0.00374(7)
CL7	0.04013(15)	0.02437(10)	0.01721(8)	-0.01972(10)	0.00214(8)	0.00375(7)
CL8	0.02805(11)	0.01617(7)	0.02195(8)	-0.01383(7)	-0.00062(7)	-0.00064(6)
CL12	0.02206(8)	0.01263(6)	0.01781(7)	-0.00677(6)	-0.00163(6)	-0.00307(5)
CL13	0.01441(7)	0.01734(7)	0.01657(7)	-0.00269(6)	-0.00249(5)	0.00221(5)
CL14	0.02089(9)	0.02650(10)	0.02892(11)	-0.01308(8)	-0.00764(8)	-0.00319(8)
CL15	0.02069(8)	0.01932(8)	0.01471(7)	-0.00627(6)	0.00392(5)	0.00333(6)

Table A.22: Anisotropic displacement parameters ($Å^2$) for KM25 from the refinement FULL, using X-ray data measured at 123K and to a $\sin\theta/\lambda$(max) of 1.08$Å^{-1}$.

A-B	d_{A-B}	A-B	d_{A-B}	A-B	d_{A-B}
C1 - C2	1.539(1)	C1 - C14	1.542(1)	C1 - C15	1.555(1)
C2 - C11	1.557(1)	C3 - C4	1.518(1)	C3 - C16	1.559(1)
C4 - C5	1.383(1)	C4 - C9	1.400(1)	C5 - C6	1.405(1)
C6 - C7	1.402(1)	C7 - C8	1.401(1)	C8 - C9	1.378(1)
C9 - C10	1.502(1)	C10 - C11	1.550(1)	C10 - C16	1.562(1)
C11 - C12	1.544(1)	C12 - C15	1.550(1)	C12 - C13	1.551(1)
C13 - C14	1.581(1)	C14 - C1	1.7663(8)	CL5 - C5	1.7172(9)
CL6 - C6	1.7128(9)	CL7 - C7	1.714(1)	CL8 - C8	1.7167(9)
CL12 - C12	1.7695(8)	CL13 - C13	1.7724(9)	CL14 - C14	1.7720(9)
CL15 - C15	1.7682(9)				

Table A.23: Bond lengths (Å) for KM25 from refinement FULL, using X-ray data measured at 123K and to a $\sin\theta/\lambda$(max) of 1.08Å^{-1}. Esds given in parentheses.

A-B-C	∠A-B-C	A-B-C	∠A-B-C
C2 -C1 -C14	111.41(6)	C2 -C1 -C15	102.42(6)
C2 -C1 -CL1	111.43(5)	C14 -C1 -C15	100.13(6)
C14 -C1 -CL1	114.83(6)	C15 -C1 -CL1	115.51(6)
C1 -C2 -C3	127.12(7)	C1 -C2 -C11	103.42(6)
C3 -C2 -C11	103.54(6)	C2 -C3 -C4	113.84(6)
C2 -C3 -C16	96.45(7)	C4 -C3 -C16	97.74(6)
C3 -C4 -C5	132.94(7)	C3 -C4 -C9	106.77(7)
C5 -C4 -C9	120.17(7)	C4 -C5 -C6	119.10(7)
C4 -C5 -CL5	120.13(6)	C6 -C5 -CL5	120.76(7)
C5 -C6 -C7	120.30(8)	C5 -C6 -CL6	119.61(7)
C7 -C6 -CL6	120.09(7)	C6 -C7 -C8	120.05(8)
C6 -C7 -CL7	120.56(7)	C8 -C7 -CL7	119.37(7)
C7 -C8 -C9	118.89(7)	C7 -C8 -CL8	121.66(6)
C9 -C8 -CL8	119.44(6)	C4 -C9 -C8	121.38(7)
C4 -C9 -C10	107.63(7)	C8 -C9 -C10	130.93(7)
C9 -C10 -C11	111.88(7)	C9 -C10 -C16	97.80(7)
C11 -C10 -C16	98.47(7)	C2 -C11 -C10	103.72(6)
C2 -C11 -C12	102.72(6)	C10 -C11 -C12	127.14(6)
C11 -C12 -C13	114.30(6)	C11 -C12 -C15	101.03(6)
C11 -C12 -CL12	111.63(5)	C13 -C12 -C15	99.08(6)
C13 -C12 -CL12	113.45(5)	C15 -C12 -CL12	116.28(5)
C12 -C13 -C14	103.03(6)	C12 -C13 -CL13	110.68(5)
C14 -C13 -CL13	113.70(5)	C1 -C14 -C13	102.19(6)
C1 -C14 -CL14	112.42(6)	C13 -C14 -CL14	114.51(6)
C1 -C15 -C12	93.26(6)	C1 -C15 -CL15	115.47(6)
C12 -C15 -CL15	114.69(5)	C3 -C16 -C10	94.54(7)

Table A.24: Bond angles (°) for KM25 from refinement FULL, using X-ray data measured at 123K and to a $\sin\theta/\lambda$(max) of 1.08Å^{-1}. Esds given in parentheses.

Atom	x	y	z	U_{eq}
C1	0.3486(1)	-0.3243(1)	0.83843(7)	0.0190(2)
C2	0.5337(1)	-0.3641(1)	0.86591(7)	0.0177(2)
C3	0.7131(1)	-0.4503(1)	0.80096(8)	0.0188(2)
C4	0.7090(1)	-0.3525(1)	0.71067(7)	0.0196(2)
C5	0.7303(2)	-0.3976(1)	0.61494(8)	0.0228(2)
C6	0.7367(2)	-0.2814(1)	0.54699(8)	0.0258(2)
C7	0.7161(2)	-0.1197(1)	0.57614(8)	0.0256(2)
C8	0.6881(1)	-0.0728(1)	0.67342(7)	0.0217(2)
C9	0.6893(1)	-0.1913(1)	0.73915(7)	0.0197(2)
C10	0.6803(1)	-0.1853(1)	0.84615(7)	0.0223(2)
C11	0.5080(1)	-0.1806(1)	0.89210(6)	0.0186(2)
C12	0.3146(1)	-0.0568(1)	0.86873(6)	0.0171(2)
C13	0.2852(1)	-0.0528(1)	0.76123(6)	0.0176(2)
C14	0.3109(1)	-0.2409(1)	0.74005(7)	0.0197(2)
C15	0.2212(1)	-0.1630(1)	0.90410(7)	0.0184(2)
C16	0.8136(2)	-0.3821(2)	0.86012(9)	0.0234(2)
CL1	0.31627(5)	-0.50772(4)	0.85242(4)	0.0298(1)
CL5	0.74853(7)	-0.59282(5)	0.58001(3)	0.0359(1)
CL6	0.76819(9)	-0.33757(7)	0.42818(3)	0.0413(1)
CL7	0.73004(8)	0.01998(6)	0.49408(3)	0.0401(1)
CL8	0.64964(6)	0.12830(4)	0.71211(3)	0.0314(1)
CL12	0.23020(5)	0.15291(3)	0.92228(2)	0.0236(1)
CL13	0.07184(4)	0.11909(4)	0.73930(2)	0.0206(1)
CL14	0.12557(6)	-0.24132(6)	0.69385(4)	0.0340(1)
CL15	0.22325(5)	-0.20026(4)	1.02782(2)	0.0248(1)

Table A.25: Atomic coordinates and U_{eq} (Å^2) for KM25 from the refinement HO, using X-ray data measured at 123K and with $\sin\theta/\lambda > 1.08$Å^{-1}.

Atom	U_{11}	U_{22}	U_{33}	U_{12}	U_{13}	U_{23}
C1	0.0133(2)	0.0121(2)	0.0185(3)	-0.0062(2)	0.0014(2)	-0.0003(2)
C2	0.0134(2)	0.0122(2)	0.0156(2)	-0.0050(2)	0.0001(2)	0.0019(2)
C3	0.0137(3)	0.0134(2)	0.0176(3)	-0.0046(2)	0.0005(2)	0.0017(2)
C4	0.0146(3)	0.0139(2)	0.0157(2)	-0.0071(2)	0.0012(2)	0.0001(2)
C5	0.0189(3)	0.0152(2)	0.0160(3)	-0.0090(2)	0.0017(2)	-0.0011(2)
C6	0.0214(4)	0.0190(3)	0.0149(3)	-0.0112(3)	0.0022(2)	-0.0009(2)
C7	0.0213(4)	0.0179(3)	0.0154(3)	-0.0117(3)	0.0013(2)	0.0011(2)
C8	0.0165(3)	0.0151(2)	0.0159(2)	-0.0091(2)	0.0002(2)	0.0005(2)
C9	0.0140(2)	0.0151(2)	0.0144(2)	-0.0079(2)	-0.0002(2)	0.0005(2)
C10	0.0156(3)	0.0185(3)	0.0150(2)	-0.0094(2)	-0.0016(2)	0.0006(2)
C11	0.0145(3)	0.0143(2)	0.0130(2)	-0.0067(2)	-0.0013(2)	0.0010(2)
C12	0.0143(2)	0.0120(2)	0.0124(2)	-0.0059(2)	-0.0005(2)	0.0002(2)
C13	0.0133(2)	0.0143(2)	0.0126(2)	-0.0056(2)	-0.0005(2)	0.0007(2)
C14	0.0138(3)	0.0154(2)	0.0164(3)	-0.0062(2)	-0.0001(2)	-0.0028(2)
C15	0.0140(3)	0.0132(2)	0.0151(2)	-0.0057(2)	0.0017(2)	0.0003(2)
C16	0.0144(3)	0.0211(3)	0.0195(3)	-0.0067(2)	-0.0033(2)	0.0036(3)
CL1	0.02039(11)	0.01452(9)	0.03425(16)	-0.01039(7)	0.00221(9)	-0.00015(8)
CL5	0.03552(18)	0.01875(10)	0.02282(12)	-0.01605(11)	0.00264(10)	-0.00413(8)
CL6	0.04046(22)	0.02969(15)	0.01487(10)	-0.02019(15)	0.00368(10)	-0.00335(8)
CL7	0.04027(21)	0.02500(13)	0.01793(10)	-0.01969(14)	0.00182(10)	0.00390(8)
CL8	0.02871(14)	0.01689(9)	0.02271(11)	-0.01406(9)	-0.00078(9)	-0.00043(7)
CL12	0.02293(11)	0.01339(8)	0.01854(10)	-0.00714(7)	-0.00175(7)	-0.00290(6)
CL13	0.01534(9)	0.01811(9)	0.01729(9)	-0.00313(7)	-0.00259(6)	0.00237(6)
CL14	0.02149(13)	0.02690(13)	0.02939(15)	-0.01313(10)	-0.00757(10)	-0.00287(10)
CL15	0.02131(11)	0.01995(10)	0.01545(9)	-0.00649(8)	0.00375(7)	0.00336(6)

Table A.26: Anisotropic atomic displacement parameters (Å^2) for KM25 from the refinement HO, using X-ray data measured at 123K and to a $\sin\theta/\lambda > 1.08$Å^{-1}.

A-B	d_{A-B}	A-B	d_{A-B}	A-B	d_{A-B}
C1 - C2	1.538(1)	C1 - C14	1.542(1)	C1 - C15	1.556(1)
C2 - C11	1.558(1)	C2 - C3	1.563(1)	C3 - C4	1.518(1)
C3 - C16	1.558(2)	C4 - C5	1.382(1)	C4 - C9	1.399(1)
C5 - C6	1.407(2)	C6 - C7	1.403(2)	C7 - C8	1.403(2)
C8 - C9	1.379(1)	C9 - C10	1.503(1)	C10 - C11	1.550(1)
C10 - C16	1.562(2)	C11 - C12	1.544(1)	C12 - C15	1.552(1)
C12 - C13	1.552(1)	C13 - C14	1.582(1)	CL1 - C1	1.766(1)
CL5 - C5	1.716(1)	CL6 - C6	1.712(1)	CL7 - C7	1.713(1)
CL8 - C8	1.716(1)	CL12 - C12	1.7683(9)	CL13 - C13	1.770(1)
CL14 - C14	1.772(1)	CL15 - C15	1.769(1)		

Table A.27: Bond lengths (Å) for KM25 from refinement HO, using X-ray data measured at 123K and with $\sin\theta/\lambda > 1.08\text{Å}^{-1}$. Esds given in parentheses.

A-B-C	∠A-B-C	A-B-C	∠A-B-C	A-B-C	∠A-B-C
C2 - C1 - C14	111.47(8)	C2 - C1 - C15	102.42(7)	C2 - C1 - CL1	111.43(6)
C14 - C1 - C15	100.06(7)	C14 - C1 - CL1	114.96(7)	C15 - C1 - CL1	115.38(7)
C1 - C2 - C3	127.15(8)	C1 - C2 - C11	103.42(7)	C3 - C2 - C11	103.49(7)
C2 - C3 - C4	113.86(8)	C2 - C3 - C16	96.51(8)	C4 - C3 - C16	97.80(8)
C3 - C4 - C5	132.92(8)	C3 - C4 - C9	106.73(8)	C5 - C4 - C9	120.23(9)
C4 - C5 - C6	119.06(9)	C4 - C5 - CL5	120.21(8)	C6 - C5 - CL5	120.74(8)
C5 - C6 - C7	120.3(1)	C5 - C6 - CL6	119.62(9)	C7 - C6 - CL6	120.06(9)
C6 - C7 - C8	120.0(1)	C6 - C7 - CL7	120.63(8)	C8 - C7 - CL7	119.31(8)
C7 - C8 - C9	118.79(9)	C7 - C8 - CL8	121.68(8)	C9 - C8 - CL8	119.52(8)
C4 - C9 - C8	121.46(9)	C4 - C9 - C10	107.66(8)	C8 - C9 - C10	130.82(9)
C9 - C10 - C11	111.87(8)	C9 - C10 - C16	97.79(8)	C11 - C10 - C16	98.48(8)
C2 - C11 - C10	103.67(7)	C2 - C11 - C12	102.77(7)	C10 - C11 - C12	127.16(8)
C11 - C12 - C13	114.33(7)	C11 - C12 - C15	100.97(7)	C11 - C12 - CL12	111.68(6)
C13 - C12 - C15	98.99(7)	C13 - C12 - CL12	113.44(6)	C15 - C12 - CL12	116.35(6)
C12 - C13 - C14	103.03(7)	C12 - C13 - CL13	110.74(6)	C14 - C13 - CL13	113.79(6)
C1 - C14 - C13	102.26(7)	C1 - C14 - CL14	112.41(7)	C13 - C14 - CL14	114.49(7)
C1 - C15 - C12	93.29(7)	C1 - C15 - CL15	115.57(7)	C12 - C15 - CL15	114.57(6)
C3 - C16 - C10	94.52(8)				

Table A.28: Bond angles (°) for KM25 from refinement HO, using X-ray data measured at 123K and with $\sin\theta/\lambda > 1.08\text{Å}^{-1}$. Esds given in parentheses.

Atom	x	y	z	U_{eq}
C1	0.3481(2)	-0.3239(2)	0.8385(1)	0.0188(3)
C2	0.5335(2)	-0.3638(2)	0.8659(1)	0.0174(3)
C3	0.7132(2)	-0.4505(2)	0.8008(1)	0.0192(4)
C4	0.7091(2)	-0.3525(2)	0.7107(1)	0.0186(3)
C5	0.7301(2)	-0.3973(2)	0.6147(1)	0.0225(4)
C6	0.7360(2)	-0.2811(2)	0.5469(1)	0.0257(4)
C7	0.7162(2)	-0.1197(2)	0.5763(1)	0.0250(4)
C8	0.6878(2)	-0.0730(2)	0.6734(1)	0.0210(4)
C9	0.6893(2)	-0.1910(2)	0.7392(1)	0.0198(3)
C10	0.6803(2)	-0.1854(2)	0.8462(1)	0.0218(4)
C11	0.5081(2)	-0.1808(2)	0.8921(1)	0.0183(3)
C12	0.3146(2)	-0.0573(2)	0.8686(1)	0.0158(3)
C13	0.2858(2)	-0.0533(2)	0.7611(1)	0.0175(3)
C14	0.3111(2)	-0.2409(2)	0.7398(1)	0.0197(4)
C15	0.2211(2)	-0.1626(2)	0.9040(1)	0.0182(3)
C16	0.8136(2)	-0.3822(2)	0.8601(1)	0.0234(4)
CL1	0.31615(5)	-.50757(4)	0.85197(3)	0.0303(1)
CL5	0.74789(6)	-.59255(5)	0.57981(3)	0.0360(1)
CL6	0.76764(6)	-.33716(6)	0.42813(3)	0.0425(1)
CL7	0.72982(6)	0.02004(5)	0.49409(3)	0.0407(1)
CL8	0.64965(5)	0.12818(4)	0.71214(3)	0.0315(1)
CL12	0.23020(5)	0.15276(4)	0.92222(2)	0.0233(1)
CL13	0.07171(4)	0.11890(4)	0.73917(2)	0.0202(1)
CL14	0.12575(5)	-.24116(5)	0.69360(3)	0.0347(1)
CL15	0.22318(5)	-.20061(5)	1.02758(2)	0.0250(1)

Table A.29: Atomic coordinates and U_{eq} (Å^2) for KM25 from the refinement LO, using X-ray data measured at 123K and to a $\sin\theta/\lambda$(max) of 0.8Å^{-1}.

Atom	U_{11}	U_{22}	U_{33}	U_{12}	U_{13}	U_{23}
C1	0.0135(5)	0.0115(4)	0.0181(5)	-0.0065(4)	0.0015(4)	-0.0010(4)
C2	0.0123(5)	0.0130(4)	0.0150(4)	-0.0053(4)	0.0008(4)	0.0013(4)
C3	0.0138(5)	0.0137(5)	0.0170(5)	-0.0057(4)	0.0009(4)	0.0016(4)
C4	0.0128(5)	0.0135(5)	0.0160(5)	-0.0063(4)	0.0016(4)	-0.0005(4)
C5	0.0187(5)	0.0140(5)	0.0165(5)	-0.0091(4)	0.0026(4)	-0.0027(4)
C6	0.0209(6)	0.0194(5)	0.0142(5)	-0.0115(5)	0.0027(4)	-0.0024(4)
C7	0.0204(6)	0.0177(5)	0.0156(5)	-0.0111(5)	0.0017(4)	0.0004(4)
C8	0.0153(5)	0.0143(5)	0.0162(5)	-0.0092(4)	0.0004(4)	-0.0005(4)
C9	0.0136(5)	0.0153(5)	0.0143(4)	-0.0084(4)	0.0002(4)	-0.0002(4)
C10	0.0149(5)	0.0183(5)	0.0141(4)	-0.0098(4)	-0.0016(4)	0.0001(4)
C11	0.0143(5)	0.0143(5)	0.0123(4)	-0.0068(4)	-0.0010(4)	0.0002(4)
C12	0.0132(5)	0.0107(4)	0.0121(4)	-0.0052(4)	-0.0003(3)	-0.0008(3)
C13	0.0130(5)	0.0140(5)	0.0126(4)	-0.0060(4)	-0.0004(4)	0.0000(3)
C14	0.0135(5)	0.0160(5)	0.0154(5)	-0.0068(4)	-0.0005(4)	-0.0030(4)
C15	0.0136(5)	0.0134(5)	0.0142(4)	-0.0059(4)	0.0020(4)	0.0001(4)
C16	0.0134(5)	0.0211(6)	0.0198(5)	-0.0074(4)	-0.0032(4)	0.0029(4)
CL1	0.0205(1)	0.0145(1)	0.0350(2)	-0.0110(1)	0.0030(1)	-0.0014(1)
CL5	0.0352(2)	0.0188(1)	0.0229(1)	-0.0165(1)	0.0030(1)	-0.0052(1)
CL6	0.0417(2)	0.0304(2)	0.0145(1)	-0.0215(2)	0.0042(1)	-0.0045(1)
CL7	0.0410(2)	0.0250(2)	0.0177(1)	-0.0204(2)	0.0025(1)	0.0033(1)
CL8	0.0287(2)	0.0168(1)	0.0223(1)	-0.0146(1)	-0.0005(1)	-0.0014(1)
CL12	0.0225(1)	0.0131(1)	0.0182(1)	-0.0073(1)	-0.0014(1)	-0.0037(1)
CL13	0.0147(1)	0.0180(1)	0.0170(1)	-0.0031(1)	-0.0022(1)	0.0015(1)
CL14	0.0216(2)	0.0275(2)	0.0296(2)	-0.0140(1)	-0.0078(1)	-0.0039(1)
CL15	0.0214(1)	0.0202(1)	0.0151(1)	-0.0070(1)	0.0042(1)	0.0029(1)

Table A.30: Anisotropic atomic displacement parameters ($Å^2$) for KM25 from the refinement LO, using X-ray data measured at 123K and to a $\sin\theta/\lambda$(max) of $0.8Å^{-1}$.

A-B	d_{A-B}	A-B	d_{A-B}	A-B	d_{A-B}
C1 - C2	1.540(2)	C1 - C14	1.543(2)	C1 - C15	1.554(2)
C2 - C11	1.555(2)	C2 - C3	1.566(2)	C3 - C4	1.517(2)
C3 - C16	1.561(2)	C4 - C5	1.385(2)	C4 - C9	1.401(2)
C5 - C6	1.403(2)	C6 - C7	1.404(2)	C7 - C8	1.400(2)
C8 - C9	1.376(2)	C9 - C10	1.503(2)	C10 - C11	1.550(2)
C10 - C16	1.562(2)	C11 - C12	1.544(2)	C12 - C15	1.547(2)
C12 - C13	1.551(2)	C13 - C14	1.580(2)	CL1 - C1	1.766(1)
CL5 - C5	1.718(1)	CL6 - C6	1.712(1)	CL7 - C7	1.713(1)
CL8 - C8	1.717(1)	CL12 - C12	1.771(1)	CL13 - C13	1.775(1)
CL14 - C14	1.772(1)	CL15 - C15	1.767(1)		

Table A.31: Bond lengths (Å) for KM25 from refinement LO, using X-ray data measured at 123K and to a $\sin\theta/\lambda$(max) of 0.8Å^{-1}. Esds given in parentheses.

A-B-C	∠A-B-C	A-B-C	∠A-B-C
C2 - C1 - C14	111.3(1)	C2 - C1 - C15	102.4(1)
C2 - C1 - CL1	111.41(9)	C14 - C1 - C15	100.2(1)
C14 - C1 - CL1	114.74(9)	C15 - C1 - CL1	115.67(9)
C1 - C2 - C3	127.1(1)	C1 - C2 - C11	103.5(1)
C3 - C2 - C11	103.6(1)	C2 - C3 - C4	113.8(1)
C2 - C3 - C16	96.3(1)	C4 - C3 - C16	97.7(1)
C3 - C4 - C5	132.9(1)	C3 - C4 - C9	106.9(1)
C5 - C4 - C9	120.1(1)	C4 - C5 - C6	119.2(1)
C4 - C5 - CL5	120.1(1)	C6 - C5 - CL5	120.8(1)
C5 - C6 - C7	120.2(1)	C5 - C6 - CL6	119.6(1)
C7 - C6 - CL6	120.1(1)	C6 - C7 - C8	120.0(1)
C6 - C7 - CL7	120.5(1)	C8 - C7 - CL7	119.5(1)
C7 - C8 - C9	119.0(1)	C7 - C8 - CL8	121.6(1)
C9 - C8 - CL8	119.4(1)	C4 - C9 - C8	121.3(1)
C4 - C9 - C10	107.6(1)	C8 - C9 - C10	131.1(1)
C9 - C10 - C11	111.9(1)	C9 - C10 - C16	97.9(1)
C11 - C10 - C16	98.5(1)	C2 - C11 - C10	103.8(1)
C2 - C11 - C12	102.6(1)	C10 - C11 - C12	127.2(1)
C11 - C12 - C13	114.3(1)	C11 - C12 - C15	101.12(9)
C11 - C12 - CL12	111.58(8)	C13 - C12 - C15	99.22(9)
C13 - C12 - CL12	113.43(8)	C15 - C12 - CL12	116.19(9)
C12 - C13 - C14	103.04(9)	C12 - C13 - CL13	110.62(8)
C14 - C13 - CL13	113.58(9)	C1 - C14 - C13	102.09(1)
C1 - C14 - CL14	112.36(9)	C13 - C14 - CL14	114.59(9)
C1 - C15 - C12	93.22(9)	C1 - C15 - CL15	115.39(9)
C12 - C15 - CL15	114.83(9)	C3 - C16 - C10	94.6(1)

Table A.32: Bond angles (°) for KM25 from refinement LO, using X-ray data measured at 123K and to a $\sin\theta/\lambda$(max) of 0.8Å^{-1}. Esds given in parentheses.

Atom	x	y	z
C(1)	0.3485(1)	-0.32419(9)	0.83847(6)
C(2)	0.5337(1)	-0.36410(9)	0.86587(6)
C(3)	0.7131(1)	-0.4504(1)	0.80094(6)
C(4)	0.7090(1)	-0.3525(1)	0.7107(6)
C(5)	0.7304(1)	-0.3975(1)	0.61483(6)
C(6)	0.7363(1)	-0.2812(1)	0.54700(6)
C(7)	0.7161(1)	-0.1197(1)	0.57616(6)
C(8)	0.6879(1)	-0.0728(1)	0.67340(6)
C(9)	0.6893(1)	-0.1912(1)	0.73918(6)
C(10)	0.6803(1)	-0.1852(1)	0.84612(6)
C(11)	0.5080(1)	-0.18058(9)	0.89212(5)
C(12)	0.3146(1)	-0.05691(9)	0.86866(5)
C(13)	0.2853(1)	-0.0530(1)	0.76118(5)
C(14)	0.3109(1)	-0.2408(1)	0.74003(6)
C(15)	0.2211(1)	-0.16290(9)	0.90402(6)
C(16)	0.8137(1)	-0.3822(1)	0.86011(7)
Cl(1)	0.31626(4)	-0.50768(2)	0.85228(2)
Cl(5)	0.74829(5)	-0.59270(4)	0.57994(2)
Cl(6)	0.76802(6)	-0.33745(5)	0.42817(2)
Cl(7)	0.72992(5)	0.02007(4)	0.49410(2)
Cl(8)	0.64961(4)	0.12827(3)	0.71214(2)
Cl(12)	0.23018(3)	0.15286(3)	0.92225(2)
Cl(13)	0.07174(3)	0.11901(3)	0.73923(2)
Cl(14)	0.12564(4)	-0.24126(4)	0.69373(3)
Cl(15)	0.22317(4)	-0.20039(3)	1.02773(2)

Table A.33: Atomic coordinates for the non-hydrogen atoms of KM25 from refinement MULT.

Atom	U_{11}	U_{22}	U_{33}	U_{12}	U_{13}	U_{23}
C(1)	0.0116(2)	0.0103(2)	0.0172(2)	-0.0053(2)	0.0013(2)	-0.0003(2)
C(2)	0.0115(2)	0.0106(2)	0.0145(2)	-0.0042(2)	0.0002(2)	0.0019(2)
C(3)	0.0121(2)	0.0115(2)	0.0164(2)	-0.0040(2)	0.0007(2)	0.0016(2)
C(4)	0.0128(2)	0.0119(2)	0.0143(2)	-0.0061(2)	0.0012(2)	-0.0002(2)
C(5)	0.0168(3)	0.0132(2)	0.0151(2)	-0.0080(2)	0.0019(2)	-0.0012(2)
C(6)	0.0192(3)	0.0166(3)	0.0137(2)	-0.0099(2)	0.0022(2)	-0.0010(2)
C(7)	0.0194(3)	0.0155(2)	0.0141(2)	-0.0104(2)	0.0013(2)	0.0012(2)
C(8)	0.0145(2)	0.0130(2)	0.0147(2)	-0.0081(2)	0.0003(2)	0.0005(2)
C(9)	0.0124(2)	0.0132(2)	0.0134(2)	-0.0071(2)	0.0000(2)	0.0004(2)
C(10)	0.0134(2)	0.0162(2)	0.0139(2)	-0.0083(2)	-0.0017(2)	0.0008(2)
C(11)	0.0125(2)	0.0123(2)	0.0118(2)	-0.0056(2)	-0.0012(2)	0.0009(2)
C(12)	0.0120(2)	0.0101(2)	0.0114(2)	-0.0049(2)	-0.0006(2)	0.0001(1)
C(13)	0.0114(1)	0.0125(2)	0.0115(2)	-0.0048(2)	-0.0006(2)	0.0006(2)
C(14)	0.0119(2)	0.0137(2)	0.0152(2)	-0.0054(2)	-0.0001(2)	-0.0027(2)
C(15)	0.0118(2)	0.0114(2)	0.0138(2)	-0.0047(2)	0.0016(2)	0.0004(2)
C(16)	0.0121(2)	0.0190(3)	0.0185(3)	-0.0059(2)	-0.0033(2)	0.0035(2)
Cl(1)	0.01813(8)	0.01260(6)	0.0334(1)	-0.00925(6)	0.00240(8)	-0.00029(7)
Cl(5)	0.0320(1)	0.01669(8)	0.02179(9)	-0.01459(9)	0.00252(9)	-0.00397(7)
Cl(6)	0.0369(1)	0.0270(1)	0.01391(8)	-0.0186(1)	0.00367(9)	-0.00328(7)
Cl(7)	0.0366(2)	0.02250(9)	0.01693(8)	-0.0180(1)	0.00189(9)	0.00379(7)
Cl(8)	0.0258(1)	0.01485(7)	0.02152(9)	-0.01269(8)	-0.00072(7)	-0.00045(6)
Cl(12)	0.02017(8)	0.01153(6)	0.01746(7)	-0.00613(6)	-0.00165(6)	-0.00285(5)
Cl(13)	0.01320(7)	0.01593(7)	0.01615(7)	-0.00232(5)	-0.00235(5)	0.00217(5)
Cl(14)	0.01929(9)	0.02429(9)	0.0284(1)	-0.01202(8)	-0.00754(8)	-0.00280(8)
Cl(15)	0.01884(8)	0.01767(7)	0.01444(7)	-0.00547(6)	0.00384(6)	0.00324(5)

Table A.34: Anisotropic atomic displacement parameters (Å^2) for the non-hydrogen atoms of KM25 from refinement MULT.

	C(1)	C(2)	C(3)	C(4)	C(5)	C(6)	C(7)	C(8)
M1	4.0(1)	4.1(1)	4.0(1)	4.0(2)	3.8(2)	3.8(2)	4.0(1)	4.2(1)
D1+	0.17(8)	0.10(8)	-0.04(8)	0.03(9)	0.15(9)	0.11(9)	0.05(9)	0.07(9)
D1-	-0.10(7)	-0.06(8)	0.06(8)	-0.2(1)	0.08(8)	0.01(8)	-0.02(8)	-0.01(8)
D0	-0.09(7)	-0.07(8)	0.00(8)	-0.04(7)	0.06(7)	-0.00(7)	-0.01(7)	0.04(7)
Q0	-0.09(7)	0.19(7)	-0.14(8)	-0.33(7)	-0.21(6)	-0.20(7)	-0.17(7)	-0.27(6)
Q1+	-0.06(6)	0.21(7)	-0.17(7)	-0.01(6)	0.22(7)	0.07(7)	0.10(7)	-0.07(6)
Q1-	0.07(6)	0.03(7)	-0.10(7)	0.10(6)	0.03(6)	0.17(6)	-0.09(6)	-0.06(6)
Q2+	0.23(7)	0.10(7)	-0.07(7)	-0.01(8)	0.27(8)	-0.10(7)	-0.04(7)	-0.07(7)
Q2-	-0.08(6)	0.09(7)	-0.01(7)	-0.00(7)	0.06(7)	0.14(7)	-0.18(7)	0.26(7)
O0	-0.09(9)	-0.10(9)	-0.25(9)	-0.12(8)	0.15(8)	0.13(8)	-0.13(8)	0.18(8)
O1+	-0.08(8)	-0.19(8)	-0.26(9)	-0.00(7)	-0.08(8)	0.09(8)	-0.10(8)	0.03(8)
O1-	-0.32(8)	-0.27(8)	-0.29(9)	0.12(8)	-0.06(7)	-0.07(7)	-0.05(7)	-0.13(7)
O2+	-0.09(8)	0.07(9)	0.01(9)	0.12(9)	0.03(8)	-0.07(8)	-0.16(8)	0.02(8)
O2-	-0.00(8)	0.00(8)	0.27(9)	-0.01(8)	-0.13(8)	0.02(8)	0.00(8)	0.09(8)
O3+	0.33(8)	0.29(8)	0.44(8)	0.41(9)	0.40(9)	0.38(9)	0.39(9)	0.37(9)
O3-	-0.17(8)	-0.04(9)	-0.05(8)	-0.0(1)	0.06(9)	0.10(9)	0.10(9)	0.02(9)

Table A.35: Multipole populations for the carbon atoms of KM25 taken from the refinement MULT.

	C(9)	C(10)	C(11)	C(12)	C(13)	C(14)	C(15)	C(16)
M1	4.0(2)	4.1(1)	3.9(1)	3.7(1)	3.9(1)	4.1(1)	4.0(1)	4.2(1)
D1+	-0.01(9)	-0.09(8)	0.17(8)	0.01(7)	-0.10(7)	-0.03(7)	-0.04(7)	0.04(8)
D1-	0.06(9)	-0.02(8)	0.02(8)	0.15(7)	-0.18(7)	-0.01(7)	0.10(8)	0.00(8)
D0	0.09(7)	-0.06(8)	0.03(8)	0.05(7)	0.12(8)	-0.28(8)	-0.16(7)	-0.02(9)
Q0	-0.20(6)	0.06(7)	0.07(7)	-0.10(7)	0.03(7)	0.02(7)	-0.13(7)	0.02(7)
Q1+	-0.07(6)	0.12(7)	0.13(6)	-0.12(6)	-0.07(6)	-0.13(7)	0.14(6)	0.04(7)
Q1-	-0.04(6)	0.14(7)	-0.07(7)	0.02(6)	0.02(6)	0.02(7)	-0.17(7)	0.04(7)
Q2+	-0.10(7)	-0.00(7)	-0.04(7)	-0.03(6)	0.00(6)	-0.05(6)	-0.06(6)	-0.10(7)
Q2-	0.10(7)	-0.02(7)	0.09(7)	-0.22(6)	-0.09(6)	0.13(6)	-0.13(6)	0.19(7)
O0	0.06(8)	-0.16(9)	-0.02(9)	0.19(9)	0.06(9)	-0.17(9)	-0.02(9)	-0.1(1)
O1+	-0.06(7)	-0.09(9)	-0.19(8)	-0.30(8)	-0.30(8)	-0.14(8)	-0.27(8)	-0.35(9)
O1-	0.03(8)	-0.24(8)	-0.19(8)	-0.31(8)	-0.33(8)	-0.35(8)	-0.28(8)	-0.40(9)
O2+	-0.02(9)	0.00(9)	0.21(9)	0.11(8)	0.13(8)	0.05(8)	-0.12(8)	0.09(9)
O2-	-0.00(8)	0.10(9)	-0.02(8)	-0.07(8)	0.03(8)	-0.10(8)	-0.06(8)	0.00(9)
O3+	0.24(9)	0.32(8)	0.16(8)	0.42(8)	0.27(7)	0.42(8)	0.36(8)	0.14(8)
O3-	-0.0(1)	-0.07(9)	-0.06(9)	0.00(8)	-0.09(7)	-0.02(8)	-0.07(8)	-0.30(9)

Table A.36: Multipole populations for the carbon atoms of KM25 taken from the refinement **MULT**.

	Cl(1)	Cl(5)	Cl(6)	Cl(7)	Cl(8)
M1	7.2(1)	7.1(1)	7.2(1)	7.4(1)	7.5(1)
D1+	-0.03(4)	-0.13(4)	-0.05(4)	-0.04(4)	0.09(4)
D1-	0.33(4)	0.24(4)	0.11(4)	0.00(4)	0.00(4)
D0	-0.21(4)	0.24(4)	0.26(4)	-0.10(4)	0.09(4)
Q0	-0.01(4)	0.15(4)	0.17(5)	0.28(5)	0.16(4)
Q1+	-0.13(4)	0.24(4)	-0.04(4)	0.31(4)	0.30(4)
Q1-	0.05(4)	0.25(4)	0.35(4)	0.15(4)	-0.19(4)
Q2+	-0.39(4)	-0.41(4)	-0.30(4)	0.14(4)	-0.35(4)
Q2-	0.43(4)	0.33(4)	-0.40(4)	-0.02(4)	-0.28(4)
O0	0.19(4)	0.19(5)	0.27(5)	0.16(5)	-0.06(4)
O1+	-0.02(4)	-0.02(4)	0.06(4)	0.16(4)	-0.03(4)
O1-	0.03(4)	0.19(4)	0.07(5)	-0.04(5)	-0.07(4)
O2+	0.33(4)	-0.18(4)	-0.11(4)	0.01(4)	-0.03(4)
O2-	-0.06(4)	0.00(4)	-0.09(4)	-0.05(4)	-0.01(4)
O3+	-0.06(4)	0.07(4)	0.10(4)	-0.08(4)	0.01(4)
O3-	-0.19(4)	-0.03(4)	0.04(4)	-0.04(4)	0.01(4)
H0	-0.20(5)	0.25(5)	0.56(6)	0.35(6)	0.26(5)
H1+	0.17(4)	-0.25(5)	-0.14(5)	-0.05(5)	-0.12(4)
H1-	-0.12(5)	-0.01(5)	-0.18(5)	-0.21(5)	0.04(4)
H2+	-0.01(4)	0.02(5)	-0.16(5)	0.17(5)	-0.11(4)
H2-	-0.25(4)	0.16(5)	-0.11(5)	0.03(5)	-0.17(4)
H3+	0.20(4)	0.05(4)	-0.06(5)	-0.13(5)	0.07(4)
H3-	0.12(4)	-0.16(4)	0.08(5)	-0.14(4)	0.15(4)
H4+	0.11(4)	-0.03(4)	0.05(4)	0.08(4)	-0.05(4)
H4-	-0.10(4)	-0.02(4)	0.05(4)	0.04(4)	-0.00(4)

Table A.37: Multipole population parameters for the chlorine atoms from refinement MULT.

	Cl(12)	Cl(13)	Cl(14)	Cl(15)
M1	7.2(1)	7.1(1)	7.3(1)	7.1(1)
D1+	0.09(4)	0.03(4)	0.00(4)	0.13(4)
D1-	-0.04(4)	-0.02(4)	0.14(4)	0.00(4)
D0	-0.04(4)	-0.05(4)	0.18(4)	-0.22(4)
Q0	-0.02(4)	-0.28(4)	0.48(4)	0.02(4)
Q1+	0.19(4)	0.08(4)	-0.37(4)	0.28(4)
Q1-	-0.04(4)	-0.08(4)	0.08(4)	0.25(4)
Q2+	-0.37(4)	0.03(4)	-0.22(4)	-0.09(4)
Q2-	-0.38(4)	-0.24(4)	0.22(4)	0.21(4)
O0	0.10(4)	0.06(4)	0.06(4)	-0.02(4)
O1+	0.01(4)	-0.05(4)	-0.01(4)	0.11(4)
O1-	-0.07(4)	-0.07(4)	0.11(4)	0.06(4)
O2+	0.03(4)	0.07(4)	-0.06(4)	-0.03(4)
O2-	-0.02(4)	0.02(4)	-0.10(4)	-0.08(4)
O3+	0.04(4)	0.06(4)	-0.15(4)	-0.01(4)
O3-	-0.05(3)	0.04(4)	0.10(4)	0.09(4)
H0	0.34(4)	0.05(4)	0.08(5)	-0.04(5)
H1+	-0.04(4)	-0.23(4)	-0.06(4)	-0.11(4)
H1-	-0.10(4)	-0.23(4)	-0.03(5)	0.18(4)
H2+	-0.05(40	0.00(4)	-0.06(5)	0.11(4)
H2-	-0.14(4)	-0.05(4)	-0.06(5)	-0.21(4)
H3+	0.03(4)	-0.09(4)	0.00(5)	-0.09(4)
H3-	0.10(4)	0.05(4)	0.19(5)	0.15(4)
H4+	0.04(3)	-0.08(4)	-0.01(4)	0.17(4)
H4-	0.05(3)	0.00(4)	0.37(4)	0.04(4)

Table A.38: Multipole population parameters for the chlorine atoms from refinement MULT cont'd.

	H(2)	H(3)	H(10)	H(11)	H(13)	H(14)
M1	0.85(8)	0.71(9)	0.89(9)	0.86(8)	0.77(8)	0.78(8)
D1+	0.07(5)	0.23(5)	0.28(6)	0.21(5)	0.19(5)	0.16(5)
D1-	0.09(5)	-0.07(6)	0.04(6)	0.03(5)	-0.00(5)	0.13(5)
D0	-0.02(5)	0.12(6)	-0.05(6)	0.07(5)	-0.06(5)	-0.00(6)
	H(15)	H(16A)	H(16B)			
M1	0.76(8)	0.68(9)	0.78(9)			
D1+	0.20(5)	0.12(6)	0.15(6)			
D1-	0.02(5)	0.05(6)	-0.06(6)			
D0	0.08(5)	0.07(6)	-0.02(6)			

Table A.39: Hydrogen atom multipole population pparameters from the refinement MULT

Atom	x	y	z	U_{eq}
Nb	0.77545(4)	0.02670(4)	0.35071(3)	0.0368(2)
C(1)	0.8037(5)	0.0514(4)	0.2401(4)	0.043(3)
C(2)	0.8533(5)	-0.0086(4)	0.2591(4)	0.044(3)
C(3)	0.9110(5)	-0.0390(5)	0.2108(4)	0.059(3)
C(4)	0.9132(5)	-0.0053(6)	0.1420(5)	0.071(4)
C(5)	0.8612(6)	0.0543(6)	0.1229(4)	0.071(4)
C(6)	0.8044(6)	0.0849(5)	0.1709(4)	0.064(3)
N(1)	0.8304(3)	0.1034(3)	0.3987(3)	0.036(2)
C(7)	0.8726(4)	0.1632(4)	0.4362(3)	0.034(2)
C(8)	0.8515(4)	0.1823(4)	0.5089(4)	0.035(2)
C(9)	0.8956(5)	0.2433(4)	0.5417(4)	0.048(3)
C(10)	0.9573(5)	0.2849(4)	0.5068(4)	0.056(3)
C(11)	0.9790(5)	0.2639(4)	0.4368(4)	0.046(3)
C(12)	0.9380(4)	0.2037(4)	0.3999(4)	0.038(2)
C(13)	0.9622(5)	0.1822(4)	0.3231(4)	0.047(3)
C(14)	0.9170(6)	0.2342(5)	0.2700(4)	0.080(4)
C(15)	1.0550(5)	0.1894(5)	0.3095(4)	0.081(4)
C(16)	0.7828(5)	0.1385(4)	0.5472(4)	0.046(3)
C(17)	0.7975(5)	0.1263(6)	0.6271(4)	0.080(4)
C(18)	0.7018(5)	0.1799(5)	0.5367(5)	0.081(4)
C(19)	0.6493(5)	0.0106(6)	0.4219(5)	0.068(4)
C(20)	0.6311(5)	0.0591(6)	0.3640(5)	0.071(4)
C(21)	0.6339(5)	0.0139(7)	0.3008(5)	0.071(4)
C(22)	0.6561(6)	-0.0610(6)	0.3191(6)	0.075(4)
C(23)	0.6654(6)	-0.0644(6)	0.3931(6)	0.076(4)
P	0.8672(2)	-0.0777(1)	0.4068(1)	0.0576(9)
C(24)	0.8623(6)	-0.1759(5)	0.3674(4)	0.093(5)
C(25)	0.9742(5)	-0.0508(5)	0.4016(5)	0.085(4)
C(26)	0.8533(6)	-0.0966(5)	0.5033(4)	0.085(4)

Table A.40: Atomic coordinates and U_{eq} (Å^2) for the non-hydrogen atoms of **1** [Nb(η^2-C_6H_4)Cp(N-2,6-^{i}Pr$_2$C$_6$H$_4$)PMe$_3$].

A-B	d_{AB}	A-B	d_{AB}	A-B	d_{AB}
Nb-C(1)	2.139(7)	Nb-C(2)	2.194(7)	Nb-N(1)	1.805(5)
Nb-C(19)	2.440(8)	Nb-C(20)	2.406(8)	Nb-C(21)	2.474(9)
Nb-C(22)	2.502(10)	Nb-C(23)	2.480(10)	Nb-P	2.528(2)
C(1)-C(2)	1.340(10)	C(1)-C(6)	1.401(10)	C(2)-C(3)	1.390(10)
C(3)-C(4)	1.396(12)	C(4)-C(5)	1.360(13)	C(5)-C(6)	1.377(12)
N(1)-C(7)	1.405(8)	C(7)-C(8)	1.425(9)	C(7)-C(12)	1.425(10)
C(8)-C(9)	1.393(10)	C(8)-C(16)	1.511(10)	C(9)-C(10)	1.380(11)
C(10)-C(11)	1.387(11)	C(11)-C(12)	1.395(10)	C(12)-C(13)	1.520(10)
C(13)-C(14)	1.507(11)	C(13)-C(15)	1.524(11)	C(16)-C(17)	1.512(10)
C(16)-C(18)	1.496(11)	C(19)-C(20)	1.382(13)	C(19)-C(23)	1.400(14)
C(20)-C(21)	1.399(14)	C(21)-C(22)	1.359(15)	C(22)-C(23)	1.379(15)
P-C(24)	1.816(8)	P-C(25)	1.789(8)	P-C(26)	1.829(8)

Table A.41: Bond lengths (Å) for **1** [Nb(η^2-C_6H_4)Cp(N-2,6-$^i Pr_2C_6H_4$)PMe_3].

A-B-C	∠A-B-C	A-B-C	∠A-B-C	A-B-C	∠A-B-C
C(1)-Nb-C(2)	36.0(3)	C(1)-Nb-N(1)	103.0(2)	C(2)-Nb-N(1)	107.1(3)
C(1)-Nb-C(19)	135.8(3)	C(2)-Nb-C(19)	149.9(3)	N(1)-Nb-C(19)	103.0(3)
C(1)-Nb-C(20)	105.0(3)	C(2)-Nb-C(20)	134.1(3)	N(1)-Nb-C(20)	105.2(3)
C(19)-Nb-C(20)	33.1(3)	C(1)-Nb-C(21)	81.7(3)	C(2)-Nb-C(21)	102.5(3)
N(1)-Nb-C(21)	134.5(3)	C(19)-Nb-C(21)	54.7(3)	C(20)-Nb-C(21)	33.3(3)
C(1)-Nb-C(22)	93.2(3)	C(2)-Nb-C(22)	95.7(3)	N(1)-Nb-C(22)	156.9(3)
C(19)-Nb-C(22)	54.4(3)	C(20)-Nb-C(22)	54.1(3)	C(21)-Nb-C(22)	31.7(3)
C(1)-Nb-C(23)	125.3(3)	C(2)-Nb-C(23)	119.1(3)	N(1)-Nb-C(23)	130.0(3)
C(19)-Nb-C(23)	33.1(3)	C(20)-Nb-C(23)	54.3(3)	C(21)-Nb-C(23)	53.3(3)
C(22)-Nb-C(23)	32.1(3)	C(1)-Nb-P	113.9(2)	C(2)-Nb-P	78.0(2)
N(1)-Nb-P	90.7(2)	C(19)-Nb-P	100.9(2)	C(20)-Nb-P	133.2(2)
C(21)-Nb-P	129.3(3)	C(22)-Nb-P	97.6(2)	C(23)-Nb-P	81.7(2)
Nb-C(1)-C(2)	74.2(4)	Nb-C(1)-C(6)	163.0(6)	C(2)-C(1)-C(6)	122.7(7)
Nb-C(2)-C(1)	69.7(4)	Nb-C(2)-C(3)	169.1(6)	C(1)-C(2)-C(3)	120.8(7)
C(2)-C(3)-C(4)	116.9(7)	C(3)-C(4)-C(5)	121.6(8)	C(4)-C(5)-C(6)	121.5(8)
C(1)-C(6)-C(5)	116.4(8)	Nb-N(1)-C(7)	179.5(6)	N(1)-C(7)-C(8)	121.0(6)
N(1)-C(7)-C(12)	118.2(6)	C(8)-C(7)-C(12)	120.9(6)	C(7)-C(8)-C(9)	117.2(6)
C(7)-C(8)-C(16)	120.5(6)	C(9)-C(8)-C(16)	122.2(6)	C(8)-C(9)-C(10)	122.8(7)
C(9)-C(10)-C(11)	119.3(7)	C(10)-C(11)-C(12)	121.6(7)	C(7)-C(12)-C(11)	118.1(6)
C(7)-C(12)-C(13)	121.1(6)	C(11)-C(12)-C(13)	120.7(6)	C(12)-C(13)-C(14)	110.3(6)
C(12)-C(13)-C(15)	112.9(6)	C(14)-C(13)-C(15)	108.8(6)	C(8)-C(16)-C(17)	114.3(6)
C(8)-C(16)-C(18)	110.6(6)	C(17)-C(16)-C(18)	109.1(6)	Nb-C(19)-C(20)	72.1(5)
Nb-C(19)-C(23)	75.1(5)	C(20)-C(19)-C(23)	106.5(8)	Nb-C(20)-C(19)	74.8(5)
Nb-C(20)-C(21)	76.0(5)	C(19)-C(20)-C(21)	108.4(9)	Nb-C(21)-C(20)	70.7(5)
Nb-C(21)-C(22)	75.3(5)	C(20)-C(21)-C(22)	108.1(9)	Nb-C(22)-C(21)	73.0(6)
Nb-C(22)-C(23)	73.1(6)	C(21)-C(22)-C(23)	108.4(9)	Nb-C(23)-C(19)	71.9(5)
Nb-C(23)-C(22)	74.8(6)	C(19)-C(23)-C(22)	108.6(9)	Nb-P-C(24)	116.7(3)
Nb-P-C(25)	111.5(3)	C(24)-P-C(25)	104.7(4)	Nb-P-C(26)	116.8(3)
C(24)-P-C(26)	103.1(4)	C(25)-P-C(26)	102.4(4)		

Table A.42: Bond angles (°) for **1** [Nb(η^2-C_6H_4)Cp(N-2,6-$^i Pr_2C_6H_4$)PMe_3].

	U_{11}	U_{22}	U_{33}	U_{12}	U_{13}	U_{23}
Nb	0.0434(3)	0.0354(3)	0.0315(3)	-0.0051(4)	-0.0045(4)	0.0017(4)
C(1)	0.061(5)	0.041(4)	0.027(4)	-0.022(4)	0.003(3)	0.000(3)
C(2)	0.048(5)	0.046(5)	0.038(4)	-0.008(4)	-0.010(4)	-0.001(4)
C(3)	0.054(5)	0.065(6)	0.059(5)	-0.008(5)	0.003(4)	-0.009(5)
C(4)	0.074(6)	0.093(8)	0.047(5)	-0.030(5)	0.021(5)	-0.021(5)
C(5)	0.099(8)	0.082(7)	0.033(5)	-0.034(6)	0.010(5)	-0.002(5)
C(6)	0.096(8)	0.055(5)	0.041(5)	-0.019(5)	-0.010(5)	0.008(4)
N(1)	0.040(4)	0.035(3)	0.033(3)	-0.004(3)	-0.004(3)	0.006(3)
C(7)	0.039(4)	0.034(4)	0.030(4)	0.008(3)	-0.003(3)	0.003(3)
C(8)	0.039(4)	0.034(4)	0.033(4)	0.002(3)	-0.002(3)	-0.005(3)
C(9)	0.059(5)	0.044(5)	0.040(4)	-0.002(4)	-0.001(4)	-0.007(4)
C(10)	0.056(6)	0.048(5)	0.064(6)	-0.013(4)	-0.005(5)	-0.013(5)
C(11)	0.047(5)	0.047(5)	0.046(5)	-0.005(4)	0.004(4)	0.001(4)
C(12)	0.046(5)	0.034(4)	0.035(4)	-0.003(4)	-0.008(4)	-0.004(4)
C(13)	0.059(5)	0.044(5)	0.038(4)	-0.005(4)	0.003(4)	0.003(4)
C(14)	0.120(9)	0.073(7)	0.047(5)	0.014(6)	-0.006(6)	-0.001(5)
C(15)	0.082(7)	0.106(8)	0.055(6)	0.007(6)	0.020(5)	-0.012(6)
C(16)	0.043(5)	0.049(4)	0.045(4)	0.004(4)	-0.002(4)	-0.003(4)
C(17)	0.082(8)	0.115(8)	0.045(5)	-0.034(6)	0.004(5)	0.007(5)
C(18)	0.061(7)	0.069(6)	0.112(8)	0.008(5)	0.021(6)	0.012(6)
C(19)	0.058(6)	0.103(8)	0.044(5)	-0.026(6)	0.001(5)	-0.007(6)
C(20)	0.052(6)	0.081(7)	0.080(7)	0.005(5)	0.004(5)	-0.012(6)
C(21)	0.046(6)	0.109(9)	0.058(6)	-0.015(6)	-0.022(5)	0.004(7)
C(22)	0.066(7)	0.084(8)	0.076(8)	-0.036(6)	0.006(6)	-0.022(6)
C(23)	0.076(8)	0.075(7)	0.078(8)	-0.029(6)	0.009(7)	0.018(7)
P	0.080(2)	0.045(1)	0.048(1)	0.014(1)	-0.010(1)	0.004(1)
C(24)	0.168(10)	0.050(6)	0.061(7)	0.025(6)	-0.009(7)	-0.002(5)
C(25)	0.074(7)	0.099(8)	0.083(7)	0.028(6)	-0.021(6)	0.001(6)
C(26)	0.136(9)	0.072(7)	0.045(5)	0.030(6)	-0.010(6)	0.021(5)

Table A.43: Anisotropic atomic displacement parameters ($Å^2$) for the non-hydrogen atoms of **1** [$Nb(\eta^2\text{-}C_6H_4)Cp(N\text{-}2,6\text{-}^iPr_2C_6H_4)PMe_3$].

Atom	x	y	z	Atom	x	y	z
H(3A)	0.9475	-0.0815	0.2238	H(4A)	0.9528	-0.0237	0.1071
H(5A)	0.8637	0.0746	0.0745	H(6A)	0.7670	0.1268	0.1582
H(9A)	0.8824	0.2565	0.5908	H(10A)	0.9843	0.3284	0.5303
H(11A)	1.0240	0.2910	0.4136	H(13A)	0.9465	0.1283	0.3144
H(14A)	0.8583	0.2297	0.2774	H(14B)	0.9337	0.2881	0.2772
H(14C)	0.9304	0.2182	0.2216	H(15A)	1.0849	0.1564	0.3427
H(15B)	1.0676	0.1736	0.2609	H(15C)	1.0710	0.2435	0.3164
H(16A)	0.7785	0.0870	0.5257	H(17A)	0.8493	0.0994	0.6340
H(17B)	0.7997	0.1771	0.6501	H(17C)	0.7536	0.0956	0.6480
H(18A)	0.6921	0.1864	0.4859	H(18B)	0.6577	0.1493	0.5575
H(18C)	0.7038	0.2308	0.5596	H(19A)	0.6496	0.0244	0.4722
H(20A)	0.6183	0.1144	0.3677	H(21A)	0.6234	0.0335	0.2530
H(22A)	0.6622	-0.1037	0.2853	H(23A)	0.6822	-0.1107	0.4194
H(24A)	0.8994	-0.2103	0.3928	H(24B)	0.8068	-0.1959	0.3710
H(24C)	0.8782	-0.1733	0.3175	H(25A)	1.0070	-0.0918	0.4234
H(25B)	0.9900	-0.0448	0.3519	H(25C)	0.9833	-0.0020	0.4268
H(26B)	0.8914	-0.1370	0.5181	H(26C)	0.8631	-0.0495	0.5309
H(26D)	0.7976	-0.1144	0.5114				

Table A.44: Atomic coordinates for the hydrogen atoms of **1** [Nb(η^2-C_6H_4)Cp(N-2,6-$^i Pr_2C_6H_4$)PMe_3].

Atom	x	y	z	U_{eq}
Mo(1)	0.13341(3)	0.30951(3)	-0.19126(3)	0.0420(1)
P(1)	0.2832(1)	0.5087(1)	-0.2043(1)	0.0545(3)
N(1)	0.1597(4)	0.2208(4)	-0.0391(3)	0.054(1)
N(2)	0.2036(4)	0.2419(4)	-0.3186(3)	0.056(1)
C(1)	-0.0397(5)	0.4838(5)	-0.2186(5)	0.064(2)
C(2)	-0.0983(4)	0.3518(5)	-0.2190(4)	0.057(1)
C(3)	-0.1540(6)	0.3233(7)	-0.3372(5)	0.079(2)
C(4)	0.2151(5)	0.1259(4)	0.0684(4)	0.055(1)
C(5)	0.2789(7)	-0.0115(6)	0.0337(6)	0.083(2)
C(6)	0.3315(7)	0.1962(7)	0.1217(6)	0.086(2)
C(7)	0.0942(7)	0.0970(7)	0.1618(5)	0.086(2)
C(8)	0.2784(5)	0.1663(4)	-0.4042(3)	0.065(2)
C(9)	0.3430(8)	0.2654(8)	-0.5055(7)	0.132(3)
C(10)	0.1745(8)	0.0845(8)	-0.4541(7)	0.132(3)
C(11)	0.3937(8)	0.0688(8)	-0.3412(7)	0.149(4)
C(12)	0.2720(9)	0.6383(7)	-0.3427(5)	0.097(3)
C(13)	0.4750(6)	0.4625(7)	-0.1957(7)	0.089(3)
C(14)	0.2549(7)	0.6100(6)	-0.0852(5)	0.076(2)

Table A.45: Atomic coordinates and U_{eq} (Å^2) for the non-hydrogen atoms of **2** [$Mo(NBu^t)_2(PMe_3)(CH_2{=}CHCH_3)$].

A-B	d_{AB}	A-B	d_{AB}	A-B	d_{AB}
Mo(1)-P(1)	2.446(1)	Mo(1)-N(1)	1.771(3)	Mo(1)-N(2)	1.772(4)
Mo(1)-C(1)	2.238(4)	Mo(1)-C(2)	2.188(4)	P(1)-C(12)	1.800(6)
P(1)-C(13)	1.811(6)	P(1)-C(14)	1.808(6)	N(1)-C(4)	1.452(5)
N(2)-C(8)	1.450(6)	C(1)-C(2)	1.431(7)	C(2)-C(3)	1.517(8)
C(4)-C(5)	1.537(7)	C(4)-C(6)	1.517(9)	C(4)-C(7)	1.517(7)
C(8)-C(9)	1.482(8)	C(8)-C(10)	1.482(9)	C(8)-C(11)	1.482(8)

Table A.46: Bond lengths (Å) for **2** [$Mo(NBu^t)_2(PMe_3)(CH_2{=}CHCH_3)$].

A-B-C	∠A-B-C	A-B-C	∠A-B-C	A-B-C	∠A-B-C
P(1)-Mo(1)-N(1)	101.9(1)	P(1)-Mo(1)-N(2)	99.4(1)	N(1)-Mo(1)-N(2)	123.0(2)
P(1)-Mo(1)-C(1)	81.0(1)	N(1)-Mo(1)-C(1)	115.9(2)	N(2)-Mo(1)-C(1)	119.3(2)
P(1)-Mo(1)-C(2)	118.5(1)	N(1)-Mo(1)-C(2)	108.1(2)	N(2)-Mo(1)-C(2)	106.5(2)
C(1)-Mo(1)-C(2)	37.7(2)	Mo(1)-P(1)-C(12)	116.3(3)	Mo(1)-P(1)-C(13)	114.7(2)
C(12)-P(1)-C(13)	101.8(3)	Mo(1)-P(1)-C(14)	116.0(2)	C(12)-P(1)-C(14)	104.1(3)
C(13)-P(1)-C(14)	102.0(3)	Mo(1)-N(1)-C(4)	162.9(3)	Mo(1)-N(2)-C(8)	168.2(3)
Mo(1)-C(1)-C(2)	69.3(2)	Mo(1)-C(2)-C(1)	73.0(3)	Mo(1)-C(2)-C(3)	115.9(3)
C(1)-C(2)-C(3)	119.0(4)	N(1)-C(4)-C(5)	109.8(4)	N(1)-C(4)-C(6)	108.7(4)
C(5)-C(4)-C(6)	109.6(4)	N(1)-C(4)-C(7)	109.2(4)	C(5)-C(4)-C(7)	110.6(4)
C(6)-C(4)-C(7)	108.8(4)	N(2)-C(8)-C(9)	110.6(4)	N(2)-C(8)-C(10)	109.1(4)
C(9)-C(8)-C(10)	109.1(5)	N(2)-C(8)-C(11)	109.7(4)	C(9)-C(8)-C(11)	109.2(5)
C(10)-C(8)-C(11)	109.1(5)				

Table A.47: Bond angles (°) for **2** [$Mo(NBu^t)_2(PMe_3)(CH_2{=}CHCH_3)$].

Atom	U_{11}	U_{22}	U_{33}	U_{12}	U_{13}	U_{23}
Mo(1)	0.0434(2)	0.0422(2)	0.0403(2)	0.0001(1)	-0.0028(1)	-0.0084(1)
P(1)	0.0587(6)	0.0576(6)	0.0494(5)	-0.0128(5)	0.0007(4)	-0.0132(4)
N(1)	0.056(2)	0.054(2)	0.050(2)	-0.008(1)	-0.012(1)	-0.003(1)
N(2)	0.057(2)	0.056(2)	0.058(2)	-0.001(1)	-0.001(2)	-0.019(2)
C(1)	0.055(2)	0.057(2)	0.079(3)	0.008(2)	-0.007(2)	-0.012(2)
C(2)	0.046(2)	0.063(2)	0.059(2)	0.003(2)	-0.003(2)	-0.008(2)
C(3)	0.060(3)	0.110(4)	0.066(3)	0.001(3)	-0.020(2)	-0.016(3)
C(4)	0.061(2)	0.052(2)	0.050(2)	0.000(2)	-0.011(2)	-0.002(2)
C(5)	0.102(4)	0.061(3)	0.081(4)	0.014(3)	-0.017(3)	-0.009(3)
C(6)	0.093(4)	0.084(3)	0.082(4)	-0.012(3)	-0.041(3)	-0.005(3)
C(7)	0.092(4)	0.090(4)	0.065(3)	-0.003(3)	0.002(3)	0.008(3)
C(8)	0.076(3)	0.063(3)	0.058(2)	0.009(2)	0.004(2)	-0.021(2)
C(12)	0.127(6)	0.090(4)	0.071(3)	-0.050(4)	-0.001(3)	0.009(3)
C(13)	0.059(3)	0.106(4)	0.111(5)	-0.020(3)	-0.001(3)	-0.032(4)
C(14)	0.085(4)	0.081(3)	0.073(3)	-0.018(3)	-0.001(3)	-0.036(3)

Table A.48: Anisotropic atomic displacement parameters ($Å^2$) of the non-hydrogen atoms of **2** [$Mo(NBu^t)_2(PMe_3)(CH_2{=}CHCH_3)$].

Atom	x	y	z	Atom	x	y	z
H(1A)	-0.0363	0.5519	-0.2930	H(1B)	-0.0031	0.5043	-0.1452
H(2A)	-0.1021	0.2830	-0.1451	H(3A)	-0.2562	0.3448	-0.3403
H(3B)	-0.1081	0.3809	-0.4048	H(3C)	-0.1333	0.2261	-0.3409
H(5A)	0.3557	0.0077	-0.0250	H(5B)	0.3151	-0.0739	0.1051
H(5C)	0.2044	-0.0544	-0.0005	H(6A)	0.4088	0.2133	0.0631
H(6B)	0.2919	0.2839	0.1397	H(6C)	0.3675	0.1371	0.1948
H(7A)	0.0205	0.0514	0.1294	H(7B)	0.1303	0.0380	0.2349
H(7C)	0.0547	0.1848	0.1798	H(9A)	0.4109	0.3192	-0.4746
H(9B)	0.3913	0.2131	-0.5611	H(9C)	0.2681	0.3277	-0.5471
H(10A)	0.1330	0.0206	-0.3881	H(10B)	0.0998	0.1470	-0.4958
H(10C)	0.2230	0.0324	-0.5098	H(11A)	0.4617	0.1219	-0.3098
H(11B)	0.3528	0.0041	-0.2753	H(11C)	0.4417	0.0176	-0.3977
H(12A)	0.3345	0.7117	-0.3389	H(12B)	0.2999	0.5952	-0.4109
H(12C)	0.1745	0.6773	-0.3522	H(13A)	0.5270	0.5454	-0.2014
H(13B)	0.4956	0.4001	-0.1198	H(13C)	0.5037	0.4163	-0.2618
H(14A)	0.3186	0.6851	-0.0989	H(14B)	0.1569	0.6484	-0.0866
H(14C)	0.2738	0.5511	-0.0074				

Table A.49: Atomic coordinates for the hydrogen atoms of **2** $[Mo(NBu^t)_2(PMe_3)(CH_2{=}CHCH_3)]$.

Atom	x	y	z	U_{eq}
Mo	0.13076(5)	0.60111(5)	0.13369(1)	0.0225(2)
C(1)	0.0965(6)	0.4926(6)	0.0875(3)	0.022(3)
C(2)	0.1763(6)	0.5218(6)	0.0670(3)	0.026(3)
C(101)	0.0271(6)	0.4233(5)	0.0818(3)	0.019(3)
C(102)	-0.0306(6)	0.3961(6)	0.1249(3)	0.026(3)
C(103)	-0.0942(7)	0.3289(6)	0.1197(3)	0.029(3)
C(104)	-0.1035(6)	0.2856(6)	0.0719(4)	0.031(3)
C(105)	-0.0501(6)	0.3109(6)	0.0277(4)	0.031(3)
C(106)	0.0136(6)	0.3781(5)	0.0324(3)	0.025(3)
C(201)	0.2443(6)	0.4988(6)	0.0243(3)	0.021(3)
C(202)	0.3320(6)	0.4578(6)	0.0358(4)	0.029(3)
C(203)	0.3965(6)	0.4384(6)	-0.0051(4)	0.028(3)
C(204)	0.3745(7)	0.4559(6)	-0.0583(3)	0.030(3)
C(205)	0.2870(6)	0.4946(7)	-0.0700(3)	0.034(3)
C(206)	0.2216(7)	0.5146(7)	-0.0303(3)	0.034(3)
N(1)	0.0378(5)	0.6773(5)	0.1256(3)	0.025(2)
C(3)	-0.0416(7)	0.7355(6)	0.1361(4)	0.032(3)
C(4)	-0.1294(7)	0.6995(10)	0.1091(4)	0.073(5)
C(5)	-0.0598(8)	0.7411(7)	0.1969(4)	0.048(4)
C(6)	-0.0182(10)	0.8252(8)	0.1143(6)	0.092(7)
N(2)	0.1579(5)	0.5669(5)	0.1992(3)	0.032(3)
C(7)	0.1702(8)	0.5482(7)	0.2557(3)	0.038(4)
C(8)	0.0871(10)	0.4919(8)	0.2728(4)	0.087(6)
C(9)	0.1697(8)	0.6326(7)	0.2872(4)	0.051(4)
C(10)	0.2657(10)	0.5033(10)	0.2636(5)	0.094(7)
P	0.2711(2)	0.6929(2)	0.1138(1)	0.0280(8)
C(11)	0.2760(7)	0.7904(7)	0.1542(4)	0.043(4)
C(12)	0.2769(7)	0.7354(7)	0.0457(3)	0.040(4)
C(13)	0.3865(6)	0.6443(7)	0.1242(4)	0.047(4)

Table A.50: Atomic coordinates and U_{eq} (Å^2) for the non-hydrogen atoms of **3** [Mo(NBu^t)$_2$(PMe$_3$)(PhC≡CPh)].

A-B	d_{AB}	A-B	d_{AB}	A-B	d_{AB}
Mo-C(1)	2.081(8)	Mo-C(2)	2.158(9)	Mo-N(1)	1.759(7)
Mo-N(2)	1.761(7)	Mo-P	2.465(3)	C(1)-C(2)	1.306(12)
C(1)-C(101)	1.446(12)	C(2)-C(201)	1.473(11)	C(101)-C(102)	1.411(11)
C(101)-C(106)	1.428(11)	C(102)-C(103)	1.367(13)	C(103)-C(104)	1.373(13)
C(104)-C(105)	1.388(13)	C(105)-C(106)	1.367(12)	C(201)-C(202)	1.408(12)
C(201)-C(206)	1.421(11)	C(202)-C(203)	1.395(13)	C(203)-C(204)	1.392(12)
C(204)-C(205)	1.390(13)	C(205)-C(206)	1.384(12)	N(1)-C(3)	1.448(12)
C(3)-C(4)	1.506(14)	C(3)-C(5)	1.543(13)	C(3)-C(6)	1.514(15)
N(2)-C(7)	1.450(11)	C(7)-C(8)	1.509(17)	C(7)-C(9)	1.515(14)
C(7)-C(10)	1.515(18)	P-C(11)	1.806(11)	P-C(12)	1.824(9)
P-C(13)	1.795(10)				

Table A.51: Bond lengths (Å) for **3** [Mo(NBu^t)$_2$(PMe$_3$)(PhC≡CPh)].

A-B-C	∠A-B-C	A-B-C	∠A-B-C	A-B-C	∠A-B-C
C(1)-Mo-C(2)	35.8(3)	C(1)-Mo-N(1)	107.3(3)	C(2)-Mo-N(1)	120.3(3)
C(1)-Mo-N(2)	109.1(3)	C(2)-Mo-N(2)	119.1(3)	N(1)-Mo-N(2)	117.6(3)
C(1)-Mo-P	121.8(2)	C(2)-Mo-P	86.0(2)	N(1)-Mo-P	100.7(2)
N(2)-Mo-P	100.7(3)	Mo-C(1)-C(2)	75.3(6)	Mo-C(1)-C(101)	142.8(6)
C(2)-C(1)-C(101)	141.8(8)	Mo-C(2)-C(1)	68.9(5)	Mo-C(2)-C(201)	152.3(7)
C(1)-C(2)-C(201)	138.8(9)	C(1)-C(101)-C(102)	121.7(7)	C(1)-C(101)-C(106)	122.0(7)
C(102)-C(101)-C(106)	116.2(7)	C(101)-C(102)-C(103)	121.5(7)	C(102)-C(103)-C(104)	120.6(8)
C(103)-C(104)-C(105)	120.4(8)	C(104)-C(105)-C(106)	119.6(8)	C(101)-C(106)-C(105)	121.7(8)
C(2)-C(201)-C(202)	121.4(7)	C(2)-C(201)-C(206)	120.7(8)	C(202)-C(201)-C(206)	117.8(8)
C(201)-C(202)-C(203)	120.6(8)	C(202)-C(203)-C(204)	121.1(8)	C(203)-C(204)-C(205)	118.5(8)
C(204)-C(205)-C(206)	121.8(8)	C(201)-C(206)-C(205)	120.2(8)	Mo-N(1)-C(3)	162.8(6)
N(1)-C(3)-C(4)	108.6(8)	N(1)-C(3)-C(5)	109.7(8)	C(4)-C(3)-C(5)	109.1(8)
N(1)-C(3)-C(6)	109.2(8)	C(4)-C(3)-C(6)	110.4(9)	C(5)-C(3)-C(6)	109.8(9)
Mo-N(2)-C(7)	171.6(7)	N(2)-C(7)-C(8)	107.4(8)	N(2)-C(7)-C(9)	109.7(8)
C(8)-C(7)-C(9)	109.7(9)	N(2)-C(7)-C(10)	108.7(8)	C(8)-C(7)-C(10)	112.4(10)
C(9)-C(7)-C(10)	108.9(9)	Mo-P-C(11)	112.9(3)	Mo-P-C(12)	115.3(3)
C(11)-P-C(12)	103.0(5)	Mo-P-C(13)	116.7(4)	C(11)-P-C(13)	103.2(5)
C(12)-P-C(13)	104.1(5)				

Table A.52: Bond angles (°) for **3** [Mo(NBu^t)$_2$(PMe$_3$)(PhC≡CPh)].

Atom	U_{11}	U_{22}	U_{33}	U_{12}	U_{13}	U_{23}
Mo	0.0200(3)	0.0311(4)	0.0163(3)	-0.0029(4)	0.0025(4)	-0.0016(4)
C(1)	0.024(5)	0.029(5)	0.013(4)	0.009(4)	-0.001(3)	0.005(4)
C(2)	0.021(5)	0.033(6)	0.023(4)	-0.001(4)	0.000(4)	-0.010(4)
C(101)	0.014(4)	0.020(5)	0.022(4)	0.010(4)	0.001(3)	0.005(4)
C(102)	0.024(4)	0.035(5)	0.018(4)	-0.004(5)	-0.002(3)	0.012(5)
C(103)	0.034(5)	0.029(6)	0.025(5)	-0.007(5)	-0.001(4)	0.004(4)
C(104)	0.021(5)	0.020(5)	0.053(6)	-0.007(4)	-0.003(4)	0.003(5)
C(105)	0.015(4)	0.042(7)	0.037(5)	0.006(5)	-0.001(4)	-0.004(5)
C(106)	0.018(4)	0.028(6)	0.030(5)	0.012(4)	-0.002(4)	-0.003(4)
C(201)	0.018(4)	0.027(5)	0.018(4)	0.001(4)	0.005(4)	0.006(4)
C(202)	0.021(5)	0.031(6)	0.035(5)	0.012(4)	0.006(4)	0.000(5)
C(203)	0.021(5)	0.024(5)	0.040(5)	0.008(4)	0.000(4)	-0.002(5)
C(204)	0.025(5)	0.039(6)	0.027(5)	0.002(5)	0.014(4)	-0.006(4)
C(205)	0.025(5)	0.060(7)	0.017(4)	0.007(5)	0.000(4)	-0.002(5)
C(206)	0.032(6)	0.048(7)	0.020(5)	0.001(5)	0.002(4)	-0.004(5)
N(1)	0.029(4)	0.027(4)	0.020(4)	-0.006(4)	0.006(3)	-0.006(4)
C(3)	0.037(5)	0.028(5)	0.031(4)	0.006(5)	0.009(5)	-0.016(5)
C(4)	0.033(6)	0.133(12)	0.054(7)	0.030(9)	-0.012(6)	-0.041(8)
C(5)	0.049(7)	0.061(8)	0.034(6)	0.002(6)	0.011(5)	-0.002(6)
C(6)	0.116(13)	0.068(10)	0.093(11)	0.045(9)	0.063(10)	0.022(9)
N(2)	0.035(5)	0.042(5)	0.020(4)	-0.021(4)	-0.001(3)	-0.002(4)
C(7)	0.060(7)	0.034(7)	0.018(5)	0.006(6)	-0.011(5)	0.006(4)
C(8)	0.144(14)	0.096(11)	0.020(5)	-0.069(11)	-0.018(7)	0.029(7)
C(9)	0.072(8)	0.057(8)	0.022(5)	-0.002(6)	-0.013(5)	-0.006(5)
C(10)	0.105(12)	0.140(15)	0.037(7)	0.056(12)	-0.034(7)	-0.011(8)
P	0.021(1)	0.037(2)	0.026(1)	-0.007(1)	0.000(1)	-0.002(1)
C(11)	0.048(6)	0.047(7)	0.034(5)	-0.021(6)	0.005(5)	-0.008(5)
C(12)	0.039(6)	0.054(8)	0.028(5)	-0.021(6)	-0.004(5)	0.005(5)
C(13)	0.021(5)	0.049(6)	0.072(8)	-0.001(5)	-0.002(5)	0.009(6)

Table A.53: Anisotropic atomic displacement parameters ($Å^2$) for the non-hydrogen atoms of **3** $[Mo(NBu^t)_2(PMe_3)(PhC{\equiv}CPh)]$.

Atom	x	y	z	Atom	x	y	z
H(102)	-0.0251	0.4263	0.1585	H(103)	-0.1322	0.3119	0.1499
H(104)	-0.1479	0.2380	0.0692	H(105)	-0.0577	0.2811	-0.0058
H(106)	0.0509	0.3957	0.0020	H(202)	0.3467	0.4429	0.0722
H(203)	0.4565	0.4113	0.0036	H(204)	0.4187	0.4413	-0.0863
H(205)	0.2718	0.5088	-0.1064	H(206)	0.1613	0.5411	-0.0390
H(4A)	-0.1184	0.6962	0.0712	H(4B)	-0.1427	0.6422	0.1227
H(4C)	-0.1829	0.7370	0.1160	H(5A)	-0.0038	0.7641	0.2141
H(5B)	-0.1133	0.7787	0.2038	H(5C)	-0.0731	0.6839	0.2106
H(6A)	-0.0071	0.8229	0.0765	H(6B)	-0.0701	0.8643	0.1217
H(6C)	0.0385	0.8455	0.1321	H(8A)	0.0271	0.5216	0.2691
H(8B)	0.0880	0.4417	0.2498	H(8C)	0.0952	0.4736	0.3093
H(9A)	0.2226	0.6674	0.2754	H(9B)	0.1109	0.6625	0.2797
H(9C)	0.1748	0.6227	0.3251	H(10A)	0.3183	0.5405	0.2541
H(10B)	0.2724	0.4850	0.3001	H(10C)	0.2652	0.4531	0.2407
H(11A)	0.3314	0.8241	0.1450	H(11B)	0.2194	0.8245	0.1482
H(11C)	0.2793	0.7741	0.1913	H(12A)	0.3332	0.7706	0.0416
H(12B)	0.2793	0.6873	0.0211	H(12C)	0.2212	0.7701	0.0385
H(13A)	0.4355	0.6857	0.1154	H(13B)	0.3933	0.6269	0.1610
H(13C)	0.3923	0.5941	0.1015				

Table A.54: Atomic coordinates for the hydrogen atoms of **3** $[Mo(NBu^t)_2(PMe_3)(PhC{\equiv}CPh)]$.

Atom	x	y	z	U_{eq}
Mo(1)	0.5000	0.30455(7)	0.2500	0.0516(8)
P(11)	0.4333(2)	0.3664(2)	0.1901(3)	0.067(2)
C(11)	0.4536(6)	0.4051(6)	0.1292(7)	0.093(8)
C(12)	0.3699(6)	0.3372(7)	0.1387(9)	0.117(9)
C(13)	0.4072(7)	0.4156(6)	0.2334(8)	0.104(9)
N(11)	0.4808(4)	0.2793(4)	0.3188(6)	0.052(4)
C(111)	0.4707(5)	0.2528(5)	0.3716(7)	0.052(3)
C(112)	0.4995(5)	0.2061(5)	0.3946(6)	0.053(3)
C(113)	0.4885(6)	0.1803(6)	0.4460(7)	0.082(4)
C(114)	0.4493(6)	0.1988(6)	0.4719(7)	0.080(4)
C(115)	0.4221(5)	0.2438(5)	0.4515(7)	0.072(4)
C(116)	0.4330(5)	0.2726(5)	0.4006(7)	0.060(4)
C(117)	0.4025(4)	0.3214(5)	0.3745(7)	0.074(3)
C(118)	0.3483(6)	0.3106(7)	0.3247(7)	0.150(4)
C(119)	0.3944(7)	0.3564(7)	0.4271(7)	0.150(4)
C(120)	0.5407(5)	0.1850(4)	0.3666(7)	0.074(3)
C(121)	0.5302(7)	0.1300(5)	0.3432(9)	0.150(4)
C(122)	0.5968(6)	0.1886(6)	0.4149(8)	0.150(4)
Mo(2)	0.0000	0.32173(6)	0.2500	0.0492(7)
P(21)	0.0366(2)	0.2602(2)	0.1901(2)	0.067(2)
C(21)	-0.0145(6)	0.2233(6)	0.1285(8)	0.101(8)
C(22)	0.0742(7)	0.2907(6)	0.1399(9)	0.120(11)
C(23)	0.0841(7)	0.2096(5)	0.2327(8)	0.103(8)
N(21)	0.0539(4)	0.3473(4)	0.3182(6)	0.053(5)
C(211)	0.0909(5)	0.3729(4)	0.3715(6)	0.047(3)
C(212)	0.1432(5)	0.3518(5)	0.3982(7)	0.056(3)
C(213)	0.1806(6)	0.3795(5)	0.4500(7)	0.073(4)
C(214)	0.1652(6)	0.4246(5)	0.4725(7)	0.079(4)
C(215)	0.1132(6)	0.4438(6)	0.4467(7)	0.081(4)
C(216)	0.0746(5)	0.4186(5)	0.3949(7)	0.055(3)
C(217)	0.0191(5)	0.4401(4)	0.3680(7)	0.070(3)
C(218)	0.0182(8)	0.4939(6)	0.3408(9)	0.160(4)
C(219)	-0.0118(7)	0.4398(7)	0.4175(8)	0.160(4)
C(220)	0.1599(5)	0.3038(5)	0.3727(7)	0.070(3)
C(221)	0.1937(7)	0.2674(7)	0.4239(7)	0.160(4)
C(222)	0.1890(7)	0.3150(7)	0.3230(7)	0.160(4)

Table A.55: Atomic coordinates and U_{eq} (Å^2) for the non-hydrogen atoms of **4** [Mo(N-2,6-^{i}Pr$_2$C$_6$H$_3$)$_2$(PMe$_3$)$_2$].

Atom	x	y	z	U_{eq}
Mo(3)	0.25851(4)	0.56216(6)	0.24931(5)	0.0491(6)
P(31)	0.1816(2)	0.6132(2)	0.1900(2)	0.066(2)
C(31)	0.1989(7)	0.6630(6)	0.1393(8)	0.112(9)
C(32)	0.1298(6)	0.5774(6)	0.1289(7)	0.096(7)
C(33)	0.1416(6)	0.6503(6)	0.2323(7)	0.104(8)
P(32)	0.2122(2)	0.5103(2)	0.3091(2)	0.064(2)
C(34)	0.2555(7)	0.4609(6)	0.3600(8)	0.108(9)
C(35)	0.1905(6)	0.5457(6)	0.3703(8)	0.098(8)
C(36)	0.1509(6)	0.4739(6)	0.2673(8)	0.104(9)
N(31)	0.2669(4)	0.5247(4)	0.1816(6)	0.054(5)
C(311)	0.2798(5)	0.5028(4)	0.1288(6)	0.047(3)
C(312)	0.2530(5)	0.4566(5)	0.0998(7)	0.062(4)
C(313)	0.2675(5)	0.4339(6)	0.0472(7)	0.075(4)
C(314)	0.3084(6)	0.4559(5)	0.0267(7)	0.079(4)
C(315)	0.3323(6)	0.5010(6)	0.0530(7)	0.078(4)
C(316)	0.3205(5)	0.5246(5)	0.1049(7)	0.058(4)
C(317)	0.3485(5)	0.5739(5)	0.1338(7)	0.078(2)
C(318)	0.3330(6)	0.6184(6)	0.0863(8)	0.151(3)
C(319)	0.4093(5)	0.5688(7)	0.1571(8)	0.151(3)
C(330)	0.2100(5)	0.4331(4)	0.1239(7)	0.078(2)
C(331)	0.2331(7)	0.3915(6)	0.1738(7)	0.151(3)
C(332)	0.1617(6)	0.4118(7)	0.0714(7)	0.151(3)
N(32)	0.3012(4)	0.5986(4)	0.3171(6)	0.050(4)
C(321)	0.3401(5)	0.6223(4)	0.3709(7)	0.050(3)
C(322)	0.3273(5)	0.6685(5)	0.3992(7)	0.060(4)
C(323)	0.3667(6)	0.6922(5)	0.4507(7)	0.072(4)
C(324)	0.4171(6)	0.6708(6)	0.4714(8)	0.083(4)
C(325)	0.4300(6)	0.6246(5)	0.4478(7)	0.080(4)
C(326)	0.3928(5)	0.6002(5)	0.3955(7)	0.062(4)
C(327)	0.4070(5)	0.5507(5)	0.3674(7)	0.078(2)
C(328)	0.4202(7)	0.5097(6)	0.4198(8)	0.151(3)
C(329)	0.4542(6)	0.5566(7)	0.3406(8)	0.151(3)
C(340)	0.2718(6)	0.6915(4)	0.3706(7)	0.078(2)
C(341)	0.2493(8)	0.7125(7)	0.4228(7)	0.151(3)
C(342)	0.2696(8)	0.7332(6)	0.3207(7)	0.151(3)

Table A.56: Atomic coordinates and U_{eq} ($Å^2$) (cont'd) for the non-hydrogen atoms of **4** [Mo(N-2,6-^{i}Pr$_2$C$_6$H$_3$)$_2$(PMe$_3$)$_2$].

A-B	d_{AB}	A-B	d_{AB}	A-B	d_{AB}
Mo(1)-P(11)	2.411(4)	Mo(1)-N(11)	1.809(13)	Mo(1)-P(11A)	2.411(4)
Mo(1)-N(11A)	1.809(13)	P(11)-C(11)	1.839(18)	P(11)-C(12)	1.833(16)
P(11)-C(13)	1.817(18)	N(11)-C(111)	1.410(19)	C(111)-C(112)	1.423(16)
C(111)-C(116)	1.399(21)	C(112)-C(113)	1.384(22)	C(112)-C(120)	1.477(20)
C(113)-C(114)	1.378(24)	C(114)-C(115)	1.362(19)	C(115)-C(116)	1.415(21)
C(116)-C(117)	1.501(17)	C(117)-C(118)	1.504(17)	C(117)-C(119)	1.504(22)
C(120)-C(121)	1.504(18)	C(120)-C(122)	1.504(16)	Mo(2)-P(21)	2.406(5)
Mo(2)-N(21)	1.807(10)	Mo(2)-P(21A)	2.406(5)	Mo(2)-N(21A)	1.807(10)
P(21)-C(21)	1.825(15)	P(21)-C(22)	1.830(21)	P(21)-C(23)	1.835(15)
N(21)-C(211)	1.407(15)	C(211)-C(212)	1.407(16)	C(211)-C(216)	1.397(18)
C(212)-C(213)	1.421(17)	C(212)-C(220)	1.470(19)	C(213)-C(214)	1.364(21)
C(214)-C(215)	1.382(19)	C(215)-C(216)	1.401(17)	C(216)-C(217)	1.482(17)
C(217)-C(218)	1.504(19)	C(217)-C(219)	1.504(26)	C(220)-C(221)	1.504(20)
C(220)-C(222)	1.504(24)	Mo(3)-P(31)	2.400(4)	Mo(3)-P(32)	2.405(5)
Mo(3)-N(31)	1.805(13)	Mo(3)-N(32)	1.797(10)	P(31)-C(31)	1.821(18)
P(31)-C(32)	1.813(14)	P(31)-C(33)	1.838(18)	P(32)-C(34)	1.823(15)
P(32)-C(35)	1.817(18)	P(32)-C(36)	1.825(15)	N(31)-C(311)	1.390(19)
C(311)-C(312)	1.422(17)	C(311)-C(316)	1.418(20)	C(312)-C(313)	1.412(22)
C(312)-C(330)	1.490(21)	C(313)-C(314)	1.385(22)	C(314)-C(315)	1.356(19)
C(315)-C(316)	1.378(22)	C(316)-C(317)	1.502(17)	C(317)-C(318)	1.504(20)
C(317)-C(319)	1.504(17)	C(330)-C(331)	1.504(19)	C(330)-C(332)	1.504(17)
N(32)-C(321)	1.414(15)	C(321)-C(322)	1.423(19)	C(321)-C(326)	1.421(17)
C(322)-C(323)	1.390(17)	C(322)-C(340)	1.501(18)	C(323)-C(324)	1.360(20)
C(324)-C(325)	1.376(22)	C(325)-C(326)	1.384(18)	C(326)-C(327)	1.504(19)
C(327)-C(328)	1.504(21)	C(327)-C(329)	1.504(24)	C(340)-C(341)	1.504(25)
C(340)-C(342)	1.504(21)				

Table A.57: Bond lengths (Å) for **4** [Mo(N-2,6-$^{i}Pr_2C_6H_3)_2(PMe_3)_2$].

A-B-C	∠ A-B-C	A-B-C	∠ A-B-C	A-B-C	∠ A-B-C
P(11)-Mo(1)-N(11)	109.9(3)	P(11)-Mo(1)-P(11A)	97.0(2)	N(11)-Mo(1)-P(11A)	97.9(3)
P(11)-Mo(1)-N(11A)	97.9(3)	N(11)-Mo(1)-N(11A)	137.6(6)	P(11A)-Mo(1)-N(11A)	109.9(3)
Mo(1)-P(11)-C(11)	115.0(5)	Mo(1)-P(11)-C(12)	114.2(6)	C(11)-P(11)-C(12)	101.3(8)
Mo(1)-P(11)-C(13)	120.7(5)	C(11)-P(11)-C(13)	101.9(8)	C(12)-P(11)-C(13)	100.9(8)
Mo(1)-N(11)-C(111)	171.1(9)	N(11)-C(111)-C(112)	118.9(12)	N(11)-C(111)-C(116)	119.8(11)
C(112)-C(111)-C(116)	121.3(13)	C(111)-C(112)-C(113)	118.0(13)	C(111)-C(112)-C(120)	122.7(12)
C(113)-C(112)-C(120)	119.3(11)	C(112)-C(113)-C(114)	120.3(13)	C(113)-C(114)-C(115)	122.6(15)
C(114)-C(115)-C(116)	119.4(15)	C(111)-C(116)-C(115)	118.3(12)	C(111)-C(116)-C(117)	120.2(13)
C(115)-C(116)-C(117)	121.4(13)	C(116)-C(117)-C(118)	112.2(11)	C(116)-C(117)-C(119)	113.9(12)
C(118)-C(117)-C(119)	109.1(12)	C(112)-C(120)-C(121)	113.9(12)	C(112)-C(120)-C(122)	111.3(12)
C(121)-C(120)-C(122)	109.1(11)	P(21)-Mo(2)-N(21)	109.7(4)	P(21)-Mo(2)-P(21A)	97.3(2)
N(21)-Mo(2)-P(21A)	98.4(4)	P(21)-Mo(2)-N(21A)	98.4(4)	N(21)-Mo(2)-N(21A)	137.1(7)
P(21A)-Mo(2)-N(21A)	109.7(4)	Mo(2)-P(21)-C(21)	114.4(6)	Mo(2)-P(21)-C(22)	113.0(6)
C(21)-P(21)-C(22)	101.5(8)	Mo(2)-P(21)-C(23)	121.4(6)	C(21)-P(21)-C(23)	102.2(7)
C(22)-P(21)-C(23)	101.7(8)	Mo(2)-N(21)-C(211)	172.0(9)	N(21)-C(211)-C(212)	118.5(11)
N(21)-C(211)-C(216)	118.9(10)	C(212)-C(211)-C(216)	122.6(10)	C(211)-C(212)-C(213)	117.5(12)
C(211)-C(212)-C(220)	122.0(10)	C(213)-C(212)-C(220)	120.4(11)	C(212)-C(213)-C(214)	120.2(12)
C(213)-C(214)-C(215)	121.2(13)	C(214)-C(215)-C(216)	121.3(14)	C(211)-C(216)-C(215)	117.1(11)
C(211)-C(216)-C(217)	122.7(10)	C(215)-C(216)-C(217)	120.2(12)	C(216)-C(217)-C(218)	113.4(13)
C(216)-C(217)-C(219)	112.6(12)	C(218)-C(217)-C(219)	109.1(13)	C(212)-C(220)-C(221)	115.4(12)
C(212)-C(220)-C(222)	111.4(12)	C(221)-C(220)-C(222)	109.1(12)	P(31)-Mo(3)-P(32)	96.9(2)
P(31)-Mo(3)-N(31)	98.9(3)	P(32)-Mo(3)-N(31)	109.0(4)	P(31)-Mo(3)-N(32)	110.1(3)
P(32)-Mo(3)-N(32)	98.5(4)	N(31)-Mo(3)-N(32)	137.1(5)	Mo(3)-P(31)-C(31)	112.8(5)
Mo(3)-P(31)-C(32)	114.3(5)	C(31)-P(31)-C(32)	101.3(7)	Mo(3)-P(31)-C(33)	121.8(5)
C(31)-P(31)-C(33)	101.4(8)	C(32)-P(31)-C(33)	102.5(7)	Mo(3)-P(32)-C(34)	113.1(6)
Mo(3)-P(32)-C(35)	114.4(6)	C(34)-P(32)-C(35)	101.1(8)	Mo(3)-P(32)-C(36)	121.8(6)
C(34)-P(32)-C(36)	102.3(7)	C(35)-P(32)-C(36)	101.5(8)	Mo(3)-N(31)-C(311)	169.8(9)
N(31)-C(311)-C(312)	119.4(12)	N(31)-C(311)-C(316)	121.1(10)	C(312)-C(311)-C(316)	119.5(13)
C(311)-C(312)-C(313)	118.9(13)	C(311)-C(312)-C(330)	120.5(13)	C(313)-C(312)-C(330)	120.6(11)
C(312)-C(313)-C(314)	119.5(13)	C(313)-C(314)-C(315)	121.1(15)	C(314)-C(315)-C(316)	122.0(15)
C(311)-C(316)-C(315)	118.8(12)	C(311)-C(316)-C(317)	120.6(13)	C(315)-C(316)-C(317)	120.6(13)
C(316)-C(317)-C(318)	112.1(11)	C(316)-C(317)-C(319)	112.8(11)	C(318)-C(317)-C(319)	109.0(12)
C(312)-C(330)-C(331)	111.1(11)	C(312)-C(330)-C(332)	115.5(12)	C(331)-C(330)-C(332)	109.1(11)
Mo(3)-N(32)-C(321)	172.3(9)	N(32)-C(321)-C(322)	120.5(10)	N(32)-C(321)-C(326)	119.4(11)
C(322)-C(321)-C(326)	120.1(11)	C(321)-C(322)-C(323)	119.7(12)	C(321)-C(322)-C(340)	118.5(10)
C(323)-C(322)-C(340)	121.7(12)	C(322)-C(323)-C(324)	118.5(13)	C(323)-C(324)-C(325)	123.2(13)
C(324)-C(325)-C(326)	120.4(13)	C(321)-C(326)-C(325)	117.8(13)	C(321)-C(326)-C(327)	121.2(10)
C(325)-C(326)-C(327)	121.0(12)	C(326)-C(327)-C(328)	109.3(13)	C(326)-C(327)-C(329)	113.0(12)
C(328)-C(327)-C(329)	109.1(12)	C(322)-C(340)-C(341)	112.2(12)	C(322)-C(340)-C(342)	113.4(14)
C(341)-C(340)-C(342)	109.1(12)				

Table A.58: Bond angles (°) for **4** [Mo(N-2,6-^{i}Pr$_2$C$_6$H$_3$)$_2$(PMe$_3$)$_2$].

Atom	U_{11}	U_{22}	U_{33}	U_{12}	U_{13}	U_{23}
Mo(1)	0.052(1)	0.0398(9)	0.067(1)	0.000	0.024(1)	0.000
P(11)	0.067(3)	0.056(2)	0.077(4)	0.010(2)	0.021(3)	0.004(2)
C(11)	0.098(12)	0.094(11)	0.086(13)	0.010(10)	0.026(10)	0.025(10)
C(12)	0.082(12)	0.119(14)	0.129(17)	0.009(11)	0.002(11)	0.006(12)
C(13)	0.117(13)	0.084(11)	0.115(15)	0.051(10)	0.040(12)	0.004(10)
N(11)	0.047(6)	0.039(6)	0.063(8)	-0.008(5)	0.007(6)	-0.009(6)
Mo(2)	0.0399(9)	0.040(1)	0.063(1)	0.000	0.0090(9)	0.0000
P(21)	0.068(3)	0.060(2)	0.071(3)	0.006(2)	0.017(2)	-0.005(2)
C(21)	0.111(13)	0.091(11)	0.080(12)	-0.005(10)	-0.003(10)	-0.021(9)
C(22)	0.158(17)	0.098(13)	0.138(18)	-0.028(12)	0.097(15)	-0.021(12)
C(23)	0.122(13)	0.087(11)	0.092(13)	0.057(11)	0.022(11)	0.002(9)
N(21)	0.050(6)	0.051(7)	0.060(9)	0.007(6)	0.021(6)	-0.002(6)
Mo(3)	0.0430(6)	0.0458(7)	0.062(1)	-0.0010(6)	0.0209(7)	-0.0067(6)
P(31)	0.060(2)	0.069(3)	0.069(3)	0.010(2)	0.018(2)	0.001(2)
C(31)	0.105(14)	0.100(13)	0.122(16)	-0.009(11)	0.022(12)	0.038(12)
C(32)	0.082(10)	0.115(13)	0.066(11)	0.020(10)	-0.012(8)	-0.003(9)
C(33)	0.093(11)	0.134(15)	0.080(12)	0.057(11)	0.021(10)	0.009(11)
P(32)	0.061(2)	0.065(3)	0.072(3)	-0.011(2)	0.027(2)	-0.003(2)
C(34)	0.130(15)	0.104(12)	0.104(15)	0.019(11)	0.058(12)	0.038(11)
C(35)	0.105(12)	0.107(13)	0.088(13)	0.002(10)	0.038(10)	-0.005(10)
C(36)	0.094(12)	0.123(14)	0.113(15)	-0.030(11)	0.056(11)	0.004(11)
N(31)	0.055(7)	0.051(6)	0.063(8)	-0.006(6)	0.027(6)	-0.002(6)
N(32)	0.045(6)	0.050(6)	0.051(8)	-0.006(5)	0.010(6)	-0.002(6)

Table A.59: Anisotropic atomic displacement parameters ($Å^2$) for the non-hydrogen atoms of **4** [Mo(N-2,6-^{i}Pr$_2$C$_6$H$_3$)$_2$(PMe$_3$)$_2$].

Atom	x	y	z	Atom	x	y	z
H(11A)	0.4251	0.4286	0.1074	H(11B)	0.4858	0.4243	0.1514
H(11C)	0.4611	0.3824	0.0974	H(12A)	0.3451	0.3637	0.1162
H(12B)	0.3778	0.3147	0.1071	H(12C)	0.3539	0.3177	0.1663
H(13A)	0.3812	0.4364	0.2017	H(13B)	0.3901	0.3996	0.2625
H(13C)	0.4366	0.4370	0.2583	H(113)	0.5076	0.1488	0.4621
H(114)	0.4417	0.1802	0.5071	H(115)	0.3954	0.2567	0.4705
H(117)	0.4230	0.3399	0.3512	H(1A)	0.3288	0.3417	0.3075
H(2A)	0.3537	0.2906	0.2893	H(3A)	0.3278	0.2908	0.3470
H(4A)	0.3753	0.3869	0.4070	H(5A)	0.3735	0.3385	0.4506
H(6A)	0.4290	0.3660	0.4571	H(120)	0.5397	0.2049	0.3283
H(7A)	0.5573	0.1179	0.3242	H(8A)	0.5321	0.1101	0.3818
H(9A)	0.4948	0.1262	0.3117	H(10A)	0.6225	0.1754	0.3946
H(10B)	0.6057	0.2238	0.4284	H(10C)	0.5979	0.1680	0.4527
H(21A)	0.0028	0.1996	0.1066	H(21B)	-0.0370	0.2044	0.1490
H(21C)	-0.0365	0.2471	0.0970	H(22A)	0.0874	0.2641	0.1174
H(22B)	0.0508	0.3136	0.1082	H(22C)	0.1043	0.3100	0.1676
H(23A)	0.0938	0.1890	0.2005	H(23B)	0.1161	0.2255	0.2614
H(23C)	0.0677	0.1879	0.2579	H(213)	0.2167	0.3660	0.4681
H(214)	0.1911	0.4425	0.5079	H(215)	0.1029	0.4751	0.4639
H(217)	0.0006	0.4190	0.3310				

Table A.60: Atomic coordinates for the hydrogen atoms of **4** [Mo(N-2,6-$^{i}Pr_2C_6H_3)_2(PMe_3)_2$].

Atom	x	y	z	Atom	x	y	z
H(1B)	-0.0181	0.5067	0.3217	H(2B)	0.0369	0.5152	0.3776
H(3B)	0.0371	0.4948	0.3084	H(4B)	-0.0476	0.4531	0.3967
H(5B)	-0.0142	0.4052	0.4324	H(6B)	0.0064	0.4613	0.4543
H(220)	0.1274	0.2854	0.3495	H(7B)	0.1750	0.2587	0.4550
H(8B)	0.2011	0.2365	0.4033	H(9B)	0.2273	0.2845	0.4461
H(20A)	0.1999	0.2838	0.3061	H(20B)	0.1655	0.3346	0.2874
H(20C)	0.2206	0.3352	0.3445	H(31A)	0.1667	0.6820	0.1168
H(31B)	0.2254	0.6862	0.1664	H(31C)	0.2133	0.6469	0.1077
H(32A)	0.1005	0.6002	0.1072	H(32B)	0.1457	0.5636	0.0973
H(32C)	0.1161	0.5496	0.1492	H(33A)	0.1129	0.6681	0.2002
H(33B)	0.1264	0.6273	0.2573	H(33C)	0.1646	0.6751	0.2613
H(34A)	0.2350	0.4416	0.3826	H(34B)	0.2681	0.4380	0.3322
H(34C)	0.2861	0.4767	0.3915	H(35A)	0.1725	0.5227	0.3921
H(35B)	0.2218	0.5604	0.4019	H(35C)	0.1661	0.5729	0.3492
H(36A)	0.1388	0.4560	0.2997	H(36B)	0.1228	0.4967	0.2425
H(36C)	0.1592	0.4492	0.2381	H(313)	0.2497	0.4026	0.0280
H(314)	0.3178	0.4399	-0.0090	H(315)	0.3594	0.5163	0.0365
H(317)	0.3369	0.5825	0.1712				

Table A.61: Atomic coordinates for the hydrogen atoms (cont'd) of **4** [Mo(N-2,6-$^{i}Pr_2C_6H_3)_2(PMe_3)_2$].

Atom	x	y	z	Atom	x	y	z
H(1C)	0.3513	0.6489	0.1076	H(2C)	0.3447	0.6106	0.0487
H(3C)	0.2945	0.6242	0.0722	H(4C)	0.4260	0.6009	0.1752
H(5C)	0.4193	0.5424	0.1901	H(6C)	0.4215	0.5592	0.1204
H(330)	0.1969	0.4594	0.1470	H(7C)	0.2633	0.4054	0.2080
H(8C)	0.2068	0.3778	0.1929	H(9C)	0.2456	0.3644	0.1512
H(50C)	0.1356	0.3976	0.0903	H(51C)	0.1452	0.4393	0.0417
H(52C)	0.1741	0.3853	0.0479	H(323)	0.3578	0.7237	0.4689
H(324)	0.4439	0.6876	0.5069	H(325)	0.4656	0.6098	0.4651
H(327)	0.3767	0.5411	0.3304	H(53C)	0.4277	0.4786	0.3994
H(54C)	0.4516	0.5191	0.4555	H(55C)	0.3900	0.5039	0.4363
H(56C)	0.4616	0.5248	0.3218	H(57C)	0.4487	0.5838	0.3086
H(58C)	0.4845	0.5652	0.3782	H(340)	0.2472	0.6650	0.3479
H(60C)	0.2139	0.7272	0.4040	H(61C)	0.2474	0.6849	0.4521
H(62C)	0.2739	0.7386	0.4466	H(63C)	0.2340	0.7479	0.3036
H(64C)	0.2948	0.7596	0.3422	H(65C)	0.2806	0.7188	0.2851

Table A.62: Atomic coordinates (cont'd) for the hydrogen atoms of **4** [Mo(N-2,6-$^{i}Pr_2C_6H_3)_2(PMe_3)_2$].

Atom	x	y	z	U(eq)
Nb(1)	0.09236(3)	0.15355(7)	0.57755(4)	0.0312(3)
O(1)	0.1149(2)	-0.0176(6)	0.5462(4)	0.041(2)
O(2)	0.0715(3)	0.2338(6)	0.4722(3)	0.045(2)
N(1)	0.1489(3)	0.2368(7)	0.6202(4)	0.037(2)
C(1)	0.0308(6)	0.2606(9)	0.6588(10)	0.044(1)
C(2)	-0.0007	0.1920	0.5967	0.044(1)
C(3)	0.0071	0.0558	0.6104	0.044(1)
C(4)	0.0435	0.0403	0.6809	0.044(1)
C(5)	0.0581	0.1669	0.7108	0.044(1)
C(1A)	0.0095(7)	0.2329(13)	0.6225(11)	0.044(1)
C(2A)	-0.0013	0.1024	0.5961	0.044(1)
C(3A)	0.0296	0.0170	0.6494	0.044(1)
C(4A)	0.0595	0.0948	0.7088	0.044(1)
C(5A)	0.0471	0.2282	0.6921	0.044(1)
C(6)	0.1881(4)	0.3062(11)	0.6730(7)	0.056(4)
C(7)	0.2071(7)	0.2211(19)	0.7436(9)	0.137(8)
C(8)	0.1624(5)	0.4242(16)	0.7117(12)	0.138(9)
C(9)	0.2308(5)	0.3504(15)	0.6262(9)	0.098(6)
C(10)	0.1577(3)	-0.0989(7)	0.5379(5)	0.058(3)

Table A.63: Atomic coordinates and U_{eq} ($Å^2$) for the non-hydrogen atoms of **5** [$NbCp(NBu^t)(OCMe_2CF_3)_2$].

Atom	x	y	z	U(eq)
C(11)	0.1557(5)	-0.1387(11)	0.4468(5)	0.086(3)
C(12)	0.2096(5)	-0.0289(14)	0.5638(8)	0.086(3)
C(13)	0.1542(4)	-0.2229(10)	0.5907(6)	0.086(3)
C(12A)	0.2118(8)	-0.0563(32)	0.5167(25)	0.086(3)
C(13A)	0.1418(9)	-0.2263(15)	0.4915(14)	0.086(3)
F(1)	0.1573(5)	-0.1801(11)	0.6662(6)	0.095(2)
F(2)	0.1090(4)	-0.2783(12)	0.5714(8)	0.095(2)
F(3)	0.1916(5)	-0.3062(12)	0.5821(8)	0.095(2)
F(1A)	0.0996(9)	-0.2801(27)	0.5137(18)	0.095(2)
F(2A)	0.1195(11)	-0.1919(27)	0.4194(15)	0.095(2)
F(3A)	0.1812(9)	-0.3070(26)	0.4974(17)	0.095(2)
C(14)	0.0850(3)	0.3244(8)	0.4142(5)	0.055(3)
C(15)	0.0949(7)	0.4551(14)	0.4603(11)	0.081(3)
C(16)	0.1346(5)	0.2838(21)	0.3761(10)	0.081(3)
C(17)	0.0403(5)	0.3426(15)	0.3452(8)	0.081(3)
F(4)	0.0408(7)	0.2276(16)	0.3102(11)	0.118(2)
F(5)	0.0510(8)	0.4359(18)	0.2949(11)	0.118(2)
F(6)	-0.0002(7)	0.3774(26)	0.3815(16)	0.118(2)

Table A.64: Atomic coordinates and U_{eq} (Å^2) (cont'd) for the non-hydrogen atoms of **5** [$NbCp(NBu^t)(OCMe_2CF_3)_2$].

A-B	d_{AB}	A-B	d_{AB}	A-B	d_{AB}
Nb(1)-O(1)	1.930(6)	Nb(1)-O(2)	1.936(6)	Nb(1)-N(1)	1.773(7)
Nb(1)-C(1)	2.440(15)	Nb(1)-C(2)	2.495(15)	Nb(1)-C(3)	2.532(15)
Nb(1)-C(4)	2.501(15)	Nb(1)-C(5)	2.443(16)	Nb(1)-C(1A)	2.477(18)
Nb(1)-C(2A)	2.531(18)	Nb(1)-C(3A)	2.525(17)	Nb(1)-C(4A)	2.467(19)
Nb(1)-C(5A)	2.436(18)	O(1)-C(10)	1.401(10)	O(2)-C(14)	1.398(10)
N(1)-C(6)	1.447(12)	C(1)-C(2)	1.420	C(1)-C(5)	1.420
C(2)-C(3)	1.420	C(3)-C(4)	1.420	C(4)-C(5)	1.420
C(1A)-C(2A)	1.420	C(1A)-C(5A)	1.420	C(2A)-C(3A)	1.420
C(3A)-C(4A)	1.420	C(4A)-C(5A)	1.420	C(6)-C(7)	1.489(19)
C(6)-C(8)	1.544(20)	C(6)-C(9)	1.480(18)	C(10)-C(11)	1.542(12)
C(10)-C(12)	1.542(15)	C(10)-C(13)	1.542(13)	C(10)-C(12A)	1.542(27)
C(10)-C(13A)	1.541(19)	C(13)-F(1)	1.307(14)	C(13)-F(2)	1.307(15)
C(13)-F(3)	1.308(16)	C(13A)-F(1A)	1.307(34)	C(13A)-F(2A)	1.307(33)
C(13A)-F(3A)	1.307(32)	C(14)-C(15)	1.542(17)	C(14)-C(15A)	1.542(16)
C(14)-C(16)	1.541(17)	C(14)-C(16A)	1.542(18)	C(14)-C(17)	1.541(15)
C(14)-C(17A)	1.542(16)	C(17)-F(4)	1.308(22)	C(17)-F(5)	1.308(24)
C(17)-F(6)	1.308(26)	C(17A)-F(4A)	1.308(23)	C(17A)-F(5A)	1.308(24)
C(17A)-F(6A)	1.308(25)				

Table A.65: Bond lengths (Å) for **5** [$NbCp(NBu^t)(OCMe_2CF_3)_2$].

A-B-C	∠A-B-C	A-B-C	∠A-B-C	A-B-C	∠A-B-C
O(1)-Nb(1)-O(2)	102.1(3)	O(1)-Nb(1)-N(1)	106.1(3)	O(2)-Nb(1)-N(1)	106.9(3)
O(1)-Nb(1)-C(1)	141.7(3)	O(2)-Nb(1)-C(1)	99.2(4)	N(1)-Nb(1)-C(1)	97.5(4)
O(1)-Nb(1)-C(2)	120.0(3)	O(2)-Nb(1)-C(2)	82.1(4)	N(1)-Nb(1)-C(2)	130.2(4)
C(1)-Nb(1)-C(2)	33.4(2)	O(1)-Nb(1)-C(3)	89.7(3)	O(2)-Nb(1)-C(3)	100.8(4)
N(1)-Nb(1)-C(3)	144.0(4)	C(1)-Nb(1)-C(3)	55.0(3)	C(2)-Nb(1)-C(3)	32.8(2)
O(1)-Nb(1)-C(4)	87.1(3)	O(2)-Nb(1)-C(4)	133.3(4)	N(1)-Nb(1)-C(4)	114.3(4)
C(1)-Nb(1)-C(4)	55.4(4)	C(2)-Nb(1)-C(4)	54.8(3)	C(3)-Nb(1)-C(4)	32.8(2)
O(1)-Nb(1)-C(5)	115.9(3)	O(2)-Nb(1)-C(5)	132.8(4)	N(1)-Nb(1)-C(5)	89.1(4)
C(1)-Nb(1)-C(5)	33.8(2)	C(2)-Nb(1)-C(5)	55.4(3)	C(3)-Nb(1)-C(5)	55.0(3)
C(4)-Nb(1)-C(5)	33.4(2)	O(1)-Nb(1)-C(1A)	132.2(4)	O(2)-Nb(1)-C(1A)	87.5(4)
N(1)-Nb(1)-C(1A)	115.6(4)	O(1)-Nb(1)-C(2A)	99.5(4)	O(2)-Nb(1)-C(2A)	90.7(4)
N(1)-Nb(1)-C(2A)	144.6(5)	C(1A)-Nb(1)-C(2A)	32.9(2)	O(1)-Nb(1)-C(3A)	81.5(4)
O(2)-Nb(1)-C(3A)	121.1(4)	N(1)-Nb(1)-C(3A)	128.9(5)	C(1A)-Nb(1)-C(3A)	54.7(4)
C(2A)-Nb(1)-C(3A)	32.6(2)	O(1)-Nb(1)-C(4A)	98.8(4)	O(2)-Nb(1)-C(4A)	142.2(4)
N(1)-Nb(1)-C(4A)	96.9(4)	C(1A)-Nb(1)-C(4A)	55.4(4)	C(2A)-Nb(1)-C(4A)	54.7(4)
C(3A)-Nb(1)-C(4A)	33.0(2)	O(1)-Nb(1)-C(5A)	132.2(4)	O(2)-Nb(1)-C(5A)	116.2(4)
N(1)-Nb(1)-C(5A)	89.5(4)	C(1A)-Nb(1)-C(5A)	33.6(2)	C(2A)-Nb(1)-C(5A)	55.1(4)
C(3A)-Nb(1)-C(5A)	55.1(4)	C(4A)-Nb(1)-C(5A)	33.7(3)	Nb(1)-O(1)-C(10)	145.7(5)

Table A.66: Bond Angles (°) for **5** [$NbCp(NBu^t)(OCMe_2CF_3)_2$].

A-B-C	∠A-B-C	A-B-C	∠A-B-C	A-B-C	∠A-B-C
Nb(1)-O(2)-C(14)	145.1(5)	Nb(1)-N(1)-C(6)	165.6(7)	Nb(1)-C(1)-C(2)	75.4(3)
Nb(1)-C(1)-C(5)	73.2(3)	C(2)-C(1)-C(5)	108.0	Nb(1)-C(2)-C(1)	71.1(3)
Nb(1)-C(2)-C(3)	75.0(2)	C(1)-C(2)-C(3)	108.0	Nb(1)-C(3)-C(2)	72.2(2)
Nb(1)-C(3)-C(4)	72.4(3)	C(2)-C(3)-C(4)	108.0	Nb(1)-C(4)-C(3)	74.8(3)
Nb(1)-C(4)-C(5)	71.1(3)	C(3)-C(4)-C(5)	108.0	Nb(1)-C(5)-C(1)	73.0(3)
Nb(1)-C(5)-C(4)	75.5(2)	C(1)-C(5)-C(4)	108.0	Nb(1)-C(1A)-C(2A)	75.6(3)
Nb(1)-C(1A)-C(5A)	71.6(4)	C(2A)-C(1A)-C(5A)	108.0	Nb(1)-C(2A)-C(1A)	71.5(3)
Nb(1)-C(2A)-C(3A)	73.4(4)	C(1A)-C(2A)-C(3A)	108.0	Nb(1)-C(3A)-C(2A)	73.9(4)
Nb(1)-C(3A)-C(4A)	71.2(4)	C(2A)-C(3A)-C(4A)	108.0	Nb(1)-C(4A)-C(3A)	75.7(4)
Nb(1)-C(4A)-C(5A)	72.0(3)	C(3A)-C(4A)-C(5A)	108.0	Nb(1)-C(5A)-C(1A)	74.8(4)
Nb(1)-C(5A)-C(4A)	74.3(3)	C(1A)-C(5A)-C(4A)	108.0	N(1)-C(6)-C(7)	109.4(11)
N(1)-C(6)-C(8)	108.9(9)	C(7)-C(6)-C(8)	104.9(12)	N(1)-C(6)-C(9)	110.8(9)
C(7)-C(6)-C(9)	112.0(11)	C(8)-C(6)-C(9)	110.5(11)	O(1)-C(10)-C(11)	107.6(7)
O(1)-C(10)-C(12)	111.9(7)	C(11)-C(10)-C(12)	109.1(8)	O(1)-C(10)-C(13)	109.8(7)
C(11)-C(10)-C(13)	109.1(7)	C(12)-C(10)-C(13)	109.2(8)	O(1)-C(10)-C(12A)	126.9(13)
O(1)-C(10)-C(13A)	112.0(10)	C(12A)-C(10)-C(13A)	109.2(17)	C(10)-C(13)-F(1)	104.7(9)
C(10)-C(13)-F(2)	108.9(9)	F(1)-C(13)-F(2)	109.8(11)	C(10)-C(13)-F(3)	112.7(9)
F(1)-C(13)-F(3)	110.3(10)	F(2)-C(13)-F(3)	110.3(10)	C(10)-C(13A)-F(1A)	113.9(20)
C(10)-C(13A)-F(2A)	106.8(16)	F(1A)-C(13A)-F(2A)	93.5(22)	C(10)-C(13A)-F(3A)	109.3(18)
F(1A)-C(13A)-F(3A)	112.5(20)	F(2A)-C(13A)-F(3A)	120.3(25)	O(2)-C(14)-C(15)	106.3(9)
O(2)-C(14)-C(15A)	115.0(9)	O(2)-C(14)-C(16)	112.1(9)	C(15)-C(14)-C(16)	109.2(11)
O(2)-C(14)-C(16A)	104.5(9)	C(15A)-C(14)-C(16A)	109.1(11)	O(2)-C(14)-C(17)	110.8(8)
C(15)-C(14)-C(17)	109.2(10)	C(16)-C(14)-C(17)	109.2(9)	O(2)-C(14)-C(17A)	109.7(8)
C(15A)-C(14)-C(17A)	109.2(9)	C(16A)-C(14)-C(17A)	109.1(10)	C(14)-C(17)-F(4)	99.9(12)
C(14)-C(17)-F(5)	110.9(12)	F(4)-C(17)-F(5)	111.5(15)	C(14)-C(17)-F(6)	106.0(14)
F(4)-C(17)-F(6)	119.3(17)	F(5)-C(17)-F(6)	108.6(18)	C(14)-C(17A)-F(5A)	111.3(13)
F(4A)-C(17A)-F(5A)	109.9(15)	C(14)-C(17A)-F(6A)	103.3(13)	F(4A)-C(17A)-F(6A)	120.6(18)
F(5A)-C(17A)-F(6A)	108.4(17)				

Table A.67: Bond Angles (°) for **5** [$NbCp(NBu^t)(OCMe_2CF_3)_2$].

Atom	U_{11}	U_{22}	U_{33}	U_{12}	U_{13}	U_{23}
Nb(1)	0.0322(4)	0.0357(5)	0.0266(4)	0.0002(4)	0.0076(3)	0.0008(4)
O(1)	0.043(3)	0.035(3)	0.047(3)	0.006(3)	0.006(3)	0.001(3)
O(2)	0.063(4)	0.041(4)	0.030(3)	0.007(3)	0.000(3)	0.004(3)
N(1)	0.038(4)	0.041(4)	0.035(4)	-0.004(3)	0.011(3)	-0.002(3)
C(6)	0.050(6)	0.065(7)	0.053(6)	-0.016(5)	0.005(5)	-0.010(5)
C(7)	0.170(18)	0.141(15)	0.081(10)	-0.064(14)	-0.076(11)	0.027(10)
C(8)	0.071(9)	0.151(16)	0.192(18)	-0.028(10)	0.013(11)	-0.129(15)
C(9)	0.053(7)	0.131(13)	0.115(12)	-0.034(8)	0.025(8)	-0.054(10)

Table A.68: Anisotropic atomic displacement parameters ($Å^2$) for **5** $[NbCp(NBu^t)(OCMe_2CF_3)_2]$.

Atom	x	y	z	U
H(1A)	0.0332	0.3540	0.6645	0.053(2)
H(2A)	-0.0234	0.2309	0.5532	0.053(2)
H(3A)	-0.0093	-0.0136	0.5777	0.053(2)
H(4A)	0.0560	-0.0415	0.7042	0.053(2)
H(5A)	0.0823	0.1857	0.7578	0.053(2)
H(1AA)	-0.0059	0.3106	0.5976	0.053(2)
H(2AA)	-0.0253	0.0764	0.5503	0.053(2)
H(3AA)	0.0302	-0.0768	0.6460	0.053(2)
H(4AA)	0.0839	0.0628	0.7524	0.053(2)
H(5AA)	0.0616	0.3022	0.7225	0.053(2)
H(7A)	0.2237	0.1449	0.7240	0.080
H(7B)	0.2316	0.2690	0.7803	0.080
H(7C)	0.1783	0.1947	0.7722	0.080
H(8A)	0.1490	0.4837	0.6694	0.080
H(8B)	0.1347	0.3938	0.7413	0.080
H(8C)	0.1879	0.4683	0.7488	0.080
H(9A)	0.2166	0.4075	0.5830	0.080
H(9B)	0.2565	0.3967	0.6616	0.080
H(9C)	0.2465	0.2760	0.6030	0.080
H(11A)	0.1236	-0.1798	0.4262	0.103(3)
H(11B)	0.1600	-0.0595	0.4167	0.103(3)
H(11C)	0.1840	-0.1970	0.4403	0.103(3)
H(12A)	0.2103	-0.0176	0.5057	0.103(3)
H(12B)	0.2113	0.0552	0.5901	0.103(3)
H(12C)	0.2387	-0.0810	0.5853	0.103(3)
H(12D)	0.2140	-0.0330	0.5738	0.103(3)
H(12E)	0.2391	-0.1165	0.5080	0.103(3)
H(12F)	0.2152	0.0211	0.4844	0.103(3)
H(15A)	0.0799	0.4492	0.5113	0.097(4)
H(15B)	0.1316	0.4695	0.4712	0.097(4)
H(15C)	0.0794	0.5266	0.4286	0.097(4)
H(16A)	0.1646	0.3007	0.4142	0.097(4)
H(16B)	0.1297	0.1909	0.3702	0.097(4)
H(16C)	0.1395	0.3213	0.3238	0.097(4)

Table A.69: Atomic coordinates for the hydrogen atoms of **5** [$NbCp(NBu^t)(OCMe_2CF_3)_2$].

Atom	x	y	z	U_{eq}
Mo(1)	0.22877(3)	0.44931(5)	0.08873(3)	0.0366(2)
O(1)	0.2380(3)	0.5433(5)	0.1885(2)	0.065(2)
O(2)	0.1311(2)	0.5414(5)	-0.0055(2)	0.058(2)
N(1)	0.2184(4)	0.2331(6)	0.0898(3)	0.074(3)
N(2)	0.3205(3)	0.5099(7)	0.0819(3)	0.065(2)
C(1)	0.2716(4)	0.5162(8)	0.2782(3)	0.058(3)
C(2)	0.2473(6)	0.6654(11)	0.3115(5)	0.140(7)
C(3)	0.3663(5)	0.5063(14)	0.3221(5)	0.150(6)
C(4)	0.2348(5)	0.3607(10)	0.2941(4)	0.100(5)
C(6)	0.0189(5)	0.6701(10)	-0.1266(5)	0.116(4)
C(7)	0.1184(5)	0.4713(11)	-0.1401(4)	0.098(4)
C(5)	0.0710(3)	0.5080(7)	-0.0937(3)	0.055(3)
C(8)	0.0147(4)	0.3596(10)	-0.0998(4)	0.090(4)
C(9)	0.2244(4)	0.0470(7)	0.0905(4)	0.063(3)
C(10)	0.2208(5)	-0.0116(8)	0.0079(5)	0.086(4)
C(11)	0.1477(5)	-0.0213(8)	0.0965(5)	0.085(4)
C(12)	0.3079(5)	-0.0097(8)	0.1688(4)	0.086(4)
C(13)	0.3995(4)	0.4871(9)	0.0807(4)	0.069(3)
C(14)	0.3848(9)	0.3958(21)	0.0047(9)	0.115(5)
C(15)	0.4629(8)	0.3956(19)	0.1671(8)	0.105(4)
C(16)	0.4361(9)	0.6652(17)	0.0811(9)	0.104(4)
C(14A)	0.3702(12)	0.5372(27)	-0.0175(11)	0.096(6)
C(15A)	0.4229(14)	0.3041(26)	0.0780(15)	0.113(7)
C(16A)	0.4621(16)	0.5870(34)	0.1403(16)	0.145(10)

Table A.70: Atomic coordinates and U_{eq} (Å^2) for non-hydrogen atoms of **6** [Mo(NBu^t)$_2$(OBu^t)$_2$].

A-B	d_{AB}	A-B	d_{AB}	A-B	d_{AB}
Mo(1)-O(1)	1.862(4)	Mo(1)-O(2)	1.877(3)	Mo(1)-N(1)	1.716(5)
Mo(1)-N(2)	1.777(6)	O(1)-C(1)	1.423(7)	O(2)-C(5)	1.427(6)
N(1)-C(9)	1.471(7)	N(2)-C(13)	1.442(10)	C(1)-C(2)	1.478(12)
C(1)-C(3)	1.483(10)	C(1)-C(4)	1.485(11)	C(6)-C(5)	1.520(9)
C(7)-C(5)	1.482(12)	C(5)-C(8)	1.515(10)	C(9)-C(10)	1.519(12)
C(9)-C(11)	1.532(12)	C(9)-C(12)	1.528(8)	C(13)-C(14)	1.443(18)
C(13)-C(15)	1.570(13)	C(13)-C(16)	1.549(16)	C(13)-C(14A)	1.614(21)
C(13)-C(15A)	1.511(23)	C(13)-C(16A)	1.355(23)		

Table A.71: Bond lengths (Å) for **6** $[Mo(NBu^t)_2(OBu^t)_2]$.

A-B-C	∠A-B-C	A-B-C	∠A-B-C	A-B-C	∠A-B-C
O(1)-Mo(1)-O(2)	107.9(2)	O(1)-Mo(1)-N(1)	110.1(3)	O(2)-Mo(1)-N(1)	109.6(2)
O(1)-Mo(1)-N(2)	108.2(2)	O(2)-Mo(1)-N(2)	108.8(2)	N(1)-Mo(1)-N(2)	112.2(3)
Mo(1)-O(1)-C(1)	143.9(4)	Mo(1)-O(2)-C(5)	141.4(4)	Mo(1)-N(1)-C(9)	169.5(6)
Mo(1)-N(2)-C(13)	157.1(5)	O(1)-C(1)-C(2)	106.8(5)	O(1)-C(1)-C(3)	109.9(7)
C(2)-C(1)-C(3)	108.6(6)	O(1)-C(1)-C(4)	111.0(5)	C(2)-C(1)-C(4)	109.4(8)
C(3)-C(1)-C(4)	111.0(6)	O(2)-C(5)-C(6)	104.8(5)	O(2)-C(5)-C(7)	108.9(5)
C(6)-C(5)-C(7)	111.3(6)	O(2)-C(5)-C(8)	109.6(5)	C(6)-C(5)-C(8)	111.1(5)
C(7)-C(5)-C(8)	110.9(6)	N(1)-C(9)-C(10)	109.1(6)	N(1)-C(9)-C(11)	106.7(6)
C(10)-C(9)-C(11)	110.8(5)	N(1)-C(9)-C(12)	109.5(4)	C(10)-C(9)-C(12)	110.6(6)
C(11)-C(9)-C(12)	110.0(6)	N(2)-C(13)-C(14)	110.7(8)	N(2)-C(13)-C(15)	106.5(8)
C(14)-C(13)-C(15)	113.8(9)	N(2)-C(13)-C(16)	107.8(8)	C(14)-C(13)-C(16)	109.6(11)
C(15)-C(13)-C(16)	108.2(7)	N(2)-C(13)-C(14A)	101.1(9)	N(2)-C(13)-C(15A)	114.2(12)
C(14A)-C(13)-C(15A)	98.3(13)	N(2)-C(13)-C(16A)	110.9(15)	C(14A)-C(13)-C(16A)	114.2(16)
C(15A)-C(13)-C(16A)	116.4(14)				

Table A.72: Bond angles (°) for **6** $[Mo(NBu^t)_2(OBu^t)_2]$.

Atom	U_{11}	U_{22}	U_{33}	U_{12}	U_{13}	U_{23}
Mo(1)	0.0413(2)	0.0264(2)	0.0379(2)	0.0010(2)	0.0165(2)	0.0008(2)
O(1)	0.082(3)	0.061(3)	0.048(2)	0.002(2)	0.028(2)	0.007(2)
O(2)	0.053(2)	0.053(2)	0.052(2)	0.001(2)	0.014(2)	0.002(2)
N(1)	0.105(4)	0.025(2)	0.074(3)	-0.003(3)	0.031(3)	0.002(3)
N(2)	0.042(3)	0.095(4)	0.054(3)	0.013(3)	0.020(2)	-0.001(3)
C(1)	0.069(4)	0.065(4)	0.040(3)	-0.001(3)	0.026(3)	0.001(3)
C(2)	0.241(12)	0.117(8)	0.080(6)	0.042(8)	0.093(7)	0.015(6)
C(3)	0.079(6)	0.274(15)	0.076(5)	-0.019(8)	0.023(4)	0.012(7
C(4)	0.128(7)	0.103(6)	0.069(4)	-0.032(6)	0.047(5)	0.008(4)
C(6)	0.076(5)	0.106(7)	0.102(6)	0.013(5)	-0.006(4)	0.019(5)
C(7)	0.105(6)	0.123(7)	0.067(4)	-0.021(5)	0.041(4)	-0.007(5)
C(5)	0.046(3)	0.055(4)	0.047(3)	0.000(3)	0.011(3)	0.002(3)
C(8)	0.059(4)	0.094(6)	0.092(5)	-0.020(4)	0.018(4)	-0.008(5)
C(9)	0.087(4)	0.022(3)	0.076(4)	0.006(3)	0.038(3)	0.002(3)
C(10)	0.125(6)	0.041(4)	0.102(5)	0.002(4)	0.064(5)	-0.001(4)
C(11)	0.096(5)	0.051(4)	0.108(6)	0.005(4)	0.052(5)	0.007(4)
C(12)	0.095(5)	0.039(4)	0.103(5)	0.006(4)	0.033(4)	0.011(4)
C(13)	0.045(3)	0.080(5)	0.077(4)	-0.006(3)	0.027(3)	-0.011(4)

Table A.73: Anisotropic atomic displacement parameters ($Å^2$) for **6** [$Mo(NBu^t)_2(OBu^t)_2$].

Atom	x	y	z	Atom	x	y	z
H(2A)	0.2688	0.7657	0.2982	H(2B)	0.1859	0.6706	0.2833
H(2C)	0.2702	0.6580	0.3726	H(3A)	0.3893	0.6089	0.3127
H(3B)	0.3899	0.4887	0.3828	H(3C)	0.3811	0.4122	0.2979
H(4A)	0.1737	0.3718	0.2667	H(4B)	0.2490	0.2661	0.2697
H(4C)	0.2578	0.3426	0.3546	H(6A)	0.0560	0.7613	-0.1228
H(6B)	-0.0254	0.6562	-0.1853	H(6C)	-0.0065	0.6958	-0.0916
H(7A)	0.1499	0.3677	-0.1183	H(7B)	0.0798	0.4603	-0.2008
H(7C)	0.1575	0.5628	-0.1300	H(8A)	0.0489	0.2587	-0.0795
H(8B)	-0.0107	0.3829	-0.0647	H(8C)	-0.0296	0.3433	-0.1584
H(10A)	0.1675	0.0231	-0.0405	H(10B)	0.2674	0.0394	0.0041
H(10C)	0.2257	-0.1329	0.0078	H(11A)	0.0955	0.0132	0.0466
H(11B)	0.1500	-0.1429	0.0999	H(11C)	0.1496	0.0242	0.1472
H(12A)	0.3551	0.0329	0.1635	H(12B)	0.3105	0.0359	0.2199
H(12C)	0.3109	-0.1312	0.1726	H(14A)	0.3985	0.2790	0.0210
H(14B)	0.3259	0.4047	-0.0393	H(14C)	0.4207	0.4382	-0.0169
H(15A)	0.4534	0.4338	0.2126	H(15B)	0.4524	0.2758	0.1589
H(15C)	0.5210	0.4186	0.1818	H(16A)	0.4650	0.7073	0.1390
H(16B)	0.4756	0.6603	0.0597	H(16C)	0.3896	0.7396	0.0454
H(14D)	0.3256	0.6207	-0.0415	H(14E)	0.4176	0.5741	-0.0241
H(14F)	0.3489	0.4313	-0.0470	H(15D)	0.4443	0.2570	0.1345
H(15E)	0.3723	0.2437	0.0379	H(15F)	0.4657	0.2941	0.0610
H(16D)	0.4761	0.5600	0.1981	H(16E)	0.5132	0.5844	0.1358
H(16F)	0.4372	0.6982	0.1257				

Table A.74: Atomic coordinates of the hydrogen atoms of **6** $[Mo(NBu^t)_2(OBu^t)_2]$.